Pharmacological characterisation of the 5-HT receptors present on mouse and human hepatic stellate cells and their role in liver fibrosis.

Thesis submitted for the degree of

Doctor of Philosophy

At the University of Strathclyde
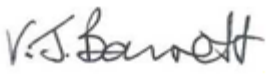
by

Victoria J Barrett

Strathclyde Institute of Pharmacy and Biomedical Sciences

University of Strathclyde

May 2017

'This thesis is the result of the author's original research. It has been composed by the author and has not been previously submitted for examination which has led to the award of a degree.'

'The copyright of this thesis belongs to GSK in accordance with the author's contract of employment with GSK under the terms of the United Kingdom Copyright Acts. Due acknowledgement must always be made of the use of any material contained in, or derived from, this thesis.'

Signed: V.J.Barrett   Date: 19ᵗʰ May 2017

Pharmacological characterisation of the 5-HT receptors present on mouse and human hepatic stellate cells and their role in liver fibrosis

Victoria J Barrett

Fibrosis and Lung Injury Discovery Performance Unit, GlaxoSmithKline Medicines Research Centre, Stevenage, Hertfordshire, UK, SG1 2NY

Abstract

The prevalence of chronic liver disease is rising worldwide with a clear unmet need for therapy: The only current treatment is liver transplant or elimnation of the underlying cause. The hepatic stellate cell (HSC) has been identified as the fibrogenic cell type responsible for scarring. Following liver injury HSCs are activated, transforming into a proliferating, perpetuating population of myofibroblast–like cells, that secrete extracellular matrix. Evidence that serotonin (5-HT) influences HSC biology has been reported, with activation up-regulating the expression of 5-HT_{2A}, 5-HT_{2B} and 5-HT_{1B} receptors and therefore have potential as targets for therapy. In this thesis an 'in-depth' quantitative pharmacological characterisation of the 5-HT receptors present on mouse and human HSCs was undertaken to fully evaluate and extend the evidence for a role of 5-HT in driving the fibrogenic process.

The 5-HT_{2A} receptor was demonstrated pharmacologically to be responsible for both 5-HT-stimulated intracellular calcium signalling in mouse and human HSCs and for extracellular regulated kinase (ERK) phosphorylation signal in mouse HSCs. A second 5-HT receptor responsible for ERK phosphorylation was found to be present on mouse HSCs, with pharmacological properties suggesting the 5-HT_{1B} receptor as the most likely candidate.

The role of 5-HT in fibrotic phenotypic endpoints of proliferation and collagen production was also investigated with no evidence of a role for 5-HT identified. Although 5-HT was reported to enhance platelet derived growth factor (PDGF)-induced proliferation, 5-HT was found only to enhance the PDGF-induced ERK phosphorylation in mouse HSCs. These data, therefore, did not support a role for 5-HT in driving HSCs fibrogenesis.

In a mouse CCl_4 liver injury model the consistent delivery of low pharmacologically selective doses of a selective 5-HT_{2A} and 5-HT_{2B} antagonist, volinanserin and GSK1606260A respectively, were evaluated. Volinanserin was found to have no anti-fibrotic effect whereas GSK1606260A was pro-fibrotic. These data highlights the challenge of reliance on *in vitro* single cell type assays and their translation into *in vivo* models. Taken together these data were not consistent with the functional 5-HT_{2A} and 5-HT_{1B} receptors present on HSCs playing a key role in driving fibrosis and suggest they do not present a viable anti-fibrotic therapy opportunity.

Acknowledgements

Abbreviations

ALD, alcoholic liver disease

ALK5, activin like kinase 5

ALT, alanine aminotransferase

Ang II, angiotensin II

AST, aspartate aminotransferase

AT1, Angiotensin 1

ATP, adenosine triphosphate

BDL, bile duct ligation

BSA, bovine serum albumin

cAMP, cyclic adenosine monophosphate

CCl_4, carbon tetrachloride

CHC, Chronic hepatitis C

CHO, chinese hamster ovary

CNS, Central nervous system

CRC, concentration-response curve

CREB, cAMP response element binding protein

CTGF, connective tissue growth factor

CYP, cytochrome P450

DAG, diacylglycerol

DC, dendritic cell

DMEM, Dulbecco's modified eagle medium

DMSO, dimethyl sulphoxide

EC_{50}, molar concentration that produces 50% of maximum response to that agent.

EC_{80}, molar concentration that produces 80% of maximum response to that agent.

ECM, extracellular matrix

EDTA, ethylenediaminetetraacetic acid

EGF, Endothelial growth factor

ELK, ETS domain-containing protein

ELISA, enzyme-linked immunosorbent assay

ERK, extracellular signal-regulated kinases

ET-1, endothelin 1

Fas ligand, death ligand

FCS, foetal calf serum

FGF, fibroblast growth factor

FLIPR, fluorescence imaging plate reader

FXR, farnesoid X receptor

GFAP, glial fibrillary acidic protein

GIT, gastrointestinal tract

GPCR, G protein-coupled receptor

GSK, GlaxoSmithKline

HBSS, Hank's balanced salt solution

HBV, hepatitis B virus

HCC, hepatocellular carcinoma

HCV, hepatitis C virus

HEPES, 4-(2-hydroxyethyl)-1-piperazineethanesulfonic acid

HSC, hepatic stellate cell

IGF-1, insulin-like growth factor

IL-1, interleukin-1

IL-6, interleukin-6

IL-8, interleukin-8

IC_{50}, molar concentration that produces 50% of maximum inhibition to that agent

IP3, inositol 1,4,5 triphosphate

IPF, idiopathic pulmonary fibrosis

LPA, lysophosphatidic acid

LPS, lipopolysaccharide

LSEC, liver sinusoidal endothelial cells

LXR, liver X receptor

MEK, Mitogen-activated protein kinase kinase

MAPK, mitogen-activated protein kinase

MDMA, 3,4-methylenedioxy-N-methylamphetamine

MHC Major histocompatibility complex

MIP-2, macrophage inflammatory protein-2

MMP, matrix metalloproteinases

MSD, Meso Scale Discovery

NADPH, nicotinamide adenine dinucleotide phosphate-oxidase

NAFLD, non-alcoholic fatty liver disease

NASH, non-alcoholic steatohepatitis

NFκB, nuclear factor-κB

NOX, nitrogen oxides

NO, nitric oxide

ONS, Office for National Statistics

OPZ, Oltipraz

pA_2, the negative log of the concentration of antagonist which would produce a 2-fold shift in the concentration-response curve for an agonist.

PAI-1, plasminogen inhibitor-1

PBS, phosphate buffered saline

PCLS, precision cut liver slice

PDGF, Platelet derived growth factor

pERK, ERK phosphorylation

pIC_{50}, negative $\log_{10} IC_{50}$

PI3K, phosphoinositide 3-kinase

PK, pharmacokinetic

PKC, protein kinase C

PKA, protein kinase A

pK_D, negative $\log_{10} K_D$

pK_i, negative $\log_{10} K_i$

fpK_i, negative $\log_{10} K_i$ measure in a functional assay

PLC, phospholipase C

PMSF, phenylmethylsulfonyl fluoride

PPARγ, peroxisome proliferator-activated receptor γ

PSR, picrosirius red

PTX, pertussis toxin

ROS, reactive oxygen species

SAMe, S-adenosyl-L-methionine

SD, standard deviation

SDS, sodium dodecyl sulphate

SEC, sinusoidal endothelial cell

SEM, standard error of the mean

SERT, serotonin reuptake transporter

SIAJ, "Scar-in- a-Jar"

SMAD, Sma and Mad related protein

SSc, Systemic sclerosis scleroderma

STAT1, Signal transducer and activator of transcription 1

TAA, thioacetamide

TGFβ, transforming growth factor-β

TβRI, TGFβ receptor I

TβRII, TGFβ receptor II

TβRIII, TGFβ receptor III

TIMP, tissue inhibitor of metalloproteinase

TNFα, Tumour necrosis factor-α

TPH, tryptophan hydroxylase

TRAIL, tumour necrosis factor-related apoptosis-inducing ligand

VHD, valvular heart disease

VEGF, vascular endothelial growth factor

α-SMA, smooth muscle-actin

5-HIAA, 5-Hydroxyindole acetic acid

5-HT, 5-Hydoxytryptamine

5-HTP, 5-Hydroxytryptophan

8-OH-DPAT, 8-Hydroxy N,N-dipropylaminotetralin

TABLE OF CONTENTS

Figures

Tables

CHAPTER 1. INTRODUCTION

1.1 Liver fibrosis.

Liver fibrosis is a reversible wound-healing response to acute or chronic injury of the liver and a structural consequence of the balancing between repair and accumulation of extracellular matrix (ECM) components, such as collagen and fibronectin, to form scarring. Wound repair is one of the most complex biological processes that occur in the body, where various intracellular and intercellular pathways are activated and coordinated, to restore tissue integrity and homeostasis (Gurtner et al., 2008; Wynn, 2008). Normal tissue repair can progress into fibrosis if the injury is severe, repetitive or if the wound healing response becomes unregulated and therefore fibrosis is a feature of most chronic inflammatory diseases (Wynn and Ramalingam, 2012).

The liver is the largest internal organ and plays an important role in metabolism, blood clotting, regulation of most substances in the body, production of bile, resistance to infection and clearance of poisons and drugs from the body. A healthy liver has substantial overcapacity and has a remarkable ability to regenerate in response to parenchymal loss of up to 70% (Wallace et al., 2008). In chronic liver injury the accumulation of the matrix proteins, along with the stimulus to regenerate, leads to the distortion of the architecture of the liver and vascular structures resulting in progressive loss of organ function and eventual irreversible damage known as cirrhosis (Friedman et al., 2013). Cirrhotic patients can have apparently normal liver function for long periods before the liver fails, along with development of ascites (accumulation of fluid in the peritoneal cavity), portal hypertension, encephalopathy and possibly hepatocellular carcinoma. Fibrosis often causes lifelong disability and has a significant economic impact leading to a huge burden on public health.

1.2 Prevalence of liver disease and patient population.

Chronic liver disease is rising worldwide with the prevalence of non-alcoholic fatty liver disease (NAFLD) escalating over the last 10 years (Lazo and Clark, 2008; Williams et al., 2011). The main causes of liver fibrosis are infection, autoimmune diseases, inherited diseases, diet (e.g. high fat diet) and chemical (e.g. alcohol). Before the 21st century, alcoholic liver disease and viral hepatitis-induced liver

disease were considered the main cause of liver morbidity but with the increased prevalence of obesity, non-alcoholic fatty liver disease (NAFLD) is now becoming the most common liver disease (Lazo and Clark, 2008). NAFLD covers the spectrum of liver disease from simple steatosis (deposition of fat in the liver) to the most extreme form of NAFLD, which is non-alcoholic steatohepatitis (NASH:-inflammation of the liver with concurrent fat accumulation), associated with metabolic syndrome and insulin resistance. Globally there are at least 400 million obese adults (Ogden et al., 2006) and it has been estimated that 75% of those with obesity will have NAFLD and with approximately 20% prevalence of NASH (Clark, 2006). NAFLD is a recognised cause of liver cirrhosis and hepatocellular carcinoma (HCC). In England the number of people dying from liver disease has risen by 40% in the last decade and is still rising. Liver disease is the 3rd biggest cause of premature mortality with over 90% of cases being due to alcohol, viral hepatitis and obesity (Verne, 2014). Overall liver disease is the fifth 'big killer' in England & Wales, after heart disease, cancer, stroke and respiratory disease, and is the only major cause of death still increasing (Department of Health: Safe, Sensible, Social – Consultation on further action Impact Assessments 22 July 2008). Up to 45% of the deaths in the developed world can be attributed to some type of fibrosis (Wynn, 2008) and thus fibrosis represents a huge unmet clinical need.

1.3   Liver fibrosis therapy.

Over the last 20 years the understanding that liver fibrosis is a dynamic and reversible process, along with the underlying sources and mediators of fibrosis progression, has led to the identification of therapeutic approaches. The progression of liver fibrosis occurs over 15-40 years depending on the patient's rate of fibrosis progression, which eventually may culminate in cirrhosis and therefore long term pharmacological intervention will be required (Cohen-Naftaly and Friedman, 2011). Most therapies for chronic liver disease target the removal of the causative agent, as there is no effective therapy for hepatic fibrosis, and therefore for some patients the only available treatment is a liver transplant (Bataller and Brenner, 2005; Said and Lucet, 2008; Wallace et al., 2008).

There are currently over 400 clinical trials ongoing for liver fibrosis around the world (http://clinicaltrial.gov) but the majority of the trials are for novel methods for the assessment of fibrosis. Elimination of the source of chronic injury is the most effective treatment and along with therapeutic strategies to treat the underlying cause such as cessation of drinking alcohol or weight reduction which fall into this category. Taking away the cause of the injury therefore stops the insult and allows the liver to repair (Novo et al., 2014). There is a great deal of evidence that liver fibrosis is reversible, not just from animal studies, but in patients too (Rockey, 2008). Reversion of the fibrosis was observed, even in some patients who exhibited histologic cirrhosis, after eradication of hepatitis C (HCV) (Poynard et al., 2002; Abergel et al., 2004) and hepatitis B (HBV) (Lai et al., 1998; Hadziyannis et al., 2003). In patients suffering with NASH treatment with peroxisome proliferator-activated receptor γ (PPARγ) agonist, rosiglitazone, for 48 weeks, demonstrated a reduction in both the steatosis and fibrosis (Neuschwander-Tetri et al., 2003). Table 1.3.1 shows a list of possible treatments that target the underlying cause.

There have been other approaches considered for fibrosis therapy which treat the underlying disease mechanism such as reducing inflammation, targeting specific signalling pathways, inhibition of matrix synthesis and blocking the function of or eliminating effector cells. (Rockey, 2008; Cohen-Naftaly and Friedman, 2011). There have been a number of clinical trials which have investigated therapy to treat the underlying disease but so far no new anti-fibrotic therapy has emerged. Table 1.3.2 highlights examples of anti-fibrotic therapy that has been tested in clinical trials over the last 10 years. These include antioxidants, which target ROS generation to reduce inflammation, such as S-adenosylmethionine (SAMe), Silybin, vitamin E and reservatol (Loguercio et al., 2007; Sanyal et al., 2010; Medici et al., 2011; Faghihzadeh et al., 2014) (Table 1.3.2). Targeting more than one mechanism in fibrosis with agents such as losartan, olptipraz and pentoxifylline have been tried with interesting results (Colmenero et al., 2009; Lebrec et al., 2010; Kim et al., 2011) (Table 1.3.2).

There are many different types of cells in the liver such as hepatocytes, Kupffer cells (fixed macrophages) endothelial cells and hepatic stellate cells (HSCs). All the cells

Disease	Therapy	Evidence
HBV	Antiviral : Lamivudine, Adefovir dipivoxil	(Lai et al., 1998; Hadziyannis et al., 2003)
HCV	Interferon alpha	(Poynard et al., 2002; Abergel et al., 2004)
Autoimmune hepatitis	Corticosteroids	(Dufour, 1997)
Hemochromatosis	Iron depletion	(Pietrangelo et al., 1995)
Alcoholic hepatitis	corticosteroids	(Ramond et al., 1992)
Primary biliary cirrhosis	Ursodeoxycholic acid, Methotrexate	(Hammel et al., 2001)
NASH	Gastric bypass surgery, PPAR γ ligands	(Neuschwander-Tetri et al., 2003; Furuya et al., 2007)

Table adapted from Rockey, 2008.

Table 1.3.1. Treatments that target the underlying cause of fibrosis.

Therapy	Trial Protocol	Trial outcome
S-adenosyl-methionine (SAMe)	**Population:** 37 Alcoholic liver disease (ALD) patients. **Type** : Double blind, randomized placebo controlled. **Treatment:** Daily: SAMe or placebo **Duration:** 24 weeks. **Extra advice**: Subjects were required to remain abstinent from alcohol	Improvement of AST, ALT, Bilirubin levels in both groups due to alcohol abstinence. 24 weeks of therapy with SAMe was no more effective than placebo.
	Pharmacology	**Evidence**
	Antioxidant: Prevents activation of TLR pathways, pro-inflammatory response, fibrogenesis, cirrhosis, and hepatocellular carcinoma	(Medici et al., 2011)

Therapy	Trial Protocol	Trial outcome
Reservatol	**Population**: 50 NAFLD patients (2 groups) **Type**: Double blind, randomized placebo controlled **Treatment**: 500-mg reservatol or placebo **Duration**: 12 weeks. **Extra advice**: Patients to follow an energy-balanced diet and received physical activity recommendation	Reduction in liver enzyme, inflammatory cytokines, and hepatocellular apoptosis. Treatment along with lifestyle modification is superior to lifestyle modification alone
	Pharmacology	**Evidence**
	Antioxidant and anti-inflammatory	(Faghihzadeh et al., 2014)

Therapy	Trial Protocol	Trial outcome
Silybin/ vitamin E / phospholipid	**Population** 85 patients (Group A: 59 NAFLD, Group B: 26 NAFLD with HCV-related chronic hepatitis) **Treatment**: 4 pills per day of silybin/phophatidylcholine/vitamin E. **Duration**: 6 months treatment followed by 6 month of no treatment.	Improved in liver enzyme levels, hyperinsulinemia, and indexes of liver fibrosis. Recommendation: use as a complementary approach to treatment of patients with chronic liver damage.
	Pharmacology	**Evidence**
	Antioxidant: suppresses HCS proliferation & collagen deposition *in vitro* in humans (Dehmlow et al., 1996)	(Loguercio et al., 2007)

Therapy	Trial Protocol	Trial outcome
Pioglitazone	**Population:** 247 NASH patients **Type** : Double blind, randomized placebo controlled. **Treatment:** Daily pioglitazone, Vit E or placebo. **Duration:** 24 months	Significant improvement of liver enzyme levels, hepatic steatosis and lobular inflammation. No significant improvement in NASH with pioglitazone but Vitamin E therapy was superior to placebo
	Pharmacology	**Evidence**
	PPARγ agonist which is expressed on HSCs. Activation inhibits fibrogenicity	(Sanyal et al., 2010)

Table 1.3.2 Examples of anti-fibrotic therapy completed trials in patients with liver disease.

Therapy	Trial Protocol	Trial outcome
Losartan	**Population:** 14 patients with chronic hepatitis C (CHC). **Type** :uncontrolled open-label study **Treatment:** Losartan 50mg daily **Duration:** 18 months	Collagen remained stable 7 patients demonstrated a reduction in fibrosis stage and inflammation. Prolonged administration of losartan, is associated with down regulation of NOX components and fibrogenic genes
	Pharmacology	**Evidence**
	Angiotensin1 (AT1) receptor antagonist which decreases expression of NADPH oxidase and inhibits proliferation and contraction of HSCs.	(Colmenero et al., 2009)

Therapy	Trial Protocol	Trial outcome
Oltipraz (OPZ)	**Population**: 83 patients suffering from liver fibrosis and cirrhosis **Type:** Double blind, randomized placebo controlled **Treatment**: 3 groups: Twice daily admin of OPZ 60mg, OPZ 90mg or Placebo **Duration** : 24 weeks	60mg OPZ group: Decreases in hepatic collagen area and plasmaTGF-β1 An association between TGF-β1 repression and improvement in the histological index of fibrosis was observed. No significant difference in liver histological outcomes between the three treatment groups.
	Pharmacology	**Evidence**
	TGF-β inhibition and inhibition of TNF-α	(Kim et al., 2011)

Therapy	Trial Protocol	Trial outcome
Pentoxifylline	**Population:** 335 cirrhosis patients **Treatment:** 3 times daily admin 400mg pentoxifylline or placebo **Duration:** 6 months	No reduction in short term mortality but probability of survival without complications was higher.
	Pharmacology	**Evidence**
	Phosphodiesterase inhibition causing increased cAMP leading to TNF-α inhibition	(Lebrec et al., 2010)

Table 1.3.2 continued.

have a potential role in the pathogenesis of liver fibrosis, but one cell which is thought to be a key mediator is the HSC due to its role in matrix production (Friedman, 2008b) (See section 1.8). In the injured liver activation of the HSC occurs which involves the cell undergoing a phenotypic and functional transformation into a myofibroblast–like cell that has enhanced collagen production (Friedman, 2000; Bataller and Brenner, 2005; Ruddell et al., 2006) (See Section 1.8 for in-depth discussion of HSC biology). The location of the HSC in the liver in the sinusoidal space of Disse allows it to come into contact with platelets and hepatocytes, as well as being in close proximity to nerve endings. HSCs can be influenced by neurotransmitters and growth factors through expression of appropriate receptors on their surface, whose expression is influenced by activation of the HSC (Wong et al., 1994; Ruddell et al., 2006; Friedman, 2008b). Targeting receptors on the HSC therefore offer an opportunity for anti-fibrotic therapy. 5-HT receptors are expressed on HSCs, with increased expression of 5-HT_{2A}, 5-HT_{2B} and 5-HT_{1B} observed following HSC activation (Ruddell et al., 2006). Links between 5-HT and fibrosis have been reported since the 1960s (Oates et al., 1966; Pavlovic et al., 1995), with 5-HT_2 receptors implicated as drivers of fibrosis in heart valves, lung, skin and liver (Reimund, 1987; Waller et al., 2005; Roth, 2007; Rothman and Baumann, 2009). Antagonists of the 5-HT_2 receptors therefore offers a prospect for fibrosis therapy.

1.4   5-Hydroxytryptamine.

5-hydroxytryptamine (5-HT), also known as serotonin, was first synthesised in 1951 (Hamlin and Fischer, 1951) and has been the subject of extensive research since then. 5-HT is a neurotransmitter and probably best known for its modulation of neural activity and neuropsychological processes, due to its wide use in psychiatry and neurology. However it also regulates numerous biological processes outside the brain (Berger et al., 2009). 5-HT is an important neurocrine and paracrine hormone and is heterogeneously distributed throughout the brain and peripheral tissues. In the CNS, 5-HT is important in regulation of virtually all brain function, controlling regulatory processes such as temperature, sleep, learning, memory, pain, feeding and motor activity (Berger et al., 2009). Therefore any dysregulation of the 5-HT system in the CNS can lead to many pathological conditions such as aggression, depression,

anxiety, suicidal behaviour and alcoholism (Figueroa et al., 2009). Outside of the CNS, 5-HT is involved in the contraction and relaxation of smooth muscle and vasculature, cardiovascular function, gastrointestinal tract (GIT) motility, bladder control and platelet aggregation (Ruddell et al., 2008; Berger et al., 2009; Figueroa et al., 2009).

Platelet-derived 5-HT has been demonstrated to be critical for normal wound healing in many organs such as liver, lung, heart and skin (Mann and Oakley, 2013). 5-HT has been shown to influence inflammatory responses and promote formation of a temporary scar, which acts as a scaffold for normal tissue to be restored (Ruddell et al., 2008; Mann and Oakley, 2013). During acute injury, 5-HT is therefore able to exert a pro-fibrogenic and pro-regenerative influence which ensures the repair and restoration of tissue architecture (Yokoyama et al., 1953; Lesurtel, 2006; Lesurtel et al., 2012; Mann and Oakley, 2013). 5-HT also plays a complex role in the regulation of processes in the body, such as digestion or pain (Berger et al., 2009). This therefore means that pharmacological intervention at a specific receptor in a disease is a challenge, as a single 5-HT receptor is likely to have effects in multiple body systems (Berger et al., 2009).

It was the discovery that platelet–derived 5-HT can initiate liver regeneration after partial hepatectomy in rodent models (Lesurtel, 2006; Papadimas et al., 2006; Tian et al., 2011) that increased the interest in its contribution to hepatic disease. During chronic liver injury, 5-HT can promote aberrant healing, which leads to tissue fibrosis and impairs organ regeneration (Papadimas et al., 2006; Ruddell et al., 2006, 2008; Mann and Oakley, 2013). 5-HT can therefore be both 'friend and foe' in the liver and has potential as a pharmacological target in liver disease (Lesurtel et al., 2012).

1.4.1 5-HT synthesis and metabolism.

About 95% of 5-HT can be found in the GIT, with 90% found in enterochromaffin cells (ECs) and the rest in the enteric neurones. The CNS contains the remaining 5%, which it makes itself, as 5-HT is unable to cross the blood brain barrier (Lesurtel et al., 2008). The 5-HT found in the blood is mainly derived from the GIT (Bertaccini,

1960), due to its presence and synthesis in ECs and enteric neurones (Dreyfus and Bornstein, 1977; Gershon and Tamir, 1981; Costa et al., 1982; Yu et al., 1999). Platelets contain 95% of the blood 5-HT, which they accumulate from the plasma due to a high-affinity uptake system for 5-HT, which allows them to become loaded with 5-HT as the blood passes through the intestinal circulation (Da Prada et al., 1967). Although we ingest 5-HT through our diet (5-HT is widely distributed in animals, fungi, plants, fruit and vegetables), this is mostly metabolised before ever entering the blood (Lesurtel et al., 2008).

5-HT is synthesised from L-tryptophan by tryptophan hydroxylase (TPH) to produce 5-hydroxytryptophan (5-HTP) followed by decarboxylation by L-aromatic acid decarboxylase (Figure 1.4.1) (Lesurtel et al., 2008). There are two isoforms of TPH, TPH1 which is present in the periphery and THP2 in the brain. 5-HT is mainly metabolised in the liver through the action of mono amine oxidase, to produce 5-hydroxyindoleacetaldehyde, with further oxidation by aldehyde dehydrogenase to form 5-hydoxyindole acetic acid (5-HTIAA), which is excreted in the urine (Tyce, 1990)(Figure 1.4.1). The GIT and CNS both have an inactivating mechanism which is a serotonin reuptake transporter (SERT) (Wade et al., 1996; Chen et al., 1998) and this has also been demonstrated to be present in rat HSCs (Ruddell et al., 2006). SERT plays an important role in terminating the action of 5-HT and maintaining transmitter homeostasis. The lack of SERT in mice manifests itself as increased colonic motility and water in the stools (Lesurtel et al., 2008).

1.4.2 5-HT receptor classification.

Pharmacology as a scientific discipline was born in the mid 19th century, to understand how therapeutic agents and poisons produced their effects in the body. Pharmacologists' big idea was the lock-and-key relationship between drugs and a specific site, to allow drugs to have the desired specificity and efficacy (Rang, 2006). For more than a century, pharmacologists have studied receptors, with G protein-coupled receptors (GPCRs) and ion channels as major examples. Experiments with isolated animal tissues have been crucial in providing data to define the interaction between chemical and tissue responses until the era of molecular research in the
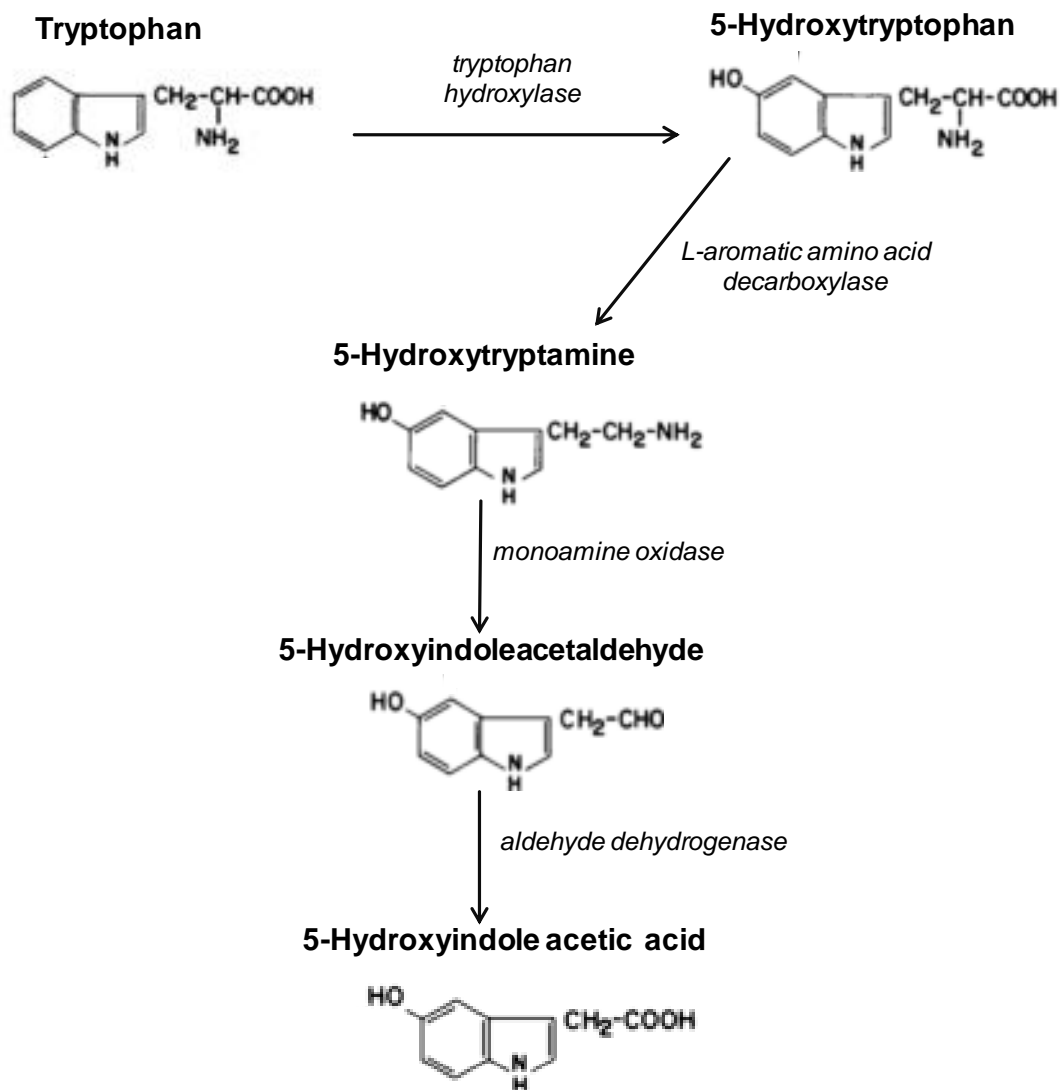
Figure 1.4.1   5-Hydroxytryptamine synthesis and metabolism. L-tryptophan undergoes hydroxylation by the enzyme tryptophan hydoxylase to produce 5-hydroxytryptophan (5-HTP). This is followed by decarboxylation of 5-HTP by L-aromatic amino acid decarboxylase to form 5-Hydroxytryptamine (5-HT). 5-HT is metabolised in the liver and kidneys by monoamine oxidase to form 5-Hydroxyindoleacetic acid which is further oxidised by aldehyde dehydrogenase to produce 5-Hydoxyindole acetic acid (5-HTIAA). 5-HTIAA is then excreted in the urine (Figure adapted from Tyce, 1990).

1970's and 80's, which provided the physical evidence of the existence of receptors (Rang, 2006).

The subdivision of the 5-HT receptors started in the 1950's when it was realised that 5-HT effects could be inhibited in part by morphine (M), and in part by dibenzyline (D) in the guinea pig ileum (Gaddum and Picarelli, 1957). The proposed division into 5-HT M, on smooth muscle, and 5-HT D, associated with intramural nervous tissue, was defined using non-selective ligands. Black's application of Schild's approach to receptor classification led to the development of propranolol (to treat angina pectoris), and cimetidine (to treat gastric and duodenal ulcers) (Black et al., 1965, 1972). Many drug companies adopted this approach to receptor classification leading to the development of a large array of new drugs with which to pharmacologically characterise different receptors (mainly GPCR) families. The development of the ability to radiolabel compounds offered a simple, but powerful way to identify and study receptors, which had a massive impact on receptor research (Hill, 2006). Radioligand binding studies in membranes and cells, along with autoradiography in brain slices and second messenger studies in cells and tissue, led to the further identification of 5-HT receptor subtypes and their renaming as 5-HT_1, 5-HT_2 and 5-HT_3, with the latter considered the previously classified M receptor (Bradley et al., 1986; Hannon and Hoyer, 2008).

It is competitive antagonist affinity which has provided the framework for the receptor classification that we have today (Kenakin, 1997). Competitive antagonists have the same affinity for a given receptor irrespective of the system or agonist used to study it. Within the 5-HT field of receptor classification there were still a number of antagonist affinity discrepancies due to the mixed populations of 5-HT receptors present in peripheral tissues. Agonists have the added complication of requiring two parameters, affinity and intrinsic efficacy, to describe their effects. This means that agonist potencies vary depending on the cellular system used to measure them (Kenakin, 1997). An approach using agonist and antagonist analogues of 5-HT to provide affinity and efficacy 'fingerprints' was proposed as a quantitative basis for differential classification of 5-HT receptors (Martin et al., 1987; Martin and

MacLennan, 1990). This approach complemented and extended the current scheme for identifying and classifying receptors for 5-HT (Martin and MacLennan, 1990).

In 1986 the molecular biology era of receptor cloning began. $5\text{-}HT_{1A}$ the first 5-HT receptor to be cloned, advanced the knowledge and understanding of 5-HT receptors (Hoyer and Martin, 1997). The use of this technology, confirming the traditional pharmacological and biochemical approaches, led to the identification of the 14 receptors we have today based on operational, structural and transductional information (Humphrey et al., 1993; Hoyer and Martin, 1997; Hannon and Hoyer, 2008). 5-HT has 7 receptor families (classified as $5\text{-}HT_1$ to $5\text{-}HT_7$), with a total of 14 receptor subtypes, comprising of 13 distinct GPCRs and one ligand gated ion channel (Table 1.4.1) (Hannon and Hoyer, 2008; Alexander et al., 2015). The GPCRs can be further grouped by their coupling to $G\alpha_{q/11}$ ($5\text{-}HT_{2A}$, $5\text{-}HT_{2B}$ and $5\text{-}HT_{2C}$), $G\alpha_{i/0}$ ($5\text{-}HT_{1A}$, $5\text{-}HT_{1B}$, $5\text{-}HT_{1D}$, $5\text{-}ht_{1e}$, $5\text{-}HT_{1F}$, $5\text{-}ht_{5a}$), $G\alpha_S$ ($5\text{-}HT_4$, $5\text{-}HT_6$ and $5\text{-}HT_7$) and no coupling has yet been designated to the $5\text{-}ht_{5b}$ receptor (Hannon and Hoyer, 2008; Alexander et al., 2015) (Table 1.4.1). With the multiplicity of receptors, transporters and metabolising enzymes it is not hard to see how 5-HT is able to regulate systems, such as behaviour or cognition, in a complex way (Cools et al., 2008).

The three main G-proteins, once activated through stimulation of the receptor, are able to trigger distinct downstream signalling events. $G\alpha_q$-coupled receptors activate phospholipase C (PLC), which hydrolyses phosphatidyl 4,5-bisphophate to diacylglycerol (DAG) and inositol phosphate (IP_3) the latter which binds to IP_3 receptors which leads to increase in intracellular calcium. The $G\alpha_{i/o}$ class of 5-HT receptors when activated reduce the cAMP levels through suppression of adenylate cyclase. Activation of $G\alpha_s$-coupled receptors results in an increase of cAMP, which causes a downstream activation of protein kinase A (PKA) and the cAMP response element binding protein (CREB). Although the 5-HT receptors can be subdivided due to their coupling it does not mean that they exclusively couple to one type of G-protein, and can couple to a variety of other types of intracellular signalling molecules (Millan et al., 2008). In the case of $5\text{-}HT_{2A,}$ non-hallucinogenic agonists can stimulate G_q whereas hallucinogenic agonists stimulate both $G_{q/11}$ and $G_{i/o}$

Receptor Class	Receptor Subtype	G protein coupling	Agonists	Antagonists
5-HT$_1$	5-HT$_{1A}$	**G$\alpha_{i/0}$**	**8-OH-DPAT**, NLX-101	**(±)WAY 100635, robalzotan**
	5-HT$_{1B}$		**CP94253**, L-694,247, naratriptan, eleptriptan, sumatriptan, zolmitriptan	**SB224289,** GR 55562, SB 236057
	5-HT$_{1D}$		**PNU109291,** sumatriptan, eletriptan	**SB714786**
	5-ht$_{1e}$		BRL-54443	-
	5-HT$_{1F}$		LY 334370, **lasmiditan, 5-BODMT,** BRL-54443, sumatriptan	-
5-HT$_2$	5-HT$_{2A}$	**G$\alpha_{q/11}$**	**DOI**	**ketanserin, pimavanserin,** volinanserin, mianserin, trazodone, sarpogrelate, ritanserin, methiothepin
	5-HT$_{2B}$		**BW723C86, Ro 60-0175,** DOI, methysergide	**BF-1, RS-127445, EGIS-7625,** mianserin, ritanserin, methiothepin
	5-HT$_{2C}$		**WAY-163909,** lorcaserin , DOI, Ro 60-0175	**SB242084, FR260010, RS-102221,** mianserin, methysergide, trazodone, olanzapine, loxapine
5-HT$_3$	5-HT$_3$	**Ligand gated ion channel**	**SR 57227,** *m*-**Chlorophenyl-biguanide**	**Granisetron, Ondansetron, Tropisetron**
5-HT$_4$	5-HT$_4$	**Gα_s**	**BIMU 8, TD-8954, RS67506, relenopride, ML 10302, velusetrag,** cisapride	**GR 113808, SB 204070, RS 100235**
5-HT$_5$	5-ht$_{5a}$	**G$\alpha_{i/0}$**	-	**SB 699551**
	5-ht$_{5b}$	?	-	-
5-HT$_6$	5-HT$_6$	**Gα_s**	**WAY-181187, E6801, WAY-208466, EMD-386088**	**Ro 630-563, SB 271046, SB 357134, SB399885, cerlapirdine**
5-HT$_7$	5-HT$_7$	**Gα_s**	**LP-12, LP-44, LP-211, AS-19, E55888**	**SB 258719, SB 269970, SB656104, DR-4004, JNJ-18038638**

Table 1.4.1   5-Hydroxytryptamine receptor classification. Classification of the receptors by class, subtype, G-protein coupling, agonists and antagonists. (Adapted from Hannon and Hoyer, 2008; Alexander et al., 2015). Selective agonist and antagonists are highlighted in bold.

in the rat frontal cortex (Gonzalez-Maeso et al., 2007). 5-HT receptors can also transactivate other pathways such as the tyrosine kinases where 5-HT$_{2A}$ receptor-mediated ERK phosphorylation is dependent on Src, calmodulin and transactivation of epidermal growth-factor receptor (in neuronal cells) or fibroblast-growth-factor receptor (in glial cells) (Quinn et al., 2002; Tsuchioka et al., 2008). It is the receptor distribution along with the cellular environment which dictates the effect of 5-HT on a target organ (Figueroa et al., 2009).

1.5   5-HT and the liver.

1.5.1   Structure of the liver.

The human liver weighs about 1.5 kilograms and contains approximately 13% of the body's blood supply (Wallace et al., 2008). The relative size of the liver and its structure varies depending on species and diet, the average for a carnivore is about 3-4% of body weight compared with about 2% for an omnivore and 1% for herbivores. The liver is a complex multifunctional organ. In man the liver is divided by fissures (fossae), on its surface, into two major lobes (right and left) and two smaller lobes (quadrate and caudate). De-oxygenated blood, which contains nutrients and potentially harmful material from the gut, is delivered via the hepatic portal vein, which divides to pass in between the lobules and terminates in the sinusoids. Oxygenated blood is supplied via the hepatic artery into the sinusoids. Blood leaves the liver via a central vein in each lobule, which drains into the hepatic vein before draining into the inferior vena cava (Figure 1.5.1 A). The liver regulates the chemical levels in the blood and secretes bile to eliminate waste products. Over 500 functions have been identified in the liver such as production of protein for blood plasma, production of cholesterol, conversion of excess glucose into glycogen for storage and regulation of blood clotting.

Microscopically, the liver parenchyma, which is the functional part of the liver filtering the blood to remove toxins, is arranged in lobules based upon blood flow (Figure 1.5.1 B). The lobule is a cylindrical structure constructed around the central
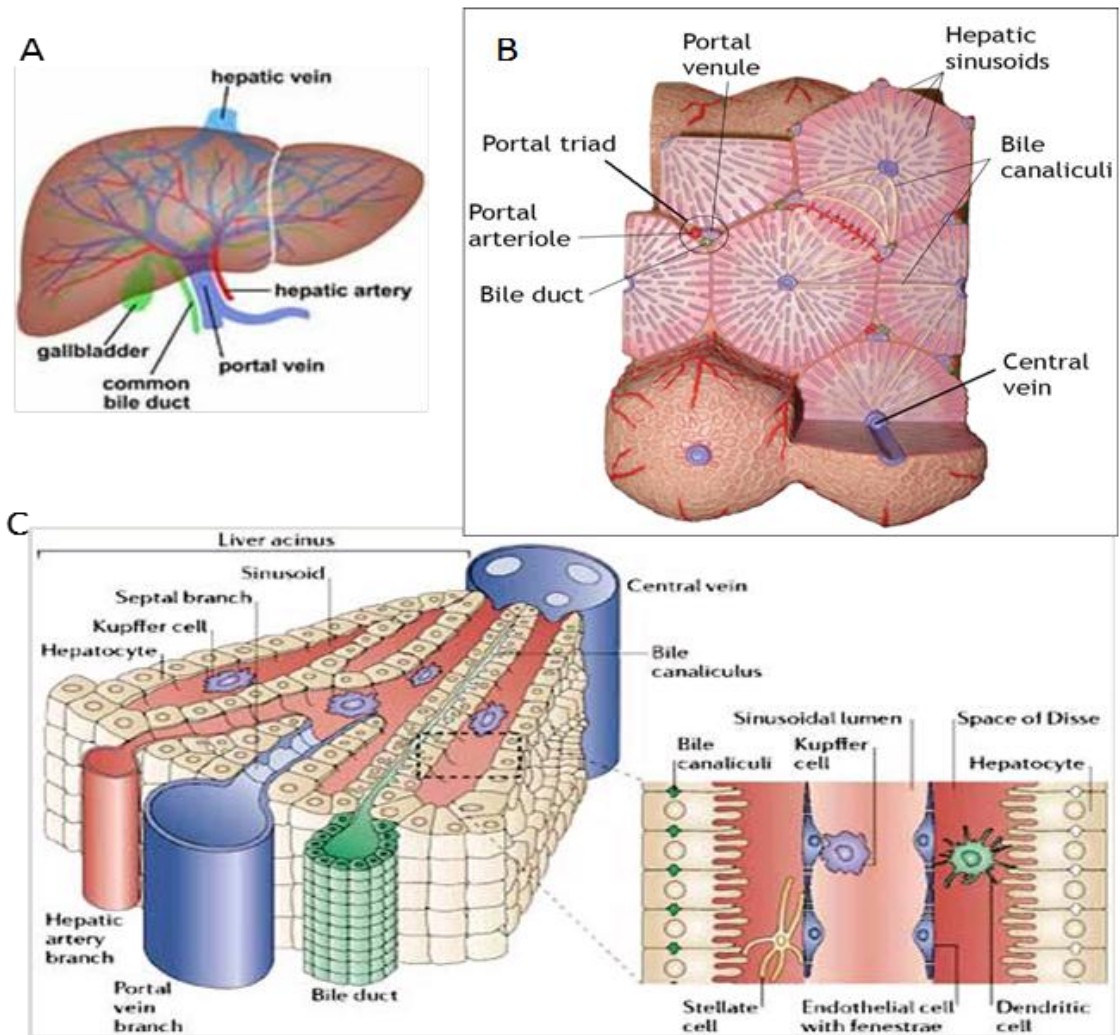
Figure 1.5.1   Liver structure. (A)**Whole liver structure** showing the blood supply network and bile duct network. (B) **Liver lobule structure**. The parenchyma is the primary functional part of the liver and supported by the connective tissue called stroma. Blood is supplied from the hepatic portal vein and hepatic artery which is discharged into capillaries of the liver. Bile ducts are surrounded by a network of small blood vessels from the hepatic artery. (C) **Three-dimensional structure of the liver lobule**. Branches of the portal vein and hepatic artery supply the sinusoids, which takes blood through the acinus to the central vein. Bile ducts transport bile from the canaliculus and eventually to the gut. The sinusoids are lined by morphologically and phenotypically unique endothelial cells (See inset) that are characterised by the absence of tight junctions, a recognisable basement membrane and the presence of open fenestrae, that are organised into sieve plates. The sinusoidal endothelium is interspersed with macrophages, known as Kupffer cells and overlies the space of Disse, which contains fibroblasts known as hepatic stellate cells. Dendritic cells from the parenchyma exit the liver through the space of Disse (Adapted from Adam and Eksteen 2006 and Google Images).

vein and composed of many hepatic cellular plates that radiate from the central vein (Figure 1.5.1 B and C) (Adams and Eksteen, 2006). Each hepatic plate is only a maximum of two hepatocytes thick, with small bile canaliculi lying between them The portal triad is composed of the bile duct along with small portal venules and that feed into the terminal bile ducts in the portal triad between adjacent liver lobules. hepatic arterioles, which deliver the blood to the flat hepatic sinusoids, that lie between the hepatic plates, and flows eventually to the central vein at the centre of the lobule (Braet and Wisse, 2002). The way in which the blood flows from the portal triad to the central vein in the lobule sets up a gradient of oxygen, nutrients, drugs and enzymes. The concentrations are highest nearest the portal triad, known as the periportal zone, and decrease as blood enters the midzonal region, with the lowest concentrations observed in the centrilobular zone nearest the central vein. One of the striking features of the liver is the heterogeneous expression of its enzymes along the sinusoids, such as cytochrome P450 genes (Oinonen and Lindros, 1998). Cytochrome P450 (CYP) enzymes are highly expressed in hepatocytes surrounding the central vein and are active in mono-oxygenation and hydroxylation of various xenobiotics, including drugs and alcohols. This therefore means that the damage will predominantly occur in the area of highest expression which will be the central vein (Wallace et al., 2008). Another consideration is that the oxygen levels will be at the lowest nearest the central vein and this will impact on the cells ability to respond to and survive injury (Wallace et al., 2008).

The sinusoids are lined by fenestrated endothelial cells and contain the Kupffer cells (tissue fixed macrophages), which are phagocytotic cells like macrophages (Braet and Wise, 2002). Between the sinusoids and hepatocytes (epithelial cells) is the space of Disse and this is where the HSCs reside and where dendritic cells can also be found (Figure 1.5.1C) (Braet and Wisse, 2002; Adams and Eksteen, 2006). Bile is secreted by the hepatocytes into the canaliculi, which causes the bile to flow towards the bile duct in the opposite direction to the flow of blood (Boyer, 2013). The bile is then delivered to the gallbladder where it is concentrated and stored. Once something is eaten, bile is discharged into the duodenum to help dissolve the fat from ingested food. Humans can produce up to a litre of bile a day, with 95% of the bile being reabsorbed in the ileum to be reused by the liver (Boyle 2013).

1.5.2 Overview of cellular composition of the liver.

There are many different types of cells in the liver with the major types being hepatocytes (60-80%), biliary epithelia, Kupffer cells (fixed macrophages) and oval cells (hepatocyte and cholangiocyte precursors). The remaining cells are endothelial cells, HSCs, lymphocytes, fibroblasts, smooth muscle cells, mesothelia, hematopoietic cells and blood cells. The hepatocytes are the major functional cells in the liver performing synthesis of protein, cholesterol, bile salts and phospholipids. They also store protein, transform carbohydrates, secrete bile and detoxify endogenous substances (Wallace et al., 2008).

The Kupffer cells are the largest group of fixed tissue macrophages (Bilzer et al., 2006; Pellicoro et al., 2014), which predominate in the uninjured liver and reside in the sinusoids. Kupffer cells are predominately located in the periportal area, to allow close contact with passing lymphocytes. This enables direct sampling of antigens in the blood coming from the gastrointestinal tract via the portal vein and ensuring early exposure to pathogenic bacteria, bacterial endotoxin and microbial debris (Bilzer et al., 2006; Pellicoro et al., 2014). Kupffer cells possesses major histocompatibility complex (MHC) antigens which allow them to recognise antigen and so are able to pass through the space of Disse to contact directly with hepatocytes. Kupffer cells like macrophages can phagocytose debris and microorganisms and clear endotoxin from the blood. They are capable of releasing cytokines such as Tumour necrosis factor-α (TNF-α), interleukin-1, -6 and -8 (IL-1, IL-6, IL-8), transforming growth factor-β (TGFβ) and interferons (Bilzer et al., 2006; Pellicoro et al., 2014). The population of Kupffer cells decreases during hepatic inflammation and fibrogenesis, which leads to increased recruitment of monocyte-derived macrophages. Once the inflammation and fibrosis resolves the Kupffer cells are gradually replenished (Ramachandran et al., 2012; Pellicoro et al., 2014). The actual mechanism of Kupffer cell depletion, through cell death or migration, and source of cell replenishment has not been established (Pellicoro et al., 2014). The pro-fibrogenic macrophages are therefore derived from the monocyte population and undergo a phenotypical switch induced by phagocytosis (Ramachandran et al., 2012). Kupffer cells play a crucial role in the early response to liver injury and then it is the monocyte-derived

macrophages, which then take over as the population switches and expands, as fibrosis progresses (Ramachandran et al., 2012; Pellicoro et al., 2014).

Liver sinusoidal endothelial cells (LSEC) make up 50% of non-parenchymal cells in the liver and constitute the sinusoid wall (Braet and Wisse, 2002). The liver sinusoids are regarded as unique capillaries because of the presence of open pores or fenestrae lacking a diaphragm and a basal lamina underneath the endothelium (Braet and Wisse, 2002). The LSECs have numerous bristle coated micropinocytotic vesicles and lysosome-like vacuoles in the cytoplasm, which indicates that these cells are capable of endocytosis (Braet and Wisse, 2002). The LSEC act as a 'selective sieve' for substances passing into and out of the space of Disse, where HSCs and hepatocytes can be found, and as a 'scavenger system' which cleans the blood of waste macromolecules from different tissues (Braet and Wisse, 2002).

Dendritic cells (DCs), are predominantly immature cells that capture and process antigen. These cells are derived from bone marrow and can also be found in the liver in the space of Disse. They reside around the central veins and portal tracts. The liver also contains lymphocytes and cholangiocytes, which are biliary epithelial cells which line the bile duct. All the cells have a potential role in the pathogenesis of liver fibrosis but one cell which is thought to be the predominant player is the HSC due to its role in matrix production (Friedman, 2008b).

1.5.3   5-HT and liver blood flow.

It has been known for many years that 5-HT regulates liver blood flow and plays a role in the regulation of portal blood flow. 5-HT was found to increase portal resistance in dogs (Richardson and Withrington, 1978) and rats (Cummings et al., 1993). The fact that the 5-HT$_2$ antagonists ketanserin and ritanserin have been demonstrated to cause significant reductions in the hepatic portal vein pressure have led to the proposition that they should be considered as a treatment of portal hypertension (Mastaï et al., 1989, 1990; Cummings et al., 1993). Studies investigating ketanserin as a clinical treatment for portal hypertension demonstrated a significant decrease in portal hypertension. However 50% of the patients developed significant side effects, such as reversible portosystemic encephalopathy (brain

dysfunction) (Vorobioff et al., 1989). There have also been studies investigating the effects of 5-HT on hepatic sinusoidal blood flow. The 5-HT$_2$ antagonist LY53857 caused inhibition of the 5-HT-induced reduction of blood flow at the inlet of the periportal and outlet of the centrivenous sinusoids. Thereby demonstrating the presence of 5-HT$_2$ receptors in the hepatic sinusoids (Cummings et al., 1993). The HSCs, which express 5-HT$_2$ receptors (Ruddell et al., 2006), reside within the sinusoids and they have been postulated to regulate sinusoidal blood flow when the cells are activated, due to their increased contractile phenotype. The HSC are not the only cell within the sinusoid which responds to 5-HT. Sinusoidal endothelial cells (SECs) have also been found to respond to 5-HT to contract the fenestrae (Brauneis et al., 1992; Gatmaitan et al., 1996). 5-HT therefore plays a role in the regulation of the hepatic blood flow through activation of individual cells within the liver and also through neuronal innervations of the liver during both normal liver function and during liver injury.

1.5.4 Evidence for involvement of 5-HT in fibrosis.

In the 1960's a link between fibrosis and 5-HT was first reported due to a condition called carcinoid syndrome, which is associated with tissue fibrosis (Oates et al., 1966). Carcinoid syndrome is caused by large amounts of 5-HT being secreted by neuroendocrine carcinoid tumours. This causes symptoms such as flushing of the skin or face, diarrhoea and heart palpitations. In addition it also causes tissue fibrosis, mainly in the heart valve, but also other organs such as lung and skin (Pavlovic et al., 1995). 5-HT was also implicated in cardiac and pulmonary fibrosis in patients taking methysergide as anti-migraine therapy (Graham, 1967). Ergotamine treatment for migraine has also been found to cause aortic and mitral valve disease (Hendrikx et al., 1996). Methysergide, a 5-HT antagonist, was found to cause retroperitoneal fibrosis due to formation of a metabolite methylergonovine, which is a 5-HT agonist (Reimund, 1987). Fenfluramine, was approved for the treatment of obesity in the US in 1973 but was withdrawn in 1997 due to the incidence of valvular heart disease (VHD) (Rothman and Baumann, 2009). Subsequent investigation determined that fenfluramine induced VHD due to its activation of 5-HT$_{2B}$ receptors by its metabolite, norfenfluramine. 3,4-

methylenedioxy-N-methylamphetamine (MDMA), a hallucinogen (Rothman et al., 2000) and dopamine agonists (pergolide and cabergoline), used to treat Parkinson's disease, which are structurally similar to 5-HT, have all been associated with the development of VHD and this involves activation of the 5-HT$_{2B}$ receptor (Waller et al., 2005). 5-HT$_{2B}$ receptors are present on human cardiac valves and are required for normal cardiac development (Roth, 2007). Valvulopathic drugs induce mitogenesis in human valvular interstitial cells via activation of 5-HT$_{2B}$ receptors and stimulation of the ERK pathway (Setola et al., 2003). Due to the association with 5-HT$_{2B}$ agonism and valvular disease, with drugs from diverse indications, this led to recommendation to drug companies and regulatory authorities ensure that candidate drugs, and their major metabolites, should be screened for 5-HT$_{2B}$ activity (Roth, 2007).

There is evidence that 5-HT can stimulate the proliferation and fibrogenic actions of lung fibroblasts (Welsh et al., 2004). 5-HT can stimulate sclerotic remodelling of the pulmonary vasculature and airways, which leads to increased pulmonary vascular resistance and lung fibrosis. The 5-HT receptor involved in this process remains to be determined (Almeida et al., 2011). 5-HT$_{2A}$ receptors were implicated due to the antagonist effect of ketanserin in treatment of pulmonary arterial hypertension (PAH) (Demoulin, 1981), but some more recent work has implicated contributions by the 5-HT$_{1B}$ and 5-HT$_{2B}$ receptors (Morecroft et al., 1999; Launay et al., 2002; Dumitrascu et al., 2011). In idiopathic pulmonary fibrosis (IPF) there is reported to be an up-regulation of both 5-HT$_{2A}$ and 5-HT$_{2B}$ receptors, with 5-HT$_{2A}$ localising to the fibroblasts and 5-HT$_{2B}$ localising mainly in the epithelium in lungs (Konigshoff et al., 2010). Terguride, a 5-HT$_{2A/2B}$ antagonist, was shown to inhibit TGFβ1 expression and reverse lung function in mice subjected to bleomycin induced fibrosis (Konigshoff et al., 2010). Another group (Fabre et al., 2008), using a similar bleomycin fibrosis model, demonstrated attenuation of the fibrosis by blockade of the 5-HT$_{2A}$ receptor with ketanserin, or the 5-HT$_{2B}$ receptor with SB215505.

Systemic sclerosis scleroderma (SSc), a rare autoimmune disease, is characterised by deposition of fibril-forming collagen in the skin, stomach, lungs, heart, and kidneys. Many SSc patients have vascular disease and Raynauds syndrome. Dermal

fibroblasts have been shown to express 5-HT$_{1B}$, 5-HT$_{2A}$ and 5-HT$_{2B}$ (Slominski et al., 2003; Dees et al., 2011). In addition 5-HT$_{2B}$ levels are up-regulated in SSc fibroblasts (Dees et al., 2011). 5-HT involvement in the disease is unclear but there is some recent evidence for a causative role of platelet-derived 5-HT (Dees et al., 2011). 5-HT stored in platelets was found to induce ECM synthesis in interstitial fibroblasts through activation of the 5-HT$_{2B}$ receptor in a TGFβ dependent manner. Dermal fibrosis was also reduced in 5-HT$_{2B}$-deficient mice using both inducible and genetic models of fibrosis (Dees et al., 2011). SB204741, a 5-HT$_{2B}$ receptor antagonist prevented the onset of fibrosis and reduced established fibrosis. 5-HT$_{2B}$ receptors were found to be up regulated in fibrotic tissue when compared to healthy controls. This study suggests a link between vascular damage, platelet activation and tissue remodelling with 5-HT$_{2B}$ receptor as a novel target to treat fibrotic disease (Dees et al., 2011).

1.6 Role of 5-HT in liver regeneration and hepatic fibrosis.

1.6.1 5-HT and liver regeneration.

The adult liver is a regenerative organ that is capable of efficiently restoring liver mass as well as rebuilding its complex structure required for normal liver function. Experiments using rodent models of liver regeneration have pointed to 5-HT having an autocrine and paracrine hepatic signalling role, which helps to regulate growth and regeneration of parenchymal liver cells. There seems to be evidence of an inverse relationship between the 5-HT driven epithelial growth mechanisms and 5-HT signalling pathways that act on myofibroblasts to stimulate fibrosis (Lesurtel et al., 2012; Mann and Oakley, 2013).

Intestinal 5-HT has been found to be quickly mobilised and accumulate in liver remnants following seventy percent hepatectomy (PHx) in mice. Initial studies demonstrated that 5-HT could enhance hepatocyte proliferation (Lesurtel, 2006). If platelets were depleted or if a platelet inhibitor (clopidogrel) was used liver regeneration was markedly reduced in mice (Lesurtel, 2006). Clinical study results demonstrate that platelets are critical for liver regeneration, as low platelet count was associated with delayed liver regeneration (Alkozai et al., 2010), and after liver

donation a platelet transfusion was associated with liver regeneration (Kim et al., 2010).

Platelets were identified as the primary source of 5-HT, with 5-HT$_{2A}$ playing a major role in hepatocyte regeneration (Lesurtel, 2006). Expression of 5-HT$_{2A}$ and 5-HT$_{2B}$ receptors in the liver increased after hepatectomy, with antagonists of these receptors, ketanserin and SB 206553 respectively, inhibiting liver regeneration in mice studies (Lesurtel et al., 2006). In thrombocytopenic mice 5-HT agonism restored hepatic proliferation and peripheral 5-HT deficient knock-out mice demonstrated impaired liver regeneration after partial hepatectomy (Lesurtel et al., 2012). Further studies have confirmed a pro-inflammatory and pro-regenerative role of 5-HT in post ischemic liver (Nocito et al., 2007). 5-HT$_{2B}$ agonism of the receptor was found to improve animal survival in small liver graft transplantation (Tian et al., 2011).

Elderly mice (2 year old), when compared with young mice (7-8 week), have been found to have impaired capacity to initiate liver regeneration, which is similar to that observed in humans (Clavien et al., 2007; Furrer et al., 2011). 5-HT$_{2B}$ agonism improved liver regeneration along with sinusoidal perfusion. Similar effects have been observed in humans (Clavien et al., 2007). Ultra-structural changes of hepatic sinusoids occur with ageing in a process called pseudocapillarisation, which includes the defenestration (reduction of porosity) and thickening of the sinusoidal endothelium (Furrer et al., 2011). 5-HT agonism has an immediate impact on the fenestration pattern of old liver (Furrer et al., 2011). 5-HT agonism allowed the re-attachment of platelets to sinusoids, a process that is required after hepatectomy, but is absent in pseudocapillarised liver (Furrer et al., 2011). These findings suggest that close communication is required between blood factors, platelets and hepatocytes through sinusoidal fenestrae to ensure initiation of liver regeneration, with 5-HT playing a role in this (Lesurtel et al., 2012). Another group, using SERT deficient mice, which lack platelet derived 5-HT, failed to show a role for this source of 5-HT in liver regeneration (Matondo et al., 2009).

Biliary remodelling that occurs in adults in response to obstruction involves paracrine crosstalk between cholangiocytes (epithelial cells of the bile duct) and

stromal cells, particularly myofibroblasts (Omenetti et al., 2011). 5-HT inhibits proliferation of cholangiocytes (Omenetti et al., 2011). It has been demonstrated that cholangiocytes are able to synthesise 5-HT and that autocrine/paracrine mechanisms that suppress biliary 5-HT production stimulate proliferation of ductular cells, liver myofibroblasts, and progenitors (Omenetti et al., 2011). $5-HT_{1A}$ and $5-HT_{1B}$ receptors has been shown to be expressed on cholangiocytes in the liver (Marzioni et al., 2005). Administration of the selective $5-HT_{1A}$ agonist 8-hydroxy N,N-dipropylaminotetralin (8-OH-DPAT) and the $5-HT_{1B}$ agonist anpirtoline to BDL rats for 1 week was shown to inhibit cholangiocyte proliferation (Marzioni et al., 2005). It has been demonstrated that activation of the $5-HT_{1A}$ and $5-HT_{1B}$ receptors is responsible for the enhanced intracellular IP_3 signalling and the consequent inhibition of the cAMP/PKA/Src/ERK1/2 pathway (Marzioni et al., 2005). This therefore means that liver-cell 5-HT functions as one of the 'brakes' that restrains the outgrowth of cholangiocytes through a negative feedback mechanism (Omenetti et al., 2011) and that the $5-HT_{1A}$ and $5-HT_{1B}$ receptor are likely to be responsible (Marzioni et al., 2005).

1.6.2   Role of 5-HT in hepatic fibrosis.

Hepatic stellate cells play a key role in hepatic wound healing and fibrosis. Quiescent rat and human HSCs have been shown to express $5-HT_{1B}$, $5-HT_{1F}$, $5-HT_{2A}$, $5-HT_{2B}$, and $5-HT_7$ receptors. Indeed, expression of $5-HT_{1B}$ $5-HT_{2A}$ and $5-HT_{2B}$ are induced once the cells are activated (Ruddell et al.,2006). This has been confirmed in rat HSCs by other groups (Li et al., 2006; Park et al., 2011). HSCs have also been found to express the SERT (Ruddell et al., 2006). $5-HT_2$ receptors couple to $G_{q/11}$ family G-proteins and therefore 5-HT stimulation will elicit an increase in intracellular calcium (Raymond et al., 2001). 5-HT stimulated a concentration-dependent increase in intracellular calcium in activated rat HSCs but not in quiescent HSCs (Park et al., 2011). Expression of L-type calcium channel and α-SMA were found to be proportional to the level of activation of the rat HSC, as was the up-regulation of the TGFβ1 receptor (Park et al., 2011). The ability of 5-HT to stimulate release of intracellular calcium in rat HSCs correlating with the increase in $5-HT_{2A}$ and $5-HT_{2B}$ receptor expression and HSC activation (Park et al., 2011). In addition, ritanserin, a

non-selective 5-HT$_2$ antagonist, was shown to attenuate the 5-HT stimulated calcium release (Park et al., 2011).

Further *in vitro* studies have implicated 5-HT$_{2B}$ as the predominant receptor in HSC function (Ebrahimkhani et al., 2011). In these studies 5-HT was shown to activate the mitogen-activated protein kinase 1 (ERK) and transcription factor JunD to mediate stimulation of TGFβ1 transcription in activated HSCs. These workers demonstrated inhibition of ERK phosphorylation following incubation with PD98059, an MEK inhibitor, and a 5-HT$_{2B}$ antagonist, SB 204741, in mouse, rat and human HSCs (Ebrahimkhani et al., 2011). However the concentration at which SB 204741 inhibited pERK levels was $\geq$ 10 μM, which would not selectively inhibit the 5-HT$_{2B}$ receptor. However, 5-HT-induced expression of TGFβ1 and SMAD4 was inhibited by ketanserin, a 5-HT$_{2A}$ antagonist, in rat HSCs (Li et al., 2006). Also using LX-2 cells, an immortalised human HSC line (Xu et al., 2005; Cao et al., 2006), an increased expression of 5-HT$_{2A}$ upon activation was demonstrated (Kim et al., 2013). Sarpogrelate and ketanserin (5-HT$_{2A}$ antagonists) were also shown to inhibit viability, apoptosis and wound healing in LX-2 cells (Kim et al., 2013). Rat HSCs proliferation studies reported that a number of 5-HT$_2$ antagonists, some not selective for a specific 5-HT subtype, suppressed the proliferation and increase the rate of apoptosis of activated HSCs (Ruddell et al., 2006).

Kidney glomerular mesangial cells, like HSCs in the liver, can be activated to become proliferative and deposit ECM in the renal glomerulus (Grewal et al., 1999). It was demonstrated that 5-HT is able induce expression of TGFβ1 in a concentration and time-dependent manner in rat mesangial cells, and that this effect is via the ERK pathway, with mapping studies implicating the 5-HT$_{2A}$ receptor being responsible (Grewal et al., 1999). Connective tissue growth factor (CTGF) expression was also induced in rat mesangial cells by 5-HT, which was inhibited by ketanserin (Hahn et al., 2000). Increased type IV collagen stimulated by 5-HT was found to be antagonised by both sarpogrelate and ketanserin in a concentration-related manner in human mesangial cells (Kasho et al., 1998). The effects of 5-HT observed in mesangial cells in the kidney seem similar to those observed in the liver with HSCs.

In vivo studies in rats and mice again have provided conflicting results as to the actual 5-HT$_2$ receptor subtype involved. In a mouse CCl$_4$ model of liver injury study, SB 204741, a 5-HT$_{2B}$ antagonist, was demonstrated to reduce fibrosis and hepatic α-SMA positive fibrogenic cells together with a reduction in TGFβ1 levels, TIMP 1 and collagen 1 expression (Ebrahimkhani et al., 2011). SB 204741, which was dosed in a BDL-induced liver fibrosis model was also shown to improve liver function and reduce concentrations of serum transaminases, ALT and AST (Ebrahimkhani et al., 2011). However in sarpogrelate, a 5-HT$_{2A}$ antagonist, was shown to reduce TAA induced liver inflammation but did not significantly attenuate periportal fibrosis in rats (Kim et al., 2013).

Evidence to date implicates 5-HT as a key player in liver fibrosis with the 5-HT$_2$ the predominant receptor. However, the subtype of 5-HT$_2$ receptor involved still remains to be confirmed and may depend on the individual cell type being investigated. 5-HT receptors of numerous classes are present throughout the liver, with expression by vascular endothelium, HSCs, hepatocytes, Kupffer cells and cholangiocytes (Ruddell et al., 2008; Ebrahimkhani et al., 2011). The 5-HT$_{2A}$ receptor is abundant on platelets and promotes their aggregation and activation, which leads to the activated platelets releasing their stored serotonin, creating a positive feedback loop (Przyklenk et al., 2010; Watts et al., 2012). Therefore a 5-HT$_{2A}$ antagonist might provide the added benefit of preventing 5-HT release from platelets, which is important in the development of fibrosis (Ruddell et al., 2008; Dees et al., 2011). The interplay between the different cells and possible different 5-HT receptor subtypes may suggest that when the liver is taken as a whole, the effect of a compound may not be as expected. For instance some mechanisms may dominate more than others. 5-HT stimulation of the 5-HT$_{2A}$ receptor has been shown to have a role in the development of portal hypertension by increasing resistance in the intrahepatic vasculature and in the portal vein itself (Kaumann and Levy, 2006; Watts et al., 2012). Therefore a 5-HT$_{2A}$ antagonist may alleviate or protect against the development of portal hypertension but may also have unwanted side effects.

1.7   Overview of the pathogenesis of hepatic fibrosis.

Hepatic fibrosis starts with an initial injury and subsequent wound-healing response to the injury, which is similar to other organs' response. If this injury persists then fibrosis occurs leading progressively towards but not always cirrhosis. Chronic liver injury can result from a number of different sources including viral infections (e.g. hepatitis B and C), obesity, alcohol, drug-induced toxicity, liver infections, immune liver disease, metabolic disorders and cholestasis (Figure 1.71) (Bataller and Brenner, 2005). 75% of the blood supply to the liver via the portal vein, which comes directly from the gastrointestinal viscera and spleen. The blood is rich in toxins, such as endotoxin, xenobiotics and alcohol, and has low oxygen tension, making the liver vulnerable to hypoxia and ischemia. The structure of the liver sinusoids, with the fenestrated endothelium, allows the blood to interact with many of the different cells of the liver including the hepatocytes. For most hepatoxic agents such as alcohol metabolites, hepatitis viruses and bile acids, hepatocytes are the main target (Higuchi and Gores, 2003). The liver, due to its function to metabolise and biotransform chemicals, is also at risk from free radical damage. Thus, if its function is compromised then this will also lead to liver injury (Higuchi and Gores, 2003). It is cell death and inflammation which are the major initiators of most liver disease (Higuchi and Gores, 2003; Bataller and Brenner, 2005). Injury to the liver will typically induce necrosis of hepatocytes and apoptosis which then leads on to a complex interplay between all the different hepatic cell types. The damaged hepatocytes undergo genomic DNA fragmentation to form apoptotic bodies and release reactive oxygen species (ROS). Hepatocytes also release cytokines, such as TNFα, TGFβ1, vascular endothelial growth factor (VEGF), insulin-like growth factor (IGF-1), release lipid peroxidation products and chemokines. Together these stimulate the activation of endothelial cells, HSC and Kupffer cells (Bataller and Brenner, 2005; Kisseleva and Brenner, 2007).

The Kupffer cell, which has a major role in liver inflammation, engulf the apoptotic bodies leading to enhanced expression of pro-fibrotic genes and Fas ligand (death ligand) (Canbay et al., 2003). Thus, Kupffer cells are a major player in liver inflammation. The clearing of apoptotic bodies is required to protect tissues from
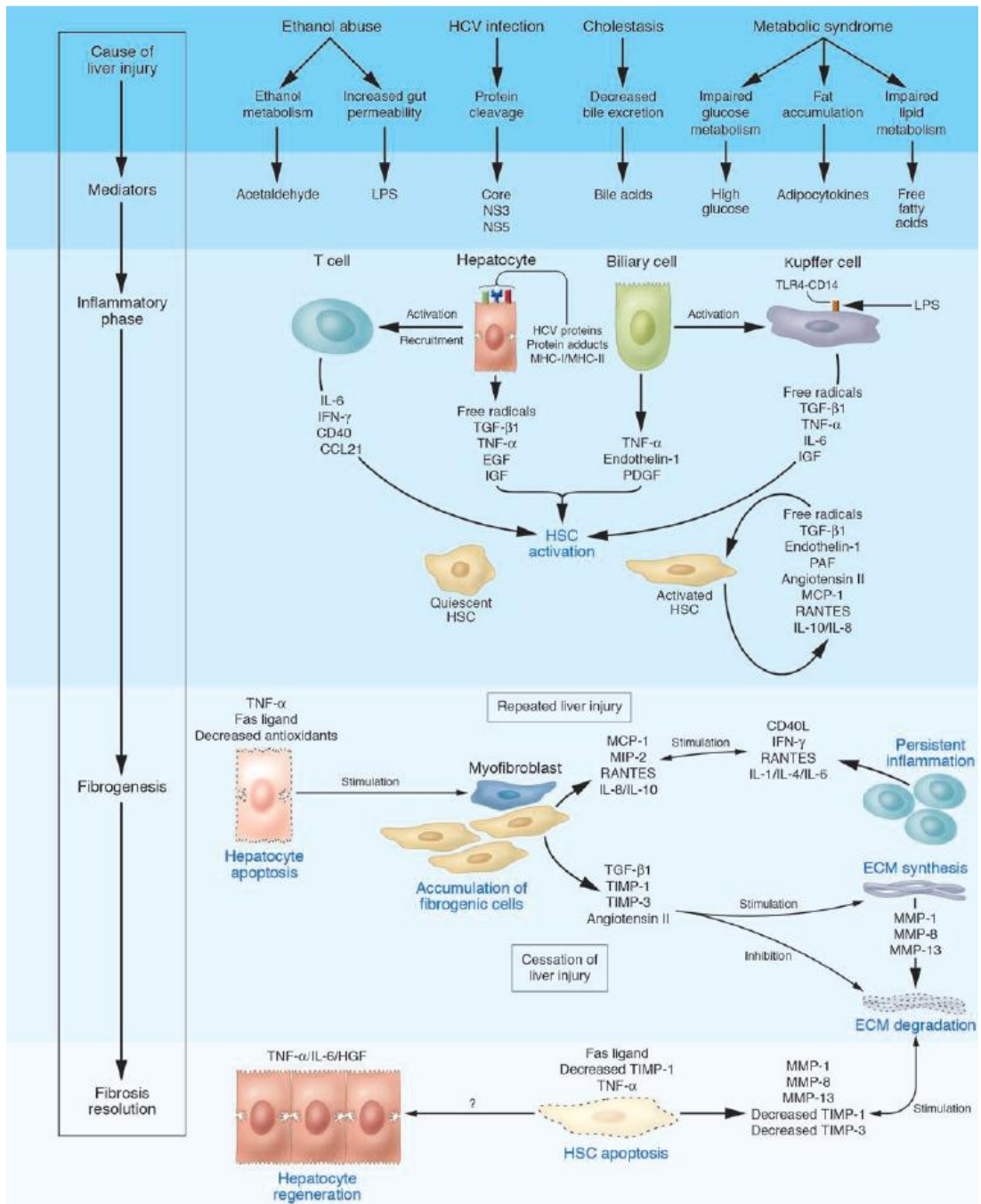
Figure 1.7.1 Illustration of the cellular mechanism of fibrosis. Many different types of agents are able to damage the liver to induce inflammation of the hepatic cell types. Damaged hepatocytes and biliary cells release inflammatory cytokines and soluble factors, which cause activation of the Kupffer cells and stimulate T-cells. The inflammatory milieu that stimulates activation of the HSC into a myofibroblast-like cell. The activated HSC secretes cytokines, which perpetuates their activated state. If the liver injury persists then accumulation of the HSCs and portal myofibroblasts occurs, synthesising large amounts of cytokines such as TIMP's. Apoptosis of damaged hepatocytes stimulates the fibrogenic actions of the HSC. If the liver injury is removed, fibrosis resolves due to apoptosis of the HSC and regeneration of hepatocytes. The remaining collagen is degraded by increased activity of the MMP's induced by decreased TIMP expression. (Taken from Bataller and Brenner, 2005).

28

their inflammatory contents. The Kupffer cells then independently initiate intracellular signalling which leads to further amplification of liver injury by release of free radicals and many cytokines (See section 1.5.2). The HSC, due its close proximity to the hepatocytes in the space of Disse, can also phagocytose the hepatocyte apoptotic bodies. This helps to activate the phenotypic change in HSCs, driving TGFβ1 expression, macrophage inflammatory protein-2 (MIP-2) expression and induction of collagen, which exacerbates hepatocyte damage (Kisseleva and Brenner, 2007). Activated HSCs (aHSCs) have also been implicated in antigen presentation and phagocytosis-dependent antigen trafficking (Viñas et al., 2003). In severe cases of liver toxicity, oxidative stress products and ROS are able to reach critical concentrations to induce fibrosis, without any significant hepatocyte damage and inflammation (Kisseleva and Brenner, 2007).

A major cytokine which plays a critical role in fibrosis progression is TGFβ. This is released by hepatocytes, Kupffer cells, LSECs and HSCs (Dooley and ten Dijke, 2012). TGFβ triggers the apoptosis of hepatocytes, activates and recruits inflammatory cells and stimulates hepatic stellate cells to transform into a myofibroblast phenotype that produces collagen. Activated HSC are myofibroblast–like cells which produce collagen types I, III and IV, proteoglycans, laminin and fibronectin and secrete TGFβ1 (Breitkopf et al., 2005). This change in the ECM composition further stimulates fibrosis and HSC activation, thus maintaining the elevated TGβ1 level (Bataller and Brenner, 2005). There are other myofibroblast-like cells that are resident in the liver, such as portal myofibroblasts. These cells are also activated by TGFβ1 and they help to further recruit circulating myofibroblasts to the injured liver (Bataller and Brenner, 2005).

Another factor, platelet derived growth factor (PDGF), is considered to be a key fibrogenic and proliferative stimulus of HSCs. High concentrations of PDGF are released by platelets and macrophages during tissue repair and inflammatory processes. There are other mitogens which play a role in the proliferation of stellate cells such as VEGF, endothelial growth factor (EGF), transforming growth factor α (TFGα), thrombin and insulin (Friedman 2008a). There is also evidence that CTGF is an important fibrogenic mediator which is downstream of TGFβ1 (Jiao et al., 2009).

After acute liver injury the damaged parenchymal cells regenerate to replace the necrotic and apoptotic cells. Persistent injury is associated with major alterations of the quantity and composition of ECM. The site of the ECM deposition in the liver is dependent on the origin of the injury. Fibrosis around the portal tracts is associated with chronic viral hepatitis and cholestatic disorders. In contrast fibrosis induced by alcohol tends to be localised in the pericentral and perisinusoidal area (Pinzani and Gentilini, 1999).

The composition and deposition of ECM alters during the progression of fibrosis. A liver in the advanced stages of fibrosis can contain 6 times more ECM than normal liver (Bataller and Brenner, 2005). The accumulation of ECM, which contains collagens (I, III and VI), fibronectin, undulin, elastin, laminin, hyaluronan and proteoglycans is due to both the synthesis and decreased degradation of matrix proteins (Arthur, 2000). The reduced matrix degradation is due to inhibition of matrix-metalloproteinases (MMP-1, -8 and -13) (Arthur, 2000), which are regulated by tissue inhibitors of metalloproteinases (TIMPs). Activated HSCs express TIMPs with TIMP-1 as the major TIMP secreted. TIMP inhibits MMPs, thus preventing matrix degradation (Iredale et al., 2013), which favours scar deposition. TIMP-1 has also been found to be anti-apoptotic towards stellate cells (Murphy et al., 2002), which ensures their persistence.

If the liver injury is removed, then resolution of the liver occurs and there is evidence to support this occurrence even after advanced fibrosis (Arthur, 2002). The time it takes to resolve is dependent on the type of injury and severity (Arthur, 2000). Increased MMP activity along with a decreased expression of TIMP's allows the degradation of the fibrillar collagen, which in turn causes apoptosis of the HSC through stimulation of death receptors (Arthur, 2000; Bataller and Brenner, 2005).

1.8   Hepatic stellate cell biology and role in fibrosis.

The hepatic stellate cell was first described by Carl von Kupffer in 1876 (Friedman, 2008b). In the beginning of the 20th century other investigators reported a macrophage-like cell that contained vitamin A. However it was not until the early 1970's that these cells were found to be different from the macrophages, and linked

with the pathogenesis of hepatic fibrosis (Wake, 1971; McGee and Patrick, 1972). Development of methods to isolate these cells in animal and human species has initiated substantial research into stellate cells (De Leeuw et al., 1984; Friedman et al., 1992). One of the earliest findings was that these cells, when cultured on plastic, proliferate and differentiate in a similar way to that had been observed in the injured liver (Friedman et al., 1992). Since then a wealth of information has been discovered about these cells and their role in fibrosis. HSCs are widely recognised as one of the key mediators in hepatic fibrosis (Friedman, 2000).

In healthy liver, HSCs are spindle shaped cells that lie in the recesses between neighbouring cells in the sub-endothelial space, known as the space of Disse. The stellate cells act as the principle storage site for retinoids (vitamin A metabolites) (Rockey, 2006). They represent 5-8% of the cells in the normal liver (Blouin et al., 1977). HSCs possess long cytoplasmic branches which allow connection with the endothelial cells and hepatocytes in the space of Disse (Friedman, 2008b). It is this contact between the cells that facilitates intercellular transport of soluble mediators and cytokines. The HSCs lie in a circumferential fashion around the sinusoidal endothelial cells with the cytoplasmic processes extending along the sinusoid (Rockey, 2001b). This anatomical feature of the HSCs is very similar to the smooth muscle-like pericytes in tissue capillaries which regulate blood flow (Sims, 1991; Soon and Yee, 2008). HSCs have been found to be adjacent to nerve endings (Ueno et al., 1997) and so can be influenced by neurotransmitters through the expression of appropriate receptors on their surface. The position of the HSCs indicates a role of HSCs in the regulation of sinusoidal blood flow (Nakatani et al., 1996; Rockey and Weisiger, 1996) which is considered to be a key function. HSCs have also been found to be influenced by growth factors, such as PDGF, whose receptor expression has been found to be enhanced by liver injury and activation of the cells (Cassiman et al., 2001; Borkham-Kamphorst et al., 2004). The average lifespan of the stellate cell is still unknown and they are considered to be long-lived cells, as proliferation is rare (Geerts, 2001). The discovery in the 1980s that the activation of HSCs, through liver injury, was key in the deposition of ECM in both normal and fibrotic liver drove an increased interest in the role of HSCs in liver fibrosis. Many scientists reported the close proximity of the HSC to the collagen fibres in the injured liver (McGee and

Patrick, 1972; Okanoue et al., 1983; Kent et al., 1984; Martinez-Hernandez, 1984). This led to development of the methods to isolate the cells from rats (Knook et al., 1982; Friedman and Roll, 1987), mice (Chen et al., 1989) and humans (Friedman et al., 1992).

1.8.1 Activation of hepatic stellate cells.

The activation of the stellate cells marks their transformation in both function and phenotype to a myofibroblast–like cell (Friedman, 2000; Bataller and Brenner, 2005). This process consists of two major stages. These are: initiation and perpetuation (Friedman, 2004). A third stage known as the resolution phase can follow where the liver injury is healed (Figure 1.8.1). The initiation stage, which is also referred to as the pre-inflammatory stage, is due to paracrine stimulation from all the neighbouring cells such as hepatocytes, sinusoidal endothelial cells and platelets. As already described (Section 1.7), once the liver is injured cellular apoptosis is the first response to the toxic event (Canbay et al., 2004). Hepatocyte necrosis and apoptosis causes release of apoptotic bodies, ROS and lipid peroxidation products. The hepatocyte apoptosis promotes HSC initiation by a process mediated through death receptors such as the Fas ligand (a type II transmembrane protein belonging to the tumour necrosis (TNF) family) and tumour necrosis factor-related apoptosis-inducing ligand (TRAIL) (Canbay et al., 2004). The clearance of the apoptotic bodies through phagocytosis directly simulates fibrosis. Kupffer cell infiltration and activation occurs, which contributes to the activation of the stellate cell. It should also be pointed out that HSCs are capable of phagocytosing the apoptotic bodies themselves due to their close proximity to the hepatocytes (Canbay et al., 2004; Kisseleva and Brenner, 2007), which stimulates further activation. The Kupffer cells stimulate release of cytokines (especially TGFβ1), matrix synthesis and promote cell proliferation (Canbay et al., 2003; Bilzer et al., 2006). Endothelial cells also contribute to the activation of the HSCs by converting the TGFβ from the latent form to the profibrogenic active form, along with a cellular isoform of fibronectin (Jarnagin et al., 1994). In addition, the platelets provide paracrine stimulation of HSCs through release of PDGF, TGFβ and EGF (Bachem et al., 1989).
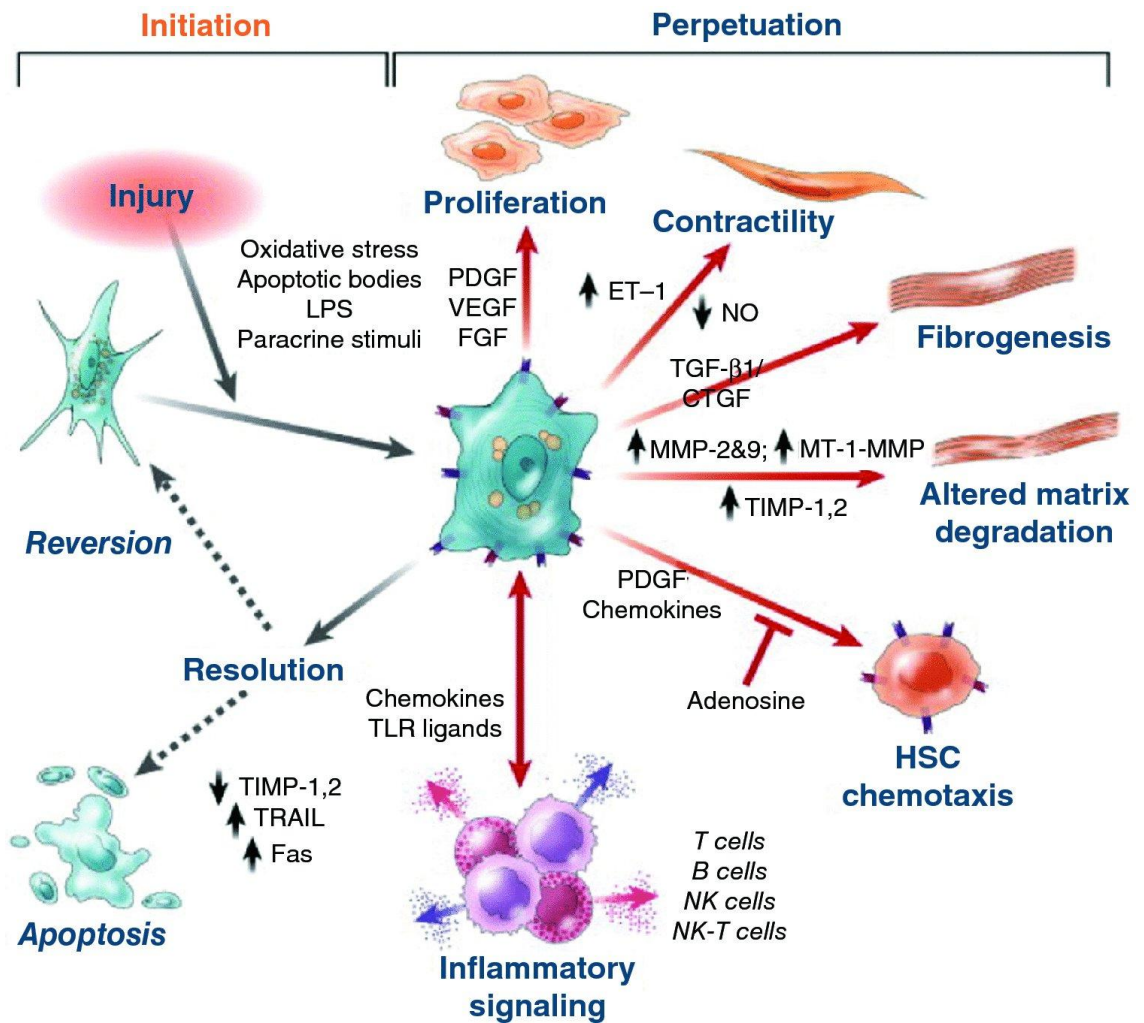
Figure 1.8.1   Hepatic stellate cells initiation, perpetuation and resolution following liver injury. During liver injury initiation of HSC activation is provoked by soluble stimuli that include oxidative stress signals, apoptotic bodies, lipopolysaccharide and paracrine stimulus from neighbouring cell types, such as Kupffer cells, sinusoidal endothelium and hepatocytes. Perpetuation follow, which is characterised by specific phenotypic changes including proliferation, contractility, fibrogenesis, altered matrix degradation, chemotaxis and inflammatory signalling. During resolution of fibrosis there is apoptosis of the fibrogenic cells along with reversion to a more quiescent phenotype (Taken from Puche et al., 2013).

1.8.2 Perpetuation of stellate cell activation.

Perpetuation of the stellate cell activation involves a number of discrete changes in function and phenotype. These are expression of α-smooth muscle-actin (α-SMA), increased production of collagen, expression of TIMP-1, loss of its retinoid storage capability, proliferation, chemotaxis, and increased contractility (Friedman, 2008) (Figure 1.8.1). The activated HSC becomes resistant to apoptosis, due to inhibition of MMPs by the increased expression of TIMP-1 (Murphy et al., 2002) and high basal nuclear factor-κB activity (Oakley et al., 2005). In the chronically injured liver, HSCs persist and produce excess deposition of collagen. This alters the constituents of the hepatic ECM, such that the liver becomes fibrotic. If ECM remodelling is allowed to continue unchecked this ultimately leads to cirrhosis of the liver (Benyon and Arthur, 2001).

1.8.2.1 Proliferation of hepatic stellate cells.

The activated HSCs change to a proliferative phenotype and become more responsive to PDGF, the most potent mitogen (Pinzani, 2002). This is due to the up-regulation of the PDGF receptor (Wong et al., 1994). PDGF exists as a dimer of two polypeptide chains, A and B chain, with three possible combinations, AA, BB, and AB. The BB dimer is the most potent at stimulating HSCs (Pinzani, 2002). The PDGF receptor comprises of an α and β subunit, which dimerises following PDGF binding. The A-chain of PDGF binds to α-receptors, whereas the B-chain of PDGF can bind to both to α- and β-receptors with high affinity (Heldin and Westermark, 1999). The PDGF cell surface receptor, which has intrinsic tyrosine kinase activity, becomes autophosphorylated on the tyrosine ligands when PDGF binds (Heldin and Westermark, 1999). This then leads to the formation of high affinity binding sites for signalling proteins with src-homology-2 (SH-2) domains or phosphotyrosine binding (PTB) domains (Pinzani, 2002). The PDGF receptor then associates with the adapter protein Grb2 which causes recruitment of the exchange factor mSos leading to recruitment and sequential activation of Ras, Raf-1, MEK and ERK, followed by ERK translocation to the nucleus. Translocation to the nucleus is associated with phosphorylation of transcription factors such as Elk-1 and SAP, and it is these that are required for proliferation (Pagès et al., 1993). Thus inhibition of this pathway

upstream of ERK causes a concentration-dependent inhibition of proliferation (Marra et al., 1999a). Pentoxifylline, a phosphodiesterase inhibitor, which causes increased levels of cAMP was found to induce a reduction in the PDGF-stimulated ERK phosphorylation (Pinzani et al., 1996). Increased levels of cAMP inhibits PDGF growth by protein kinase A (PKA) catalysed phosphorylation of Raf kinase, which is upstream of ERK (Graves et al., 1993; Wu et al., 1993) and by inhibition of STAT1 (Kawada et al., 1997).

Phosphatidylinositol 3-kinase (PI3K) activation by the PDGF receptor is required for proliferation and chemotaxis in human HSCs (Marra et al., 1997; Pinzani, 2002). PI3K activation is able to mediate the PDGF stimulated proliferation through both a Ras-ERK pathway and ERK-independent pathways. Thus, PI3K inhibitors, such as LY294002 and Wortmanin, are only able to inhibit ERK activation by at most 50% (Marra et al., 1995; Gentilini et al., 2000; Pinzani, 2002). It should also be noted as previously stated that other mitogens such as VEGF, EGF, TFGα, thrombin and insulin have been found to have a potential role in liver fibrosis (Friedman, 2008a).

1.8.2.2 Hepatic stellate cell chemotaxis.

The accumulation of activated HSCs at sites of injury and alignment within inflammatory septae *in vivo* is caused by chemotaxis (Pinzani and Marra, 2001b; Hasegaea et al., 2015). Monocyte chemoattractant protein-1 (MCP-1) has been found to induce concentration-dependent chemotaxis of HSCs, but not via activation of its CCR2 receptor (Marra et al., 1999b). Instead, this might possibly occur via CCR11 or due to a direct profibrotic action on the HSC (Pinzani and Marra, 2001b). It is possible that MCP-1 (Marra et al., 1999b), like PDGF (Ikeda et al., 1999), VEGF (Novo et al., 2007), EGF (Yang et al., 2003) and CXCL10 (Bonacchi et al., 2001) are all chemoattractants for the stellate cells. These mediators might act via activation of the Ras/ERK or PI3K/AKT pathways to induce migration (Marra et al., 1999a; Novo et al., 2011). Chemotaxis has been observed in the absence of any exogenous applied chemoattractants and this has been found to be caused by ROS generated from hepatocytes or via local tissue hypoxia (Novo et al., 2011). HSCs respond to changes in the local ECM, as the fibrosis continues, such that they may even migrate towards

collagen type 1 and MMP-1. These potentially may act in a feedback loop to further amplify the fibrotic response (Yang et al, 2003).

1.8.2.3 Contractility of hepatic stellate cells.

HSCs are reported to be contractile and this may affect the portal resistance observed during liver fibrosis. The large numbers of HSCs that are found in the end-stage fibrotic collagenous bands cause constriction of the individual sinusoids, which constricts the liver causing portal hypertension. (Rockey, 2001a, 2001b). In primary HSC culture, it has been shown that stellate cells acquire the ability to contract when they become activated. This is mediated by receptors that interact with the ECM (Melton et al., 2006). Although Endothelin-1 (ET-1) and nitric oxide are considered to be the key players in stellate cell contractility there are other agents such as angiotensins, eicosanoids and somatostatin that have been implicated (Rockey, 2003). HSC expression of the cytoskeletal protein α-SMA increases upon activation, and this correlates with the increased expression of L-type voltage-operated calcium channels (Bataller et al., 1998, 2001; Park et al., 2011). HSCs upon activation have the ability to release calcium following stimulation with arginine, vasopressin (Bataller et al., 1997) and endothelin (Goto et al., 1989). This leads to an increased contractile potential of the stellate cell (Reynaert, 2002; Rombouts et al., 2002). Contraction of HSCs generates sufficient force to contract the sinusoids (Thimgan and Yee, 1999). There are also reports that the HSC contractile response can be driven by a calcium-independent mechanism (Melton et al., 2006). The new scheme for the regulation of contractile force generation by rat hepatic stellate was proposed where ET-1 stimulates contraction via a pathway signalling through Rho-associated kinase rather than calcium (Melton et al., 2006). This proposal will have implications for our understanding of sinusoidal blood flow and hepatic fibrosis (Melton et al., 2006).

1.8.2.4 Fibrogenesis.

One of the key characteristics of HSCs is their fibrogenic potential driven by increased cell numbers, due to both proliferation, resistance to apoptosis and increased ECM production (Forbes and Parola, 2011). During hepatic fibrosis, TGFβ

has an important role in initiation, promotion and progression of transdifferentiation of the HSC into a myofibroblast (Gressner et al., 2007). TGFβ1 is the most potent stimulus for ECM synthesis in HSCs and this is derived from both a paracrine and autocrine source (Inagaki and Okazaki, 2007). TGFβ1 stimulates the production of other ECM components, such as collagen 1, fibronectin and proteoglycans (George et al., 1999), as well as α-SMA organisation and stress-fibre formation (Dooley et al., 2003; Uemura et al., 2005). Increased TGFβ activity during fibrogenesis is observed along with increased production and deposition of collagen from HSCs, leading to increased scarring and eventual loss of liver function (Gressner et al., 2007).

TGFβ is a multifunctional cytokine that regulates a large array of cellular responses. It exists in three isoforms (TGFβ1, TGFβ2 and TGFβ3), which all function through the same signalling pathways (Inagaki and Okazaki, 2007; Kubiczkova et al., 2012). Three types of TGFβ receptors are present in most cells. These are: type I (TβRI) Activin Like Kinase 5 (ALK5), type II (TβRII) receptors and type III (TβRIII) (Kubiczkova et al., 2012). TGFβ signalling is mediated through interactions between TβRI and TβRII receptors (Dooley et al., 2000). These receptors exist as independent homodimers in the absence of ligand (Massagué, 1996). TβRII is activated by the binding of TGFβ which recruits the TβRI receptor through transphosphorylation of the glycine serine rich (GS) domain (Massagué, 1998). This forms a heteromeric complex of TβRI and TβRII which leads to activated TGFβ receptor kinase activity and subsequent downstream signalling (Verrecchia and Mauviel, 2007). TβRI initiates the intracellular signalling cascade by phosphorylating intracellular proteins known as SMA and MAD proteins (SMADS) (Figure 1.8.2). There are three classes of SMADs: receptor activated SMADs (R-SMAD), common-mediator SMADs (Co-SMAD) and the inhibitory SMADs (I- SMAD). The R- SMADs, SMAD2 and 3, are restricted to the TGFβ pathway (Tsukazaki et al., 1998). Upon activation, SMAD2 and 3 are presented to the TGFβ receptor complex via the SMAD anchor for receptor activation (SARA) (Tsukazaki et al., 1998). Once phosphorylated by the TGFβR, the R-SMADs form heteromeric complexes with SMAD4 (a Co-SMAD) and translocate from the cytoplasm to the nucleus (Verrecchia and Mauviel, 2007). Within the nucleus, the SMADs bind directly to transcription factors to induce transcription of collagen type I and III (Inagaki and Okazaki, 2007) (Figure 1.8.2).
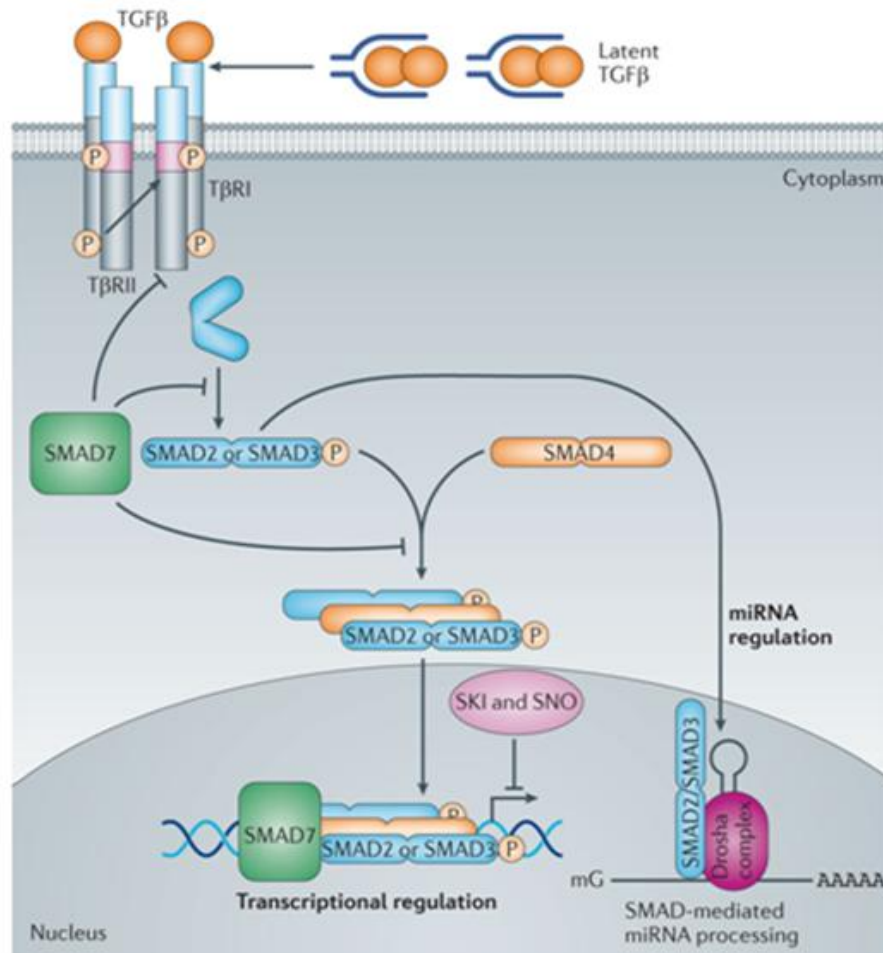
Figure 1.8.2   Schematic diagram of the canonical TGFβ-SMAD signalling pathway.
Free TGFβ can bind to the transmembrane TGFβ receptor II (TβRII). This then results in the recruitment of and hetrodimerisation with the TGFβ receptor type I (TβRI). This heterodimerisation initiates signalling through transphosphorylation of TβRI by the TβRII which is transmitted into the cell via phosphorylation of the TGFβ receptor-specific SMADs (R-SMADs: SMAD2 and SMAD3). They form heteromeric complexes with the common mediator SMAD (co‑SMAD: SMAD4) and translocate to the nucleus. Upon entry into the nucleus the R-SMAD/co-SMAD complex binds, with high affinity and specificity, to the genomic SMAD-binding element (SBE) sequence, requiring additional DNA binding transcription factors that associate with specific sequences flanking the SBE. Inhibitors of the different stages of the pathway are also shown (SMAD7 and the nuclear proteins SKI and SNO). mG and AAAAA, represents 5' capping and 3' polyadeylation of mRNAs respectively (Taken from (Akhurst and Hata, 2012)).

The effects of TGFβ on HSCs will depend on whether they are quiescent or activated (Dooley et al., 2000; Gressner et al., 2007; Dooley and ten Dijke, 2012). In quiescent HSCs, TGFβ will inhibit proliferation and this involves phosphorylation and translocation of SMAD2 to the nucleus (Dooley et al., 2000). Once the HSCs have activated TGFβ has no effect on proliferation and causes phosphorylation and translocation of SMAD3 (Liu et al., 2003). It has been found that SARA, which is required for SMAD2 signalling, is not present in activated HSCs (Liu et al., 2003) and that a constitutively phosphorylated SMAD2 is found in the nucleus (Liu et al., 2003). This therefore means that SMAD3 is a direct mediator of matrix production in the activated HSC (Uemura et al., 2005). Another important SMAD for HSC with respect to TGFβ responses, which has been investigated is the I-SMAD, SMAD7, which acts as a feedback inhibitor of TGFβ signalling (Stopa et al., 2000; Dooley et al., 2003). This is the case in quiescent HSC, but in the activated HSC there is a lack of SMAD7 induction, which could explain the excessive effect of TGFβ observed in liver fibrosis (Stopa et al., 2000; Tahashi et al., 2002; Dooley et al., 2003).

Non-canonical TGFβ signalling (Figure 1.8.3) as well as crosstalk with other pathways has been reported to occur (Inagaki and Okazaki, 2007). Non-SMAD TGFβ signalling via Ras/Raf-1MAPK signalling has been reported (Reimann et al., 1997), as well as p38/Jun amino-terminal kinase (JNK)/MAP kinase (Furukawa et al., 2003). MAPK-mediated SMAD3 linker phosphorylation is thought to be associated with HSC migration and disease progression (Furukawa et al., 2003; Yoshida et al., 2005; Matsuzaki et al., 2007).

1.8.2.5   Matrix turnover.

Fibrosis is a consequence of an imbalance between matrix production and degradation. Disruption of the normal hepatic matrix by matrix-degrading proteases hastens matrix replacement by scar tissue. The ECM in normal liver is composed of collagens (types I, III, IV, V and VI), the non-collagenous glycoproteins which encompass laminin and fibronectin amongst others and proteoglycans (Iredale et al., 2013). In the liver sinusoid the basement membrane comprises of laminin and type IV collagen which is progressively replaced by rich interstitial collagens, such as collagens I and III (Maher et al., 1988; Friedman, 1993). It is the accumulation of
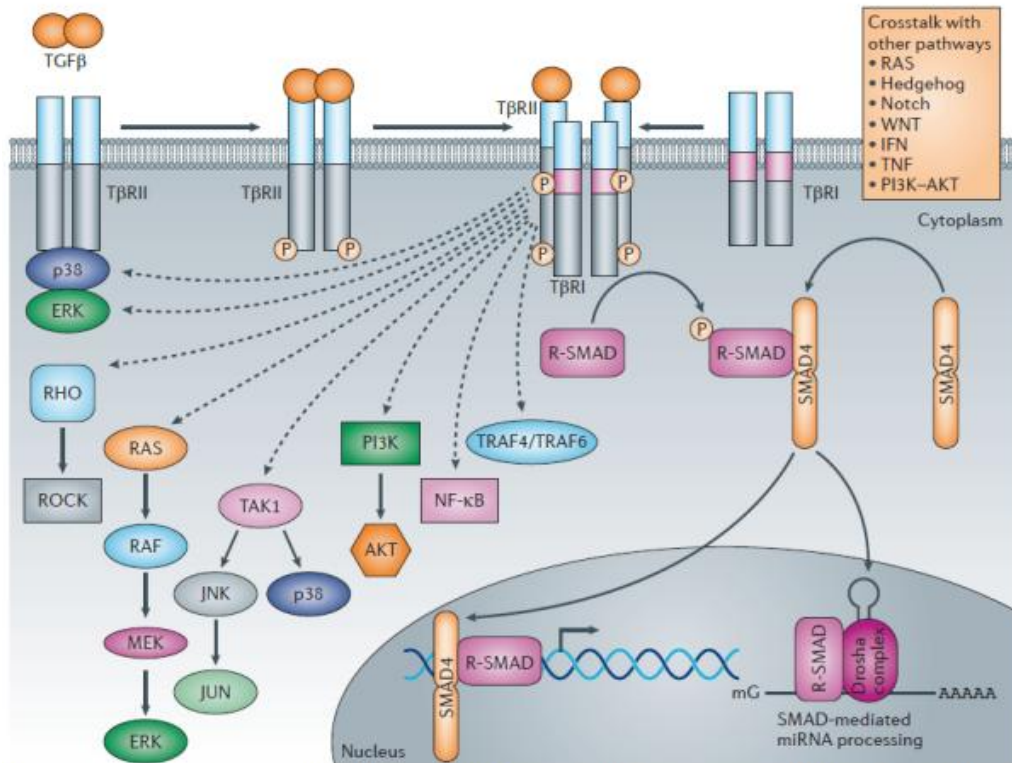
Figure 1.8.3   Schematic diagram of the non-canonical TGFβ signalling and crosstalk with other signalling pathways. Free TGFβ can bind to the transmembrane TGFβ receptor II (TβRII). This then results in the recruitment of and hetrodimerisation with the TGFβ receptor type I (TβRI). This heterodimerisation initiates signalling through transphosphorylation of TβRI by the TβRII which is transmitted into the cell via the non-canonical TGFβ pathways. These include signalling through p38 mitogen-activated protein kinase (p38 MAPK), extracellular signal-regulated kinases (ERK), RHO, TGFβ-activated kinase 1 (Tak1), phosphoinositide 3-kinase (PI3K) , nuclear factor‑κB (NF-κB, JUN N-terminal kinase (JNK) and TNF receptor associated factor 4 (TRAF4) or TRAF6. TGFβ signalling can be influenced by pathways other than the canonical and non-canonical TGFβ signalling pathways, such as the WNT, Hedgehog, Notch, interferon (IFN), tumour necrosis factor (TNF) and RAS pathways. mG and AAAAA, represents 5' capping and 3' polyadeylation of mRNAs respectively (taken from (Akhurst and Hata, 2012)).

the collagens which eventually distorts the sinusoid and vasculature, such that the architecture of the liver is significantly disrupted (Iredale et al., 2013). The discovery of the family of matrix-metalloproteinases (MMP), which are calcium-dependent enzymes which specifically degrade collagens and non-collagenous substances, were found to be a key element in the understanding of matrix remodelling (Benyon and Arthur, 2001; Iredale, 2001). MMPs are categorised based on their substrate specificity. HSCs produce MMP-2 and MMP-9 (specific for gelantinases), MMP-13 (specific for interstitial collagenases) and stromelysin (Friedman, 2008a). Increased MMP-2 expression has been demonstrated in cirrhosis (Benyon et al., 1996). The regulation of these enzymes occurs at many levels with their inactivation by binding to Tissue Inhibitors of MMPs (TIMPs) (Iredale, 2001). HSCs produce functional TIMP-1 and TIMP-2 during liver injury. This enables the inhibition of interstitial collagenases (MMP-2 and MMP-9) which will result in reduced degradation of the accumulating matrix (Murphy et al., 2002). TIMP-1 has been shown to be anti-apoptotic toward stellate cells through MMP inhibition, therefore if its expression is sustained then this will lead to an increased population of stellate cells due to the prevention of their clearance (Murphy et al., 2002).

1.8.3 Resolution of Fibrosis.

Reversibility of advanced hepatic fibrosis and even early cirrhosis has been demonstrated across a range of diseases (Ellis and Mann, 2012). The actual mechanism by which fibrosis may be reversed has yet to be completely characterised but it is believed that regression of activated HSCs and myofibroblasts are critical for this (Hasegaea et al., 2015). There are two potential pathways for reduction of activated HSCs, either reversion to a quiescent phenotype or through clearance via apoptosis (Friedman, 2008b). A study investigating the fate of activated HSCs after CCl$_4$-induced and alcohol-induced liver fibrosis, using genetically labelled activated HSCs, demonstrated that half of the activated HSCs escaped apoptosis. This involved down regulating fibrotic genes and acquiring a phenotype similar to, but distinct from, quiescent HSCs, during regression of fibrosis (Kisseleva et al., 2012). Although the stellate cells reacquired markers of quiescence during fibrosis

resolution, these inactivated HSCs adopted an intermediate phenotype, with a heightened capacity to reactivate when treated with TGFβ1 (Kisseleva et al., 2012).

1.8.3.1 Hepatic stellate cell apoptosis.

Apoptosis of HSCs is an important feature during regression of liver fibrosis (Iredale, 2001). The removal of the collagen and TIMP producing cells leads to restoration of a normal baseline MMP activity along with remodelling of the ECM to a near normal state (Oakley et al., 2005). Nuclear factor-κB (NF-κB) was speculated to function as a survival factor for HSCs through the prevention of apoptosis (Lang et al., 2000; Wright et al., 2001; Oakley et al., 2003; Elsharkawy et al., 2005). Cultured rat and human HSCs have been shown to contain constitutively active NF-κB transcriptional activity (Wright et al., 2001). Experimental evidence in rat HSCs, as well as in an *in vivo* rat CCl_4 liver injury model, has shown that HSC apoptosis can be stimulated via a caspase-dependent mechanism. This involves inhibition of the anti-apoptotic transcription factor NF-κB (Oakley et al., 2005). In the rat CCl_4 model of liver injury, NF-κB inhibition caused rapid clearance of α-SMA positive myofibroblasts, reduced hepatic expression of pro-collagen I and TIMP1 and increased hepatic MMP activity, along with an accelerated resolution of liver fibrosis (Oakley et al., 2005). Nerve growth factor, which can be derived from hepatocytes, is known to be apoptotic towards stellate cells through inhibition of NF-κB (Oakley et al., 2003) and this activity has been shown to be blocked by a serotonin antagonist (Ruddell et al., 2006). Human HSCs are relatively resistant to apoptosis when compared to rat HSCs, due to increased expression of regulator protein B-cell lymphoma 2 (Bcl-2), that regulates cell death (Novo, 2006). Therefore caution must be taken with extrapolation from rodent models to humans. There is a hypothesis that natural killer (NK) cells limit liver fibrosis by induction of HSC apoptosis via TRAIL and it has been reported that cultured HSCs are sensitive to TRAIL-mediated apoptosis (Radaeva et al., 2006). Patients with rapid progression of disease exhibit impaired NK cell function compared with patients with slow disease progression (Radaeva et al., 2006). NK cell function also declines with age which may explain the acceleration of fibrosis with age (Poynard et al., 2003).

1.9 Animal models of fibrosis.

Animal models have been used for many decades to study both fibrosis and evaluate potential anti-fibrotic therapies. *In vivo* models of liver fibrosis offer a way to investigate molecules in intact organs and have been crucial in increasing our understanding of the pathophysiological processes of fibrosis. Animal models remain a vital experimental tool, despite being unable to replicate the human disease (Constandinou et al., 2005; Starkel and Leclercq, 2011). The choice of animal model and the fibrosis-inducing stimulus is based on the expectation that the response will engage mechanisms that are similar to the human disease, although this may not be the case. It is not always possible to replicate the human disease in an animal model, for example HCV does not infect rats, and specific inducing agents will have differing effects depending on the species (Starkel and Leclercq, 2011). An important difference in the human disease is the significant impact of the alteration of the vasculature in the disease progression, causing liver loss due to secondary hypoxia, which does not occur commonly in animal models (Wallace et al., 2008). There are many different types of animal models used in research from toxin-induced, dietary-induced, surgically-manipulated, genetically-modified and infection-induced, that have and are used to advance our knowledge of liver fibrosis. The availability of knockout mice has increased the understanding of the molecular mechanisms and the significance of targeted genes in hepatic function and disease (Hayashi and Sakai, 2011). The stimulus, design, species and strain of animal are important factors that need to be considered when choosing the animal model to study, as they will influence the specific characteristics, location and development of the disease (Wallace et al., 2008; Starkel and Leclercq, 2011). It is important to choose a model that will match the mode of action of the potential anti-fibrotic agent being tested. Another important consideration is that the potential anti-fibrotic agents are not toxic or modulate the experimental agent being used to generate the liver injury, as this will compromise the data interpretation of the study (Marek et al., 2005a; Wallace et al., 2008). It is advisable when investigating the anti-fibrotic potential of a drug to test it in at least two animal models, which should be mechanistically distinct, to avoid model specific artefacts (Wallace et al., 2008; Popov and Schuppan, 2009). The models that will be discussed further in this thesis will focus on those that have

been used experimentally in the thesis and in the literature to provide evidence and insight to the research being addressed. The models discussed further will be the CCl_4 liver injury model, thioacetamide (TAA) induced liver injury model and bile duct ligation model (BDL), with the HSC playing an important role in the fibrogenesis observed in all three of these models.

1.9.1 Carbon tetrachloride liver injury model.

The CCl_4 liver injury model is one of the classical and most widely used. It is the best characterised model as it induces fibrosis through repeated insult with a hepatoxin, which is CCl_4 (Constandinou et al., 2005; Starkel and Leclercq, 2011; Crespo Yanguas et al., 2015). It mirrors the pattern of disease seen in human fibrosis and cirrhosis caused by toxic damage in many respects (Tamayo, 1983; Tsukamoto et al., 1990), but with a more pronounced cholangiolar cell hyperplasia is observed in advanced CCl_4-induced fibrosis in rat. There is also a failure to progress to hepatocellular carcinoma (Tamayo, 1983).

After administration, CCl_4 (a halokane), is bio-transformed by CYP2E1 to produce trichloromethyl radical, which causes lipid peroxidation. The lipid peroxides can then react with sulphydryl group of proteins (Tamayo, 1983; Tsukamoto et al., 1990; Basu, 2003; Weber et al., 2003). This therefore causes an acute-phase reaction, which is characterised by necrosis of centrilobular hepatocytes, activation of Kupffer cells and the induction of an inflammatory response (Hendrikx et al., 1996). This in turn causes the production of cytokines, which activates the HSC leading to liver fibrosis (Iwaisako et al., 2014). It has been demonstrated that the ERK pathway, which regulates proliferation and chemotaxis of HSC has been found to be activated following administration of CCl_4 (Marra et al., 1999a).

Most commonly CCl_4 (0.3-1mg/kg) is dosed 2-3 times weekly intraperitoneally for 4-12 weeks, depending on the level of fibrosis required to be achieved, in rats or mice (Constandinou et al., 2005; Wallace et al., 2008; Crespo Yanguas et al., 2015). Twice-weekly dosing of CCl_4 fibrosis will induce fibrosis after 4 weeks, cirrhosis after 8 week and advanced micronodular cirrhosis after 12 weeks (Constandinou et al., 2005). CCl_4 can also be administered orally, subcutaneously or inhaled using

different dosing regimens (Crespo Yanguas et al., 2015). The use of mice in this model are preferred due to their higher metabolic rate of CCl_4 (Thrall et al., 2000) and also because of the lower amount of agents required (Popov and Schuppan, 2009) in comparison to rats. The strain of mice is also important as BALB/c mice develop more liver fibrosis compared with C57BL/6 and DBA/2 counterparts upon CCl_4 administration (Shi et al., 1997; Walkin et al., 2013). This model can also be used to study fibrosis recovery after the cessation of CCl_4 administration and has been used in conjunction with knockout and transgenic animals for mechanistic studies (Iredale et al., 1998; Constandinou et al., 2005). Once the model is established it provides predictable and reproducible fibrosis (Constandinou et al., 2005).

The fibrosis observed in the histological examination of the liver demonstrates fibrosis emerging from the central vein eventually leading to central-central bridging fibrosis (Constandinou et al., 2005; Wallace et al., 2008). Histological analysis of the liver, with different immunochemical stains is used to assess fibrosis. Hemotoxylin and eosin (H&E) staining provides assessment on the overall architecture, degree of inflammation, necrosis, cellular apoptosis and cellular mitosis that has been induced. α-SMA stains areas of inflammation identifying activated HSCs and other tissue myofibroblasts. Sirius Red stain identifies areas of the combination of collagen 1 and collagen 3 deposition. These two stains provide a visual assessment of the extent and distribution of fibrosis (Constandinou et al., 2005).

1.9.2   Thioacetamide induced liver injury model.

TAA, like CCl_4, is another toxin widely used for fibrosis-induction, with it being bio-transformed by CYP450 isoenzymes, into thioacetamide sulphur dioxide. This causes centrilobular necrosis of the liver, with a more prominent periportal injury being observed (Starkel and Leclercq, 2011; Crespo Yanguas et al., 2015; Wallace et al., 2015). TAA is administered intraperitoneally, 2-3 times a week, for 4-12 weeks or administered in drinking water for up to 16 weeks (Crespo Yanguas et al., 2015; Wallace et al., 2015). The actual mechanism by which TAA causes liver injury is still not fully understood. Severe oxidative damage associated with activation of HSCs is observed (Palacios et al., 2008; Crespo Yanguas et al., 2015; Wallace et al.,

2015). TAA administered in drinking water in mice was found to cause activation of HSCs, as assessed by increased expression of glial fibrillary acidic protein (GFAP, specific hepatic biomarker for HSCs) and cysteine- and glycine-rich protein 2 (CRP2, specific marker of HSC transdifferentiation). The increased expression positively correlated with the increased collagen, α-SMA expression, and PDGF-BB expression (Palacios et al., 2008). Therefore hepatic stellate cell activation is essential for the observed fibrosis and cirrhosis (Palacios et al., 2008; Wallace et al., 2015). A reliable, dose- and time-dependent pattern of liver injury can be achieved with this model (Al-Bader et al., 2000; Laleman et al., 2006; Wallace et al., 2015) but does require a longer time to develop liver injury when compared with the CCl_4 model (Zimmermann et al., 1987; Wallace et al., 2015). Microscopic investigation of rodent livers following TAA demonstrates a more periportal infiltrate with a greater ductal proliferation and hepatic necrosis, than CCl_4 (Wallace et al., 2015). Chronic intoxication, 18 weeks or longer, of TAA frequently results in malignancy with mitotic figures being observed (Fitzhugh and Nelson, 1948; Laleman et al., 2006; Wallace et al., 2015). TAA model of liver, like CCl_4, can be assessed by the percentage of Sirius Red staining observed as well as α-SMA and H&E staining (Wallace et al., 2015).

1.9.3 Bile Duct Ligation model.

This model was first established in rat and then later in mice (Rodríguez-Garay et al., 1996; Miyoshi et al., 1999) and involves doubly ligating the bile duct and transecting between the two ligatures (Rodríguez-Garay et al., 1996). This ligation causes obstruction of the bile duct leading to increased biliary pressure, mild inflammation and cytokine secretion from biliary epithelial cells to cause cholestasis (cessation of the flow of bile). It is the bile acid toxicity that stimulates the proliferation of biliary epithelial cells, with increased expression of fibrogenic markers α-SMA, TIMP-1, Collagen I and TGFβ1, along with accumulation of B and T-cells in the portal tract. This causes liver damage and generation of ROS (Georgiev et al., 2008). HSCs play an important role in the fibrogenesis as they are the major source of myofibroblasts (>87%) in CCl_4 or TAA animal models. However in the BDL model, it is the portal fibroblasts (PF) that are the major source of myofibroblasts (aPF) (> 70%) at the

onset of injury. The HSCs contribution increases as the injury progresses (Iwaisako et al., 2014). Activated PF (aPF) respond to stimulation with taurocholic acid and IL-25 by induction of collagen-α1 and IL-13, which is not observed with HSCs (Iwaisako et al., 2014). The aPFs have been found by gene expression to express a number of novel markers, such as the mesothelial-specific marker mesothelin (Iwaisako et al., 2014). In mice marked dilatation of the gall bladder upon ligation of the common bile duct can occur. There is therefore an increased risk of perforation, bilioperitoneum and interindividual variability in expansion of the gall bladder resulting in a variable parenchymal response (Starkel and Leclercq, 2011). Addition of a surgical clip on the cystic duct or cholecystectomy alleviates this problem (Fickert et al., 2002). This complication does not occur in rats due to the absence of the bile duct. Early mortality in rodents occurs due to bile leakage, rupture of biliary cysts or gall bladder, with the mortality rate at 5−6 weeks post BDL in rats of about 20 %, but for mice the mortality rate peaks after 10 days (Starkel and Leclercq, 2011). Biliary fibrosis develops within weeks with portal hypertension, hyperdynamic circulation, porto-systemic shunting and ascites observed in rats after 6-8 weeks (Tsukamoto et al., 1990; Geerts et al., 2008; Popov and Schuppan, 2009) Seldom seen is the architectural changes observed in cirrhosis (Georgiev et al., 2008).

1.10 Profile of 5-HT compounds used in the receptor characterisation.

Many of the studies carried out to pharmacologically characterise 5-HT receptors in a specific cell or tissue have involved using a variety of 5-HT antagonists and agonists. Although these compounds are reported to be selective there is often only a small window of selectivity and the concentrations studied are often at levels which could affect multiple receptor subtypes. Evidence for a particular receptor's involvement may be compromised by its ability to interact with other receptors, not just a particular subtype of 5-HT receptors at the concentrations used. There is also conflicting information on the true selectivity of these compounds. In drug discovery, the use of recombinant receptor systems has enabled selective compounds to be defined not only against human receptors, but against different animal species, which is important if the compound of interest is to be profiled in animal models. To really

understand the therapeutic potential of a compound, it needs to be characterised in a physiologically relevant tissue or cell assay (Figueroa et al., 2009). The determination of the true selectivity of compounds in the single receptor recombinant systems is crucial in defining the concentration range, which can be used to block selectively the receptor of interest, especially for antagonists in a physiologically relevant assay. With the increased availability of human and animal primary cells, similar techniques to those used to characterise receptors in tissues need to be employed, combined with the added selectivity knowledge gained from simpler single receptor recombinant systems. The 5-HT receptors of interest expressed on the HSCs were 5-HT_{2A}, 5-HT_{2B} and 5-HT_{1B} due their increased expression upon activation of the HSCs (Ruddell et al., 2006).

Ketanserin and volinanserin are potent 5-HT_{2A} receptor antagonists with greater than 100-fold selectivity over the 5-HT_{2B} receptor (Table 1.10.1 A and B). Volinanserin, also known as MDL 100907, which has been tested in clinical trials as a potential antipsychotic (Offord et al., 1999), antidepressant (Marek et al., 2005b) and treatment for insomnia (Teegarden et al., 2008), exhibits the most selective profile over the receptors of interest. Ketanserin, which was discovered by Janssen Pharmaceutica in 1980 and is used clinically as an antihypertensive agent, also has a high affinity (pKi ~ 8) at α_1-adrenoceptors (Yoshio et al., 2001). The α_{1B} and α_{1D}-adrenoceptor are reported to be present on the HSCs (Oben, 2004). It also has affinity at the 5-HT_{1D} receptor in the 30 nM range but rather lower affinity at 5-HT_{1B} receptor (around 2 µM) (Table 1.10.1 A) (Lesage et al., 1998). No antagonism of 5-HT mediated inhibition of responses to forskolin by ketanserin was observed in cells expressing the 5-HT_{1B} receptor at concentrations up to 10 µM (Lesage et al., 1998). A novel potent, selective 5-HT_{2A} agonist, NBOH-2C-CN, reported in the literature (Table 1.10.1C) was also used, although no data exists as to it activity at 5-HT receptors other than 5-HT_{2A} and 5-HT_{2C} receptors (Hansen et al., 2014). It was also shown to behave as a partial agonist ($pEC_{50} = 8.7$ and intrinsic activity = 0.86) in a functional 5-HT_{2A} assay (Hansen et al., 2014).

A Receptor affinity values for ketanserin			
Receptor	Affinity pK_i	Species	Reference
5-HT$_{2A}$	8.1-9.7	Human	(Bryant et al., 1996; Rashid et al., 2003; Knight et al., 2004)
α_1	8.2-7.8	Human	(Yoshio et al., 2001)
5-HT$_{1D}$	7.5	Human	(Leysen et al., 1996; Lesage et al., 1998)
5-HT$_{2C}$	7.2	Human	(Knight et al., 2004)
5-HT$_{2B}$	6.1-6.7	Human	(Rashid et al., 2003; Knight et al., 2004)
D1	6.7	Human	(Sunahara et al., 1991)
5-HT$_7$	5.8-6.1	Human	(Bard et al., 1993; Thomas et al., 1998)
5-HT$_{1B}$	5.4-5.8	Human	(Lesage et al., 1998)

B Receptor affinity values for volinanserin			
Receptor	Affinity pK_i	Species	Reference
5-HT$_{2A}$	8.7-8.9	Human	(Reavill et al., 1999; Knight et al., 2004)
5-HT$_{2C}$	7.5	Human	(Knight et al., 2004)
5-HT$_{2B}$	6	Human	(Knight et al., 2004)

C Receptor affinity values for NBOH-2C-CN			
Receptor	Affinity pK_i	Species	Reference
5-HT$_{2A}$	8.9	Human	(Hansen et al., 2014
5-HT$_{2C}$	6.9	Human	(Hansen et al., 2014)

Table 10.1   Affinity values for A) ketanserin, B) volinanserin and C) NBOH-2C-CN reported in the literature.

RS-127445 and GSK1606260A are potent antagonists of the 5-HT$_{2B}$ receptor and exhibit greater than 1000-fold selectivity over the 5-HT$_{2A}$ receptor (Table 1.10.2 A and B) but are not in clinical use. These compounds exhibit higher affinity and greater selectivity than SB 204741 (Table 1.10.2 C), which was reported in the literature (Ebrahimkhani et al., 2011). No suitable 5-HT$_{2B}$ agonist was identified that had a suitable selectivity window over the 5-HT$_{2A}$ receptor.

Sumatriptan has been reported to be a selective 5-HT$_{1B}$ partial agonist (Table 1.10.3 A) and is used in the treatment of migraine. There is no reported agonist activity at the 5-HT$_{2A}$ or 5-HT$_{2B}$ receptor. Therefore it is a good candidate to use for stimulation of the 5-HT$_{1B}$ receptor. Cyanopindolol, which is also a potent β-adrenoceptor antagonist, is a potent 5-HT$_{1B}$ antagonist (Table 1.10.3 B) and has been shown functionally to antagonise 5-HT CRCs in a competitive manner to yield a pK$_B$ estimate of 8.7 (Giles et al., 1996). β$_2$- and β$_1$-adrenoceptors have been reported to be present on HSCs with expression of the β$_2$-adrenoceptor increased upon activation (Trebicka et al., 2009) and these receptors require consideration when using cyanopindolol.

1.11 Summary of study aims.

The evidence of increased expression of 5-HT$_2$ receptors on HSC, once activated, along with a body of literature implicating a role for 5-HT in fibrosis, makes inhibition of 5-HT$_2$ receptors a possible target for fibrosis therapy. The activation of the HSC is a central event in fibrosis and once activated these cells differentiate into a proliferative, persistent myofibroblast-like cell which secretes ECM and TGFβ1 (Bachem et al., 1992: Friedman 2008). If HSC activation can be inhibited by a small molecule 5-HT$_2$ receptor antagonist, with 5-HT$_{2B}$ as the preferred receptor due to key target validation work that had been published (Ebrahimkhani et al., 2011), then this could be developed into a drug therapy for liver fibrosis.

The primary aim of these studies was to pharmacologically characterise the 5-HT receptor present on activated HSCs to fully evaluate and extend the evidence for a role 5-HT$_2$ antagonists in fibrosis. There is conflicting data reported in the

A Receptor affinity values for RS-127445			
Receptor	Affinity pK_i	Species	Reference
5-HT$_{2B}$	9-9.5	Human	(Bonhaus et al., 1999; Knight et al., 2004)
5-HT$_{2C}$	7.5	Human	(Knight et al., 2004)
5-HT$_{2A}$	6	Human	(Knight et al., 2004)

B Receptor affinity values for GSK1606260A			
Receptor	Affinity fpK_i	Species	Reference
5-HT$_{2B}$	9.2	Human	(Bruton et al., 2009)
5-HT$_{2C}$	<5.3	Human	(Bruton et al., 2009)
5-HT$_{2A}$	<5.3	Human	(Bruton et al., 2009)
5-HT$_6$	7.6	Human	(Bruton et al., 2009)

C Receptor affinity values for SB-204741			
Receptor	Affinity pK_i	Species	Reference
5-HT$_{2B}$	6.9	Human	(Knight et al., 2004)
5-HT$_{2C}$	5.6	Human	(Knight et al., 2004)
5-HT$_{2A}$	<5	Human	(Knight et al., 2004)

Table 10.2   Affinity values for A) RS-127445, B) GSK1606260A and C) SB-204741 reported in the literature.

A Receptor affinity values sumatriptan			
Receptor	Affinity pK_i	Species	Reference
5-HT$_{1D}$	7.9-8.5	Human	(Leysen et al., 1996; Napier et al., 1999)
5-HT$_{1B}$	7.4-8	Human	(Napier et al., 1999)
5-HT$_{1A}$	6	Human	(Napier et al., 1999)
5-HT1f	7.9	Human	(Napier et al., 1999)
5-HT$_7$	5.9	Human	(Napier et al., 1999)

B Receptor affinity values for cyanopindolol			
Receptor	Affinity pK_i	Species	Reference
5-HT$_{1B}$	8.6	Mouse	(Maroteaux et al., 1992; Giles et al., 1996)
	8.7*	Human	
5-HT$_{1D}$	7.1	Human	(Hamblin and Metcalf, 1991)
β-Adrenoceptors	10.3	Human	(Niclauss et al., 2006)

Table 10.3 Affinity values for A) sumatriptan and B) cyanopindolol reported in the literature.
* pK$_B$

literature as to the 5-HT$_2$ subtype involved (Ebrahimkhani et al., 2011; Park et al., 2011; Kim et al., 2013) due to the use of non-selective concentrations of 5-HT$_2$ antagonists and absence of analysis of 5-HT concentration-response data. The literature has focussed on the effect of 5-HT and its antagonists on the expression of proteins on HSCs, which has not been undertaken in a quantitative manner (Ebrahimkhani et al., 2011; Kim et al., 2013). *In vitro* assays in this thesis were therefore chosen to allow classical 'in-depth' pharmacological analysis of 5-HT concentration-response curves using selective ligands, as outlined in section 1.10. This will be used in combination and at selective concentrations, to characterise the 5-HT receptor present on both mouse and human HSCs and which has not been previously undertaken in the literature. These assays range from simple *in vitro* assays investigating early receptor signalling events, such as calcium release and phosphorylation of ERK production, to downstream 'phenotypic' fibrotic end points, such as proliferation and collagen production of HSC. Further analysis of data obtained from a mouse CCl$_4$ model, after treatment with selective 5-HT$_{2A}$ and 5-HT$_{2B}$ antagonists was also undertaken to provide evidence of the relevance of 5-HT in liver fibrosis. The overall aim of this thesis is to provide a robust pharmacological characterisation of the 5-HT receptor present on mouse and human HSCs, determine its role in fibrosis and potential to provide a target for therapy.

Chapter 2: Materials and methods.

2.1 Materials.

Volinanserin and GSK1606260A used in this study were synthesised by the Medicinal Chemistry department at GSK, Medicines Research Centre (Stevenage, UK). All compounds, pertussis toxin and OptiPrep™ used in this study were purchased from Sigma-Aldrich Co. Ltd (Gillingham, UK),) unless otherwise stated. NBOH-2C-CN hydrochloride was purchased from Tocris Bioscience (Bristol, UK). All cell culture media and reagents (including recombinant mouse and human platelet-derived growth factor-BB (PDGF-BB) and recombinant human transforming growth factor-β1) were obtained from Gibco (Invitrogen Ltd., Paisley, UK). All tissue culture flasks and plates were obtained from Thermo Fisher Scientific (Cheshire, UK) unless otherwise stated.

All primary antibodies, secondary antibodies, isotype controls and nuclear stains used in the immunocytochemistry (ICC) for both the characterisation of the isolated HSC's and collagen deposition assays were commercially available. Primary antibodies used were: polyclonal rabbit anti-mouse desmin (Thermo Fisher Scientific, Cheshire, UK), mouse monoclonal anti-human synaptophysin (Sigma-Aldrich Co Ltd, Gillingham, UK), mouse monoclonal anti-human CD31 (BioLegand, San Diego, CA, USA), mouse monoclonal anti-human CD68 (Sigma-Aldrich Co Ltd, Gillingham, UK), sheep polyclonal anti-human GFAP (R&D Systems, Minneapolis, MN, USA), rabbit monoclonal anti-mouse α-smooth muscle actin (Abcam, Cambridge, MA, USA) and mouse monoclonal anti-human collagen type 1 (Invitrogen Ltd., Paisley, UK). Isotype controls include: rabbit monoclonal IgG1 isotype control (Sigma-Aldrich Co Ltd, Saint Louis, USA) and mouse monoclonal IgG1 isotype control (Sigma-Aldrich Co Ltd, Saint Louis, USA). The secondary antibodies, all obtained from Invitrogen Ltd. (Paisley, UK) include: Alexa Fluor 488 goat anti-mouse IgG, Alexa Fluor 488 goat anti-rabbit IgG, Alexa Fluor 647 goat anti-rabbit IgG and Alexa Fluor 647 goat anti-sheep IgG. Nuclear stain used was Hoechst 33342 solution (Invitrogen Ltd.,Paisley, UK).

The calcium sensitive dye, Fluo4-AM, was obtained from Molecular Probes, (Invitrogen Ltd., Paisley,UK). DNase, collagenase and pronase were purchased from Fisher Scientific Ltd (ThermoFisher Scientific Inc. New York USA). MSD

Phospho/Total ERK1/2 assay plates were purchased from Meso Scale Discovery (Rockville, USA) and cell proliferation ELISA BrdU (colourimetric) assay kits were purchased from Roche applied Science (Mannheim, Germany). All studies were completed with a final dimethyl sulphoxide (DMSO) assay concentration of 0.1% unless otherwise stated.

2.2 Isolation of hepatic stellate cells from mouse and human livers.

HSCs were isolated from C57BL/6 mouse and human livers as described by Ebrahimkhani et al. (2011). All animal studies were ethically reviewed and carried out in accordance with the Animals (Scientific Procedures) Act 1986 and the GSK policy on the care, welfare and treatment of animals. Human HSCs were isolated from cirrhotic and margins of normal resected livers. The human biological samples were sourced ethically, and their research use was in accord with the terms of informed consents. The livers were used within 2 h of retrieval for mouse and within 18h for human.

The liver tissues were chopped to a soup-like consistency in Hank's Balanced Salt Solution (HBSS) containing DNase (0.1 mg/ml), collagenase (1.5 mg/ml) and pronase (5 mg/ml), with scissors or a scalpel in a petri dish, before incubation at 37ºC for 20-30 minutes in a 50 ml falcon tube. The digested tissue was filtered through 100 μm sterile nylon gauze stretched over a glass beaker. The cell suspension was washed by centrifugation at 500g for 7 min in HBSS containing 4 μg/ml DNase and aspiration of the supernatant twice. The resulting pellet was resuspended in HBSS containing 4 μg/ml DNase, before dilution in OptiPrep™ density gradient medium at 11.7% OptiPrep™ solution for mouse and 13.5% for human cells. For mouse, the cells were isolated using three layers in 15 ml Falcon tubes (15.5% OptiPrep™ bottom layer, 11.7% OptiPrep™ middle and a top layer of HBSS). For human, the cells were isolated using two layers in a 50 ml Falcon (13.5% OptiPrep™ and HBSS). The gradients were centrifuged at 1500g for 30 min. HSCs were recovered from the interface between the HBSS layer and the OptiPrep™ layer below. The isolated stellate cells were resuspended in HBSS containing 4 μg/ml DNase before being washed at 500g for 7 min twice. The supernatant was removed and the cell pellet resuspended in growth medium (Dulbecco's Modified

Eagles Medium (DMEM) containing 4.5 g/l glucose supplemented with 16% heat-inactivated foetal calf serum (FCS), 100 U/ml penicillin and 100 U/ml streptomycin and 2 mM L-glutamine for mouse or, for human, Iscoves modified Dulbecco's medium supplemented with 20% heat-inactivated foetal calf serum (FCS), 100 U/ml penicillin and 100 U/ml streptomycin, 2.5 μg/ml Amphotericin B, 4 mM L-glutamine, 0.1 mM non-essential amino acids, 1 mM sodium pyruvate and 0.6 IU/ml insulin). The cells were plated out in uncoated plastic tissue culture flasks (0.5-1 $X10^6$ cells/ml) and incubated at 37ºC in 5% CO_2.

2.3   Cell culture.

2.3.1   Culture of isolated hepatic stellate cells.

Following isolation, cells (mouse of human) were grown in growth medium for 24 h before medium was replaced to remove any residual cellular debris. Cells were kept in culture using sterile techniques. When cells were deemed to be 80-90 % confluent the medium was removed from the culture flask followed by washing of the cells with phosphate buffered saline (PBS) and detached with TrypLE Express trypsin solution. Once the cells were detached they were resuspended in culture medium and either maintained in culture or frozen down for future experiments (see below). After the second passage, the growth medium for cells were altered to contain dialysed FCS, as using heat-inactivated serum in early cell culture was found to lead to earlier activation of hepatic stellate cells and dialysed FCS contains less 5-HT which led to less basal activation in the phosphoERK assay. HSC were used between passage 2 and passage 5. Batches of cells were frozen following detachment from the flask, as described above, centrifuged at 350g for 5 min and re-suspended in 90% FCS:10% DMSO at a concentration of 1 X 10^6 cells/ml. The 1 ml aliquots were frozen down and stored in liquid nitrogen until required and cultured as above.

2.4   Immunocytochemistry staining.

Human and mouse HSC's were plated out onto a clear, flat-bottomed, 96 well, black plate (BD Bioscience, Bedford, MA, USA) to give a 90-100% confluent monolayer. The cells were incubated overnight at 37ºC in 5% CO_2 before the cells were fixed by the addition of 100 μl of ice-cold methanol for 2 min. The fixed cells were

permeabilised by treating with 0.1% Triton-X-100 solution in PBS for 90 s at room temperature and washed with PBS three times. The cells were incubated at 4°C with an appropriate dilution of one or two primary antibodies (anti-α-SMA (1 in 500), anti-synaptophysin (1 in 100), anti-desmin (1 in 300), anti-GFAP (1 in 500), anti-CD68 (1 in 100) and anti-CD31 (1 in 50)) overnight. The primary antibody was removed and the cells washed with 0.05% Tween-20 in PBS. The secondary antibodies were added at a 1:500 dilution and the Hoechst 33342 solution at a 1:10000 dilution (to stain nuclei via binding to AT regions).

Following a 1 h incubation at room temperature, the plates were washed with 0.05% Tween-20 in PBS and stored in PBS at 4°C. The fluorescence was visualised by the InCell Analyser 2000 or InCell Analyser 6000. The image data was then transferred into Columbus (v 2.7) to allow visualisation and analysis of the images.

2.5   Measurement of 5-HT stimulated intracellular calcium signal using the Fluorescence Imaging Plate Reader (FLIPR™).

2.5.1   Principle of the measurement of intracellular calcium using the FLIPR™.

Cells were plated out onto a clear, flat-bottomed, 96 well, black plate to give a 90-100% confluent monolayer. The cells were loaded with the fluorescent calcium-sensitive dye by incubating them with Fluo4-AM in the presence of a masking dye (Brilliant Black). Fluo-4 AM is a non-fluorescent acetoxymethyl ester of Fluo4 which once inside the cell is cleaved to give the free, fluorescent Fluo-4. The plate was placed in the Fluorometric Imaging Plate Reader (FLIPR™) and the dye excited at 488nm wavelength using an optic LED and the signal detected using 510-570nm emission filter. Compounds were added to the plate to stimulate the intracellular calcium signal and the change in fluorescence intensity is recorded over time (Figure 2.5.1).

2.5.2   FLIPR™ assay protocol.

Mouse and human hepatic stellate cells were plated out at 10,000 cells per well in flat-bottomed, 96 well, clear plate in serum-free growth medium and incubated overnight at 37ºC in 5% CO_2. For pertussis toxin treatment, 100 ng/ml was added to
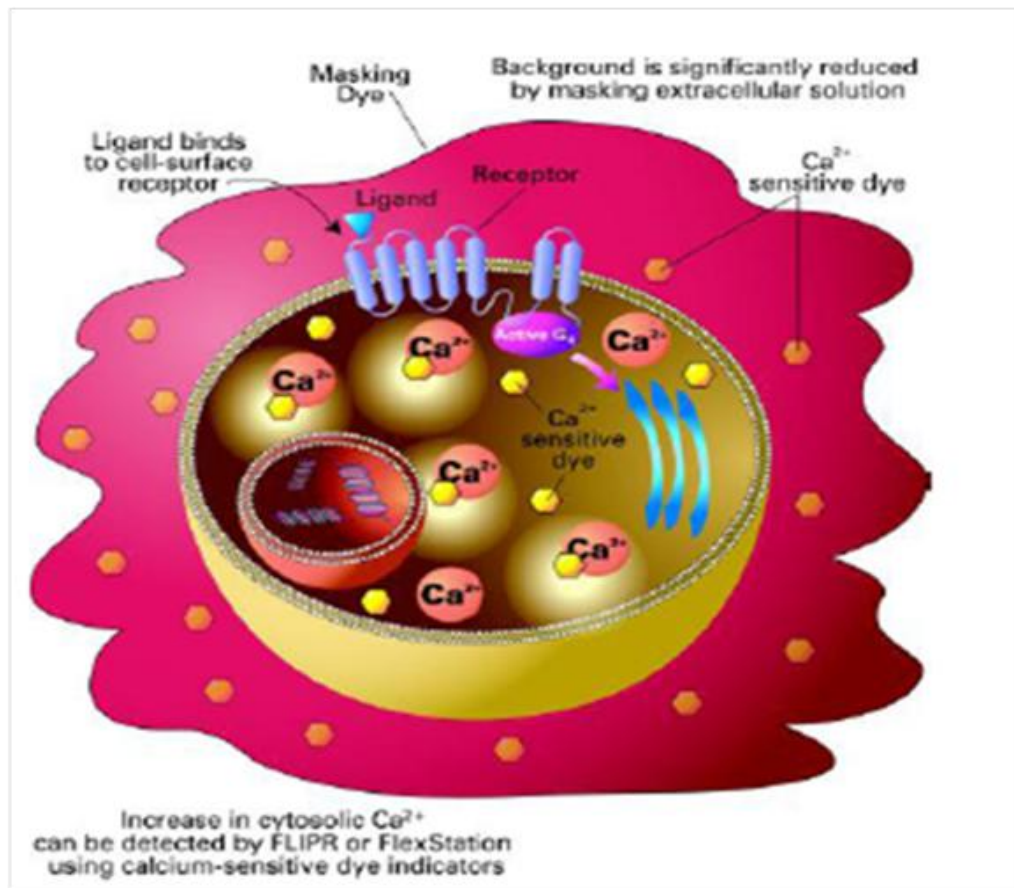
Figure 2.5.1   Principle of FLIPR™ assay. Cells are loaded with Fluo4-AM in the presence of brilliant black to reduce background fluorescence. The Fuo4-AM once inside the cell is cleaved to give the free Fluo-4 which can bind to the free cytosolic calcium. The cells are stimulated with a ligand which causes an increase in cytosolic calcium. The FLIPR™ microplate reader detects the increase in cytosolic calcium as an increase in fluorescence intensity emissions (51-570nm) (From Molecular Device website. Lydford *et al*.).

the serum-free medium before plating out. On the day of the assays the serum-free medium were aspirated and replaced with loading assay buffer (Tyrodes solution (137 mM NaCl, 13.4 mM NaHCO$_3$, 5.6 mM glucose, 2.7 mM KCl, 1.8 mM CaCl$_2$, 1.1 mM MgSO$_4$, 0.4 mM Na$_2$HPO$_4$ and 20mM N-2-hydroxyethylpiperazine-N'-ethanesulphonic acid (HEPES) pH 7.4) with the addition of 2.5 mM probenicid (to inhibit dye leakage from the cells), 500 μM brilliant black (to quench any excess unloaded Fluo-4 AM dye) and 2 μM Fluo4-AM (Molecular probes, Invitrogen Ltd., Paisley,UK). The plate was then incubated for 1 h at 37ºC. The antagonist or vehicle (0.1% DMSO) was added for 15 min before the plate was placed in the FLIPR where the fluorescence was measured every second for 10 s before (basal reading) and every second over 2 min following the addition of the agonists. All experiments were carried out at room temperature.

For washout experiments the plates were incubated with antagonist or vehicle (0.1% DMSO) for 15 min before being washed three times with FLIPR buffer. After the final wash FLIPR buffer containing 2 μM Fluo4-AM with or without the antagonists was added back to the plates for 15 min before being read on the FLIPR.

Basal (average of 10 s initial reading) and maximum response (max response - basal response) obtained were determined for each well. The data was then expressed as % basal fluorescence (((Max fluorescence response - basal fluorescence response)/basal fluorescence response) x100) for each well.

2.6   Measurement of the phosphorylated ERK in hepatic stellate cell lysates.

2.6.1   Principle of Meso Scale Discovery (MSD) Phospho/Total ERK1/2 assay.

The MSD phospho (Thr202/Tyr204;Thr185/Tyr187) ERK1/2 and TotalERK1/2 assay is a sandwich immunoassay. The capture antibodies for phosphoERK and total ERK are patterned on distinct electrodes (spots) in the same well of the plates. The sample is incubated to allow attachment of the analyte in the sample to the capture antibody, which is immobilised on the working electrode surface. The plates are washed before incubation with the SULPHO-TAG labelled anti-ERK detection antibody. The conjugated detection antibody is recruited by the bound analyte to complete the sandwich. The MSD read buffer, which provides the appropriate

chemical environment for electrochemiluminescence, is added and the plate loaded into the MSD SECTOR®. The SECTOR imager plate reader applies a voltage to the plate electrodes whereby the label bound to the electrode emits light. The instrument measures the intensity of emitted light to provide a quantitative measure of phospho ERK and total ERK present in the sample (See Figure 2.6.1).

2.6.2 PhosphoERK assay protocol.

HSCs were plated out (human and mouse cells at 10,000 per well) in flat-bottomed, 96 well plates and incubated overnight at 37ºC in 5% CO_2 in serum-free growth medium. For pertussis toxin treatment, pertussis toxin (100 ng/ml) was added to the serum-free medium before plating out. The serum-free medium were replaced with HBSS (without Ca^{2+} and $Mg^{2+)}$ on the day the assay was performed. The assay was carried out at room temperature. Cells were incubated with antagonists for up to 30 min before stimulation by addition of stimulant or vehicle. Cells were then incubated for up to 3 h, depending on the protocol, at room temperature. For the 24 h time course experiment the cells were kept in serum-free growth medium and incubated at 37ºC in 5% CO_2 throughout the time. The supernatant was aspirated and ice-cold lysis buffer (MSD Lysis buffer made up as per kit instructions containing protease inhibitors, phosphatase inhibitors, phenylmethylsulfonyl fluoride (PMSF) and sodium dodecyl sulphate (SDS). The plates were left for a minimum of 15 min on ice to ensure complete lysis of the cells. The percentage of phosphoERK was determined using Meso Scale Discovery (MSD) Phospho/Total ERK1/2 assay following the manufacturer's instructions.

The assay was carried out at room temperature. Briefly phospho/total ERK1/2 MSD plates were incubated on a plate shaker (600 rpm) for 1 h with blocking solution before being washed three times with TRIS wash buffer. The cell lysate was transferred to the Phospho/Total ERK1/2 assay plate and incubated on a plate shaker (600 rpm) for 3 h. After 3 h, the plate was washed three times with TRIS wash buffer and sulfo-tag detection antibody was added. The plate was incubated with the antibody on a plate shaker for a further 1 h. The plate was washed three times with TRIS wash buffer before addition of MSD read buffer. The MSD plates were then
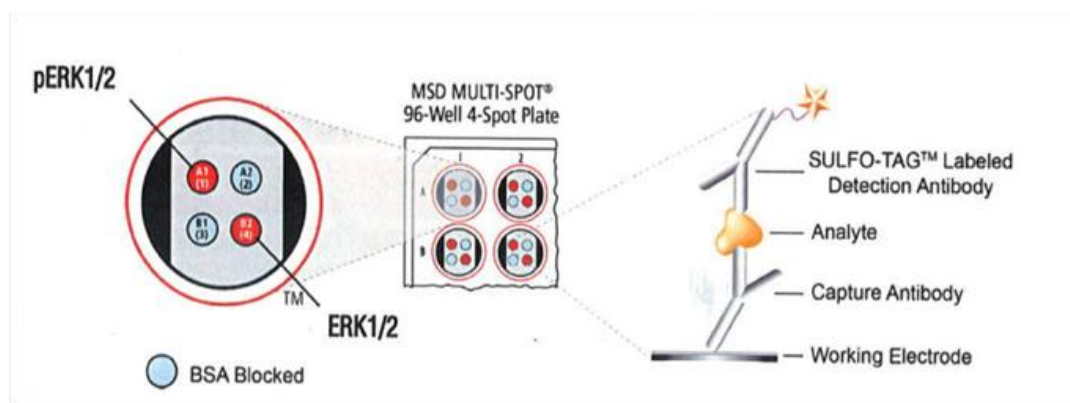
Figure 2.6.1 Diagram of the principle of the MSD phosphoERK /Total ERK sandwich immunoassay. A multiplex MSD plate which has been pre-coated with capture antibodies for phosphorylated ERK1/2 (Thr202/Tyr204; Thr185/Tyr187) and total ERK1/2 on spatially distinct spots is used. The user adds the sample and a solution containing the detection antibody—anti-total ERK1/2 conjugated with an electrochemiluminescent compound, MSD SULFO-TAG label—over the course of one or more incubation periods. The Analyte in the sample binds to the capture antibody which is immobilized on the working electrode surface; recruitment of the conjugated detection antibody by bound analyte completes the sandwich The user adds an MSD read buffer that provides the appropriate chemical environment for electrochemiluminescence and loads the plate into an MSD SECTOR® Imager for analysis. Inside the SECTOR Imager, a voltage applied to the plate electrodes causes the labels bound to the electrode surface to emit light. The instrument measures intensity of emitted light to provide a quantitative measure of phosphorylated ERK1/2 (Thr202/Tyr204; Thr185/Tyr187) and total ERK1/2 present in the sample. (Taken from MSD protocol).

read immediately using the SECTOR imager (MSD) and Discovery Workbench software. The SECTOR imager expresses the amount of phosphoERK and total ERK bound in each well in arbitrary light units. The percentage phosphoERK is calculated using the following equation, as recommended by the manufacturer:

((2 x phosphoERK signal)/(phosphoERK signal + Total ERK signal))*100

The above equation assumes that the capture antibodies for both phosphoERK and total ERK have similar binding affinities and so half the phosphoERK will bind to the phospho-specific and half to the total. The data are then expressed as the % phosphoERK (pERK).

2.7 Proliferation assay.

2.7.1 Principle of the BrdU proliferation assay.

Cellular proliferation requires replication of genomic DNA, therefore DNA synthesis is an indirect measure of cell proliferation. Traditionally [^{3}H]-thymidine incorporation had been used to label the DNA of replicating (cycling) cells but this has now been replaced by a non-radioactive alternative, 5-bromo-2'-deoxyuridine (BrdU). The assay is based on the detection of BrdU which has been incorporated into the genomic DNA of proliferating cells following incubation with the BrdU label for 4 hours (Figure 2.7.1).

2.7.2 Proliferation assay protocol.

Hepatic stellate cells were plated out (human and mouse cells at 100,000 per well) in flat-bottomed 96 well plates were incubated overnight at 37°C in 5% CO_2 in growth medium. The following day the growth medium was replaced with 0.1% serum-containing medium for 24 h. 24 h later the medium was replaced with 100 μl of 0.1% serum-containing medium with the addition of 0.2 mM ascorbic acid. Mouse and human PDGF-BB was reconstituted at 10 μg/ml in sterile 4 mM hydrochloric acid containing 0.1% bovine serum albumin (BSA) and stored in small aliquots at -20°C Cells were then incubated with PDGF-BB and compounds for 24 h at 37°C in 5% CO_2. After 24 h, 10μl of BrdU labelling solution as per kit's instructions was added to the cells plates. The plates were then incubated for a further 4 h at 37°C in 5%
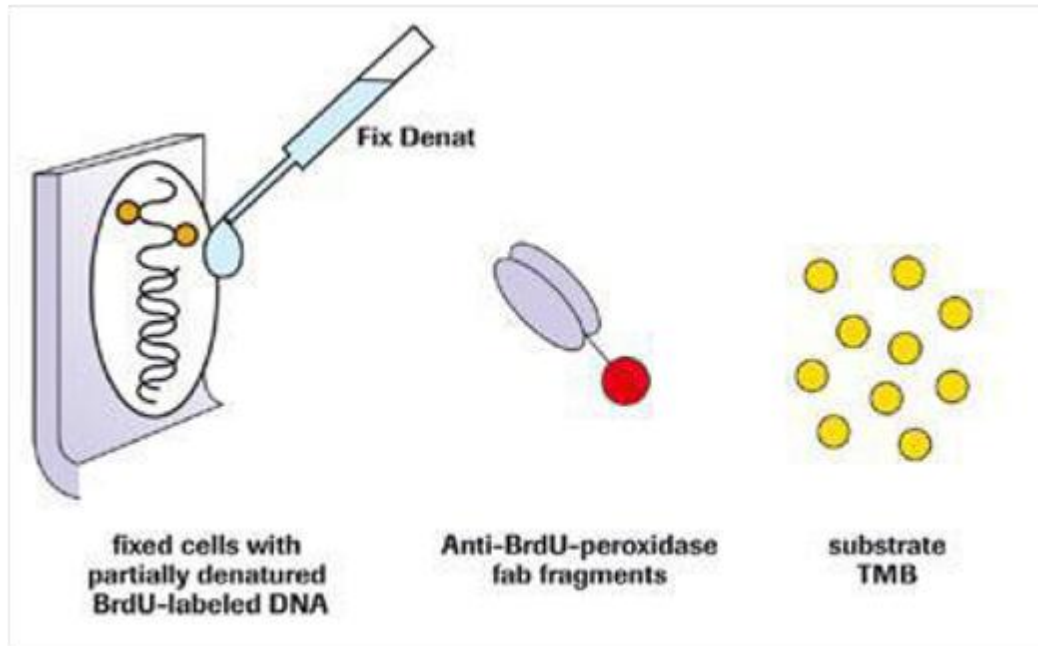
Figure 2.7.1   Picture showing the principle of the BrdU colorimetric proliferation assay. The cells are incubated with the test substance for a period of time. The pyrimidine analogue BrdU is added and incubated for a period of time (2-24 h). This allows incorporation in place of thymidine into the DNA of the proliferating cells. The cells are then fixed and the DNA denatured. Addition of the anti-BrdU-POD binds to the newly synthesised cellular DNA. The immune complex is detected by addition and incubation of tetramethyl-benzidine (TMB) substrate as absorbance in a spectrophotometer. The developed colour and absorbance values directly correlating with the amount of DNA synthesis, which correlates to the number of proliferating cells. (Taken from the kit protocol).

CO_2. The medium was aspirated and replaced with 200 µl of FixDenature solution and incubated at room temperature for 30 min. The FixDenature solution was removed and replaced with 100 µl per well of the anti-BrdU-POD solution (anti-BrdU-peroxidase fab fragment), as per kit's instructions.

The plates were incubated for 90 min at room temperature before being washed 3 times with 200 µl of washing solution followed by a wash with 200 µl of PBS. 100 µl of tetramethyl-benzidine (TMB) substrate solution was added to the wells and the plates placed on the plate shaker for 5 min at 6000 rpm. Plates were then read on a Tecan Sapphire at 370 nm with a reference wavelength of 492 nm after 20 min.

2.8   Scar-in-a-jar assay protocol.

2.8.1   Principle of the Scar-in-a-jar assay.

The Scar-in-a-jar model allows an *in vitro* study of fibrogenesis. In a monolayer fibroblast culture, collagen deposition is slow due to the limiting enzymatic conversion of pro-collagen to collagen (Lareu et al., 2007). This is overcome by the introduction of macromolecule 'crowding', with addition of a neutral ficoll cocktail, into the culture media, mimicking the highly crowded environment found *in vivo* (Chen et al., 2009). The macromolecules occupy a significant volume resulting in the excluded volume effect. This enhances the protelytic cleavage of procollagen to collagen and the activity of lysyl oxidase catalysing the formation of collagen triple helices, resulting in an accelerated mode of collagen I deposition in a reticular formation in a 6 day culture (Chen, 2009). Collagen deposition can then be quantified by immunofluorescence and *in situ* optical analysis. This allows study at all stages of the biosynthetic cascade of collagen production and the assessment of anti-fibrotic compounds targeting epigenetic to an extracellular level (Chen, 2009).

2.8.2   Scar-in-a-jar assay protocol.

HSCs were plated at the required seeding density, which unless specified is routinely 10000 cells per well, on clear-bottomed, black, tissue culture-treated sterile 96-well plates. Following overnight incubation the growth medium was replaced with 85 µl of low-serum medium (growth medium with only 0.4% FCS) for 24 h. The crowding

medium (low-serum growth medium containing Ficoll 70 at 112.5 mg/ml, Ficoll 400 at 75 mg/ml and L-ascorbic acid at 50 μg/ml) was prepared. Mouse and human TGFβ$_1$ was reconstituted at 10 μg/ml in sterile 4 mM hydrochloric acid containing 0.1% BSA and stored in small aliquots at -20ºC. TGFβ$_1$ was diluted into the crowding medium and compounds were diluted in crowding medium and added to the plates to give a final volume of 150 μl per well. Following 72 h incubation at 37ºC in 5% CO$_2$ the plates were fixed by the addition of 100 μl of ice-cold methanol for 2 min.

2.8.3 Scar-in-a-jar immunocytochemistry.

The fixed cells were permeabilised by treating with 0.1% Triton-X-100 solution in PBS for 90 s at room temperature and washed with PBS three times. The primary anti-collagen 1 antibody was incubated with the permeabilised cells overnight at 4°C following the PBS wash. Cells were washed with 0.05% (v/v) Tween-20 in PBS to remove non-specific staining. The Alexa Fluor 488 goat anti-mouse IgG secondary antibody was added at a 1:500 dilution and Hoechst 33342 solution was added at 1:10000 dilution to detect the anti-collagen primary antibody and stain nuclei. Following a 1 h incubation at room temperature, the plates were washed with 0.05% Tween-20 in PBS and stored in PBS at 4°C.

For mouse HSCs the fluorescence was visualised by the Cell Insight with the total cell number via the Hoechst nuclei staining in Channel 1, and extracellular type I collagen deposited within the matrix, with Alexa Fluor 488 detection antibody in Channel 2. The MEAN_CircRingAvgIntenDiffCh2 (measures the average pixel intensity of the nuclei minus the average pixel intensity of defined areas without the nuclei (representing collagen deposition)) was determined by an algorithm, which was inverted (multiplied by -1) before CRC analysis. For the human HSCs, data was collected from the InCell2000 using the following parameters; Total Granule Area, Total Granule Area/Cell, Total Granule Intensity and Nuclei Count for analysis in Excel.

2.9 *In Vivo* liver injury model.

This assay was carried out by a multidisciplinary group within GSK. The methodology for this assay is set out in Chapter 9: Appendix (Section 9.4). I was involved in determining the dose selection for the experiment and the further interpretation of the data obtained.

2.9.1 Compound dose selection.

Before embarking on the *in vivo* model work, identification of the compounds to use, formulation and dose to administer was carried out. Three 5-HT$_{2A}$ and three 5-HT$_{2B}$ antagonists were identified as suitable candidates to investigate. Based on their selectivity across other receptors, stability of formulation and results from naïve mice pilot pharmacokinetic (PK) studies, volinanserin and GSK1606260A were chosen. The doses required to achieve about 90 and 99% occupancy were determined using the receptor specific functional pK$_i$ and data generated from the pilot PK study (See Chapter 9: Appendix, Section 9.4.2 for dose selection).

2.9.2 PK/PD analysis.

Further PK/PD analysis of the mean blood concentrations data was performed in which the mean blood concentrations of the different compounds doses (Figure 9.4.2) were expressed as a fraction of their K$_i$ at the target receptor (See Table 9.4.1). This normalises the mean blood concentrations for each compound dose to their respective 5-HT receptor affinities. Data generated from the assays was fitted using nonlinear regression analysis (four-parameter logistic equation with variable slope or a fixed slope (=1) "Y=Bottom + (Top-Bottom)/(1+10^(($LogEC_{50}$-X)*Hill Slope))"(Hill, 1909)) in Prism 6.04 (GraphPad Software San Diego, CA, USA) A statistical comparison of the data were carried out to determine the preferred model of analysis. The data was then plotted against the % PSR area obtained for each dose and the control (week 3 and week 8 controls) mean blood concentrations.

2.10 Data Analysis.

Concentration-response curves (CRC) were fitted to the data generated from the assays using nonlinear regression analysis (four-parameter logistic equation with

variable slope "Y=Bottom + (Top-Bottom)/(1+10^((LogEC$_{50}$-X)*HillSlope))"(Hill, 1909)) to obtain values for logEC$_{50}$, Hill slope, minimum response and maximum asymptote response using Prism 6.04 (GraphPad Software San Diego, CA, USA). Any pA$_2$ values were calculated using the equation :

pA$_2$ = log$_{10}$ (concentration ratio-1) - log$_{10}$ concentration of the antagonist used.

For the purpose of presentation of the mean fitted data, due to the variation in % basal fluorescence and % pERK response between experiments, the data was normalised to the maximum response of the control 5-HT CRC. Representative plots were used where data could not be normalised to maximum response.

All statistical analyses were completed using 6.04 (GraphPad Software, San Diego, CA, USA). All statistical comparisons were made using Student's unpaired or paired t-test and differences of $p < 0.05$ were considered to be statistically significant.

2.10.1 Two-Site Receptor Binding Model

A model was developed in order to investigate the interaction of two signals coming from the two receptors activated by the same agonist which contribute to the ERK response (Courtesy of David Hall). The final equation was used to construct CRCs (Equation 2.10.1). Full derivation of the model can be found in Chapter 9: Appendix (Section 9.3).

$$E = \frac{Emax\left(\frac{\tau_A[H]}{K_a} + \frac{\tau_B[H]}{K_b} + \frac{[H]^2(\tau_{A+B})}{K_aK_b}\right)}{1 + \frac{[H]}{K_b}(1 + \tau_B) + \frac{[H]}{K_a}(1 + \tau_A) + \frac{[H]^2(1 + \tau_{A+B})}{K_aK_b}}$$

Equation 2.10.1.

The parameters of affinity and efficacy for each individual receptor were adjusted in an iterative manner to define the final parameter values to model the experimental CRCs observed i.e. Emax of the system =1 , affinity of receptor 1, K$_A$ =30nM, affinity of receptor 2 K$_B$= 3μM, efficacy for receptor Aτ_A = 5 and efficacy for receptor Bτ_B = 5

CHAPTER 3: PHENOTYPING OF MOUSE HEPATIC STELLATE CELLS.

3.1 Introduction.

The development of methods to isolate HSCs from rodents in the 1980's has been key in defining the role of HSCs in the pathogenesis of hepatic fibrosis (Friedman and Roll, 1987; Friedman et al., 1992). This method has been further modified for human tissue to allow the isolation, and culture of HSCs from normal human liver sections within 48 hr of harvest (Friedman et al., 1992). HSCs when grown in culture on plastic have been demonstrated to differentiate into myofibroblast-like cells which proliferate, showing reduced retinoid content and secreting ECM after being in culture for over a week (Friedman et al., 1992). The ability to culture the HSCs for *in vitro* assays has enabled their role in driving fibrogenesis to be explored.

The method of isolation employed in these studies relied on isolating the HSC using density gradient centrifugation. The HSCs are isolated at the top of the gradient due to their retinoid droplet content, which makes them less dense and more buoyant. This method tends to yield HSCs of high viability and purity (Friedman and Roll, 1987; Friedman et al., 1992) with low contamination from other cells in the liver, such as hepatocytes, Kupffer and sinusoidal endothelial cells (Friedman and Roll, 1987). Immunocytochemical identification of the population of cells in culture needs to be undertaken to confirm the cells are HSCs and that they have activated in culture.

This chapter explores the immunocytochemical characterisation of the cells isolated from the mouse that have been used in the experiments in this thesis in Chapters 4 and 5. Confirmation of the identity of the cells, and that a single population of HSCs were isolated, is crucial for the interpretation of the data in this thesis.

3.2 Results.

3.2.1 Antibody staining of mouse hepatic stellate cells.

Mouse HSCs were isolated from livers and cultured on plastic for 21- 28 days before being used for *in vitro* experiments or characterisation of the cells using immunocytochemical staining. Culturing the isolated HSCs on plastic provides the stimulus, due its stiffness, to activate the cells, causing them to undergo a phenotypic

change into a myofibroblast cell. These cells express distinct cytoskeletal and cell surface markers. The fluorescent Hoechst nuclear stain (blue) has been used in all the experiments to identify individual cells.

Cells from three different batches of mouse HSC cells were found to immunofluorescently stain positively for expression of α-SMA (red), which is the most reliable marker of stellate cell activation (Figure 3.2.1). The α-SMA staining highlighted the cytoskeletal fibre definition of the HSCs in all three batches. This confirmed that the stellate cells have undergone a phenotypic change during culture to become activated stellate cells. These feature are consistent with cells observed *in situ* during liver fibrosis (Figure 3.2.1). In all the images the stain was coincident with the nuclear stain, with no other discrete cells visible, suggesting the presence of just activated HSCs in the population of cells in culture.

The three batches of mouse cells were also immunofluorescently stained for the presence of desmin, which is considered as a phenotypic marker for HSCs in rat HSCs (Yokoi et al., 1984). Not all the cells in each batch were found to stain positively for desmin (green) (Figure 3.2.2), as there are blue nuclei with no desmin staining associated. This indicates that there are two distinct populations of mouse HSCs, a desmin and α-SMA positive population and a desmin negative and α-SMA positive population.

Glial fibrillary acidic protein (GFAP), a marker for quiescent HSCs, was evaluated in these batches of cells along with α-SMA. As expected no staining with GFAP (red) was observed in these cells, just blue nuclei although positive for α-SMA (green) (Figure 3.2.3). Positive staining was observed with synaptophysin (green) (Figure 3.2.4), a marker of quiescent and activated HSCs (Cassiman et al., 1992), in two batches tested. α-SMA (red) was also found to be present on the same cells (Figure 3.2.4). Once the two stains were merged, both markers were demonstrated to be present on the same population of cells (Figure 3.2.4).

Kupffer and sinusoidal endothelial cells are the most likely cell types that can contaminate the HSCs population following isolation. Two markers, anti-CD68, a
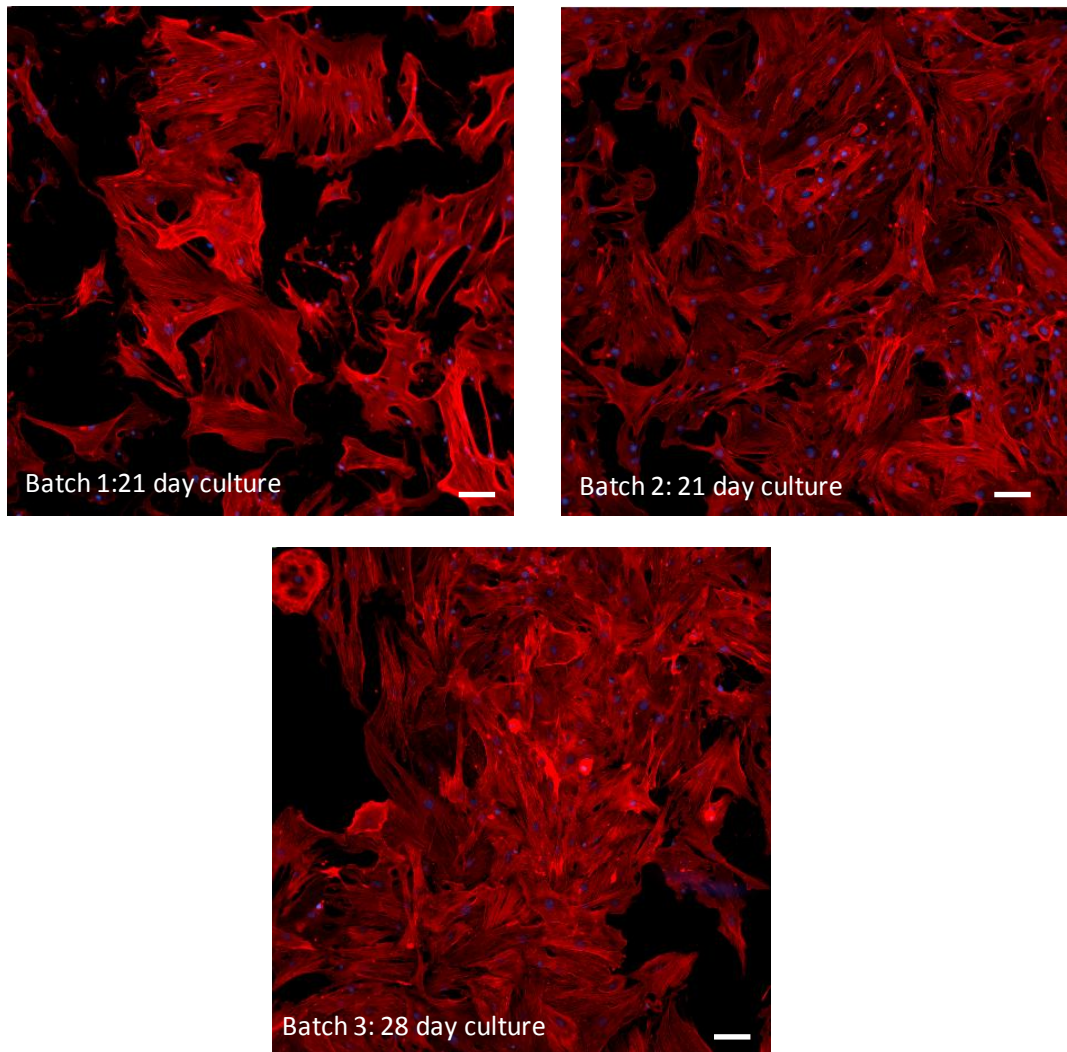
Figure 3.2.1   α-SMA immunofluorescent staining (red) of three batches of mouse HSCs kept in culture on plastic. Isolated mouse HSC, which had been in culture on plastic for 21 or 28 days, were plated out at 5000 cells per well in a black 96 well plate in growth medium. Cells were fixed with ice cold methanol, stained first with primary antibody, rabbit α-smooth muscle actin and then the secondary antibody Alexa Fluor® 647, along with Hoechst nuclear stain (blue stain). The plate was imaged on an InCell Analyser 6000 and image analysis carried out using Columbus software (See Chapter 2: Material and Methods). Data shown are a representative area from a single well for each batch. Scale bar =100 μm for all images.
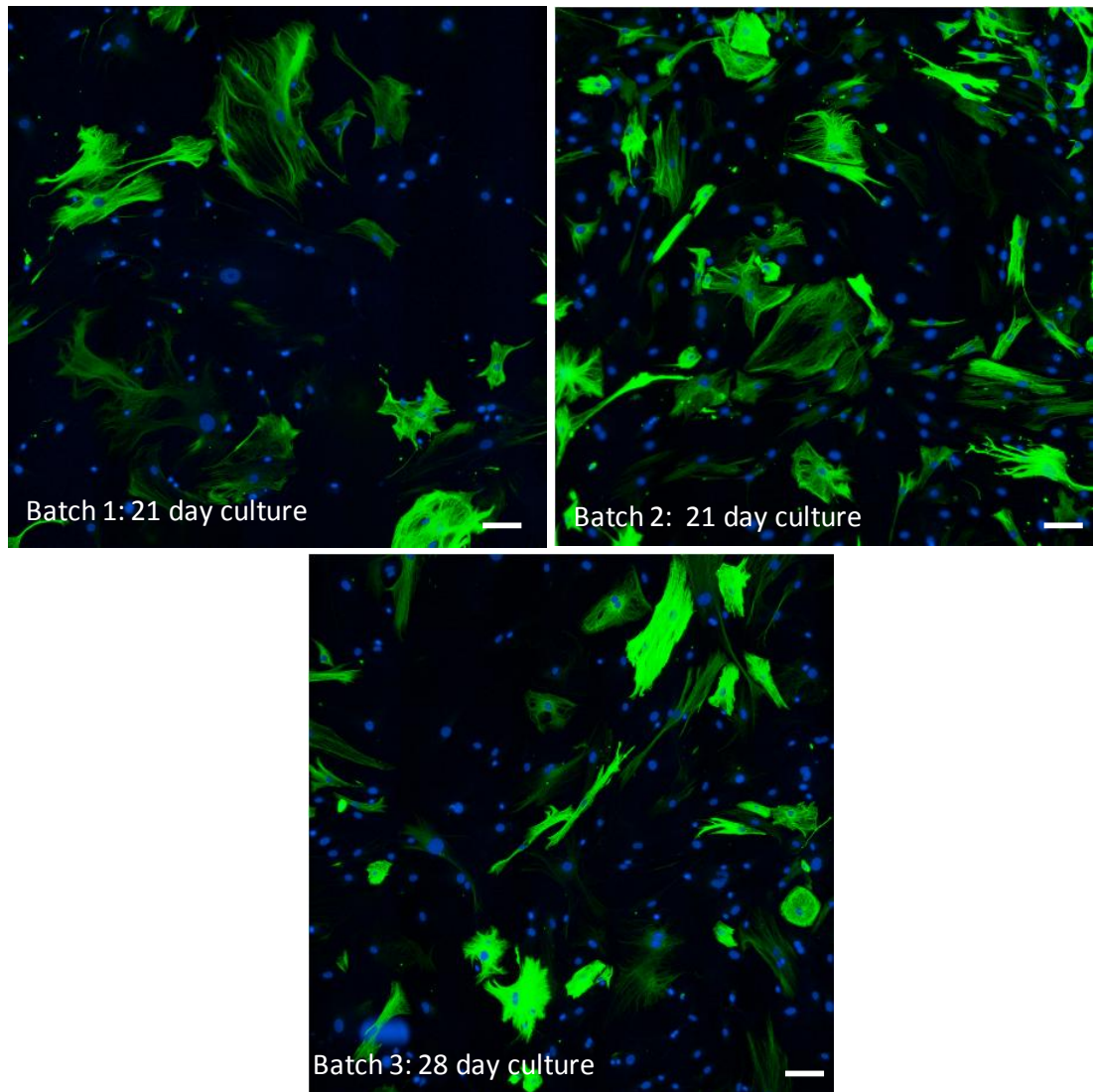
Figure 3.2.2   Desmin immunofluorescent staining of three batches of mouse HSCs kept in culture on plastic. Isolated mouse HSC, which had been in culture on plastic for 21 or 28 days, were plated out at 5000 cells per well in a black 96 well plate in growth medium. Cells were fixed with ice cold methanol, stained first with primary antibody, rabbit desmin and then secondary antibody Alexa Fluor® 647, along with Hoechst nuclear stain. (blue stain) The plate was imaged on n InCell Analyser 6000 and image analysis carried out using Columbus software (See Chapter 2: Material and Methods). Data shown are a representative area from a single well for each batch. Scale bar =100 μm for all images.
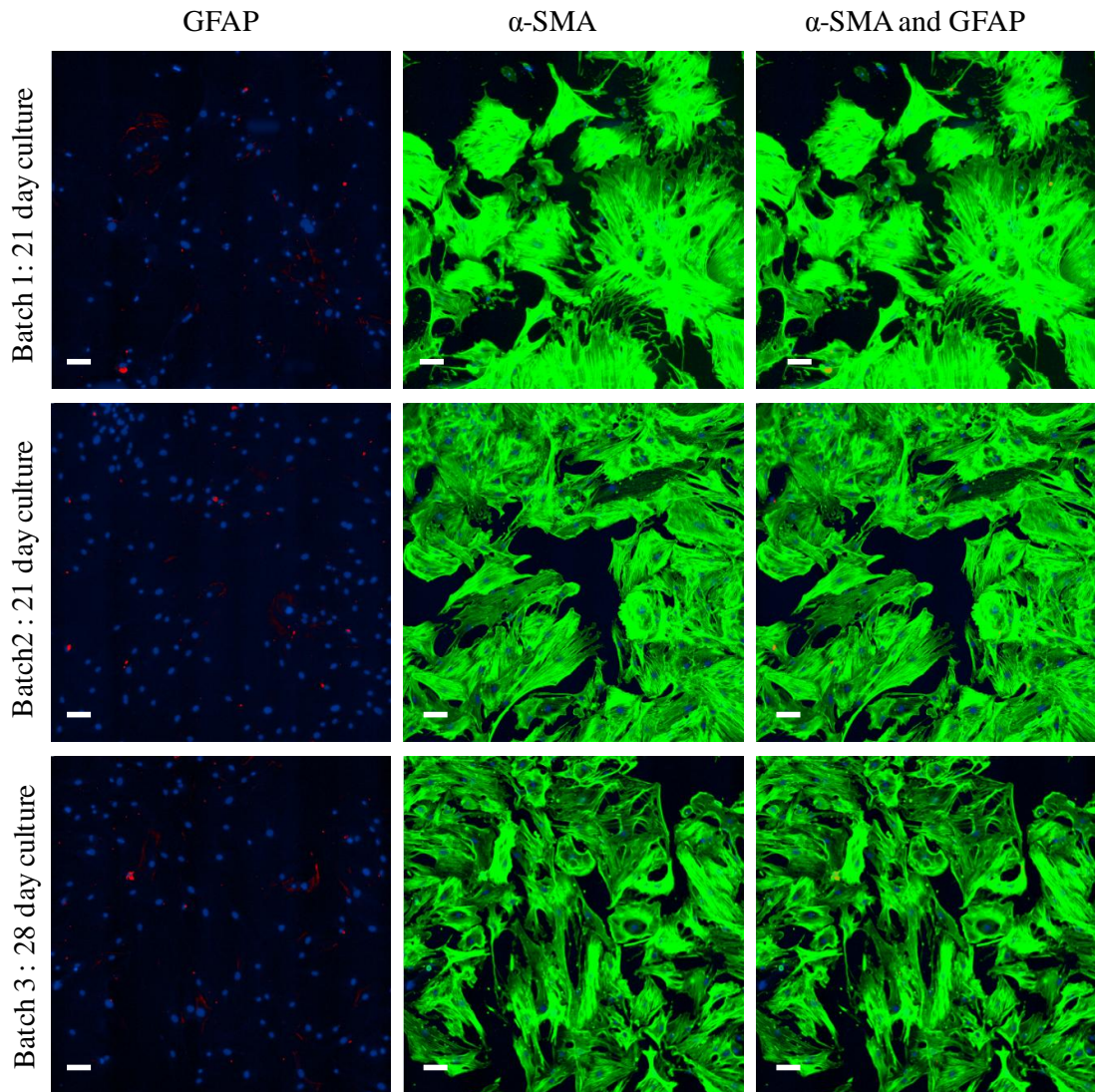
Figure 3.2.3 **Immunofluorescent co-staining of α-SMA (Green) and GFAP (Red) of three batches of mouse HSCs kept in culture on plastic**. Isolated mouse HSC, which had been in culture on plastic for 21 or 28 days, were plated out at 5000 cells per well in a black 96 well plate in growth medium. Cells were fixed with ice cold methanol, stained first with primary antibody, rabbit α-smooth muscle actin and sheep GFAP, then secondary antibodies Alexa Fluor® 647 (red stain) and Alexa Fluor® 488 (green stain) along with Hoechst nuclear stain. (blue stain) The plate was imaged on an InCell Analyser 6000 and image analysis carried out using Columbus software (See Chapter 2: Material and Methods). Data shown are representative area from a single well for each batch. Scale bar =100 μm for all images.
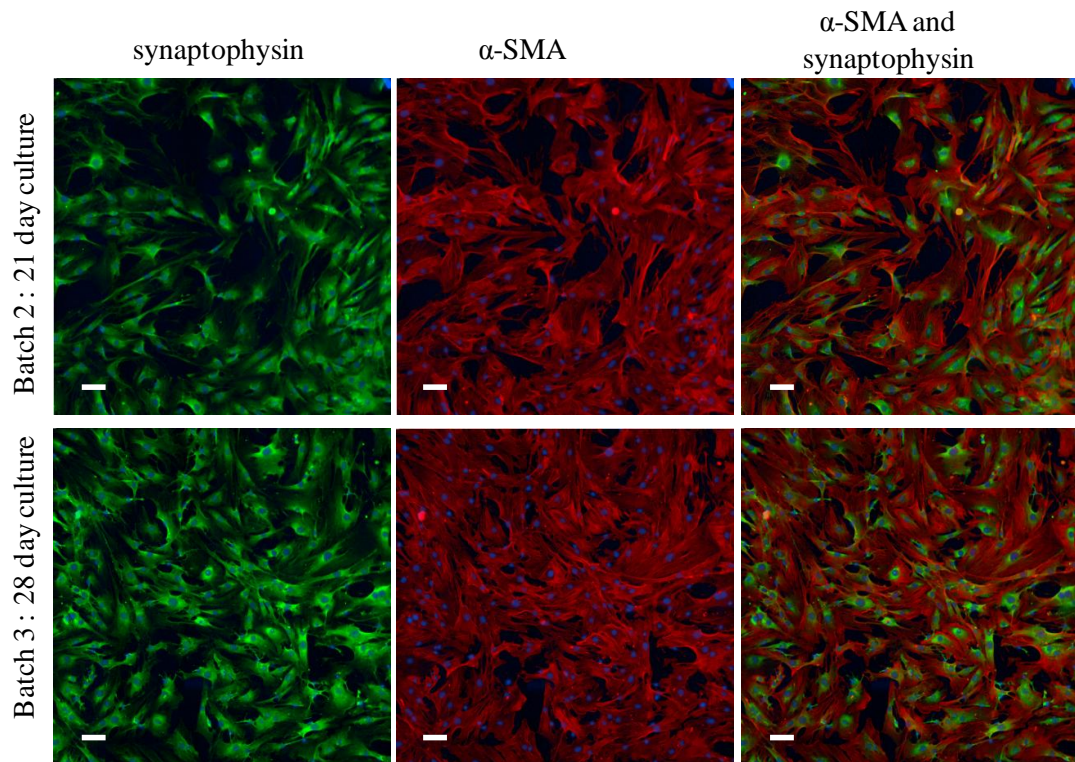
Figure 3.2.4   Immunofluorescent co-staining of synaptophysin (green) and α-SMA (red) of two batches of mouse HSCs kept in culture on plastic. Isolated mouse HSC, which had been in culture on plastic for 21 or 28 days, were plated out at 5000 cells per well in a black 96 well plate in growth medium. Cells were fixed with ice cold methanol, stained first with primary antibody, rabbit α-smooth muscle actin and mouse synaptophysin, then secondary antibodies Alexa Fluor® 647 (red stain) and Alexa Fluor® 488 (green stain) along with Hoechst nuclear stain. (blue stain) The plate was imaged on an InCell Analyser 6000 and image analysis carried out using Columbus software (See Chapter 2: Material and Methods). Data shown are representative area from a single well for each batch. Scale bar = 100 μm for all images.

Kupffer cell marker, and anti-CD31, present on both endothelial cells and Kupffer cells, were chosen to determine if these cell types were present in the batches of cells. No staining of any of the batches of positive α-SMA cells was observed with anti-CD68 (green) (Figure 3.2.5) or anti-CD31 (green) (Figure 3.2.6) alone or in combination with either anti-CD68 (Figure 3.2.5) or anti-CD31 antibodies (Figure 3.2.6). These results confirm no contamination with Kupffer cells and endothelial cells in the batches of HSCs isolated, which had been kept in culture for either 21 or 28 days.

A summary of the immunocytochemical staining obtained in these experiments confirms that the three batches of HSC stain positively for α-SMA and synaptophysin, with a population of cells staining for positively desmin (Table 3.2.1). No staining was observed with either GFAP, anti-CD68 and anti-CD31 in all three batches of cells (Table 3.2.1).

3.3   Discussion.

HSCs are recognised as one of the key mediators in the pathogenesis of hepatic fibrosis (Friedman 2000) and once activated these cells differentiate into a proliferative, persistent myofibroblast-like cell (Bachem et al., 1992: Friedman 2008). The experiments carried out in this thesis are reliant on these isolation methods of HSCs from the livers of mice. The cells, once isolated, were cultured on plastic to enable them to activate and differentiate into a myofibroblast-like cell. Immunocytochemical staining of the cells was undertaken to characterise the cells that had been isolated from the mouse livers and kept in culture.

α-SMA presence is a phenotypic marker for myofibroblasts and contractile fibroblasts, with the induction of α-SMA being the most reliable identifier of HSC activation (Friedman, 2008b). Marked α-SMA staining, with the cytoskeletal fibres being clearly visible, was observed in all three batches of cells which had been in culture for 21 or 28 days. All the cells stained positively for α-SMA indicating a pure population of activated HSCs. The mouse HSCs used in the *in vitro* experiments in this thesis were used between 14 and 35 days in culture, as after 14 days there were sufficient numbers of cells, following isolation, for immediate use in experiments,
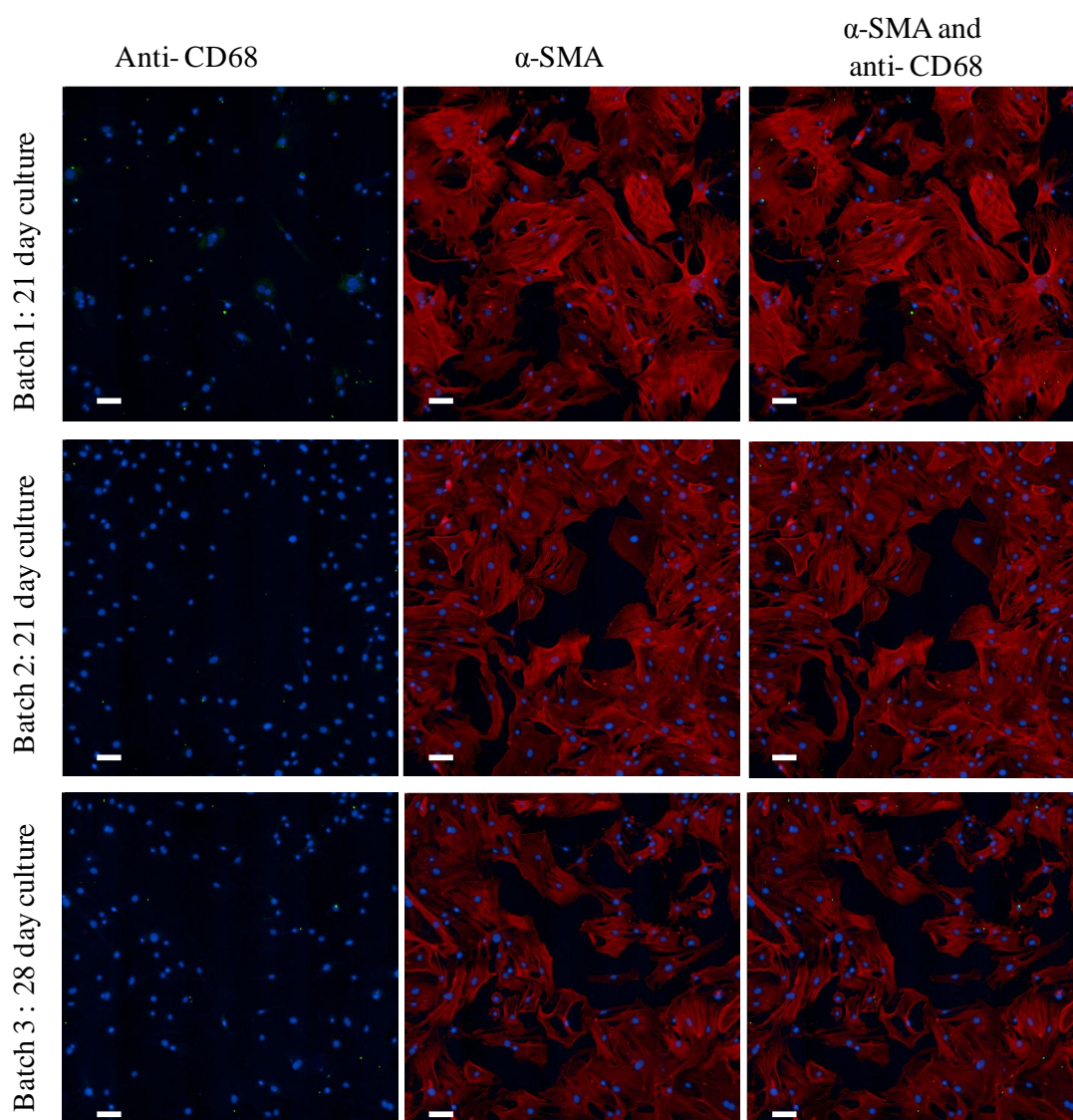
Figure 3.2.5 Immunofluorescent co-staining of α-SMA and anti-CD68 of three batches of mouse HSCs kept in culture on plastic. Isolated mouse HSC, which had been in culture on plastic for 21 or 28 days, were plated out at 5000 cells per well in a black 96 well plate in growth medium. Cells were fixed with ice cold methanol, stained first with primary antibody, rabbit α-smooth muscle actin and mouse anti-CD68, then secondary antibodies Alexa Fluor® 647 (red stain) and Alexa Fluor® 488 (green stain) along with Hoechst nuclear stain. (blue stain) The plate was imaged on an InCell Analyser 6000 and image analysis carried out using Columbus software (See Chapter 2: Material and Methods). Data shown are representative area from a single well for each batch. Scale bar = 100 μm for all images.
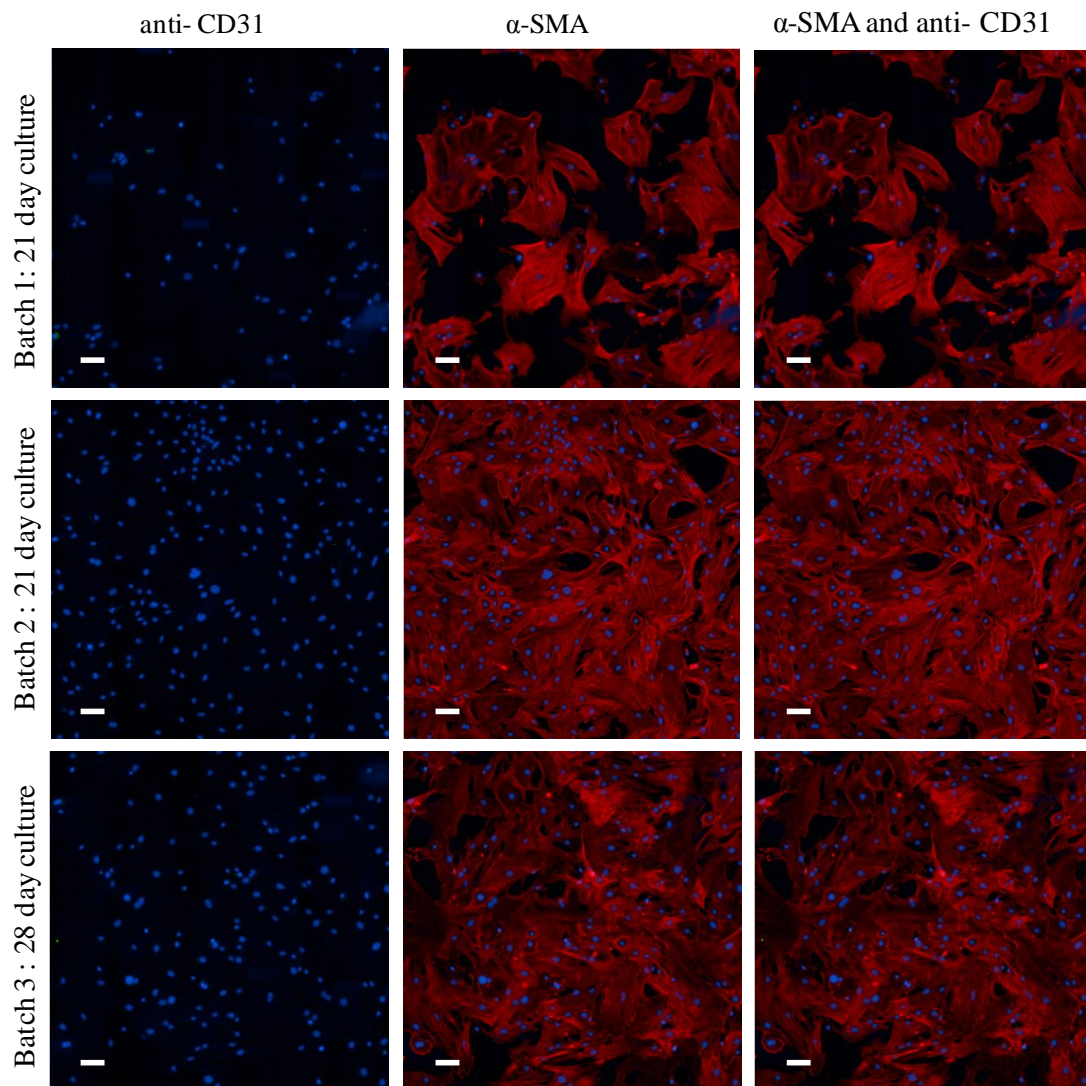
Figure 3.2.6 Immunofluorescent co-staining of α-SMA and anti-CD31 of three batches of mouse HSCs kept in culture on plastic. Isolated mouse HSC, which had been in culture on plastic for 21 or 28 days, were plated out at 5000 cells per well in a black 96 well plate in growth medium. Cells were fixed with ice cold methanol, stained first with primary antibody, rabbit α-smooth muscle actin and mouse anti-CD31, then secondary antibodies Alexa Fluor® 647 (red stain) and Alexa Fluor® 488 (green stain) along with Hoechst nuclear stain. (blue stain) The plate was imaged on an InCell Analyser 6000 and image analysis carried out using Columbus software (See Chapter 2: Material and Methods). Data shown are representative area from a single well for each batch. Scale bar = 100 μm for all images.

Marker	Batch 1	Batch 2	Batch 3
α-SMA	+	+	+
desmin	+/-	+/-	+/-
GFAP	-	-	-
synaptophysin	+	+	+
Anti-CD68	-	-	-
Anti-CD31	-	-	-

Table 3.2.1   Summary of the immunocytochemical staining of the different markers present on the three batches of HSCs tested. + = positive staining, - = no staining, **+/- =** not all cells stained positive.

or to keep in culture and freeze down for future experiments.

Another marker that is considered to identify activated HSCs is desmin (Yokoi et al., 1984), which is an intermediate filament protein of smooth muscle and is a marker of smooth-muscle related cells (Ballardini et al., 1994). The staining conducted identified cells that were positive for desmin in all the cultures but there were blue nuclei without out any evidence of associated desmin staining. It is reported that desmin is a phenotypic marker for HSCs in rats (Yokoi et al., 1984) where it is used to evaluate the purity of separated and cultured rat HSCs (Geerts et al., 1998). Desmin negative HSCs have been reported in rats and humans (Schmitt-Gräff et al., 1991; Friedman et al., 1992; Ballardini et al., 1994). In rat liver desmin positive HSC can be found in the periportal areas of the liver and in the pericentral area only 50% of the HSCs stain positively for desmin (Ballardini et al., 1994). The conclusion drawn was that desmin may only stain for a particular state of HSCs and may not be considered as a phenotypic marker of all HSCs, but a differentiation marker for HSCs (Ballardini et al., 1994). Vimentin, like desmin, is an intermediate filament protein of smooth muscle, is reported to be uniformly expressed on HSCs regardless of how long the cells have been in culture (Friedman et al., 1992) and is worth considering investigating in future studies.

Glial fibrillary acidic protein (GFAP) is an astrocyte marker and intermediate filament protein, which is closely related to vimentin and desmin, is also involved in the structure and function of cells' cytoskeleton (Neubauer et al., 1996). The expression of GFAP was demonstrated to be present on freshly isolated HSCs which was found to decrease with time in culture, whilst the expression of α-SMA increased (Buniatian et al., 1996; Neubauer et al., 1996). Maintenance of quiescent HSC has been achieved in culture, with the addition of a combined treatment of insulin and vitamin A, resulting in maintained GFAP without α-SMA expression (Yoneda et al., 2016). The cells stained in this chapter demonstrated no GFAP expression, but expression of α-SMA, providing further evidence that the cells used in these studies were activated HSCs. Synaptophysin, a transmembrane glycoprotein involved in neurotransmitter exocytosis, is reported to stain both quiescent and activated HSCs (Cassiman et al., 1992). Both cultures of HSCs tested co-stained for

the presence of synaptophysin and α-SMA, as would be expected from an activated HSC culture.

The HSC isolation method used is not expected to produce a completely pure population of HSCs. The most likely cell types expected to contaminate the HSC population are Kupffer cells, but also possibly sinusoidal endothelial cells (Friedman and Roll, 1987). To examine this the cells were co-stained with anti-α-SMA and either anti-CD68: specific for human macrophage (Kunisch, 2004), or anti-CD31, expressed on both endothelial cells and Kupffer cells, to determine if either of these cells types were present. None of the cells, which were positive for α-SMA expression, stained positively for either anti-CD68 or anti-CD31 suggesting that neither cell type was present in the culture. The cells had been in culture for over 14 days and it is reported that Kupffer cells are only able to be maintained in the HSC co-culture for about 14 days, before being overgrown by the HSCs (Friedman et al., 1992). This therefore may explain the absence of Kupffer cells in the cultures of HSCs tested.

Isolated human HSCs were also used in this thesis but the same 'in-depth' characterisation was not undertaken. The results of the studies with the human cells isolated are reported in Chapter 6. In conclusion the immunocytochemistry confirms that the mouse HSCs used in the experiments in this thesis were activated HSCs. We can therefore be confident that the data generated in Chapter 4 and 5 of this thesis is from the activated mouse HSCs.

Chapter 4: Pharmacological characterisation of the 5-HT receptor responsible for intracellular calcium release and ERK phosphorylation in mouse activated hepatic stellate cells.

4.1 Introduction.

As described in the introduction HSCs are recognised as one of the key mediators in the pathogenesis of hepatic fibrosis (Friedman, 2000). Once activated these cells differentiate into a proliferative, persistent myofibroblast-like cell which secretes ECM and TGFβ1 (Bachem et al., 1992; Friedman, 2008a). 5-HT now has been reported to promote the fibrogenic activity of HSCs (Ruddell et al., 2006, 2008; Ebrahimkhani et al., 2011; Kim et al., 2013). When HSCs are activated up-regulation of the 5-HT_{1B}, 5-HT_{2A} and 5-HT_{2B} receptors has been observed, suggesting that 5-HT may drive the fibrotic process by activating these receptor subtypes (Li et al., 2006; Ruddell et al., 2006; Park et al., 2011). The signalling pathway which follows 5-HT stimulation of the HSCs was shown to involve the activation of phospholipase C (PLC) leading to an increase in calcium (Park et al., 2011) and phosphorylation of ERK, followed by the activation of the transcription factor JunD and enhanced TGFβ1 expression (Ebrahimkhani et al., 2011).

The focus for this chapter is the pharmacological characterisation of the functional 5-HT receptors expressed on activated mouse HSCs, responsible for both the calcium release and phosphorylation of ERK responses, using selective agonists and antagonists at concentrations that only bind to the specific receptor of interest. The experiments will also explore the nature of the antagonism obtained in the assays and whether the presence of multiple 5-HT receptors contributes the response. The effects of 5-HT on calcium release in activated HSCs were investigated using measurement of a fluorescent calcium dye over time, in a 96 well plate format, following stimulation with different concentrations of 5-HT in the presence and absence of antagonists. A similar analysis of the ERK phosphorylation using a 96-well plate-based ELISA assay was performed to provide a quantitative measurement of ERK phosphorylation in HSCs, when stimulated. This 'in-depth' pharmacological analysis of the 5-HT concentration response in the presence of selective antagonists has not been carried out previously in the literature. Together these two assays providing a wealth of data with which to carry out the pharmacological characterisation. This analysis will provide a definitive identification of the 5-HT receptor subtype present on HSCs which is lacking in the literature.

4.2 Results.

4.2.1 Measurement of 5-HT stimulated intracellular calcium signal in mouse hepatic stellate cells.

Initial studies were carried out to investigate whether 5-HT was capable of stimulating an intracellular calcium signal in the mouse HSCs. A standard calcium-stimulated release protocol for the FLIPR assay, which had been used for different primary cells, was followed. A concentration-dependent increase in fluorescent intracellular calcium signal (Fluo-4) was observed following addition of 5-HT with a pEC_{50} of approximately 7.0 (Figure 4.2.1). To confirm that the cells were responding as expected, 100 µM adenosine triphosphate (ATP) was used as a positive control, through its stimulation of a calcium response via endogenously expressed P2Y receptor (Dranoff et al., 2004). Examination of the kinetics of the 5-HT response showed a rapid increase with a sustained maximum response being reached about 10 s after addition of 5-HT (Figure 4.2.2). The kinetics and peak response to ATP was similar to that of the 5-HT response (Figure 4.2.2), although there was a small reduction in signal upon addition of the 5-HT/ATP. This is a pipetting artefact due to the increase in the volume of the well following the addition, which has a small effect on the fluorescence signal.

4.2.2 Pharmacological characterisation of the 5-HT receptor responsible for the $[Ca^{2+}]$ increase in mouse hepatic stellate cells.

$5-HT_{2A}$, $5-HT_{2B}$ and $5-HT_{1B}$ receptors are reported to be up-regulated in activated HSCs (Ruddell et al., 2006; Li et al., 2006; Park et al., 2011) and due to their coupling through G_q, are most likely to be involved in the 5-HT stimulation of calcium. However the $5-HT_{1B}$ receptor couples through G_i and this cannot be ruled out, as it is possible to activate G_i coupled receptors in this assay format (Hall et al., 1999; Werry et al., 2002). To characterise the 5-HT receptor involved in stimulating the calcium response, selective antagonists for the $5-HT_{2A}$ (ketanserin and volinanserin), $5-HT_{2B}$ (GSK1606260A and RS127445) and $5-HT_{1B}$ (cyanopindolol) receptors were used. The concentration of the antagonists used were chosen carefully based on their selectivity range for the receptor of interest. The affinities for both
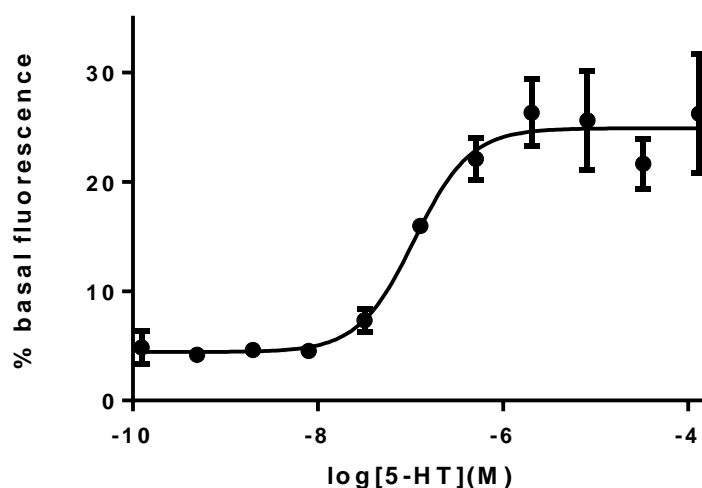
Figure 4.2.1   5-HT concentration-response curve obtained in mouse HSCs in the FLIPR assay. Stellate cells were loaded with fluorescent dye (FLUO-4AM) for 1 h before being stimulated with increasing concentrations of 5-HT in the FLIPR. (See Chapter 2: Materials and Methods). Data was captured and analysed to obtain the basal signal and maximum stimulated fluorescence above basal for each concentration, with the response being expressed as a percentage of the basal fluorescence. CRC was fitted using non-linear regression analysis (four-parameter logistic equation with variable slope (Hill, 1909)) (See Chapter 2: Data Analysis section). 5-HT CRC are from the mean ± SEM from 3 replicate CRCs in singlicate.
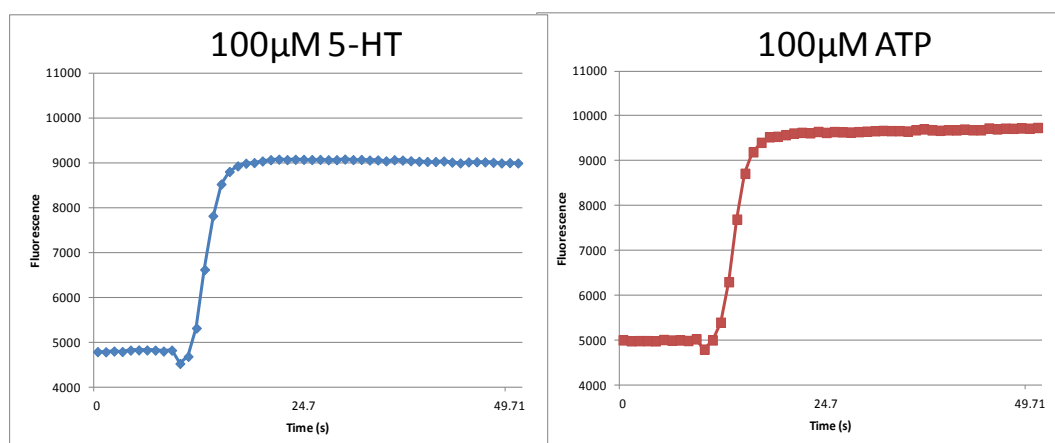
Figure 4.2.2   5-HT and ATP response obtained in mouse HSCs in the FLIPR assay. Stellate cells were loaded with fluorescent dye (FLUO4) for 1 h before being stimulated with 5-HT (100 μM) and ATP (100 μM) in the FLIPR. (See Chapter 2: Materials and Methods). Data was captured and analysed to obtain the basal signal, before addition of the stimulus and maximum stimulated fluorescence. Data presented are the response taken from a single well from an individual experiment.

mouse $5\text{-}HT_{2A}$ and $5\text{-}HT_{2B}$ receptors have been confirmed in a simple recombinant assay system (Table 4.2.1 See Chapter 9: Appendix, Section 9.2 for recombinant CHO cell assay method). Literature data was also used to determine acceptable concentration ranges to use for $5\text{-}HT_{2A}$, $5\text{-}HT_{2B}$ and $5\text{-}HT_{1B}$ compounds (See section 1.10, Table 1.10.1 to 1.10.3). To confirm if any of the antagonists used have a non-specific effect on calcium signalling, single concentrations of ketanserin (100 nM), GSK1606260A (1 μM) and cyanopindolol (1 μM) were tested against ATP concentration-response curves (CRCs). The ATP CRCs in the presence of all three of the antagonists overlaid the ATP CRC in the absence of the antagonists (Figure 4.2.3) showing that the antagonists were not acting non-specifically on calcium signalling.

To investigate the relative contributions of $5\text{-}HT_{2B}$ and $5\text{-}HT_{1B}$ receptor to the response, 5-HT CRCs were generated in the presence (15 min pre-incubation) and absence of 1 μM GSK1606260A or 100 nM RS-127445 or 1 μM cyanopindolol. 5-HT produced a concentration-dependent increase in intracellular calcium associated with a similar pEC_{50} to that obtained previously (Figure 4.2.1). GSK1606260A or RS-127445 or cyanopindolol did not produce a rightward shift in 5-HT CRC, and pEC_{50} values were similar to those obtained in the absence of the antagonists (Figure 4.2.4, Table 4.2.2). A concentration of either 1 μM GSK1606260A or 100 nM RS-127445 (assuming a competitive interaction with the $5\text{-}HT_{2B}$ receptor) would be expected to produce a > 1000-fold rightward shift of the 5-HT CRC, as predicted from its fpK_i of 10.2 and 10.8 respectively (Table 4.2.1). If 5-HT had been eliciting the response through the $5\text{-}HT_{1B}$ receptor then a > 500-fold shift of the 5-HT CRC would be expected to have been observed with cyanopindolol. These results indicate that the $5\text{-}HT_{2B}$ and $5\text{-}HT_{1B}$ receptor are not responsible for the 5-HT-stimulated calcium response in the HSCs.

To determine if the $5\text{-}HT_{2A}$ receptor was the receptor mediating the 5-HT stimulated calcium response, 5-HT CRCs were generated in the presence of three different concentrations (1, 10 and 100 nM) of ketanserin or volinanserin. Rightward shift and depression of the maximum 5-HT response was observed with ketanserin (Figure 4.2.5, Table 4.2.3 A), with the 100 nM concentration completely blocking

	mouse 5-HT$_{2A}$ fpK$_i$	mouse 5-HT$_{2B}$ fpK$_i$
Ketanserin	10.1 ± 0.2	<5
Volinanserin	10.8 ± 0.1	5.4 ± 0.2
GSK1606260A	5.4 ± 0.3	10.2 ± 0.2
RS-127445	6.9 ± 0.1	10.8 ± 0.1

Table 4.2.1   fpK$_i$ value obtained for ketanserin, volinanserin, GSK1606260A and RS-127445 in mouse recombinant 5-HT$_{2A}$ and 5-HT$_{2B}$ receptor calcium assays. CGE222 cell expressing mu5-HT$_{2A}$ or 5-HT$_{2B}$ were loaded with fluorescent dye (FLUO-4AM) for 1 h before stimulation with an EC$_{80}$ concentration of 5-HT in the presence or absence of increasing concentrations of antagonists. (See Chapter 9: Appendix, Section 9.2). Data presented are mean values $\pm$ SEM from three experiments.

A T P
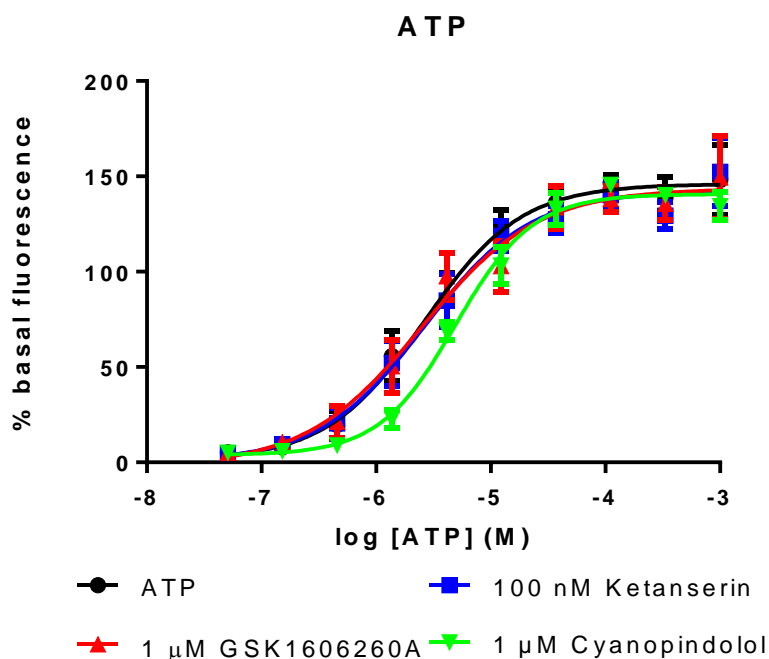
	ATP	100 nM Ketanserin	1 μM GSK1606260A	1 μM cyanopindolol
Max Response	144.4 ± 7.7	140.8 ± 6.7	148.3 ± 9.7	140.9
pEC_{50}	5.62 ± 0.2	5.63 ± 0.2	5.55 ± 0.2	5.32
Hill slope	1.20 ± 0.1	1.09 ± 0.04	1.11 ± 0.1	1.32

Figure 4.2.3   ATP CRCs and fitted curve parameters obtained in the presence and absence of ketanserin, GSK1606260A and cyanopindolol in mouse HSCs in the FLIPR™ assay. HSCs were loaded with fluorescent dye (FLUO-4AM) for 1 h before stimulation with increasing concentrations of ATP in the presence and absence of a single concentration of the antagonists in the FLIPR™. (See Chapter 2: Materials and Methods). Data were captured and analysed to obtain the basal fluorescence response and maximum stimulated fluorescence response above basal fluorescence response for each concentration, with the response being expressed as a percentage of the basal fluorescence. CRCs were fitted using non-linear regression analysis (four-parameter logistic equation with variable slope (Hill, 1909)) (See Chapter 2: Data Analysis section). ATP CRC and fitted curve parameters shown are mean values ± SEM from 3 experiments carried out in duplicate except cyanopindolol which was from 2 experiments.
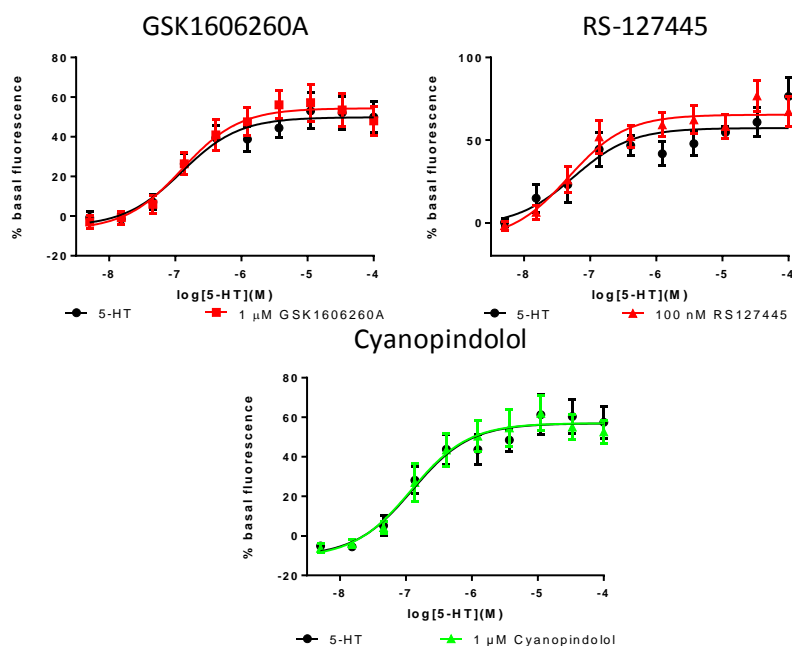
Figure 4.2.4 Effect of GSK1606260A (1 μM), RS-127445 (100 nM) and cyanopindolol (1 μM) on the 5-HT CRC in the mouse HSC FLIPR™ assay. HSCs were loaded with fluorescent dye (FLUO-4AM) for 1 h before stimulation with increasing concentrations of 5-HT in the presence and absence of a single concentration of the antagonists in the FLIPR™. (See Chapter 2: Materials and Methods). Data were captured and analysed to obtain the basal fluorescence response and maximum stimulated fluorescence response above basal fluorescence response for each concentration, with the response being expressed as a percentage of the basal fluorescence. CRCs were fitted using non-linear regression analysis (four-parameter logistic equation with variable slope (Hill, 1909)) (See Chapter 2: Data Analysis section). Data shown are mean values ± SEM from 3 or more individual experiments carried out in duplicate.

	5-HT	**1 μM GSK1606260A**		**5-HT**	**100 nM RS-127445**
Max Response	50.0 ± 11.8	54.3 ± 11.3		58.0 ± 8.0	66.1 ± 7.9
pEC_{50}	6.89 ± 0.1	6.82 ± 0.1		7.37 ± 0.4	7.29 ± 0.2
Hill slope	1.25 ± 0.3	1.47 ± 0.3		0.97 ± 0.03	1.01 ± 0.01

	5-HT	**1 μM cyanopindolol**
Max Response	57.6 ± 13.0	56.1 ± 10.9
pEC_{50}	6.89 ± 0.1	6.83 ± 0.1
Hill slope	0.99 ± 0.1	1.42 ± 0.3

Table 4.2.2 5-HT CRC parameters obtained in the presence and absence of GSK1606260A (1 μM), RS-127445 (100 nM and cyanopindolol (1 μM) in the mouse HSC FLIPR™ assay. Data represents the mean of the individual parameters obtained from fitting the data from individual experiments represented in Figure 4.2.4 using non-linear regression analysis (four-parameter logistic equation with variable slope (Hill, 1909)) (See Chapter 2: Data Analysis section). Data shown are mean values ± SEM from 3 or more individual experiments carried out in duplicate.
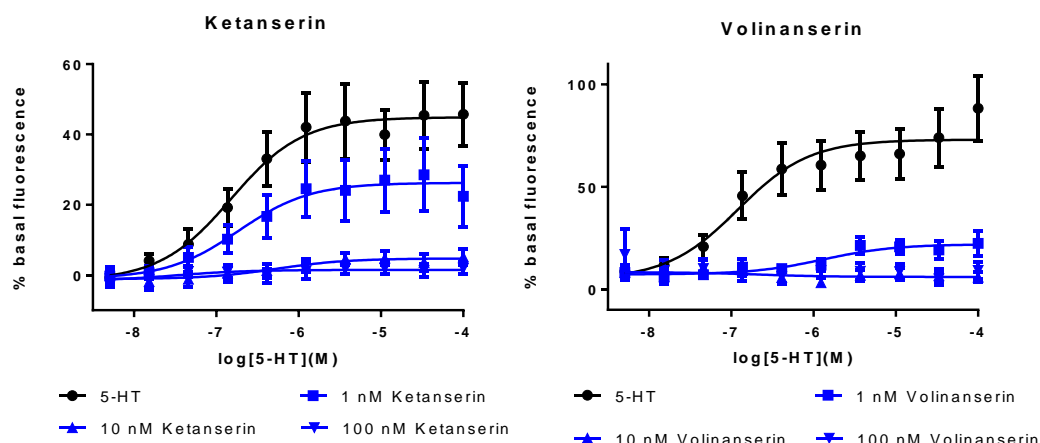
Figure 4.2.5 Effect of ketanserin and volinanserin (1, 10 and 100 nM) on the 5-HT CRC in the mouse HSC FLIPR™ assay. HSCs were loaded with fluorescent dye (FLUO-4AM) for 1 h before stimulation with increasing concentrations of 5-HT in the presence and absence of the antagonists in the FLIPR™. (See Chapter 2: Materials and Methods). Data were captured and analysed to obtain the basal fluorescence response and maximum stimulated fluorescence response above basal fluorescence response for each concentration, with the response being expressed as a percentage of the basal fluorescence. CRCs were fitted using non-linear regression analysis (four-parameter logistic equation with variable slope (Hill, 1909)) (See Chapter 2: Data Analysis section). Data shown are mean values ± SEM from 3 or more experiments carried out in duplicate.

A	Ketanserin			
	5-HT	1 nM	10 nM	100 nM
Max Response	44.5 ± 13.4	26.2 ± 15.5	*9.2± 2.3	*4.5 ± 2.2.
pEC$_{50}$	6.67 ± 0.2	6.31 ± 0.4	#6.38	
Hill slope	1.33 ± 0.2	1.16 ± 0.2		

B	Volinanserin			
	5-HT	1 nM	10 nM	100 nM
Max Response	71.5 ± 19.6	25.5 ± 7.9	*8.9 ± 4.0	*11.6 ± 5.6.
pEC$_{50}$	6.75 ± 0.2	6.07 ± 0.2	#6.67	
Hill slope	1.16 ± 0.1	0.79 ± 0.1		

Table 4.2.3   5-HT CRC parameters obtained in the presence and absence of (A) ketanserin and (B) volinanserin (1, 10 and 100 nM) in the mouse HSC FLIPR™ assay. Data represents the mean of the individual parameters obtained from fitting the data from individual experiments represented in Figure 4.2.5. using non-linear regression analysis (four-parameter logistic equation with variable slope (Hill, 1909)) (See Chapter 2: Data Analysis section). Data shown are mean values ± SEM from 3 or more experiments carried out in duplicate. * Maximum response reached.# value from one curve fit.

the 5-HT CRC. Volinanserin, like ketanserin, caused insurmountable antagonism with a rightward shift and depression of maximum 5-HT CRC. 10 and 100 nM volinanserin concentrations completely inhibiting the 5-HT CRCs (Figure 4.2.5, Table 4.2.3 B). The insurmountable nature of the antagonism obtained with ketanserin and volinanserin does not allow antagonist affinity values to be determined due to the criteria for competitive antagonism not being met. However an estimate of the affinity was determined from the 1 nM shifts which yielded pA_2 values of 9.1 and 9.6 for ketanserin and volinanserin respectively. Qualitatively the concentration range over which the antagonism is observed and the pA_2 estimates indicate the involvement of the $5-HT_{2A}$ receptor in the 5-HT response. The profile of the antagonism observed may indicate that ketanserin and volinanserin are behaving as non-competitive antagonists but alternatively could also be explained by the antagonist, agonist and receptor being unable to reach equilibrium in the time frame of the agonist response (hemi-equilibrium conditions) (Kenakin et al., 2006).

To provide further evidence of $5-HT_{2A}$ receptor involvement in the 5-HT-stimulated response in the activated stellate cells, a selective $5-HT_{2A}$ agonist, NBOH-2C-CN (Hansen et al 2014) was tested. NBOH-2C-CN was found to behave as a low efficacy agonist in one out of the three experiments with different preparations of mouse HSCs. The combined data is shown in Figure 4.2.6 A. NBOH-2C-CN was therefore investigated as an antagonist. Three concentrations of NBOH-2C-CN (0.3, 1 and 3 μM) were to found to cause rightward shift of the 5-HT CRC (Figure 4.2.6 B) in a concentration-dependent manner with depression of the maximum response to 60% of the 5-HT CRC response. Although the criteria for competitive antagonism is not met, a pA_2 of 7.6 was estimated from the 300 nM NBOH-2C-CN shift of the 5-HT CRC. The nature of the antagonism again suggests a hemi-equilibrium with a partial re-equilibration for this antagonist due to its lower affinity.

To further investigate whether the $5-HT_{1B}$ receptor could stimulate the release of calcium in the cells, sumatriptan, a $5-HT_{1B}$ selective agonist, was tested. No agonist response was observed with sumatriptan thereby providing further evidence that the $5-HT_{1B}$ receptor is not involved in inducing calcium release in this assay (Figure 4.2.7). Another method to confirm that the 5-HT was not stimulating the release of
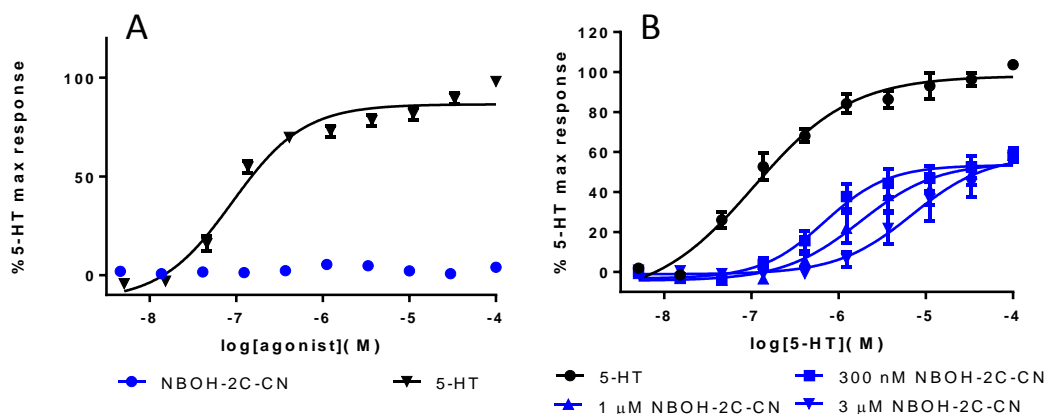
Figure 4.2.6 (A) NBOH-2C-CN agonist response observed in comparison with 5-HT, (B) 5-HT CRC curves in the presence of NBOH-2C-CN (0.3, 1 and 3 μM) in the mouse HSC FLIPR™ assay. HSCs were loaded with fluorescent dye (FLUO-4AM) for 1 h before stimulation with increasing concentrations of 5-HT or NBOH-2CN in the presence and absence of the NBOH-2C-CN in the FLIPR™. (See Chapter 2: Materials and Methods). Data were captured and analysed to obtain the basal fluorescence response and maximum stimulated fluorescence response above basal fluorescence response for each concentration, with the response being expressed as a percentage of the basal fluorescence. The data was normalised to the control 5-HT maximum response. CRCs were fitted using non-linear regression analysis (four-parameter logistic equation with variable slope (Hill, 1909)) (See Chapter 2: Data Analysis section). Data shown are mean values ± SEM from 3 or more individual experiments carried out in duplicate.

		NBOH-2C-CN		
	5-HT	300 nM	1 μM	3 μM
Max response (% 5-HT max resp)	94.8 ± 4.7	63.2 ± 3.4	70.8 ± 12.2	61.3 ± 3.8
pEC$_{50}$	6.95 ± 0.1	5.84 ± 0.4	5.39 ± 0.6	5.12 ± 0.4
Hill slope	1.07 ± 01	1.09 ± 0.3	1.19 ± 0.3	1.73 ± 0.1

Table 4.2.4 5-HT CRC parameters obtained in the presence and absence of NBOH-2C-CN (0.3, 1 and 3 μM) in the mouse HSC FLIPR™ assay. The data was normalised to the control 5-HT maximum response on each plate before fitting the CRCs. Data represents the mean of the individual parameters obtained from fitting the data from individual experiments represented in Figure 4.2.2.4 B using non-linear regression analysis (four-parameter logistic equation with variable slope (Hill, 1909)) (See Chapter 2: Data Analysis section). Data shown are the mean values ± SEM from 3 or more individual experiments carried out in duplicate.
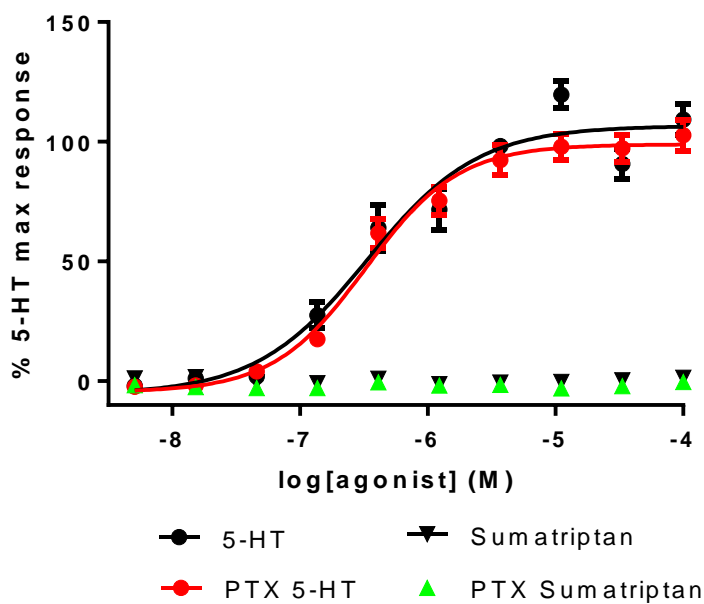
Figure 4.2.7   5-HT and sumatriptan CRC in the presence and absence of overnight treatment with pertussis toxin (100 ng/ml) in the mouse HSC FLIPR™ assay Plated out Stellate cells were loaded with fluorescent dye (FLUO4) for 1 h before stimulation with increasing concentrations of 5-HT or sumatriptan in the FLIPR™. (See Chapter 2: Materials and Methods). Data were captured and analysed to obtain the basal fluorescence response and maximum stimulated fluorescence response above basal fluorescence response for each concentration, with the response being expressed as a percentage of the basal response. The data was normalised to the control 5-HT maximum response on each plate before fitting the CRCs. CRCs were fitted using non-linear regression analysis (four-parameter logistic equation with variable slope (Hill, 1909)) (See Chapter 2: Data Analysis section). Data shown are the average values from 2 experiments carried out in duplicate.

calcium through a G_i-linked signalling cascade cells is via pre-treatment overnight with PTX (100 ng/ml). PTX which should impair the G_i interaction with 5-HT$_{1B}$ receptor and therefore remove any influence of the 5-HT response. Following pre-treatment with PTX there was no effect on the 5-HT CRC, when compared with the 5-HT CRC in the absence of pre-treatment (Figure 4.2.7), thus confirming lack of involvement of the 5-HT$_{1B}$ receptor or any other G_i-linked receptor.

4.2.3 Investigation of the insurmountable antagonism obtained with ketanserin and volinaserin in the FLIPR™ assay.

The insurmountable profile of the antagonism observed with both ketanserin and volinanserin may indicate that they are behaving as non-competitive antagonists. However this could also be explained by the fact that the antagonist, agonist and receptor are unable to reach an equilibrium in the timeframe of the agonist response (hemi-equilibrium conditions) (Paton and Rang, 1966; Kenakin et al., 2006). To investigate whether hemi-equilibrium was a possible explanation for the insurmountable antagonism observed with ketanserin and volinaserin a 'wash off experiment' was carried out. The compounds were incubated with the cells for 15 min before washing off. 'Wash off' was compared with 'control' data obtained from a plate which had undergone the same washing procedure but had the compounds added back for 15 min before stimulation with 5-HT.

There was little difference between the 5-HT CRCs obtained from the washed and control wash plates, as the pEC$_{50}$ and maximum responses were similar (Figure 4.2.8 and 4.2.9). All three concentrations of ketanserin and volinanserin tested demonstrated less antagonism of the 5-HT CRC after being washed off. This was in terms of less depression and rightward shift of the 5-HT CRCs in comparison to the control CRCs (Figure 4.2.8 and 4.2.9). At the highest concentrations of volinanserin (10 and 100 nM) and ketanserin tested (100 nM), the 5-HT response was almost completely abolished but following 'washoff' there was recovery of the 5-HT CRC response (Figure 4.2.8 and 4.2.9). The 'wash off' protocol was designed to produce a greater than 1000-fold dilution of the antagonist. The 100 nM concentration of volinaserin and ketanserin would therefore have been less than 0.1 nM and likely to produced little or no antagonism of the 5-HT CRC if they had
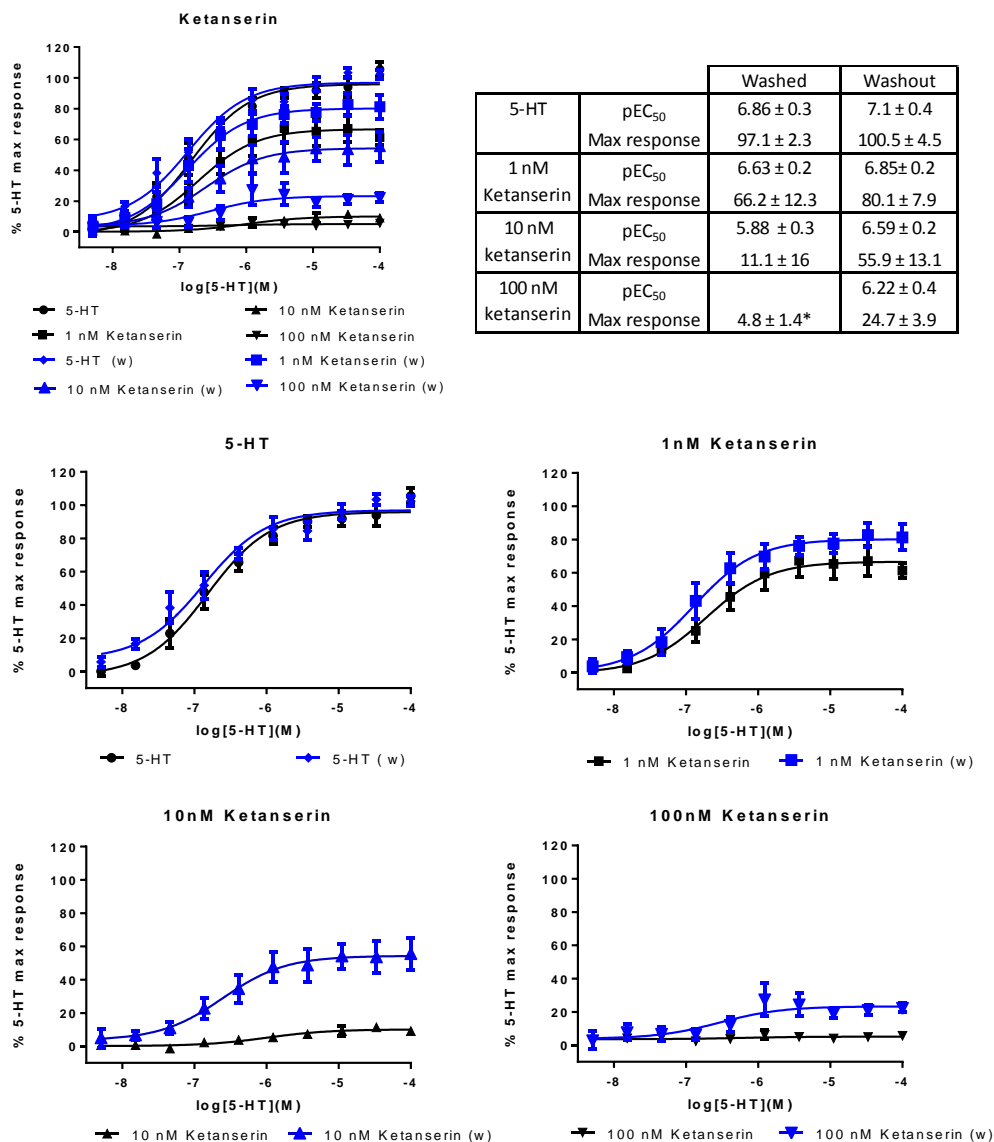
Figure 4.2.8   Effect of 'washoff' on ketanserin antagonism of the 5-HT CRCs in the mouse HSC FLIPR™ assay with accompanying table of 5-HT CRC fitting parameters. HSCs were loaded with fluorescent dye (FLUO4) for 1 h. Antagonist or vehicle was added for 15 min before being washed off before either re-addition of antagonist or just vehicle. The cells were stimulated with 5-HT   in the FLIPR™. (See Chapter 2: Materials and Methods). Data were captured and analysed to obtain the basal fluorescence response and maximum stimulated fluorescence response above basal fluorescence response for each concentration, with the response being expressed as a percentage of the basal response. The data was normalised to the control 5-HT maximum response on each plate before fitting the CRCs. CRCs were fitted using non-linear regression analysis (four-parameter logistic equation with variable slope (Hill, 1909)) (See Chapter 2: Data Analysis section). Data for each plate was normalised to the control 5-HT maximum response for fitting curves above. Data shown are the mean values ± SEM from 3 experiments carried out in duplicate. * mean of max response achieved.

Volinanserin

		Washed	Washout
5-HT	pEC$_{50}$	7.12 ± 0.3	7.25 ± 0.4
	Max response	89.6 ± 4.1	93.93 ± 3.2
1 nM Volinanserin	pEC$_{50}$	6.74	6.68 ± 0.2
	Max response	29.9 ± 14.7	86.3 ± 7.9
10 nM Volinanserin	pEC$_{50}$		6.35 ± 0.4
	Max response	-2.3 ± 2.6*	38.5 ± 15.6
100 nM Volinanserin	pEC$_{50}$		7.42
	Max response	10.4 ± 12.0*	22.4 ± 8.2

Figure 4.2.9   Effect of 'washoff' on volinanserin antagonism of the 5-HT CRCs in the mouse HSC FLIPR™ assay with accompanying table of 5-HT CRC fitting parameters. HSCs were loaded with fluorescent dye (FLUO4) for 1 h. Antagonist or vehicle was added for 15 min before being washed off before either re-addition of antagonist or just vehicle. The cells were stimulated with 5-HT in the FLIPR™. (See Chapter 2: Materials and Methods). Data were captured and analysed to obtain the basal fluorescence response and maximum stimulated fluorescence response above basal fluorescence response for each concentration, with the response being expressed as a percentage of the basal response. The data was normalised to the control 5-HT maximum response on each plate before fitting the CRCs. CRCs were fitted using non-linear regression analysis (four-parameter logistic equation with variable slope (Hill, 1909)) See Chapter 2: Data Analysis section). Data for each plate was normalised to the control 5-HT maximum response for fitting curves above. Data shown are mean values ± SEM from 3 experiments carried out in duplicate.* mean of max response achieved.

completely washed off. These data demonstrated that the antagonism observed with ketanserin and volinaserin was not irreversible as it was possible reduce the level of antagonism following washing. Hemi-equilibrium can explain the insurmountable antagonism observed due to the slow dissociation kinetics of the antagonist combined with the fast 5-HT stimulated intracellular release of calcium.

4.2.4 Pharmacological characterisation of the 5-HT receptor responsible for ERK phosphorylation in mouse hepatic stellate cells.

4.2.4.1 Assay optimisation.

Initial studies were carried out to determine the nature and time course of the 5-HT stimulated ERK phosphorylation (pERK) responses in HSCs over a 3 h period at room temperature to determine the optimum incubation time for future studies. Room temperature was used to make it easier to control conditions when running multiple plates through the assay. 10 µM 5-HT was found to cause an increase in pERK response, with a maximum response observed at 10-15 min (Figure 4.2.10). A decline in the pERK response was then observed, reaching a minimum response at 60 min, which then increased a small amount over the next following 30 min. After this response was sustained over the remainder of the time. From these results 10 min stimulation time was chosen for all subsequent experiments, as there was no significant difference in the maximum response obtained at 10 and 15 min time point ($P > 0.05$ Student paired t-test).

The effect of cell density on the 5-HT response was investigated to determine the optimal cell concentration to use in subsequent experiments. The 10 min time point was analysed at 3 different cell densities; 10000, 20000 and 40000 cells per well. The pERK response window was calculated from the maximum response (10 µM 5-HT). It was observed that as cell density increased, the 5-HT-stimulated pERK response decreased, as did the basal ERK phosphorylation (Figure 4.2.11). 10000 cells per well gave the largest signal window and was used in future experiments.

4.2.4.2 Pharmacological characterisation of the 5-HT response in mouse activated HSC.

To characterise the 5-HT-stimulated pERK response increasing concentrations (1.79
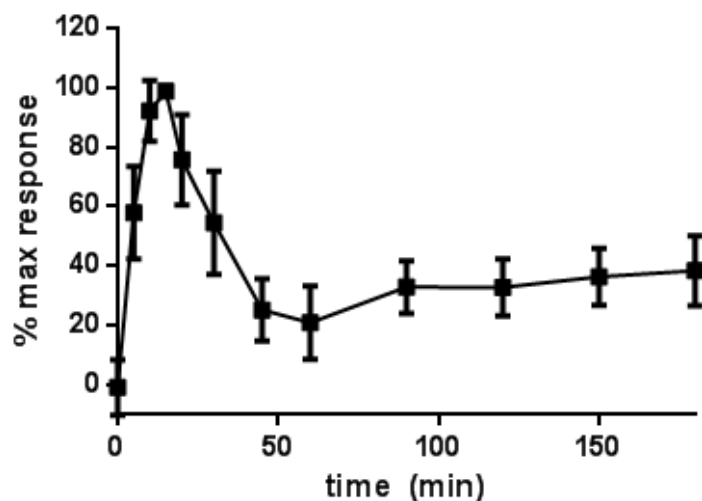
Figure 4.2.10   5-HT stimulated ERK phosphorylation response over 3 h in mouse hepatic stellate cells. Mouse hepatic stellate cells were stimulated with 10 μM 5-HT at different times over a period of 3 h. The pERK and total ERK levels were measured in the cell lysates using an MSD pERK/Total ERK kit (See Chapter 2: Materials and methods). The data was normalised to the maximum response obtained in each assay. Data shown are mean values ± SEM from 3 individual experiments carried out in duplicate.
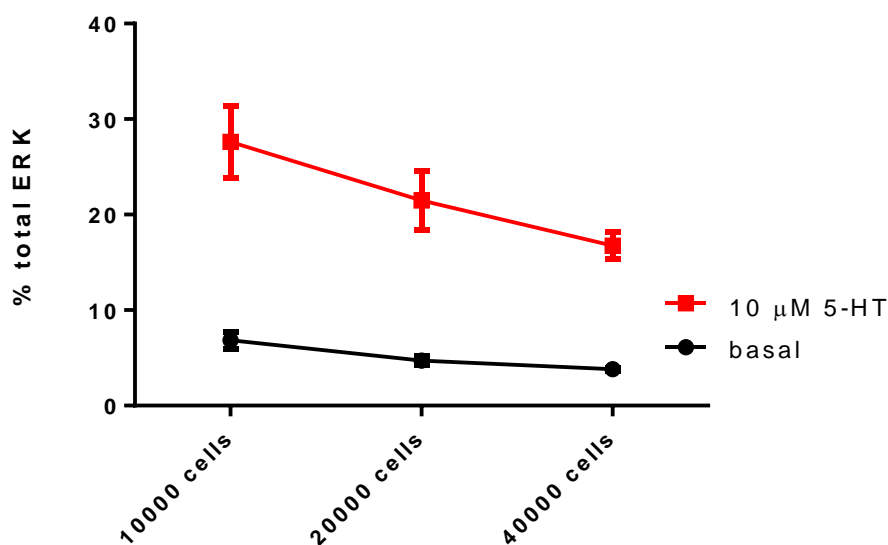
Figure 4.2.11   Effect of cell density on the 10 μM 5-HT stimulated and basal ERK phosphorylation in mouse hepatic stellate cells. The graph shows the % total ERK increase in ERK phosphorylation following a 10 min stimulation with 5-HT stimulation in comparison to the associated basal %total ERK phosphorylation for 3 cell well plating densities (10000, 20000 and 40000 cells per well). Data shown are the mean values ± SEM for at least three experiments, with the 40000 cells value data determined from 2 experiments.

nM - 100 μM) of 5-HT were incubated with the stellate cells for 10 min. A concentration-dependent increase in pERK signal was obtained. Characterisation of this response was carried out in similar way to that performed for the FLIPR assay. In the literature a 5-HT-stimulated pERK response was reported to signal via the 5-HT$_{2B}$ receptor (Ebrahimkhani et al 2011). More recent evidence, however, suggests that the up-regulated 5-HT$_{2A}$ receptor mediates an increase in the pERK level (Kim et al., 2013). The effect of 5-HT$_{2A}$ antagonists (ketanserin and volinaserin) and 5-HT$_{2B}$ antagonists (GSK1606260A and RS-127445) were used to identify the 5-HT receptor responsible for eliciting the pERK assay response. The concentrations chosen were known to be selective for the chosen receptor of interest as predicted from in-house assays, with cells expressing recombinant mouse 5-HT$_{2A}$ or 5-HT$_{2B}$ receptors (Table 4.2.1).

In HSCs, no rightward shift of the 5-HT CRCs in the presence of either GSK1606260A (1 μM) or RS-127445 (100 nM) was observed (Figure 4.2.12). A rightward shift of > 1000-fold, with GSK1606260A (1 μM) and > 10000-fold, with RS-127445 (100 nM), of the 5-HT CRC would have been observed if there was a competitive interaction with the 5-HT$_{2B}$ receptor. As can be seen from the table of CRC parameters, the pEC$_{50}$ values for 5-HT in the presence of either GSK1606260A (1 μM) or RS-127445 (100 nM) are similar to that of the 5-HT CRC alone (Table 4.2.5). These results indicate that the 5-HT$_{2B}$ receptor is not the receptor mediating the 5-HT-stimulated increase in pERK response in the HSCs.

Ketanserin, a 5-HT$_{2A}$ antagonist (10 nM, 100 nM and 1 μM) was found to produce a rightward shift and depression of the 5-HT CRC (Figure 4.2.13 A, Table 4.2.6). The Hill slopes of the curves appeared to become shallower with increasing concentrations of ketanserin when compared with the 5-HT CRC alone (Table 4.2.13 A). The CRCs in the presence of ketanserin appeared to exhibit a biphasic profile (Figure 4.2.13 A). Volinanserin (1 nM, 10 nM and 100 nM) caused considerable depression of the maximum but little rightward shift of the 5-HT CRC (Figure 4.2.13 B, Table 4.2.6 B).
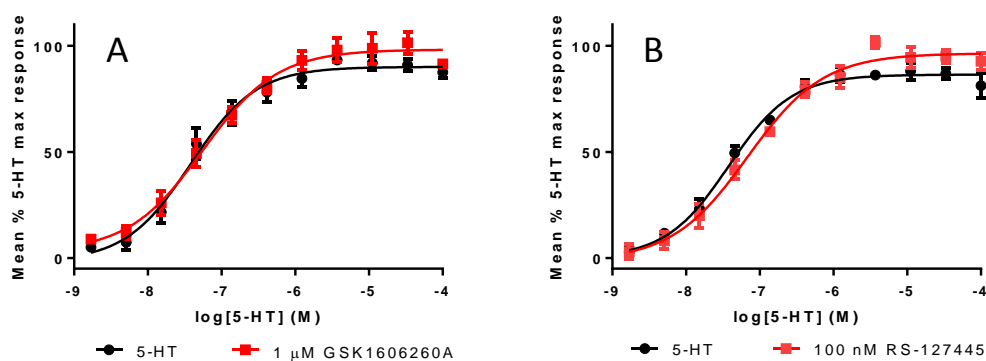
Figure 4.2.12   Effect of A) GSK1606260A (1 μM) and B) RS-127445 (100 nM) on the 5-HT CRCs in the mouse HSC pERK assay. HSCs were incubated with antagonists or vehicle for 30 min before 10 min stimulation with 5-HT. The pERK and total ERK levels were measured in cell lysates using MSD pERK/Total ERK kit (See Chapter 2: Materials and Methods). pERK response was expressed as the % total ERK was normalised to the 5-HT maximum response. CRCs were fitted using non-linear regression analysis (four-parameter logistic equation with variable slope (Hill, 1909)) (See Chapter 2: Data Analysis section). Data shown are mean values ± SEM from > 3 experiments carried out in duplicate.

A	5-HT	GSK1606260A (1 μM)
pEC_{50}	7.35 ± 0.2	7.23 ± 0.2
Hill Slope	0.99 ± 0.1	0.99 ± 0.1

B	5-HT	RS-127445 (100 nM)
pEC_{50}	7.44 ± 0.04	7.18 ± 0.03
Hill Slope	1.03 ± 0.1	0.83 ± 0.1

Table 4.2.5   Mean pEC_{50}, and Hill slope obtained for 5-HT CRCs fitted in the presence of A) GSK1606260A (1 μM) and B) RS-127445 (100 nM) in mouse HSC pERK assay. HSCs were incubated for with antagonists for 30 min before being stimulated with 5-HT for 10 min (See materials and methods). pERK response was expressed as the % total ERK was normalised to the 5-HT maximum response. CRCs were fitted using non-linear regression analysis (four-parameter logistic equation with variable slope (Hill, 1909)) (See Chapter 2: Data Analysis section). Data shown are mean values ± SEM from > 3 experiments carried out in duplicate.
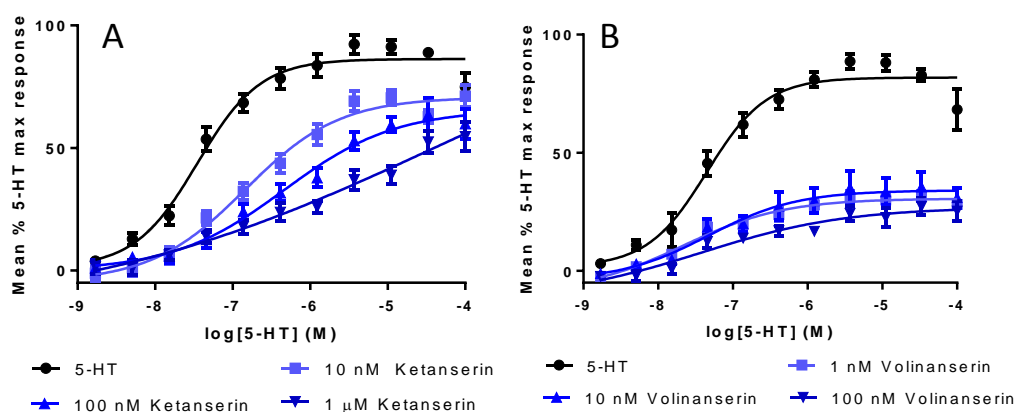
Figure 4.2.13 Effect of A) Ketanserin (10 nM, 100 nM & 1 μM) and B) Volinaserin (1 nM, 10 nM & 100 nM) on the 5-HT CRCs in the mouse HSC pERK assay. HSCs were incubated with antagonists or vehicle for 30 min before 10 min stimulation with 5-HT. The pERK and total ERK levels were measured in cell lysates using MSD pERK/Total ERK kit (See Chapter 2: Materials and Methods). pERK was expressed as the % total ERK was normalised to the 5-HT maximum response. CRCs were fitted using non-linear regression analysis (four-parameter logistic equation with variable slope (Hill, 1909)) (See Chapter 2: Data Analysis section). Data shown are mean values ± SEM from > 4 experiments carried out in duplicate.

A		Ketanserin		
	5-HT	10 nM	100 nM	1 μM
pEC_{50}	7.41 ± 0.1	6.83 ± 0.2	6.32 ± 0.2	6.1*
Hill Slope	1.44 ± 0.3	0.76 ± 0.1	0.62 ± 0.1	0.38*
Max % 5-HT Maximu response	86.6 ± 3.5	72.1 ± 4.42	69.7 ± 9.3	60.3 ± 6.8[#]

B		Volinanserin		
	5-HT	1 nM	10 nM	100 nM
pEC_{50}	7.38 ± 0.2	7.64 ± 0.3	7.08 ± 0.2	6.93 ± 0.4
Hill Slope	1.04 ± 0.1	1.21 ± 0.7	0.83 ± 0.1	2.35 ± 1.7
Max % 5-HT Max response	82.7 ± 4.3	31.0 ± 1.9	38.9 ± 7.8	28.7 ± 9.0

Table 4.2.6 Mean pEC_{50}, Hill slope and maximum response obtained for 5-HT CRCs fitted in the presence of A) Ketanserin (10 nM, 100 nM and 1 μM) and B) Volinanserin (1 nM, 10 nM and 100 nM) in mouse HSC pERK assay. HSC were incubated with antagonists or vehicle for 30 min before 10 min stimulation with 5-HT. (See materials and methods). pERK was expressed as the % total ERK was normalised to the 5-HT maximum response. CRCs were fitted using non-linear regression analysis (four-parameter logistic equation with variable slope (Hill, 1909)) (See Chapter 2: Data Analysis section). Data shown are mean values ± SEM from > 4 experiments carried out in duplicate. * data from 2 fitted curves. [#] Max response incorporates max response reached for CRC from unfitted curves.

The antagonism observed with ketanserin and volinanserin was insurmountable and no affinity could be determined using the standard methods (e.g. Schild analysis). As the antagonism observed with ketanserin and volinanserin was at concentrations expected to selectively inhibit the 5-HT$_{2A}$ receptor, then it can be concluded that 5-HT$_{2A}$ receptor is most likely mediating the 5-HT stimulation of ERK phosphorylation.

To provide further evidence of the identification of the 5-HT receptor subtype, a selective 5-HT$_{2A}$ agonist, NBOH-2C-CN was used to explore the assay system. A concentration-dependent increase in pERK was obtained with an average pEC$_{50}$ of 7.2 (Figure 4.2.14 A). NBOH-2C-CN behaved as a partial agonist with an intrinsic activity of 0.38, when compared to the 5-HT CRC. (Figure 4.2.14 A, Table 4.2.7). To further confirm that NBOH-2C-CN is acting as a 5-HT$_{2A}$ agonist, the CRC was carried out in the presence of ketanserin (100 nM). Ketanserin caused a rightward shift and depression of the NBOH-2CN CRC (Figure 4.2.14 B, Table 4.2.6) providing further evidence of 5-HT$_{2A}$ receptor involvement.

4.2.4.3 Investigation of the insurmountable antagonism.

Ketanserin and volinanserin both behaved as insurmountable antagonists of 5-HT in the pERK aHSC experiments (Figure 4.2.13. A and B). Studies were undertaken to investigate whether the pre-incubation time of the antagonist could be influencing the nature of the antagonism observed in the experiment. Experiments were carried out which investigated antagonism obtained where the antagonists were added at the same time as 5-HT stimulation, compared with the standard 30 min pre-incubation time prior to 5-HT stimulation used, for ketanserin (100 nM) and volinanserin (10 nM). The antagonism observed with no pre-incubation (red curves) for both compounds was similar to the antagonism observed if the compounds were pre-incubated for 30 min (black curves) prior to stimulation with 5-HT (Figure 4.2.15 A and B, Table 4.2.8. A and B). The antagonism observed with both volinanserin and ketanserin was still insurmountable, so it can be concluded that incubation time does not influence the nature of the antagonism observed.
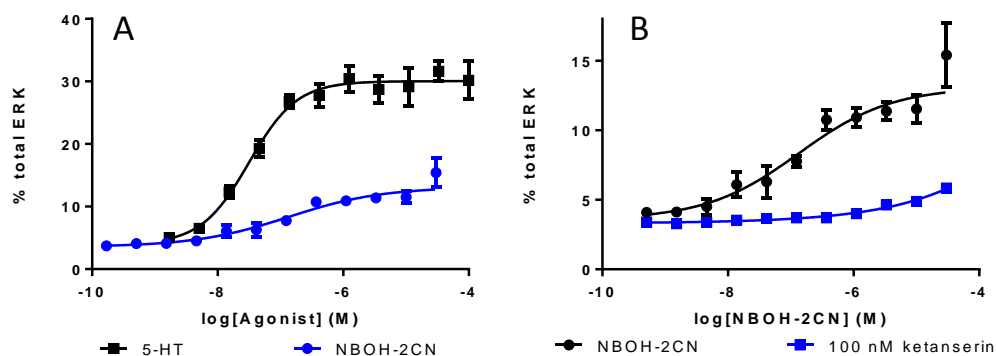
Figure 4.2.14 A) NBOH-2C-CN agonism in comparison with 5-HT & B) Effect of ketanserin (100 nM) on the NBOH-2C-CN CRCs in the mouse HSC pERK assay. HSCs were incubated with antagonists or vehicle were incubated for 30 min before they were stimulated for 10 min with 5-HT or NBOH-2C-CN. The pERK and total ERK levels were measured in cell lysates using MSD pERK/Total ERK kit (See Chapter 2: Materials and Methods). pERK was expressed as the % total ERK. CRCs were fitted using non-linear regression analysis (four-parameter logistic equation with variable slope (Hill, 1909)) (See Chapter 2: Data Analysis section). Data shown are mean values ± SEM from 3 experiments for NBOH-2C-CN and 5-HT. Data is average n=2 for ketanserin.

	5-HT	NBOH-2C-CN
Max Response	27.3 ± 4.7	8.7 ±1.7
pEC_{50}	7.53 ± 0.1	7.22 ± 0.4
Hill slope	1.16 ± 0.2	0.8 ± 0.1
Intrinsic activity	1.00	0.38 ± 0.04

Table 4.2.7 pEC_{50}, Hill slope, maximum response (% Total ERK) and intrinsic activity obtained for 5-HT and NBOH-2C-CN **CRCs in mouse HSC pERK assay.** HSC were incubated for 30 min with vehicle or antagonist before stimulation with 5-HT or NBOH-2C-CN for 10 min (See materials and methods). pERK was expressed as the % total ERK. CRCs were fitted using non-linear regression analysis (four-parameter logistic equation with variable slope (Hill, 1909)) (See Chapter 2: Data Analysis section). Data shown are mean values ± SEM from 3 experiments carried out in duplicate.
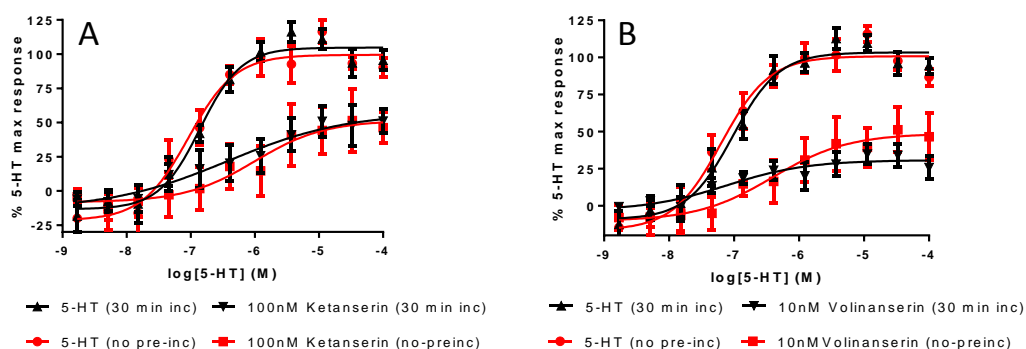
Figure 4.2.15 Effect of A) Ketanserin (100 nM) and B) Volinaserin (10 nM) on the 5-HT CRCs after 30 min pre-incubation (Black) or no pre-incubation (Red) in the mouse HSC pERK assay. HSCs were incubated with antagonists or vehicle were incubated for 30 min before stimulation with 5-HT for 10 min. The pERK and total ERK levels were measured in cell lysates using MSD pERK/Total ERK kit (See Chapter 2: Materials and Methods). pERK was expressed as the % total ERK was normalised to the 5-HT maximum response. CRCs were fitted using non-linear regression analysis (four-parameter logistic equation with variable slope (Hill, 1909)) (See Chapter 2: Data Analysis section). Data shown are mean values $\pm$ SEM from $\geq$ 3 experiments carried out in duplicate.

A	No pre-incubation		30 min pre-incubation	
	5-HT	100 nM Ketanserin	5-HT	100 nM Ketanserin
Max response % 5-HT	99.7 ± 1.2	64.0 ± 15.1	105.5 ± 3.0	58.3 ± 12.3
pEC_{50}	7.04 ± 0.2	5.78 ± 0.7	6.92 ± 0.1	6.38 ± 0.4
Hill slope	1.25 ± 0.1	0.74 ± 0.1	1.33 ± 0.3	0.5 ± 0.1
B	No pre-incubation		30 min pre-incubation	
	5-HT	10 nM volinanserin	5-HT	10 nM volinanserin
Max response % 5-HT	98.8 ± 4.1	47.0 ± 23.5	103.8 ± 2.9	29.4 ± 12.3
pEC_{50}	7.22 ± 0.1	6.44 ± 0.2	7.10 ± 0.2	7.17 ± 0.3
Hill slope	1.35 ± 0.2	1.06 ± 0.2	1.32 ± 0.2	0.77 ± 0.1

Table 4.2.8   5-HT CRC mean fitting parameters obtained for A) Ketanserin (100 nM) and B) Volinaserin (10nM) after 30 min pre-incubation or no pre-incubation in the mouse HSC pERK assay. HSCs were incubated with antagonists or vehicle were incubated for 30 min or no pre incubation before stimulation for 10 min with 5-HT. pERK was expressed as the % total ERK was normalised to the 5-HT maximum response. CRCs were fitted using non-linear regression analysis (four-parameter logistic equation with variable slope (Hill, 1909)) (See Chapter 2: Data Analysis section). Data shown are mean values $\pm$ SEM from $\geq$ 3 experiments carried out in duplicate.

4.2.4.4 Investigation into the presence of a second 5-HT receptor contributing to the 5-HT response.

On closer inspection of the 5-HT CRC obtained in the pERK assay, the slope was shallow and the curve was possibly biphasic in nature, with the second phase being evident at 300nM to 100μM (Figure 4.2.16.A). The 5-HT CRC was repeated but with a 1:2 dilution series instead of the usual 1:3 dilution series to help better define the CRC (Figure 4.2.16.B). A clear biphasic CRC was obtained using the 1:2 dilution (Figure 4.2.16.B), with the first phase reaching a plateau at around 300 nM (Figure 4.2.16.C). The second phase continuing to stimulate two receptor populations, which both contribute to the pERK response. A computer model was generated (Courtesy of David Hall) (Equation 2.11.1) to investigate the hypothesis that 5-HT stimulates two receptor populations which both contribute to the pERK response (See Chapter 9: Appendix , Section 9.3).

By inputting different affinities (K) and efficacies (τ) for 5-HT stimulation of each receptor into the model, the shape of the CRC was adjusted until it best reflected the experimental data (Figure 4.2.17). The model demonstrates that a system containing two receptors for the same ligand can generate CRCs with a similar profile to those observed in the HSC pERK assay. Therefore supports the hypothesis that more than one 5-HT receptor subtype is present on the HSCs and contributes to the 5-HT response in the pERK assays.

Further evidence that a second receptor could be contributing to the 5-HT CRC is obtained from the 5-HT CRCs in the presence of ketanserin and volinanserin. The 5-HT CRC in the presence of ketanserin is shallow and become progressively shallower with increasing ketanserin concentrations. There is also some indication of this occurring with volinanserin. However not all 5-HT CRCs in the presence of volinanserin could be defined in all the experiments (Table 4.2.6 B). This phenomenon of shallow curves in the presence of antagonists can be observed when a second receptor contributes to the 5-HT CRC. As the 5-HT$_{2B}$ receptor is unlikely to be involved due to lack of activity of 5-HT$_{2B}$ antagonists in this assay, then most likely potential candidate is the 5-HT$_{1B}$ receptor. Indeed the expression of the 5-HT$_{1B}$ receptor has been reported to be increased upon HSC activation (Ruddell et al.,
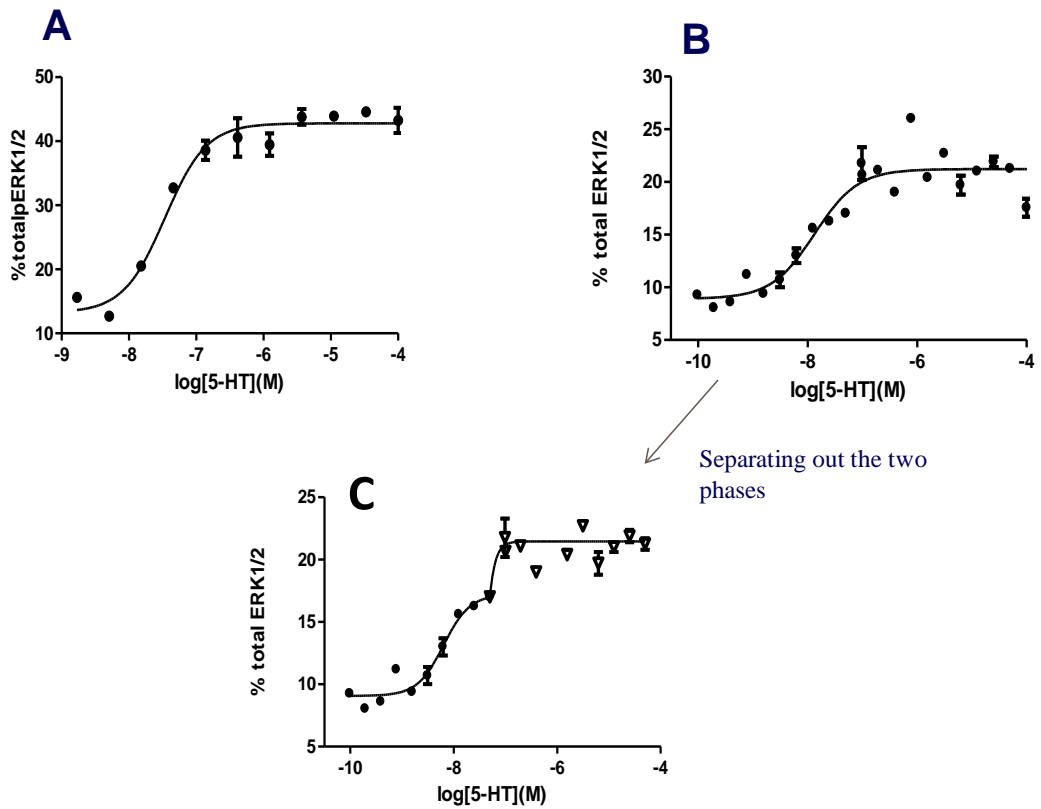
Figure 4.2.16 Biphasic 5-HT CRC investigation. A) 1 in 3 dilution 5-HT CRC, B) 1 in 2 dilution 5-HT CRC and C) 5-HT CRC fitted with two curves to show definition of biphasic 5-HT CRC. The mouse HSCs were stimulated for 10 min with 5-HT. The pERK and total ERK levels were measured in cell lysates using MSD pERK/Total ERK kit (See Chapter 2: Materials and Methods). pERK was expressed as the % total ERK. CRCs were fitted using non-linear regression analysis (four-parameter logistic equation with variable slope (Hill, 1909)) (See Chapter 2: Data Analysis section). Data is from a representative experiment.
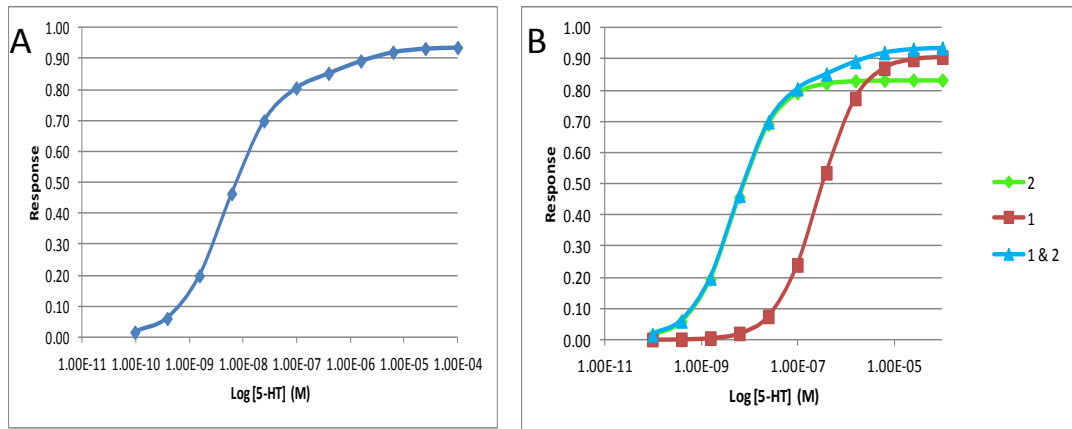
Figure 4.2.17   5-HT CRC generated using a computer model to investigate 5-HT stimulating two receptors which both contribute to the pERK response. A) 5-HT CRC generated from the combined stimulus, B) Separate 5-HT CRC for each receptor which contribute to the overall 5-HT CRC, C) The parameters used to generate the CRC and D) Schematic of the receptor activation that is thought to occur through dual 5-HT receptor activation of ERK.

2006). The next experiments were therefore focussed on addressing the possibility that 5-HT$_{1B}$ receptors contribute to the 5-HT induced ERK phosphorylation in HSCs.

Sumatriptan is reported to be a selective 5-HT$_{1B}$/5-HT$_{1D}$ agonist so the activity of sumatriptan was investigated in the assay. Sumatriptan (1.7 nM to 100 μM) produced a concentration-dependent increase in pERK response with a mean pEC$_{50}$ of 4.86 (Figure 4.2.18, Table 4.2.9). Sumatriptan behaved as a partial agonist with an intrinsic activity of 0.56 when compared to 5-HT maximum response in the same experiments (Table 4.2.9).

To further investigate the identity of the second receptor, sumatriptan was tested in the absence or presence of ketanserin or cyanopindolol (a 5HT$_{1B}$ antagonist (pK$_B$ = 8.1 - 8.7, (Maroteaux et al., 1992; Giles et al., 1996)). Ketanserin (100 nM) produced no rightward shift of the sumatriptan response but there was a 35% depression of the maximum response observed although this was not significant (p>0.05, paired Student t-test) (Figure 4.2.19, Table 4.2.10). Cyanopindolol (100 nM) was found to cause a rightward shift of the sumatriptan CRC which can be interpreted as being consistent with interaction at the 5-HT$_{1B}$ receptor (Figure 4.2.20, Table 4.2.11). Due to the low potency of sumatriptan (pEC$_{50}$= 4.61, Table 4.2.9) the rightward shift of the sumatriptan CRC by cyanopindolol (100 nM) made it difficult to accurately define a CRC over the concentration range used. An estimate of a pA$_2$ (assuming, same maximum response and parallel rightward shift) > 7.7 was calculated. This estimated pA$_2$ being in the range expected for a 5-HT$_{1B}$ interaction for cyanopindolol. Taken together, the sumatriptan agonism, lack of antagonism with ketanserin and antagonism with cyanopindolol this suggests that the second receptor involved in the response is likely to be the 5-HT$_{1B}$ receptor.

To confirm the 5-HT$_{1B}$ receptor involvement a combined antagonist study was undertaken. Experiments were carried out to investigate ketanserin antagonism in the presence of cyanopindolol. This will inhibit the 5-HT$_{1B}$ response, and should therefore effectively reveal a 'pure' 5-HT$_{2A}$ receptor system. There was no significant effect of cyanopindolol (1 μM) on the 5-HT CRC (p>0.05, Student paired t-test, pEC$_{50}$ and Hill slope comparisons with 5-HT CRC alone) (Figure 4.2.21, Table 4.2.12). Ketanserin (100 nM) caused a 50-fold rightward shift along with
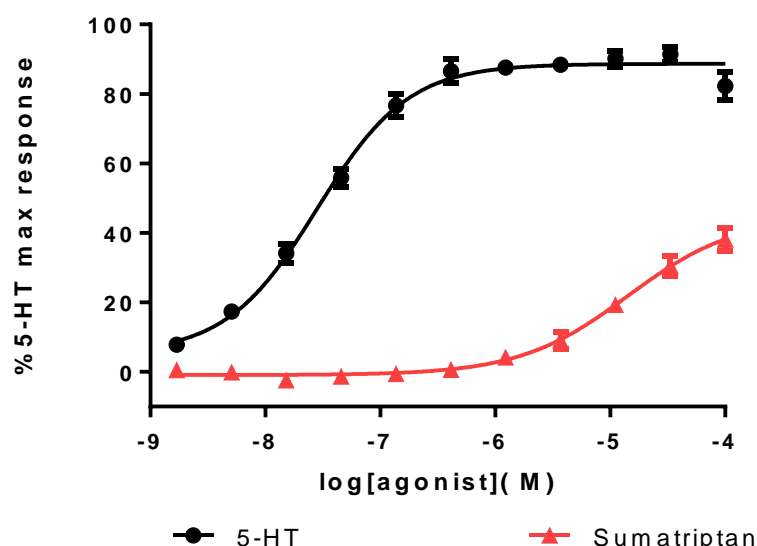
Figure 4.2.18   Sumatriptan CRC in comparison with 5-HT CRC in the mouse HSC pERK assay. HSCs were stimulated for 10 min with 5-HT or sumatriptan. The pERK and total ERK levels were measured in cell lysates using MSD pERK/Total ERK kit (See Chapter 2: Materials and Methods). pERK was expressed as the % total ERK and normalised to 5-HT max for the purpose of presentation of the CRC. CRCs were fitted using non-linear regression analysis (four-parameter logistic equation with variable slope (Hill, 1909)) (See Chapter 2: Data Analysis section). Data shown are mean values ± SEM from 9 experiments carried out in duplicate.

	5-HT	Sumatriptan
% Total ERK Max Response	23.6 ± 2.9	14.1 ± 3.1
% 5-HT max Max response	100	56.3 ± 7.6
pEC_{50}	7.58± 0.1	4.86 ±0.1
Hill slope	1.04 ± 0.1	0.97 ± 0.1
Intrinsic activity	1	0.56 ± 0.1

Table 4.2.9 pEC_{50}, Hill slope, intrinsic activity, maximum % Total ERK response and Maximum % 5-HT response obtained for sumatriptan CRCs in comparison with 5-HT CRCs in mouse HSC pERK assay. HSCs were stimulated with sumatriptan or 5-HT for 10 min (See materials and methods). pERK was expressed as the % total ERK. CRCs were fitted using non-linear regression analysis (four-parameter logistic equation with variable slope (Hill, 1909) (See Chapter 2: Data Analysis section). Data shown are mean values ± SEM from 9 experiments carried out in duplicate.

109
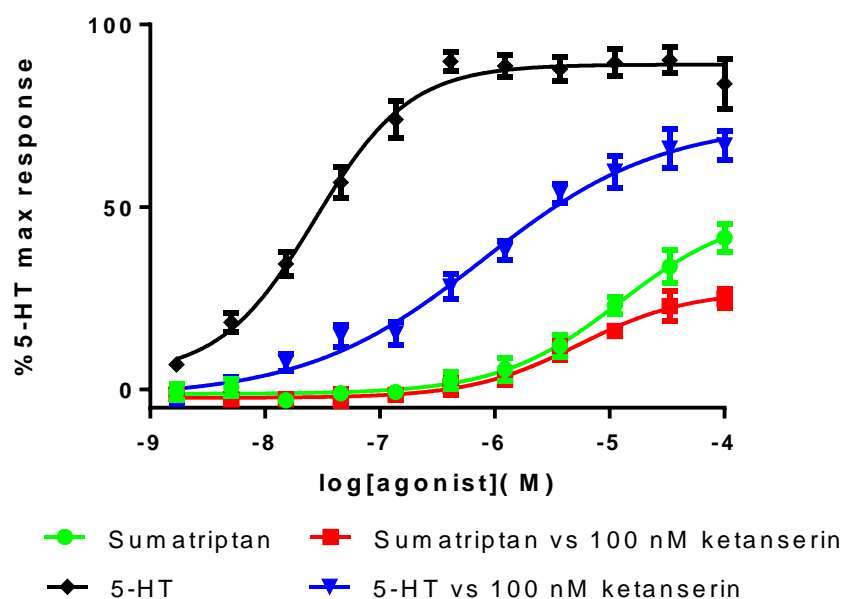
Figure 4.2.19 Antagonism of sumatriptan CRC by ketanserin (100 nM) in comparison with 5-HT CRC ± ketanserin in the mouse HSC pERK assay. HSCs were stimulated for 10 min with 5-HT or sumatriptan following a 30 min incubation with vehicle or antagonist. The pERK and total ERK levels were measured in cell lysates using MSD pERK/Total ERK kit (See Chapter 2: Materials and Methods). pERK was expressed as the % total ERK and normalised to 5-HT max for the purpose of presentation of the CRC. CRCs were fitted using non-linear regression analysis (four-parameter logistic equation with variable slope (Hill, 1909)) (See Chapter 2: Data Analysis section). Data shown are mean values ± SEM from 5 experiments carried out in duplicate.

	5-HT	5-HT + 100 nM Ketanserin	Sumatriptan	Sumatriptan +100 nM Ketanserin
Max % total ERK resp	24.1 ± 4.2	24.2 ± 6.4	14.6 ± 4.3	9.4 ± 2.6
Max % 5-HT max resp	100	97.1 ± 14.5	58.7 ± 9.7	38.1 ± 6.3
pEC_{50}	7.57 ± 0.1	5.89 ± 0.3	5.01 ± 0.1	5.35 ± 0.3
Hill Slope	1.06 ± 0.1	0.67 ± 0.2	0.99 ± 0.1	0.85 ± 0.1

Table 4.2.10 pEC_{50}, Hill slope, maximum % Total ERK response and Maximum % 5-HT response obtained for sumatriptan and 5-HT CRCs ± ketanserin (100 nM) in mouse HSC pERK assay. HSCs were stimulated with sumatriptan or 5-HT for 10 min following a 30 min pre-incubation with ketanserin or vehicle (See materials and methods). pERK was expressed as the % total ERK. CRCs were fitted using non-linear regression analysis (four-parameter logistic equation with variable slope (Hill, 1909)) (See Chapter 2: Data Analysis section). Data shown are mean values ± SEM from 5 experiments carried out in duplicate.
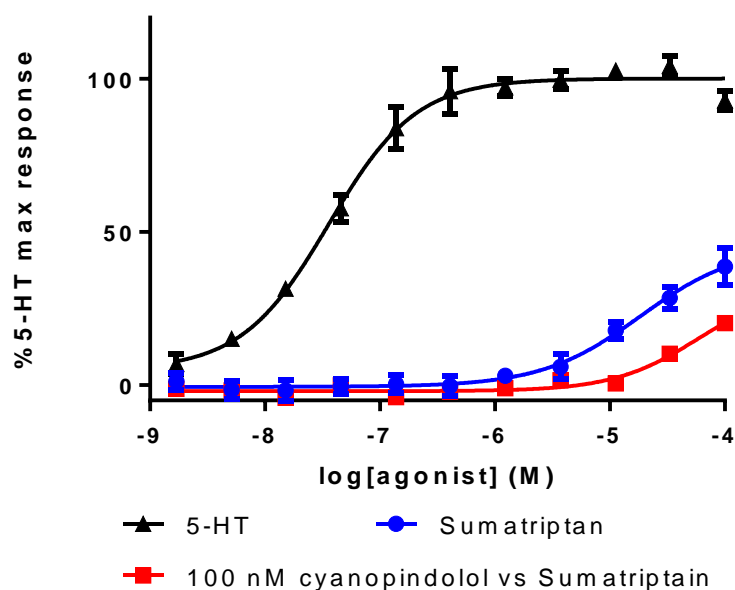
Figure 4.2.20   Antagonism of sumatriptan CRC by cyanopindolol (100 nM) in comparison with 5-HT CRC in the mouse HSC pERK assay. HSCs were stimulated for 10 min with 5-HT or sumatriptan following a 30 min pre-incubation with vehicle or antagonist. The pERK and total ERK levels were measured in cell lysates using MSD pERK/Total ERK kit (See Chapter 2: Materials and Methods). pERK was expressed as the % total ERK and normalised to 5-HT max for the purpose of presentation of the CRC. CRCs were fitted using non-linear regression analysis (four-parameter logistic equation with variable slope (Hill, 1909)) (See Chapter 2: Data Analysis section). Data shown are mean values ± SEM from 4 experiments carried out in duplicate.

	5-HT	Sumatriptan	Sumatriptan + 100 nM cyanopindolol
pEC_{50}	7.47± 0.1	4.61 ± 0.1	< 3.82 ± 0.2
Hill Slope	0.96 ± 0.1	0.88 ± 0.2	0.84 ± 0.2

Table 4.2.11 pEC_{50} and Hill slope obtained for sumatriptan ± cyanopindolol (100nM) and 5-HT CRCs in mouse HSC pERK assay. HSCs were stimulated with sumatriptan or 5-HT for 10 min following a 30 min pre-incubation with cyanopindolol or vehicle (See materials and methods). pERK was expressed as the % total ERK. CRCs were fitted using non-linear regression analysis (four-parameter logistic equation with variable slope (Hill, 1909)) (See Chapter 2: Data Analysis section). Data shown are mean values ± SEM from 4 experiments carried out in duplicate.
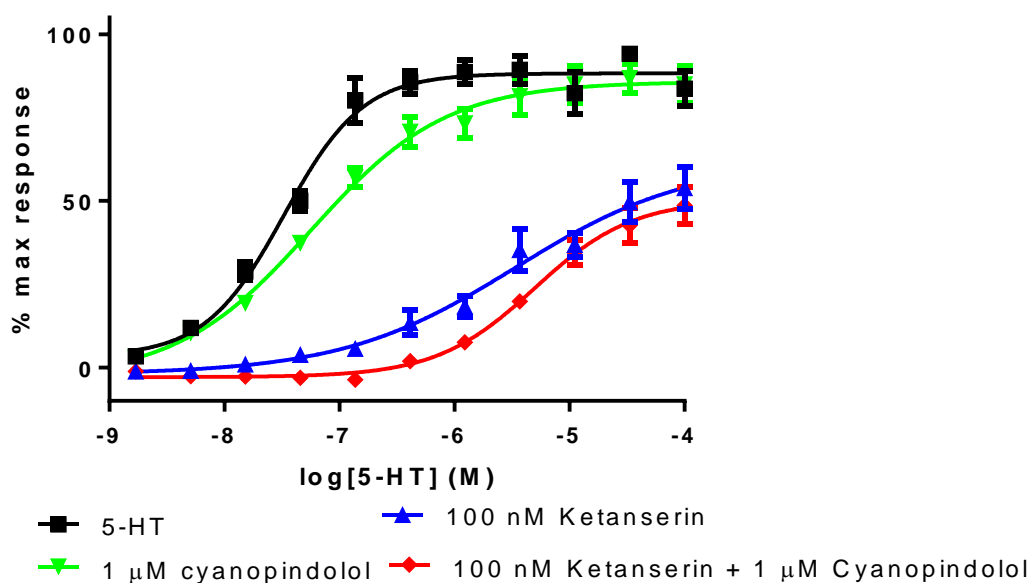
Figure 4.2.21   Effect of ketanserin (100 nM) and cyanopindolol (1 μM) alone and in combination on the 5-HT CRCs in the mouse HSC pERK assay. HSCs were stimulated for 10 min with 5-HT or sumatriptan following a 30 min incubation with vehicle or antagonist. The pERK and total ERK levels were measured in cell lysates using MSD pERK/Total ERK kit (See Chapter 2: Materials and Methods). pERK was expressed as the % total ERK and normalised to 5-HT max for the purpose of presentation of the CRCs. CRCs were fitted using non-linear regression analysis (four-parameter logistic equation with variable slope (Hill, 1909)) (See Chapter 2: Data Analysis section). Data are mean values ± SEM from 3 experiments carried out in duplicate.

	5-HT	100 nM Ketanserin	1 μM Cyanopindolol	Combined 100 nM ketanserin & 1 μM cyanopindolol
pEC_{50}	7.46 ± 0.1	5.75 ± 0.2	7.25 ± 0.1	5.33 ± 0.1
Hill Slope	1.26 ± 0.2	0.75 ± 0.1	0.76 ± 0.01	$*1.06 \pm 0.04$

Table 4.2.12   Effect of ketanserin (100 nM) and cyanopindolol (1 μM) alone and in combination on the 5-HT CRCs pEC_{50} and Hill slope in mouse HSC pERK assay. HSCs were stimulated with sumatriptan or 5-HT for 10 min following 30 min pre-incubation with cyanopindolol and or ketanserin, or vehicle (See materials and methods). pERK was expressed as the % total ERK. CRCs were fitted using non-linear regression analysis (four-parameter logistic equation with variable slope (Hill, 1909)) (See Chapter 2: Data Analysis section). Data shown are mean values ± SEM from 3 experiments carried out in duplicate. * Hill slope in presence of combination (cyanopindolol + ketanserin) is significantly different Hill slope in presence of ketanserin alone (p= 0.033, Student paired t-test).

depression of the 5-HT CRC (Figure 4.2.21, Table 4.2.12.). The 5-HT CRC in the presence of both ketanserin (100 nM) and cyanopindolol (1 μM) exhibited a Hill slope of 1.06, which was significantly different to the Hill slope of the 5-HT CRC in the presence of ketanserin (100 nM) alone (p= 0.033, Student paired t-test) (Figure 4.2.21, Table 4.2.12). In the presence of cyanopindolol, ketanserin is able to cause a 134-fold shift of the 5-HT CRC, with a pA_2 of about 9, which is similar to the affinity that is expected for ketanserin (See table 1.10.1). However ketanserin is clearly behaving as an insurmountable antagonist as the maximum response is clearly depressed. Therefore an affinity cannot be accurately determined as not all criteria for a competitive interaction are met. Overall these data would suggest that the 5-HT_{1B} receptor is the second 5-HT receptor mediating the 5-HT stimulated ERK phosphorylation.

Another way to pharmacologically investigate the removal of the 5-HT_{1B} response is to treat the cells with PTX. As 5-HT_{1B} couples through $G_{i/0}$ protein and therefore PTX impairs the $G\alpha_i$ interaction with 5-HT_{1B} receptor. Cells were pre-treated with PTX to remove the influence of the 5-HT_{1B} receptor. PTX pre-treatment caused less than a 2-fold rightward shift of the 5-HT CRC with no real depression of maximum response (Figure 4.2.22, Table 4.2.13). 100 nM ketanserin caused a 26-fold rightward shift of the 5-HT CRC in the absence of PTX, but this increased to > 90-fold after PTX treatment. The Hill slope of the PTX 5-HT CRC in the presence of 100 nM ketanserin was nearer unity than the 5-HT CRC in the presence of 100 nM ketanserin, which was shallow (Figure 4.2.22, Table 4.2.13). This is similar to the effect observed with cyanopindolol (1 μM) in combination with ketanserin (100 nM) on the 5-HT CRC (Figure 4.2.21, Table 4.2.12). These data suggest that PTX pre-treatment removes the component of the response that is G_i-linked.

One further experiment was designed to investigate the effect of PTX treatment on the sumatriptan CRC, as PTX treatment would block the effect of sumatriptan acting via the 5-HT_{1B} receptor. There was no effect of PTX treatment on the 5- HT CRC. (Figure 4.2.23, table 4.2.14) The PTX treatment did not fully inhibit the sumatriptan CRC but rightward shift of the CRC was observed (Figure 4.2.23, Table 4.2.14).
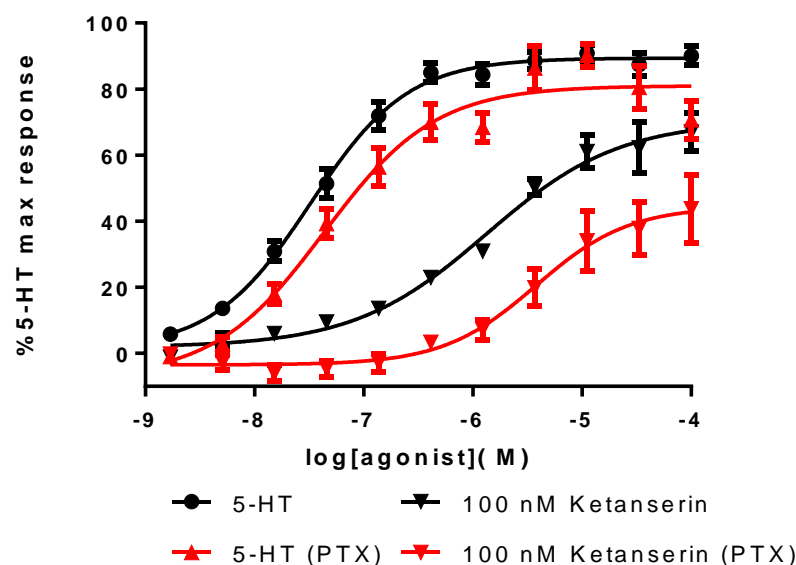
Figure 4.2.22   5-HT CRCs in the presence and absence of 100 nM ketanserin following PTX (100 ng/ml) overnight pre-treatment or no PTX pre-treatment in the mouse HSC pERK assay. HSC were pre-treated overnight with 100ng/ml PTX or vehicle. HSCs were stimulated for 10 min with 5-HT or sumatriptan following a 30 min pre-incubation with vehicle or 100nM ketanserin. The pERK and total ERK levels were measured in cell lysates using MSD pERK/Total ERK kit (See Chapter 2: Materials and Methods). pERK was expressed as the % total ERK and normalised to 5-HT max for the purpose of presentation of the CRC and to allow comparisons between the ± PTX pre-treatment. CRCs were fitted using non-linear regression analysis (four-parameter logistic equation with variable slope (Hill, 1909)) (See Chapter 2: Data Analysis section). Data shown are mean values ± SEM from 7 experiments carried out in duplicate.

	No PTX		PTX	
	5-HT	100 nM Ketanserin	5-HT	100 nM ketanserin
Max % total ERK response	17.7 ± 1.8	13.4 ± 2.0	10.9 ± 1.7	5.54 ± 1.6
Maximum % 5-HT response	100	77.5 ± 11.5	100	55.46 ± 18.2
pEC50	7.49 ± 0.1	6.07 ± 0.2	7.26 ± 0.1	<5.28 ± 0.1
Hill Slope	0.95 ± 0.1	0.76 ± 0.1	1.04 ± 0.1	1.14 ± 0.2 *

Table 4.2.13   5-HT CRC mean fitting parameters obtained in the presence and absence of 100nM ketanserin following PTX (100ng/ml) overnight pre-treatment or no PTX treatment in the mouse HSC pERK assay. HSCs were stimulated with 5-HT for 10 min following a 30 min pre-incubation with ketanserin or vehicle and following ± overnight pre-treatment with 100ng/ml PTX (See materials and methods). pERK was expressed as the % total ERK. CRCs were fitted using non-linear regression analysis (four-parameter logistic equation with variable slope (Hill, 1909)) (See Chapter 2: Data Analysis section). Data shown are mean values ± SEM from 7 experiments. * slope from n=5 fits.
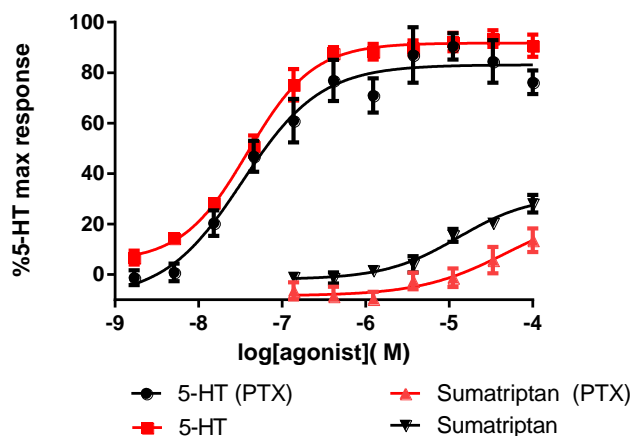
Figure 4.2.23   Effect of PTX (100 ng/ml) overnight pre-treatment on 5-HT and sumatriptan CRCs in the mouse HSC pERK assay. HSC were pre-treated overnight with 100 ng/ml PTX or vehicle. HSCs were stimulated for 10 min with sumatriptan or 5-HT. The pERK and total ERK levels were measured in cell lysates using MSD pERK/Total ERK kit (See Chapter 2: Materials and Methods). pERK was expressed as the % total ERK and normalised to 5-HT maximum response for the purpose of presentation of the CRC and to allow comparisons between the ± PTX pre-treatment. CRCs were fitted using non-linear regression analysis (four-parameter logistic equation with variable slope (Hill, 1909)) (See Chapter 2: Data Analysis section). Data shown are mean values ± SEM from 4 experiments carried out in duplicate.

	5-HT	5-HT PTX	Sumatriptan	Sumatriptan PTX
Max % total ERK response	19.3 ± 2.4	12.4 ± 2.3	5.72 ± 1.1	4.8 ± 1.4
Max % 5-HT max response	100	100	36. 3 ± 0.76	35.3 ± 17.7
pEC_{50}	7.43 ± 0.1	7.40 ± 0.1	4.92 ± 0.1	<4.18 ± 0.3
Hill slope	0.95 ± 0.1	1.04 ± 0.1	0.99 ± 0.01	1.1 *

Table 4.2.14   5-HT and Sumatriptan CRC mean fitting parameters following PTX (100 ng/ml) overnight pre-treatment or no PTX treatment in the mouse HSC pERK assay. HSCs were stimulated with 5-HT or sumatriptan for 10 min following ± overnight pre-treatment with 100 ng/ml PTX (See materials and methods). pERK was expressed as the % total ERK. CRCs were fitted using non-linear regression analysis (four-parameter logistic equation with variable slope (Hill, 1909)) (See Chapter 2: Data Analysis section). Data shown are mean values ± SEM from 4 experiments carried out in duplicate. * slope from n=2 fits.

4.3   Discussion.

4.3.1   Characterisation of the 5-HT receptor responsible for calcium signalling in mouse hepatic stellate cells.

During fibrosis the stellate cell undergoes a transformation to a myofibroblast-like cell and this involves increased expression of α-SMA along with the L-type voltage operated calcium channels and 5-HT$_2$ receptors (Bataller et al., 2001; Park et al., 2011). This up-regulation of L-type voltage operated channels mediate Ca^{2+} influx and is associated with the HSCs transforming into a myofibroblast–like contractile cells. This process may therefore contribute to the increased resistance to blood flow in fibrosis (Bataller et al., 2001). The activated HSCs are known to have increased expression of 5-HT$_{2A}$ and 5-HT$_{2B}$ receptors and these receptors are most likely to be involved in the calcium signalling, due to their coupling through Gαq, which will elicit a downstream increase in intracellular calcium. Another receptor, 5-HT$_{1B,}$ whose expression is also up-regulated on activation of the HSCs, couples through Gαi and it is possible that this receptor will cause release of calcium in this assay format (Hall et al., 1999; Werry et al., 2002). G$_i$ linked receptors can elicit release of calcium by direct stimulation of PLC through the Gβγ subunits (Selbie and Hill, 1998).

In the mouse activated HSC 5-HT was demonstrated to cause a concentration-dependent increase in release of intracellular calcium, confirming observations in the literature with rat HSCs (Park et al., 2011). To identify the receptor involved in eliciting the calcium release, selective agonists and antagonists were selected to probe and pharmacologically dissect the response. ATP was used as a positive control in the assay (to enable stimulation of the endogenously expressed P2Y receptor) (Dranoff et al., 2004). Ketanserin, GSK1606260A and cyanopindolol had no effect on the ATP CRC confirming that any effect of the antagonists was specific to the 5-HT response and not interfering with the calcium release in a non-specific manner.

5-HT$_{2B}$ antagonists, GSK1606260A (1 µM) and RS-27455 (100 nM), caused no rightward shift of the 5-HT CRC, confirming the lack of 5-HT$_{2B}$ receptor

116

involvement in mediating the 5-HT stimulated calcium release. The concentrations of the $5\text{-}HT_{2B}$ antagonists would have been expected to cause a > 100-fold rightward shift of the 5-HT CRC if the response was due to activation of the $5\text{-}HT_{2B}$ receptors. No $5\text{-}HT_{1B}$ receptor involvement was observed due to a lack of effect of the $5\text{-}HT_{1B}$ antagonist, cyanopindolol (1 μM) and lack of agonism observed with sumatriptan, a $5\text{-}HT_{1B}$ agonist. Further evidence against $5\text{-}HT_{1B}$ involvement in the 5-HT stimulation of calcium release was evident from the lack of effect of PTX treatment on the 5-HT CRC. Overnight pre-treatment of PTX, which catalyses ADP-ribosylation of the G-proteins, G_i, G_0 and Gt, thus impairing the G-protein heterotrimer interaction with the receptors, will eliminate any response via a G_i linked mechanism in the HSCs.

$5\text{-}HT_{2A}$ receptor involvement was investigated with $5\text{-}HT_{2A}$ antagonists, ketanserin and volinanserin (1, 10 and 100 nM). Both antagonists behaved as insurmountable antagonists of 5-HT stimulated calcium release in the mouse HSC (Figure 4.2.5). 1 nM concentrations of both ketanserin and volinanserin caused rightward shift and depression of the maximum 5-HT response, with the 10 and 100 nM concentrations causing substantial depression of 5-HT CRC. Due to the insurmountable nature of the antagonism observed and although the criteria for competitive antagonism has not being met, pA_2 values of 9.1 and 9.6 were estimated for ketanserin and volinanserin respectively which are consistent with $5\text{-}HT_{2A}$ receptor inhibition. The inhibition observed with ketanserin and volinanserin provides strong evidence that the calcium response is driven by the activation of $5\text{-}HT_{2A}$ receptors.

To further confirm the 5-HT response was elicited by $5\text{-}HT_{2A}$ receptors, a selective but partial $5\text{-}HT_{2A}$ agonist, NBOH-2C-CN was investigated (Hansen et al., 2014; Fantegrossi et al., 2015). In the calcium release assay this was found to produce only partial agonism in one out of three experiments carried out. The ability of an agonist to cause a response will depend on whether the stimulus is strong enough and if the cell is capable of converting the stimulus to an observable response (Kenakin, 2006). It may be that there are not sufficient receptors available for NBOH-2C-CN to elicit a response or that as the calcium release assay is quite close to the initial receptor activation insufficient amplification of the stimulus has occurred due to the receptor

coupling efficiency (Giles et al., 1996; Wilson et al., 1996; Kenakin, 2006). The ability of an agonist to produce a response is very dependent on the assay system. As no agonist CRC could be defined (Figure 4.2.6 A) NBOH-2C-CN was therefore tested as an antagonist. To ensure that NBOH-2C-CN was not desensitising the 5-HT receptor in the calcium release assay, as this would compromise the antagonism observed, NBOH-2C-CN was tested as an agonist at the same time as being tested as an antagonist. No agonism was observed with NBOH-2C-CN in any of the antagonist experiments performed. NBOH-2C-CN was found to cause insurmountable antagonism of the 5-HT CRC (Figure 4.2.6). NBOH-2C-CN caused a concentration-related rightward shift of the 5-HT CRC with about 30% depression of the maximum response. Due to insurmountable nature of the antagonism observed no definite affinity could be determined. Although the criteria for competitive antagonism is not met, a pA_2 of 7.6 was estimated from the 300 nM NBOH-2C-CN shift of the 5-HT CRC.

There was only one previous study investigating the ability of 5-HT to stimulate an increase in intracellular calcium in HSCs (Park et al., 2011). It was reported that activated HSC express voltage activated calcium channels (Oide et al., 1999). The expression level of the α-SMA and L-type calcium channels has been shown to be proportional to the activation period, with no L-type currents being observed in quiescent cells (Park et al., 2011). Thus the increased expression of L-type channels is evident during activation of HSCs. The cells used in the studies for this thesis were in culture for at least two weeks before being used in the calcium assay and have been shown to be an activated phenotype as evidenced by the expression of α-SMA. In this thesis, I have been able to show that, in mouse activated HSCs, 5-HT produces a concentration-dependent increase in intracellular calcium which is concordant with the literature in rat HSCs (Park et al., 2011). The literature (Park et al., 2011) studies were performed by measuring the increase in intracellular calcium using fura-2, a fluorescent calcium sensing dye, loaded rat HSCs on a fluorescence microscope. This is similar to the FLIPR^{TM} methodology used in this thesis but on a smaller scale with a different calcium sensing dye. Although Park et al., (2011) demonstrated a concentration-dependent response with 5-HT, they only examined the effect of a single concentration of ritanserin (10 μM) on a 10 μM 5-HT response.

Ritanserin, a 5-HT$_2$ antagonist (5-HT$_{2A}$ pK$_i$ = 8.34, 5-HT$_{2B}$ pK$_i$ = 8.7; (Knight et al., 2004)) was found to inhibit the 10 µM 5-HT response and a phospholipase C inhibitor, U73122 (1 µM) completely abolished the 5-HT response (Park et al., 2011). These data therefore provide further characterisation of the subtype of 5-HT$_2$ receptor involved in the 5-HT stimulated release of calcium. The data generated in this chapter builds on this knowledge and provides a classical 'in-depth' pharmacological analysis, using selective antagonists and agonists to definitively determine that the 5-HT$_{2A}$ receptor subtype mediates the 5-HT stimulated calcium response in activated mouse HSCs. Park et al. (2011) also demonstrated that 5-HT$_{2A}$ receptor expression increased 17-fold compared to a 3-fold increase of 5-HT$_{2B}$ receptor expression, after the cells had been in culture for 2 weeks. This adds further weight to the hypothesis that the 5-HT$_{2A}$ receptor is responsible for the observed increase in calcium following 5-HT stimulation in activated HSCs.

4.3.1.1 Investigation of the insurmountable antagonism obtained with ketanserin and volinaserin in the FLIPR™ assay.

The insurmountable profile of the antagonism observed with ketanserin, volinanserin and NBOH-2C-CN, may indicate that they are behaving as non-competitive antagonists. However another explanation could be that these compounds establish a hemi-equilibrium. This is where the antagonist and agonist together are unable to reach a proper equilibrium with the receptor in the timeframe of the agonist response (Hemi-equilibrium) (Paton and Rang, 1966; Kenakin et al., 2006). In the antagonists experiments ketanserin, volinanserin and NBOH-2C-CN were pre-incubated with the receptor for 15 min prior to 5-HT stimulation, thus allowing the antagonists to reach equilibrium with the receptor, ensuring correct receptor occupancy according to the concentration. When the agonist, 5-HT, is added to the cells then the system undergoes a re-equilibration between the agonist and the antagonist already bound to the receptor (Paton and Rang, 1966; Kenakin et al., 2006). During re-equilibration there must be sufficient time for the antagonist to dissociate from the receptors in order to allow the agonist to bind to the unbound receptors (Figure 4.3.1 A). If the antagonist has a slow off rate and the agonist response is rapid, then the antagonist is unable to dissociate fully from the receptor to allow the agonist to bind to the unbound receptors to achieve the correct receptor occupancy according to the

concentration. This is the most likely explanation for the observations in the calcium release assay with the HSCs (Kenakin et al., 2006; Charlton and Vauquelin, 2010).

To determine if the hemi-equilibrium phenomenon was occurring with ketanserin and volinanserin a 'wash off' experiment was carried out. If the antagonists cannot be washed off then this would indicate that the antagonists are acting as irreversible antagonists. All three concentrations of ketanserin and volinanserin tested demonstrated less antagonism of the 5-HT CRC after washing off, when compared to the antagonism observed with no washing off (Figure 4.2.8 and 4.2.9). The washing off of the antagonist allows the dissociation of the antagonist from the receptor thus reducing the amount of antagonist bound to the receptors. Once the cells are stimulated with 5-HT greater agonism is observed may be due to the increased availability of free receptors (provided by the dissociation of the antagonist) for the agonist to bind to. Another possibility that should also be considered it that these compounds maybe acting as reversible non-competitive antagonists. Ketanserin is reported in the literature to behave as a competitive antagonist (Frenken and Kaumann, 1984; Leff and Martin, 1986) so it is unlikely that ketanserin is acting as a reversible non-competitive antagonists. Volinanserin is a highly selective high affinity antagonist and has been shown to demonstrate slow dissociation ($t_{1/2}$) of 13.5 min from the 5-HT$_{2A}$ receptor (Kristiansen et al., 2005). There has been no data published to confirm that volinanserin is acting as a competitive antagonist but due to its slow dissociation kinetics hemi-equilibrium is a phenomenon which could explain the effects in the calcium release assay in HSCs. These experiments demonstrate that ketanserin and volinanserin are observed to behave as insurmountable antagonists due to there being insufficient time for re-equilibration of the agonist, antagonist and receptor complex (Paton and Rang, 1966; Kenakin et al., 2006; Charlton and Vauquelin, 2010). The data obtained with ketanserin (Figure 4.2.5 A) does resemble the data depicted in Figure 4.3.1 B, Panel 1.
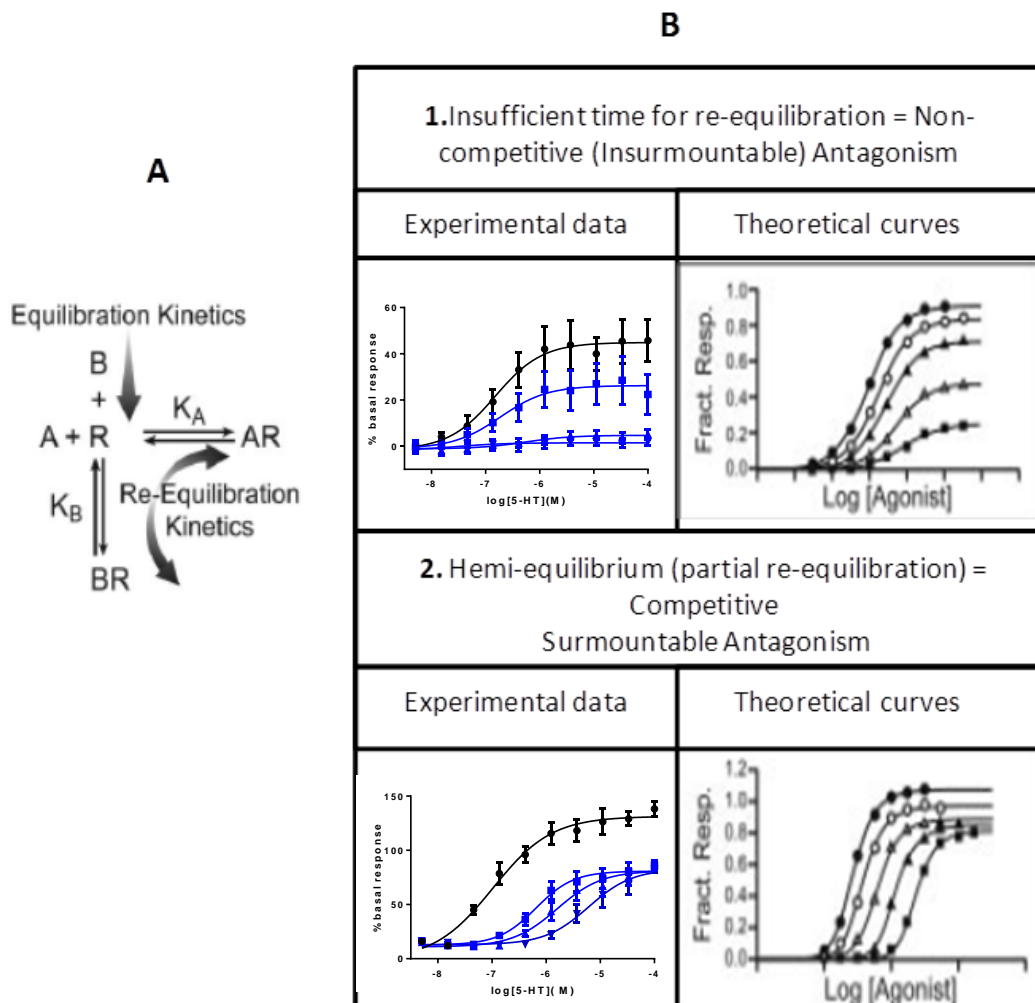
Figure 4.3.1 Schematic depicting two types of antagonist kinetics. A) Equilibrium kinetics refers to the process of antagonist binding to the receptors and reaching equilibrium according to the K_B and concentration. Re-equilibration kinetics refers to the binding of added agonist to a preparation pre-equilibrated with antagonist and the process of the agonist and antagonist achieving equilibrium with the receptor population according to their respective equilibrium dissociation constants and relative concentrations within the time allowed for measurement of agonist response . B) Summary of the kinetic for orthosteric antagonism obtained experimentally and theoretically whereby the agonist and antagonist do not (Panel 1: includes Figure 4.2.5 A) or partially do (Panel 2 : includes Figure 4.2.6 B) equilibrate according to mass action kinetics in the time allotted for observation of the response. (Adapted from Kenakin et al., 2006)

121

The nature of the antagonism observed with NBOH-2C-CN (Figure 4.2.6.) does resemble a profile expected for a competitive insurmountable antagonist, as partial equilibration occurs (Paton and Rang, 1966). This is where agonist, antagonist and receptor are able to partially re-equilibrate and where the re-equilibration occurs at the higher receptor occupancy (Kenakin et al., 2006). Some further experiments could investigate NBOH-2C-CN concentrations lower than 300 nM, to establish whether gradual depression of the 5–HT CRC maximum can be achieved. A 'wash off' experiment could also be carried out to further determine how this affects the antagonism profile observed with NBOH-2C-CN. Indeed this would hopefully demonstrate an antagonist profile as observed for the theoretical data shown in Figure 2, panel 2.

Another observation from the data obtained with ketanserin and volinanserin demonstrates there is little or no receptor reserve in the system. Rightward shift of the 5-HT CRC would be observed, with no depression of the maximum response, if there were a pool of free receptors that the agonist could bind to (Paton and Rang, 1966; Kenakin et al., 2006). With ketanserin and volinanserin there is rightward shift with depression of the maximum response. This suggests that all the receptors are bound by the antagonist, and there is no available pool of free receptors for the agonist to bind to (Figure 4.3.1. B). Hence the maximal attainable response is diminished.

4.3.2 Pharmacological characterisation of the 5-HT receptor responsible for ERK phosphorylation in mouse hepatic stellate cells.

It was demonstrated the 5-HT can stimulate ERK phosphorylation, which leads to activation of the transcription factor JunD and enhanced TGFβ1 expression. The 5-HT$_{2B}$ receptor has been reported to be the receptor in activated HSCs (Ebrahimkhani et al., 2011). The ERK pathway can be stimulated by a many different receptor types (Figure 4.3.2). These studies set out to investigate the ability of 5-HT to stimulate the ERK phosphorylation and pharmacologically characterise the 5-HT receptors responsible.

The optimum time to measure the pERK response was determined to be around 10 min (Figure 4.2.10) where the response reached its peak. This time point was therefore used in subsequent studies. It would also be of interest to investigate the later sustained response out to 3 h but also further to 24 h, because the fibrotic processes involved in phenotypic end points such as proliferation (See Chapter 5) are subjected to a sustained 5-HT stimulus throughout the incubation. The pERK response was found to be inversely correlated by the cell density (Figure 4.2.11) with final assay cell number of 10000 cells chosen to achieve a robust signal.

As with the FLIPR assay, the 5-HT stimulated pERK response was characterised in this assay format using the same 5-HT$_{2A}$, 5-HT$_{2B}$ and 5-HT$_{1B}$ antagonists and agonists at selective concentrations. GSK1606260A (1 μM) and RS-127445 (100 nM) caused no rightward shift of the 5-HT CRC at concentrations expected to shift the curve >1000-fold indicating that the 5-HT$_{2B}$ receptor was not driving the 5-HT ERK phosphorylation in HSCs (Figure 4.2.12, Table 4.2.5). With the 5-HT$_{2A}$ antagonist ketanserin (10 nM, 100 nM and 1 μM) a progressive rightward shift of the 5-HT CRC with depression of the maximum response was observed. The Hill slope coefficients obtained for the CRCs were shallow and biphasic in nature. Therefore the 5-HT response in the presence of ketanserin may act via a second 5-HT receptor. It is difficult to determine the antagonist affinity at the 5-HT$_{2A}$ receptor because of the complex behaviour of the CRC. Volinanserin (1 nM, 10 nM and 100 nM) did not produce a rightward shift in the 5-HT CRC but with increasing concentrations substantially depressed the maximum response. Although no affinity could be determined for the 5-HT$_{2A}$ antagonists the concentration range over which the antagonism was observed does suggest that the 5-HT$_{2A}$ receptor is the receptor responsible for the 5-HT stimulated ERK phosphorylation.

NBOH-2C-CN was also investigated as an agonist in this pERK assay. It was found to behave as a partial agonist, eliciting about 30% of the 5-HT maximum response, which is consistent with its reported activity in the literature (Hansen et al., 2014; Fantegrossi et al., 2015). The ERK response is further down the signalling cascade than the stimulated intracellular calcium release (Figure 4.3.2). This therefore may explain why NBOH-2C-CN behaves as a partial agonist in this ERK phosphorylation
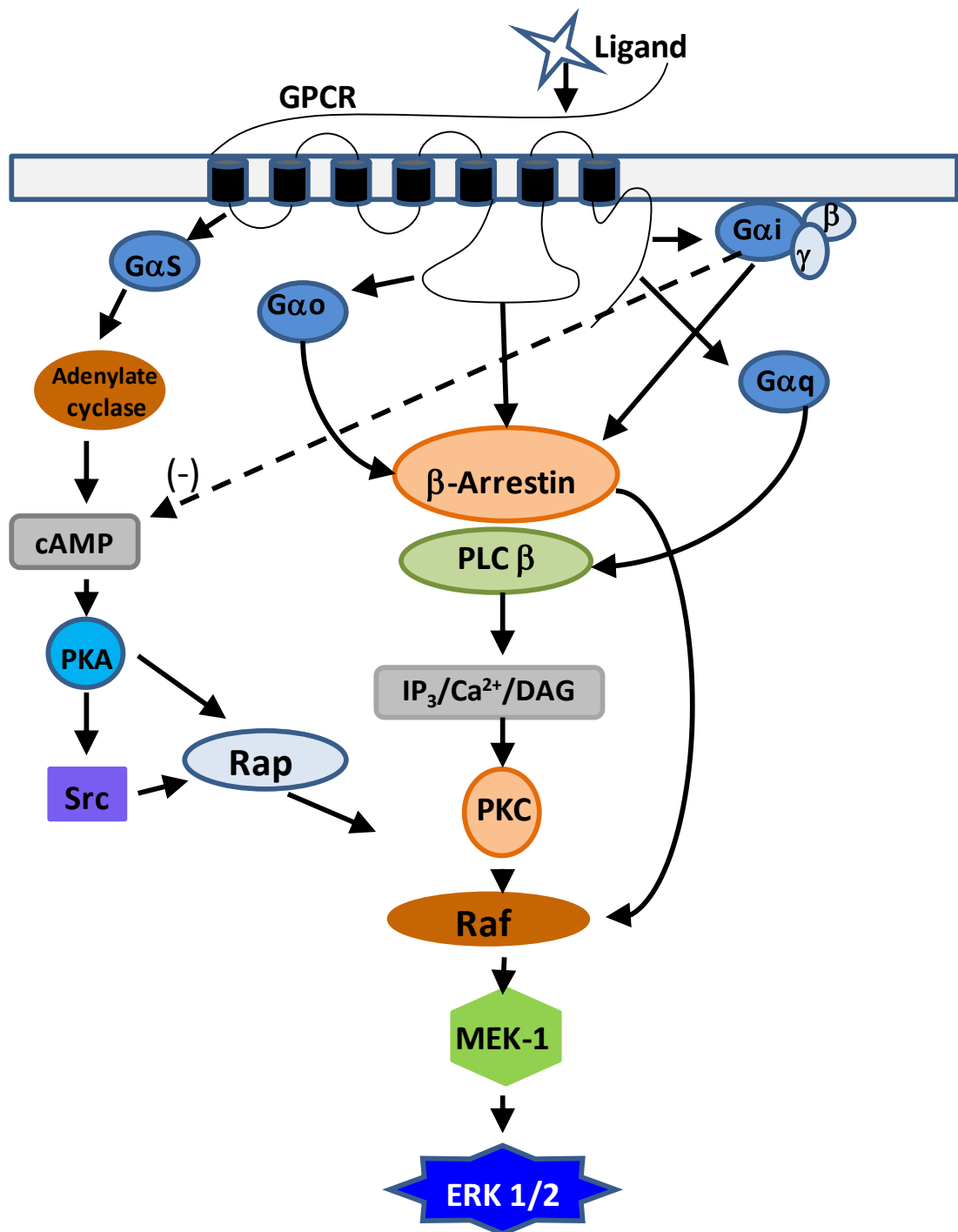
Figure 4.3.2 G protein-coupled receptor (GPCR) signalling pathways via ERK1/2.
ERK1/2 can be activated by GPCRs, which couple to different G-proteins (Gi,Gs,Gq,Go)
which transduce the signal by different pathways.

assay. The further down the signalling cascade the greater the amplification of signalling response is observed (Kenakin, 1997, 2006). The efficacy of the agonist is determined by agonist occupancy, but it is the cellular amplification of receptor signal, through a succession of saturable biochemical reactions, that will determine the strength of amplification of receptor stimulus inherent to the cells (Kenakin, 2006). This means that NBOH-2C-CN is unable to stimulate intracellular release of calcium, as it does not occupy sufficient receptors. Further down the signalling pathway there are sufficient receptors occupied for NBOH-2C-CN to be observed as a low efficacy agonist due to amplification of the signal in the cells (Kenakin, 2006). NBOH-2C-CN was antagonised by ketanserin confirming 5-HT_{2A} involvement. The pEC_{50} is consistent with the range of antagonism observed with this partial agonist in the FLIPR assay. These data provide further evidence of 5-HT_{2A} receptor involvement in the pERK response.

Interestingly the conclusion that the 5-HT_{2A} receptor is mediating the 5-HT stimulation of pERK response does not agree with the interpretation of the inhibition of the pERK response using SB-204741, a 5-HT_{2B} selective antagonist (Ebrahimkhani et al., 2011). SB-204741 is documented in the literature as having a binding affinity at the human 5-HT_{2A} receptor of $> 10\ \mu M$, compared with a 5-HT_{2B} affinity of about 100 nM (Knight et al., 2004). Upon examination of the data presented by Ebrahimkhani et al. (2011) the inhibition of 5-HT-induced ERK phosphorylation by SB-204741 occurred at concentrations of $\geq 10\ \mu M$ in rat, mouse and human HSCs. At these concentrations the inhibition is more likely due to an action at the 5-HT_{2A} receptor and not 5-HT_{2B}. 5-HT_{2B} inhibition should have been observed at lower concentrations as its affinity is around 100 nM. The data generated in this chapter seem to agree with other literature findings reported in LX-2 cells (a human HSC immortalised cell line (Xu et al., 2005)), where it was demonstrated that 5-HT_{2A} antagonists (ketanserin and sarpogrelate) induced apoptosis, inhibited cell viability and inhibited wound healing (Kim et al., (2013). Overall the data obtained at the concentrations tested are consistent with the selective pharmacology of the 5-HT_{2A} receptor and not the 5-HT_{2B} receptor, to produce a pERK response in HSCs.

4.3.3 Investigation of the non-surmountable antagonism obtained with ketanserin and volinaserin in the ERK phosphorylation assay.

Ketanserin is reported to be a competitive antagonist (Frenken and Kaumann, 1984; Leff and Martin, 1986). In the pERK assay we observe insurmountable antagonism with both ketanserin and volinaserin. Experiments were undertaken to investigate whether antagonist incubation time would influence the nature of the antagonism observed by ketanserin and volinaserin. Similar antagonism of the 5-HT CRCs was obtained after 30 min incubation of the antagonists compared to no pre-incubation of the antagonists, ketanserin (100nM) and volinanserin (10nM), indicating antagonist incubation time does not influence the nature of the antagonism. The antagonist would have been expected to demonstrate less insurmountable antagonism with no pre-incubation if the antagonists were acting irreversibly.

In the literature there are reports that the nature of the antagonism observed with ketanserin can be dependent on the assay selected (Leff and Martin, 1986). Four 5-HT_2 antagonists, ketanserin, spiperone, trazodone and methysergide were investigated in isolated preparations of rabbit aorta, rat jugular vein and rat caudal artery (Leff and Martin, 1986). It was reported that spiperone and trazodone were competitive antagonists in all three preparations. Ketanserin behaved as a competitive antagonist in all except the rat caudal artery, where it behaved as a non-competitive antagonist and methysergide behaved as competitive antagonist in the rat aorta preparation only (Leff and Martin 1986). The rat caudal artery, of the three tissue preparations used, had the fastest response to 5-HT (Leff and Martin, 1986). Thus when ketanserin is pre-incubated with the tissue for 60 min it is unable to dissociate sufficiently to allow 5-HT to reach its proper equilibrium with the receptor in the timeframe of the agonist response (hemi-equilibrium) (Paton and Rang, 1966; Kenakin et al., 2006). We observe hemi-equilibrium with ketanserin in the calcium release assay and so it may be this could be true for the pERK assay as well. The pERK assay response is a fairly quick response (~10 min). The insurmountable antagonism observed with ketanserin and volinaserin in the pERK assay (Figure 4.2.13) shows a lesser degree of depression of the 5-HT CRCs when compared with the 5-HT CRCs obtained in the calcium release assay (Figure 4.2.5). The pERK ketanserin antagonism has a similar insurmountable antagonism profile compared

with NBOH-2C-CN (Figure 4.2.6.) in the calcium release assay, in that there is rightward shift and reduction of the maximum response to a similar level with all three ketanserin concentrations. A 'wash off' experiment could be undertaken to determine if hemi-equilibrium could explain the nature of the antagonism observed with ketanserin and volinanserin in the pERK assay.

4.3.4 Investigation into the presence of a second 5-HT receptor contributing to the 5-HT response in mouse HSCs.

On closer inspection of the 5-HT CRC it was observed that there was a possibility that it was biphasic in nature. This was supported further by the data obtained for the 5-HT CRC in the presence of ketanserin. The 5-HT CRCs becomes progressively more shallow in the presence of increasing concentrations of ketanserin, this suggesting activation of more than one receptor by 5-HT. It is the nature of the antagonism observed with ketanserin which rules out an alternative hypothesis which is that 5-HT is stimulating two different G-protein signalling pathways via the 5-HT_{2A} receptor. In this alternative pathway 5-HT would stimulate the 5-HT_{2A} receptors at the lower concentrations through the G_q but at higher concentrations 5-HT is then able to stimulate the 5-HT_{2A} receptor via another G protein such as G_i. The antagonism profile for ketanserin expected, if the alternative hypothesis was correct, would depict 5-HT CRCs shifting in a similar manner to that observed with the 10 nM concentration, with similar Hill slopes.

Construction of a 5-HT CRC with greater definition supported this further (Figure 4.2.16.) and suggested that more than one 5-HT receptor subtype could be mediating the pERK response. A model was constructed to explore the influence of two receptor sub-types signalling via ERK. The model allowed the alteration of the affinity and efficacy of the response of the two receptors. By investigating different values for the affinity and efficacy of the receptors, a similar response profile as observed in the experimental assay was obtained. The model suggests that two receptors involved have differing affinities (K_A = 30 nM, K_B = 3 μM, 100-fold difference) and that these receptors also exhibit different efficacies for 5-HT (τ_A = 5, τ_B = 10). These tau values imply that 5-HT is behaving as partial agonist at both receptors. This model could be further explored by the addition of antagonists to

predict their behaviour in the experimental situation. The antagonism observed with ketanserin and volinanserin is insurmountable in the pERK assay and this avenue was not explored further in this study.

As three 5-HT receptors (5-HT_{2A}, 5-HT_{2B} and 5-HT_{1B}) have been reported to be induced upon activation of the cells, these were considered to be most likely to be signalling through pERK, but the 5-HT_{2B} receptor was ruled out as antagonists failed to inhibit the 5-HT CRC. Therefore the 5-HT_{1B} receptor seems to be the most likely candidate. However it is worth noting that 5-HT_7 and 5-HT_{1F} receptors have also been reported to be present on stellate cells (Ruddell et al 2006). The expression of 5-HT_{1F} remained stable over the 6 days the HSCs were kept in culture compared to 5-HT_7, which showed a 90% reduction after day 1 in rat HSC (Ruddell et al., 2006).

The role of the 5-HT_{1B} receptor was investigated to determine if activation of this 5-HT receptor subtype contributed to the biphasic response. Two methods were employed to investigate this. The first was to use a 5-HT_{1B} agonist and antagonist and the second was by blocking receptor G-protein activation with PTX. Sumatriptan is reported to be a selective $5\text{-HT}_{1B/1D}$ receptor agonist (Table 1.10.3). Sumatriptan behaved as partial agonist in the pERK assay with no inhibition by GSK1606260A. However ketanserin caused about a 30% depression of the sumatriptan CRC, but this was not significant. A greater shift of the sumatriptan CRC would have been expected with ketanserin if it was acting via the 5-HT_{2A} receptor as is the case with 5-HT. To try to define the interaction further, the effect of cyanopindolol, a reported antagonist at the 5-HT_{1B} receptor ($pK_B = 8.1 - 8.7$) (Maroteaux et al., 1992; Giles et al., 1996), on the sumatriptan CRC was investigated. Cyanopindolol (100nM) caused a rightward shift of the sumatriptan CRC, which was consistent with sumatriptan interacting at the 5-HT_{1B} receptor to elicit the pERK response. Due to the low potency of sumatriptan, it was not possible to clearly define the CRC in the presence of cyanopindolol but an affinity of 8 was estimated which is in the expected range for 5-HT_{1B} effect.

To further test whether a 5-HT_{1B} receptor was causing the biphasic 5-HT response, an experiment was carried to investigate the effect of cyanopindolol, ketanserin alone and in combination on the 5-HT CRC. The aim being to use cyanopindolol to block

the 5-HT$_{1B}$ receptor and therefore reveal a pure 5-HT$_{2A}$ response when stimulated with 5-HT in the pERK assay. Cyanopindolol at 1 μM (which should produce >100-fold shift of the 5-HT$_{1B}$ component) had no significant effect on the 5-HT CRC although there was some flattening of the Hill slope. The 5-HT CRC constructed in the presence of ketanserin (100 nM) was biphasic and had a shallow Hill slope. In the presence of both ketanserin (100 nM) and cyanopindolol (1μM) the 5-HT CRC was more sigmoid in shape, with a Hill slope similar to unity (Figure 4.2.21., Table 4.2.12). The 5-HT$_{1B}$ receptor influence has been removed by cyanopindolol, with the shift of the 5-HT CRC by ketanserin (100 nM) indicating of a single receptor interaction and that the receptor involved is 5-HT$_{2A}$.

Another approach to pharmacologically dissect the 5-HT$_{1B}$ response is to treat cells with PTX, as the 5-HT$_{1B}$ receptor couples through G$_{i/o}$ proteins. PTX catalyzes ADP-ribosylation of G-proteins, G$_i$, G$_o$ and G$_t$, thus impairing G protein heterotrimer interaction with receptors and blocking receptor coupling. Overnight PTX pre-treatment caused a non-significant 1.7-fold rightward shift of the 5-HT CRC. The 5-HT CRC Hill slope in the presence of ketanserin (100nM) alone was 0.76 but was 1.1 with the addition of PTX pre-treatment (Figure 4.2.22, Table 4.2.13), suggesting that 5-HT was only stimulating the 5-HT$_{2A}$ receptor after PTX pre-treatment. The effects observed with PTX treatment of the 5-HT CRC are similar to those observed in the cyanopindolol/ketanserin combination experiment. Taken together the effect of PTX treatment and the cyanopindolol/ketanserin combination experiment suggests that the 5-HT$_{1B}$ receptor is likely to be the second 5-HT receptor mediating the 5-HT stimulated ERK phosphorylation.

The effect of PTX pre-treatment on the response to the 5-HT$_{1B}$ agonist, sumatriptan, was investigated to provide further evidence of 5-HT$_{1B}$ involvement in the 5-HT stimulated pERK response. If the influence of the 5-HT$_{1B}$ receptor is effectively removed in the cells then sumatriptan would be unable to elicit an agonist response. Following PTX treatment the response to sumatriptan was not completely abolished and there was a > 5-fold shift of the sumatriptan CRC. Due to the low potency (pEC$_{50}$ ~5) of sumatriptan it is feasible that at the higher concentrations sumatriptan is causing phosphorylation of ERK via the 5-HT$_{2A}$ receptor. Indeed we observed that

ketanserin (100 nM) reduced the maximum sumatriptan response but not by as much as would have been expected if mediated solely by 5-HT$_{2A}$ receptor. Alternatively sumatriptan is behaving non-specifically. Future experiments could investigate the effect of PTX on antagonism of the sumatriptan response to cyanopindolol to ascertain if sumatriptan is eliciting the response through a different receptor. Another way could be to investigate sumatriptan agonism following PTX pre-treatment in the presence and absence of ketanserin as this may be able to further define whether 5-HT$_{2A}$ is activated or sumatriptan is acting in a non-specific way at these high concentrations.

Sumatriptan is a partial agonist and the amount of agonism observed will depend on the 5-HT$_{1B}$ receptor expression level in the HSCs used in the experiment. Mouse HSCs from different batches of mice were used for these experiments after they had been in culture for 2-5 weeks. The receptor expression levels are likely to vary from batch to batch, as well as within the batch depending on the time in culture. The amount of 5-HT$_{1B}$ induction, when compared with quiescent HSCs receptor levels, was less than observed for 5-HT$_{2A}$ or 5-HT$_{2B}$ after rat HSCs had been cultured on plastic for 6 days (5-HT$_{1B}$ ~ 4-fold, 5-HT$_{2A}$ ~120-fold and 5-HT$_{2B}$ ~60-fold (Ruddell et al., 2006)). Here the induction was only followed over a 6 day period, where 5-HT$_{1B}$ had a low level of receptor expression until day 4. After this time it increased 3-fold and maintained at this level for the remaining 2 days (Ruddell et al., 2006). 5-HT$_{1B}$ expression was also observed in rat HSCs after 2 weeks of culture.

Further research could explore the receptor expression over a longer period of time. It would be worthwhile exploring the possibility of radioligand binding saturation studies using selective radioligands for the receptors of interest. This would allow tracking of the actual number of receptors expressed over time in culture with the cells.

4.3.5   Summary

These data taken together are consistent with 5-HT stimulating both calcium release and phosphorylation of ERK through stimulation of the 5-HT$_{2A}$ receptor. This is the first time that this 'in-depth', thorough, pharmacological characterisation of the 5-HT

CRCs have been conducted. The 5-HT$_{2B}$ receptor, although shown to be expressed in these cells does not seem to play a role functionally. There is evidence for an additional 5-HT receptor subtype being activated that is not Gq-coupled. The second receptor is likely to be the 5-HT$_{1B}$ receptor due to the effect of cyanopindolol and PTX on the ketanserin antagonism, along with the agonism observed with sumatriptan, antagonism by cyanopindolol and previously reported receptor expression profile (Ruddell et al., 2006). The PTX experiment data with sumatriptan seems to contradict this but it is feasible that at the sumatriptan concentrations being explored 5-HT$_{2A}$ receptors are activated which could be further investigated as discussed earlier.

CHAPTER 5: CHARACTERISATION OF THE ROLE OF 5-HT IN PRODUCING PHENOTYPIC RESPONSES IN MOUSE HEPATIC STELLATE CELLS.

5.1 Introduction.

HSCs are the key cell type which orchestrates the pathogenesis of hepatic fibrosis (Friedman, 2000). HSCs differentiate into a persistent proliferative myofibroblast-like cell expressing α-SMA, which is increasingly contractile and migratory. They also secrete ECM proteins (e.g. collagen), TGFβ1, PDGF, CTGF and other cytokines (Bachem et al., 1992; Friedman, 2008a). 5-HT has been reported to promote the fibrogenic activity of HSCs (Li et al., 2006; Ruddell et al., 2006; Ebrahimkhani et al., 2011; Kim et al., 2013). Literature evidence, indicating a role of 5-HT in proliferation of HSCs has been reported (Ruddell et al., 2006). PDGF has been shown to be the most potent mitogen for HSC *in vitro* (Pinzani, 2002). High concentrations of PDGF are released, by a number of different cells during liver injury, which cause HSCs to proliferate and migrate (Ross et al., 1986; Pinzani and Marra, 2001a). Investigation of 5-HT's ability to stimulate proliferation and the 5-HT receptor mediating this response was therefore undertaken. As evidence suggesting synergy between 5-HT and PDGF in a proliferation assay has previously been reported (Ruddell et al., 2006) investigation of this was also carried out to develop a greater understanding of the signalling pathways involved and the implications in fibrosis.

A Scar-in-a-Jar (SIAJ) model, allows the study of fibroblast collagen deposition through culture in the presence of a neutral ficoll cocktail (Chen et al., 2009). The presence of the neutral ficoll cocktail causes 'macromolecular crowding' which mimics the highly crowded environment found *in vivo* (Chen et al., 2009). This crowded environment accelerates the collagen deposition in monolayer fibroblast culture, which can be quantified by immunofluorescence and *in situ* optical analysis. Study of all stages of the biosynthetic cascade of collagen production is possible allowing assessment of anti-fibrotic compounds (Chen et al., 2009). This assay was adapted for HSCs to investigate the ability of 5-HT to stimulate TGFβ driven collagen deposition.

Fibrosis is a multi-cellular process and animal models of liver injury offer the opportunity to study the impact of novel compounds in a multi-cellular fibrotic

environment. A number of groups have investigated 5-HT antagonists in rodent models of liver injury (Ebrahimkhani et al., 2011; Kim et al., 2013). ERK activation has been shown to occur in rat HSCs following *in vivo* liver injury with CCl_4 (Marra et al., 1999a) and the mouse CCl_4 model of liver injury has been used in the literature to investigate the effect of $5-HT_2$ antagonists in the liver (Ruddell et al., 2006; Ebrahimkhani et al., 2011). It has been established that 5-HT is able to activate the ERK pathway through the $5-HT_{2A}$ receptor in mouse HSCs (Chapter 4 pERK data). There is literature evidence to support $5-HT_{2B}$ involvement in the CCl_4 liver injury model with an anti-fibrotic effect reported with a $5-HT_{2B}$ antagonist, SB-204741 (Ebrahimkhani et al., 2011).

Chapter 4 focussed on pharmacologically characterising the 5–HT receptors expressed on activated HSCs involved in calcium release and pERK stimulation. This chapter extends the characterisation to the downstream consequences of 5-HT receptor activation in 'phenotypic fibrotic' assays. Investigations were carried out using proliferation and collagen deposition assays to characterise the 5-HT phenotypic responses in mouse HSCs. To help to develop a greater understanding of the contribution of 5-HT in fibrosis, investigation into the concentration-relationship of $5-HT_2$ antagonists in a CCl_4 animal model of liver injury were also conducted.

5.2 Results.

5.2.1 Hepatic stellate cell proliferation assay.

The bromodeoxyuridine (BrdU) colourimetric ELISA was developed to measure proliferation by assaying increased DNA synthesis. Mouse HSCs were stimulated with a range of concentrations of 5-HT (1.8 nM-100 μM) and PDGF-BB (1.6 pM-1.6 nM). No increase in proliferation was observed with 5-HT (Figure 5.2.1.A), but there was a trend to inhibition of proliferation at concentrations >10 μM. PDGF caused a concentration-dependent increase in proliferation with a pEC_{50} value of 9.8 (Figures 5.2.1B, Table 5.2.1.) which confirmed that HSCs were capable of proliferating in the assay. The concentration-dependent effects of ketanserin and GSK1606260A on the basal level of proliferation were investigated, with a small reduction in proliferation being observed at concentrations around 1 μM (Figure 5.2.2 A & B). The relatively
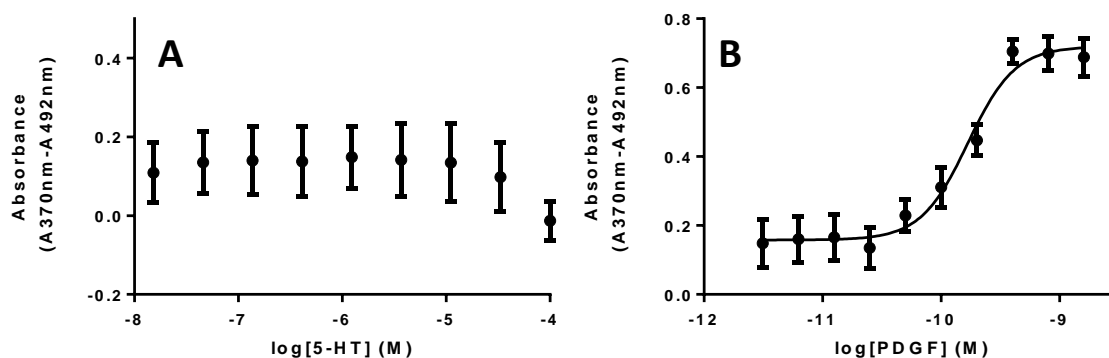
Figure 5.2.1   Effect of 5-HT and PDGF on proliferation of mouse HSCs. Culture-activated mouse HSCs were cultured in medium containing 0.1% FCS for 24 h before addition of increasing concentrations of 5-HT (A) and PDGF (B) for a further 24 h. The BrdU label was added for a further 4 h incubation at 37°C in 5% CO_2. The proliferation was determined as incorporation of BrdU into the genomic DNA of the proliferating cells using a colourimetric ELISA (See Chapter 2: Material and methods). Response values were normalised to basal and data was expressed as absorbance. CRCs were fitted using non-linear regression analysis (four parameter logistic equation with variable slope (Hill, 1909)) (See Chapter 2: Data analysis). Data shown are the mean ± SEM of at least 4 independent experiments carried out in duplicate.

	PDGF
Maximum response	0.60 ± 0.1
pEC$_{50}$	9.81 ± 0.1
Slope	3.21 ± 1.0

Table 5.2.1   Mean maximum response, pEC$_{50}$ and slope values obtained from the fitting of the PDGF CRCs obtained in the mouse HSC proliferation assay. Data represents fitting parameters obtained from fitting all the individual data using non-linear regression analysis (four parameter logistic equation with variable slope (Hill, 1909)) (See Chapter 2: Data analysis) which is graphically represented in Figure 5.2.1. Data shown are the mean ± SEM of 6 independent experiments carried out in duplicate.
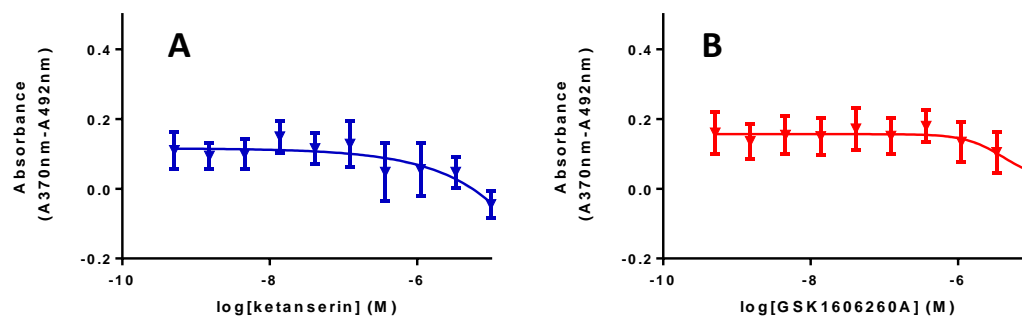
Figure 5.2.2 **Effect of increasing concentrations of (A) ketanserin and (B) GSK1606260A on basal proliferation of mouse HSCs.** Culture-activated mouse HSCs were cultured in medium containing 0.1% FCS for 24 h before addition of increasing concentrations of ketanserin or GSK1606260A for a further 24 h. The BrdU label was added for a further 4 h incubation at 37°C in 5% CO_2. The proliferation was determined as incorporation of BrdU into the genomic DNA of the proliferating cells using a colourimetric ELISA (See Chapter 2: Material and methods). Response values were normalised to basal and data was expressed as absorbance. CRCs were fitted using non-linear regression analysis (four parameter logistic equation with variable slope (Hill, 1909)) (See Chapter 2: Data analysis). Data shown are the mean ± SEM of at least 3 independent experiments carried out in duplicate.

high concentrations at which these compounds caused their effects are not consistent with the 5-HT$_{2A}$ affinity of ketanserin or 5-HT$_{2B}$ affinity of GSK1606260A, and therefore are more likely to be a non-specific effect.

5.2.2   5-HT and PDGF interaction studies in the proliferation and pERK assay.

As there had been reports of enhancement of PDGF proliferation following addition of 5-HT (10 µM), this was also investigated (Ruddell et al., 2006). No significant effects were observed in the proliferation assay on the PDGF CRC parameters, compared to the control PDGF CRC, in the presence of a maximal concentration of 5-HT (10 µM) (Figure 5.2.3, Table 5.2.2). The effect of the ketanserin (100 nM) and GSK1606260A (1 µM) on PDGF proliferation was investigated, with no effect being observed on the PDGF CRC parameters compared to the control PDGF CRC (Figure 5.2.4, Table 5.2.3), thus confirming no direct effect of the antagonists. PDGF, like 5-HT signals through ERK. The pERK assay provides a platform to investigate enhancement of PDGF response in the presence of 5-HT, that was observed in the proliferation assay by Ruddell et al. (2006). This despite not being able to confirm these findings in the current study.

The time course of PDGF (1.6 nM) stimulated ERK phosphorylation was investigated and compared to 5-HT (10 µM), to determine the profile of response of both stimuli over 24 h at 37°C in mouse HSCs. A rapid increase in ERK phosphorylation was observed with PDGF, with a maximal response around 10 to 15 min followed by a slower decline to ~12% of the maximum response at 75 min, which was then maintained out to 4 h, with a small decline to (~ 9 %) at 24 h. (Figure 5.2.5). The 5-HT response followed a similar pattern of stimulation over time as PDGF, but after 75 minutes the residual response was about 6 % of the 5-HT maximum response, which returned to baseline at 8 h. It is possible that the residual response observed with PDGF is important for driving the ongoing proliferation.

PDGF and 5-HT CRCs were generated in the presence of sub-maximal concentrations of 5-HT (100 nM) and PDGF (0.2 nM) respectively to explore the potential for synergy. 5-HT (100 nM) caused a significant 4-fold leftward shift of
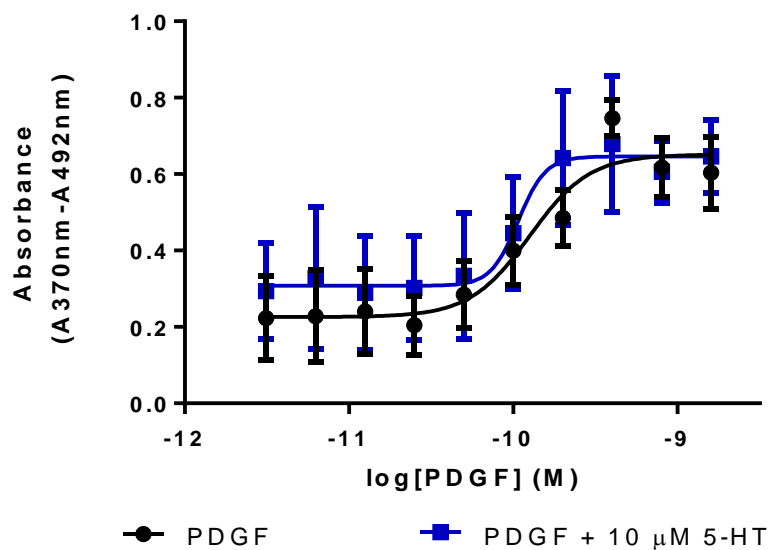
Figure 5.2.3   Effect of 5-HT (10 μM) on PDGF–induced mouse HSC proliferation. Culture-activated mouse HSCs were cultured in medium containing 0.1% FCS for 24 h before addition of various concentrations of PDGF in the presence and absence of 5-HT (10μM) for a further 24 h. The BrdU label was added for a further 4 h incubation at 37^oC in 5% CO_2. The proliferation was determined as incorporation of BrdU into the genomic DNA of the proliferating cells using a colourimetric ELISA (See Chapter 2: Material and Methods). Response values were normalised to basal and data were expressed as absorbance. CRCs were fitted using non-linear regression analysis (four parameter logistic equation with variable slope (Hill, 1909)) (See Chapter 2: Data analysis). Data shown are the mean ± SEM of at least 3 independent experiments carried out in duplicate.

	PDGF	**PDGF + 5-HT (10 μM)**
Basal Response	0.11 ± 0.1	0.3 ± 0.2
Maximum response	0.56 ± 0.2	0.64 ± 0.2
pEC$_{50}$	9.98 ± 0.2	10.09 ± 0.3
Slope	4.37 ± 1.9	3.2 ± 2.0

Table 5.2.2   Mean basal response, maximum response, pEC$_{50}$ and slope values obtained from the fitting of the PDGF CRCs in the presence and absence of 5-HT (10 μM) obtained in the mouse HSC proliferation assay. Data represents fitting parameters obtained from fitting all the individual data using non-linear regression analysis (four parameter logistic equation with variable slope (Hill, 1909)) (See Chapter 2: Data analysis) which is graphically represented in Figure 5.2.4 Data shown are the mean ± SEM of 3 independent experiments carried out in duplicate.
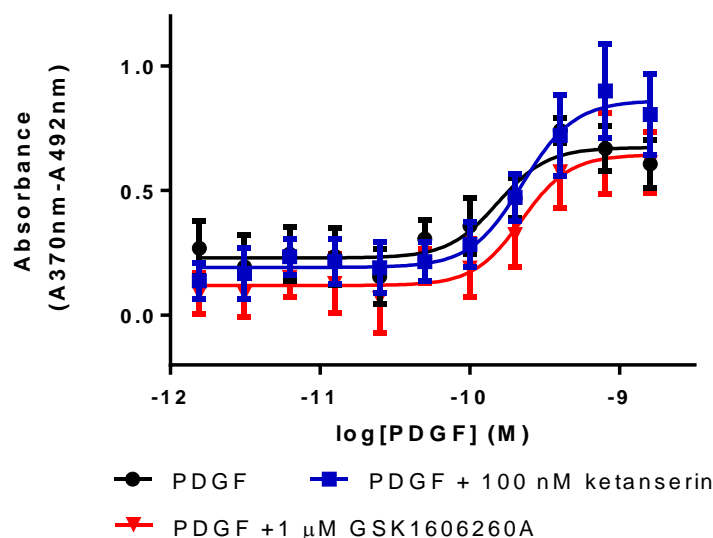
Figure 5.2.4 Effect of ketanserin (100 nM) and GSK1606260A (1 μM) on PDGF CRCs generated in the mouse HSC proliferation assay. Culture-activated mouse HSCs were cultured in medium containing 0.1% FCS for 24 h before addition of increasing concentrations of PDGF in the presence and absence of ketanserin (100nM) and GSK1606260A (1μM) for a further 24 h. The BrdU label was added for a further 4 h incubation at 37°C in 5% CO_2. The proliferation was determined as incorporation of BrdU into the genomic DNA of the proliferating cells using a colourimetric ELISA (See Chapter 2: Material and methods). Response values were normalised to basal and data was expressed as absorbance. CRCs were fitted using non-linear regression analysis (four parameter logistic equation with variable slope (Hill, 1909)) (See Chapter 2: Data analysis). Data shown are the mean ± SEM of at least 3 independent experiments carried out in duplicate.

	PDGF	PDGF + ketanserin (100 nM)	PDGF + GSK1606260A (1 μM)
Basal response	0.10 ± 0.2	0.20 ± 0.1	0.12 ± 0.2
Maximum Response	0.58 ± 0.2	0.91 ± 0.3	0.65 ± 0.2
pEC$_{50}$	9.95 ± 0.2	9.49 ± 0.2	9.82 ± 0.2
Hill Slope	4.53 ± 1.8	2.26 ± 0.8	2.48 ± 0.8

Table 5.2.3   Mean maximum response, pEC$_{50}$ and slope values obtained from the fitting of the PDGF CRCs in the presence and absence of ketanserin (100 nM) and GSK1606260A (1 μM) obtained in the mouse HSC proliferation assay. Data represents fitting parameters obtained from fitting all the individual data using non-linear regression analysis (four parameter logistic equation with variable slope (Hill, 1909)) (See Chapter 2: Data analysis) which is graphically represented in Figure 5.2.2. Data shown are the mean ± SEM of 3 independent experiments carried out in duplicate.
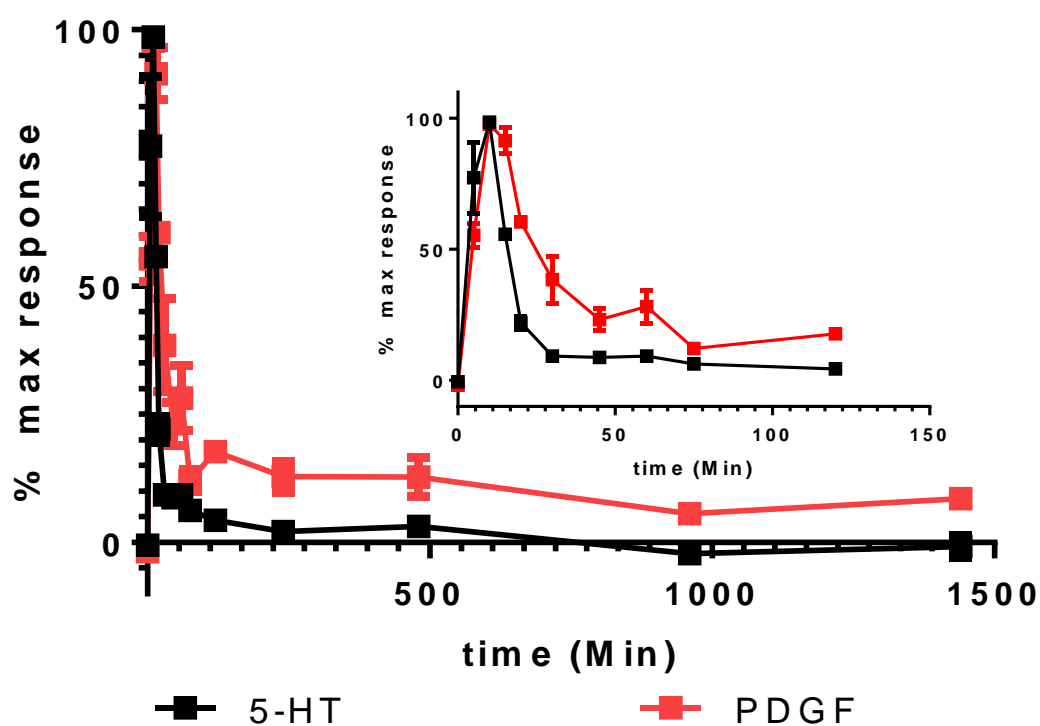
Figure 5.2.5 5-HT (10 μM) and PDGF (1.6 nM) stimulated ERK phosphorylation response over 24 h generated in mouse HSCs. Inset graph highlights the response observed over the first 2 h of the 24 h experiment. Culture-activated mouse HSCs were cultured in serum-free medium at $37^{\circ}C$ in 5% CO_2 for 24 h before addition of 5-HT (10 μM) or PDGF (1.6 nM) or medium at different time points over 24 h incubation. The pERK and total ERK levels were measured in the cell lysates using an MSD pERK/Total ERK kit (See Chapter 2: Materials and methods). The data was normalised to the maximum response obtained in each assay and expressed as % maximum response. Data shown are the mean ± range from 2 individual experiments carried out in duplicate.

the PDGF CRC (p <0.05, Student paired *t*-test), causing an increase in potency from 370 pM to 91 pM (Figure 5.2.6, Table 5.2.4). The signal window of the PDGF CRC was reduced in the presence of 5-HT (100 nM), due to the increased baseline response caused by 5-HT. However the actual maximum response achieved by both PDGF curves was not significantly different (p>0.05, Student paired *t*-test).

The reciprocal experiment where the 5-HT CRCs were generated in the absence and presence of PDGF (0.2 nM) was performed. The 5-HT CRC, in the presence of PDGF (0.2 nM) was found to produce a similar pEC_{50} and signal window (Figure 5.2.6 B, Table 5.2.4). The 5-HT CRC baseline, in the presence of PDGF (0.2 nM) increased, suggesting an additive effect. The actual maximum pERK response attained by 5-HT, in the presence of PDGF (0.2nM), was not significantly different from the maximum pERK response reached with PDGF alone (p>0.05, Student paired *t*-test). In this system 5-HT is unable to stimulate pERK to the same level as PDGF.

5.2.3 Role of 5-HT in driving TGF-β collagen deposition using the Scar in a jar assay.

Collagen deposition was investigated using mouse HSCs in a high-content imaging method adapted from Chen et al. (2009). In a preliminary study 5-HT, TGFβ, PDGF, or ketanserin applied to mouse HSCs did not elicit a concentration-related increase in collagen deposition (Figure 5.2.7). 5-HT did not affect the collagen deposition until concentrations of 10 μM or above but this is most likely due to the increase in cell numbers observed at these concentrations (Figure 5.2.7 C). A small gradual increase in collagen was observed with ketanserin in this single experiment with two different batches of cells but this is due to the differences in the cell numbers observed (Figure 5.2.7 D). No collagen deposition was observed with TGFβ, which would have been expected to cause an increase in collagen deposition (Figure 5.2.7 B). PDGF caused a small increase in collagen deposition at the lower 3 concentrations but this may have been due to a lower overall cell count observed in one of the plates (Figure 5.2.7 C). A subsequent experiment was carried out investigating just TGFβ1 alone with a further three different batches of mouse HSCs.
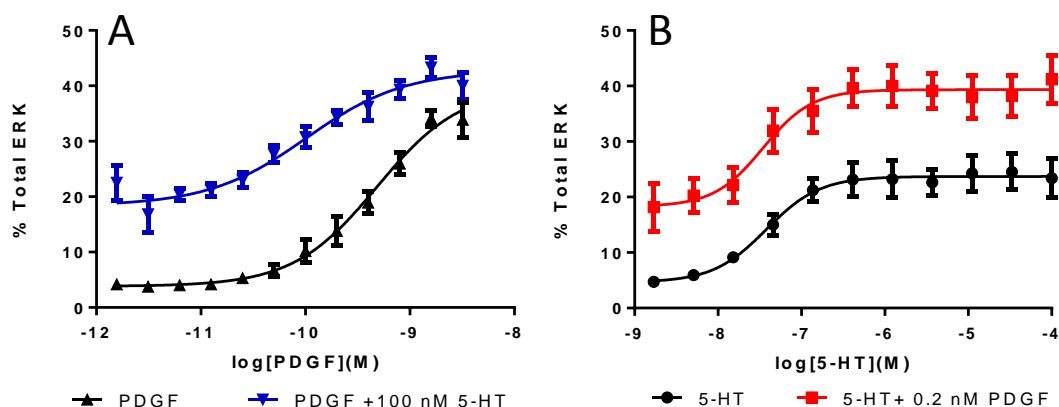
Figure 5.2.6 (A) PDGF CRC (± 5-HT (100 nM)) and (B) 5-HT CRC (± PDGF (0.2 nM)) generated in the mouse HSCs pERK assay. Culture-activated mouse HSCs were cultured in serum-free medium at 37°C in 5% CO_2 for 24 h before replacing the medium with HBSS. PDGF ± 5-HT (100 nM) or 5-HT ± PDGF (0.2 nM) were incubated for 10 min at room temperature before aspiration and addition of ice cold lysis buffer to the cells. The pERK and total ERK levels were measured in the cell lysates using an MSD pERK/Total ERK kit (See Chapter 2: Materials and methods). The data was expressed as the % Total ERK. CRCs were fitted using non-linear regression analysis (four parameter logistic equation with variable slope (Hill, 1909)) (See Chapter 2: Data analysis). Data shown are the mean ± SEM from 3 independent experiments carried out in duplicate.

	PDGF	PDGF + 5-HT (100 nM)	5-HT	5-HT + PDGF (0.2 nM)
Basal % pERK	3.8 ± 0.1	18.7 ± 1.6	3.8 ± 0.3	19.7 ± 4.9
Max % pERK	38.2 ± 4.0	43.0 ± 2.7	23.8 ± 4.9	39.3 ± 5.6
pEC$_{50}$	9.43 ± 0.3	10.04 ± 0.3*	7.44 ± 0.1	7.39 ± 0.02
slope	1.46 ± 0.1	0.99 ± 0.1	1.11 ± 0.1	1.91 ± 0.6
Max % pERK window	34.5 ± 4.1	24.3 ± 1.8	20.0 ± 4.6	19.6 ± 3.5

Table 5.2.4 Mean fitting parameters obtained from fitting PDGF CRC (± 5-HT (10 µM) and 5-HT CRC (± PDGF (0.2 nM)) in the mouse HSC proliferation assay. Data represents fitting parameters obtained from fitting all the individual data using non-linear regression analysis (four parameter logistic equation with variable slope (Hill, 1909)) (See Chapter 2: Data analysis) which is graphically represented in Figure 5.2.6. Data shown are the mean ± SEM of 3 individual experiments carried out in duplicate. * p <0.05 (Student paired *t*-test) when compared with PDGF pEC$_{50}$.
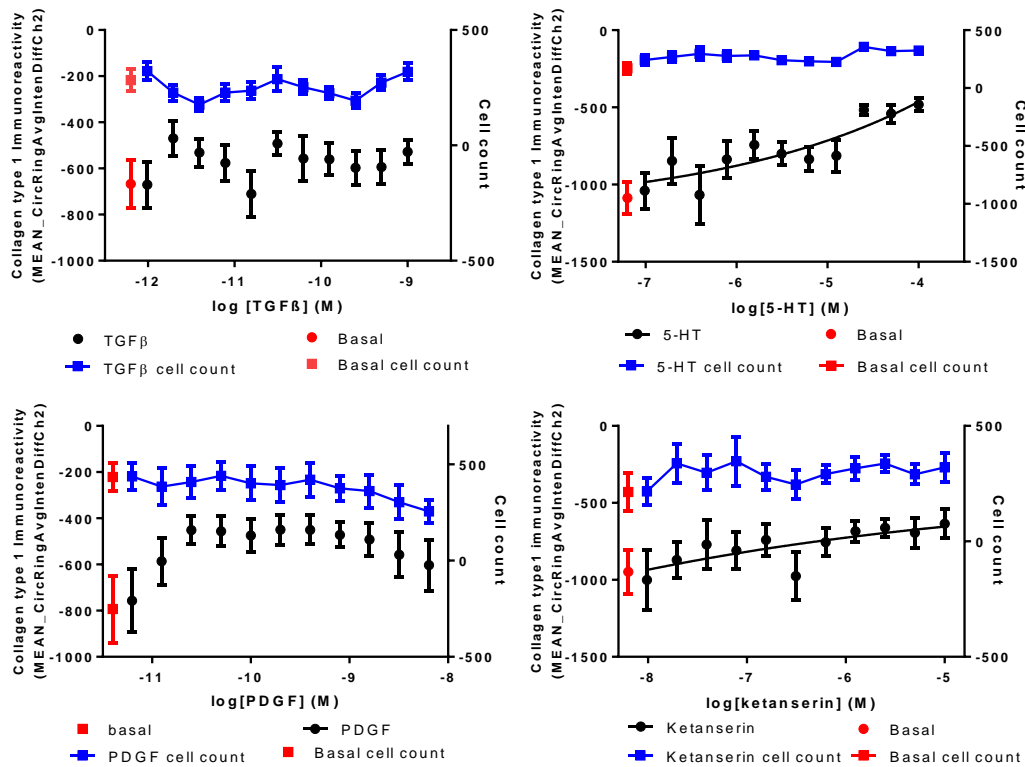
Figure 5.2.7   Effect of (A) 5-HT, (B) TGFβ1, (C) PDGF and (D) ketanserin on collagen 1 deposition and cell count in mouse HSCs. Culture-activated mouse HSC were cultured in low serum (0.4%) medium at 37°C in 5% CO_2 for 24 h before replacing the medium with Ficoll mix made up in low serum medium containing 0.2mM ascorbic acid. Compounds were added and incubated for 72 h at 37$^°$C in 5% CO_2. Cells were fixed and stained to detect collagen 1 and the nucleus of the cells. The fluorescence was then visualised and an algorithm was used to determine cell number and collagen deposition (See Chapter 2: Materials and methods). The data were expressed as the amount of collagen type 1 immunoreactivity (Mean circle ring 2 average intensity difference). Data shown are the mean ± SEM from 8-16 replicate curves from 2 different batches of cells in a single experiment.

Out of the three batches only one batch produced a TGFβ1 concentration-dependent increase in collagen 1 deposition (Figure 5.2.8 A), with no change in cell count over the same concentration range (Figure 5.2.8 B). A CRC was fitted to the data generating a pEC_{50} value of 10.91 (Table 5.2.5). Interestingly, the basal level of collagen deposition was markedly lower than with the other two batches of cells. The maximum collagen deposition was similar to the basal levels of the two other batches of cells. The cell number was lower in this batch of cells (Figure 5.2.8 B). This suggests there was a reduced level of activation of this batch of HSCs compared to the other batches of cells. This could be due to a mixed population of activated and non-activated cells. The cells which produced the TGFβ-induced collagen deposition CRC had been in culture for 5 weeks, compared to 3 weeks for the two other batches of cells. The effect of time in culture could be investigated further.

5.2.4 *In vivo* CCl₄ liver injury model.

Two compounds volinaserin, a 5-HT$_{2A}$ antagonist, and GSK1606260A, a 5-HT$_{2B}$ antagonist were identified as suitable candidates for the *in vivo* CCl₄ experiment from an initial list of 6 possible 5-HT$_{2A}$ and 5-HT$_{2B}$ antagonists. The selection of volinanserin and GSK1606260A was based on their selectivity against other receptors, solubility, stability of *in vivo* formulation, % protein binding and results of naïve mouse pilot PK studies. In order to fully assess the effect of target inhibition, doses of the compounds were selected to achieve 90% and 99% receptor occupancy, as calculated from their receptor functional pK_i (Table 4.2.1). For volinaserin the delivery doses were identified as 0.06 mg/kg/day (90% occupancy dose) and 0.64 mg/kg/day (99% occupancy dose), but due to unexpected formulation issues at the start of the study this was reduced to 0.32 mg/kg/day, which achieved about 98% occupancy at the 5-HT$_{2A}$ receptor (Chapter 9: Appendix, Table 9.4.1). For GSK1606260A, 0.15 and 1.53 mg/kg/day doses required to achieve the 90 and 99% receptor occupancy at the 5-HT$_{2B}$ receptor (Chapter 9: Appendix, Table 9.4.1).

5.2.4.1 PK/PD analysis of the in vivo CCl₄ model results.

The blood concentrations achieved were as predicted over the study (Figure 9.4.2). Liver from animals dosed with the 5-HT$_{2B}$ antagonist GSK1606260A had
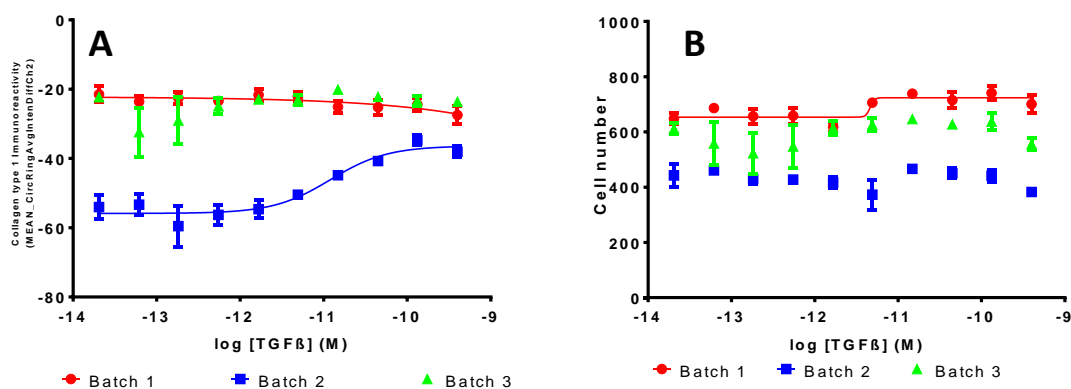
Figure 5.2.8 Effect of TGFβ1 on (A) collagen 1 deposition and (B) cell count in mouse HSCs. Culture-activated mouse HSC were cultured in low serum (0.4%) medium at 37°C in 5% CO_2 for 24 h before replacing the medium with Ficoll mix made up in low serum medium containing 0.2mM ascorbic acid. TGFβ1 was added and incubated for 72 h at 37°C in 5% CO_2. Cells were fixed and stained to detect collagen 1 and the nucleus of the cells. The fluorescence was then visualised and an algorithm was used to determine cell number and collagen deposition (See Chapter 2: Materials and methods). The data were expressed as the amount of collagen type 1 immunoreactivity (Mean circle ring 2 average intensity difference). CRCs were fitted using non-linear regression analysis (four parameter logistic equation with variable slope (Hill, 1909)) (See Chapter 2: Data analysis). Data shown are mean values ± SEM from 8 replicate curves for each of the 3 batches of cells in a single experiment.

	TGFβ1
Basal	-55.87
Maximum Response	-36.39
pEC$_{50}$	10.92
Slope	1.27

Table 5.2.5 Fitting parameters obtained from fitting TGFβ1 CRC curve obtained for Batch 2 in the collagen deposition assay in mouse HSCs. Data represents fitting parameters obtained from fitting all the data using non-linear regression analysis (four parameter logistic equation with variable slope (Hill, 1909)) (See Chapter 2: Data analysis) which is graphically represented in Figure 5.2.9. Data shown are the fit from 8 individual curves from a single experiment.

significantly increased % PSR area at both doses compared to the 8 week vehicle (*Dunnetts adjusted p-value=0.0445 for 0.15mg; **Dunnetts adjusted p-value=0.0036 for 1.53mg) (Figure 9.4.4). Liver from animals dosed with the $5\text{-}HT_{2A}$ antagonist, volinanserin (0.06 and 0.32 mg/kg/day) showed no significant difference in the % PSR area staining compared with liver from vehicle animals at week 8 (Figure 9.4.5).

Further PK/PD analysis of the picrosirius red (PSR) (for collagen) staining data obtained for GSK1606260A in the *in vivo* study demonstrated that there was a concentration-dependent effect relationship, with $5\text{-}HT_{2B}$ antagonism producing a pro-fibrotic effect in the mouse liver injury model (Figure 5.2.9). A similar analysis was carried out for volinanserin but no evidence of a concentration-dependent effect relationship for the involvement of a $5\text{-}HT_{2A}$ receptor in fibrosis was found (Figure 5.2.10).

5.3 Discussion.

5.3.1 Hepatic stellate cell proliferation response to 5-HT.

The proliferation studies demonstrated that 5-HT was unable to induce proliferation of mouse HSCs, whereas PDGF was able to induce proliferation in a concentration-dependent manner (Figure 5.2.1). These results agree with the findings of Ruddell et al. (2006) as they observed no proliferation with 5-HT alone in rat HSCs. The methodology used to isolate, culture and measure proliferation of the mouse HSCs were similar to that of Ruddell et al. (2006) for the rat HSCs. However other groups using myofibroblasts derived from either mesangial cells (Eto et al., 1997) or fibroblasts (Welsh et al., 2004; Chen et al., 2014) have reported a proliferative effect of 5-HT. This may indicate a difference in sensitivity of a particular cell type to 5-HT as a mitogen.

Following on from reports in the literature of $5\text{-}HT_2$ antagonist inhibiting proliferation (Ruddell et al., 2006; Lee et al., 2012; Kim et al., 2013) both ketanserin and GSK1606260A were tested to see if they could inhibit proliferation, at
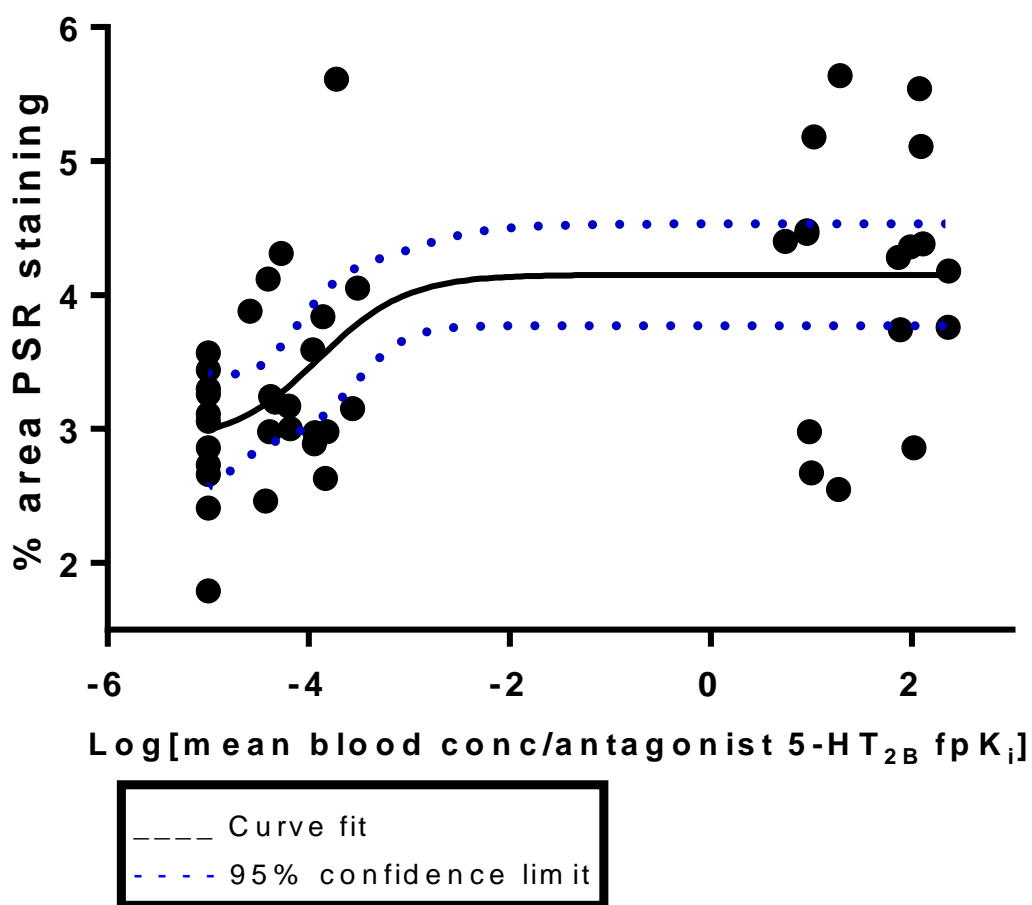
Figure 5.2.9 Concentration-response analysis of GSK1606260A percent picrosirius red staining area. Animals were injected i.p. with CCl$_4$ twice weekly for up to a total of 8 weeks to induce fibrosis. One group was culled at 3 weeks to determine baseline and the rest of the groups of animals were surgically implanted with minipumps (flow rate 3.6 µL/day) that had been loaded with vehicle (DMSO : PEG200 : water 10:45:45 (v/v/v), 0.15 mg/kg/day GSK1606260A and 1.53 mg/kg/day GSK1606260A respectively. The blood samples were taken throughout the in-life phase and as a terminal procedure to determine the drug exposure levels (Figure 5.2.10.) (Chapter 9: Appendix Section 9.4). Histological assessment of fibrosis was determined as % area picrosirius red staining of liver slices. The mean blood concentrations were scaled to the 5-HT$_{2B}$ fpK$_i$ (see table 4.2.1) of the antagonists. Data were fitted using non-linear regression analysis (three parameter logistic equation with slope =1) (See Chapter 2: Data analysis).
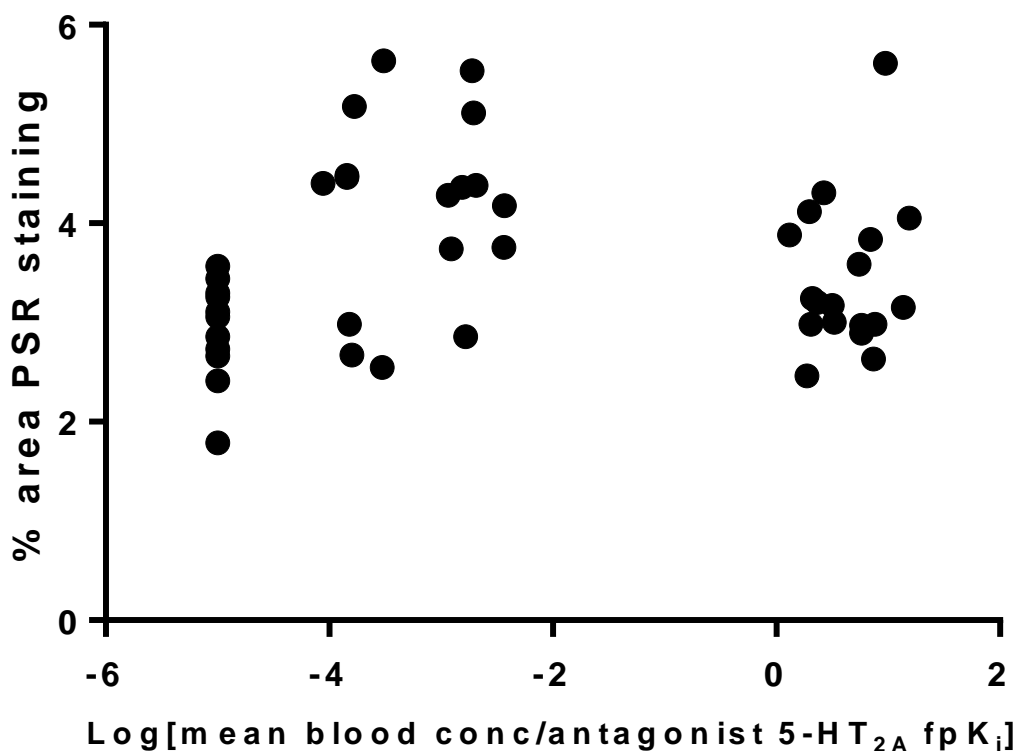
5.2.10 Concentration-response analysis of volinanserin percent picrosirius red staining area. Animals were injected i.p. with CCl_4 twice weekly for up to a total of 8 weeks to induce fibrosis. One group was culled at 3 weeks to determine baseline and the rest of the groups of animals were surgically implanted with minipumps (flow rate 3.6 μL/day) that had been loaded with vehicle (DMSO : PEG200 : water 10:45:45 (v/v/v), 0.06 mg/kg/day volinanserin and 0.32 mg/kg/day volinanserin respectively. The blood samples were taken throughout the life phase and as a terminal procedure to determine the drug exposure levels (Figure 5.2.10.) (See Chapter 9: Appendix, Section 9.4). Histological assessment of fibrosis was determined as % area picrosirius red staining of liver slices. The mean blood concentrations were scaled to the 5-HT_{2A} fpK_i (see table 4.2.1) of the antagonists. Data were fitted using non-linear regression analysis (three parameter logistic equation with slope =1) (See Chapter 2: Data analysis).

concentrations that could indicate the 5-HT receptor subtype mediating the response. In the experiments inhibition of proliferation did occur, but at concentrations above 1μM, suggesting an affinity of greater than 1μM. It is therefore unlikely that either 5-HT_{2A} or 5-HT_{2B} receptor is involved, as both compounds have nM affinity for their respective 5-HT_2 receptor subtypes. These data are similar to those previously reported for ketanserin and a number of different 5-HT_2 antagonists in rat HSCs where the IC_{50} values were all greater than 1 μM and therefore difficult to determine the specific 5-HT receptor subtype responsible (Ruddell et al., 2006). In apoptosis assays, using LX2 cells (Kim et al., 2011) and rat HSCs (Ruddell et al., 2006), 5-HT_2 antagonists demonstrated an increase in apoptosis, at concentrations greater than 1 μM, similar to that which caused reduced proliferation. One possible interpretation is that the increase of apoptosis may be due to a non-specific toxic effect of the compounds at these $> \mu M$ concentrations. This highlights the problem of using high concentrations of antagonists when trying to confirm a specific receptor effect and subsequent potentially erroneous interpretation of the result.

5.3.2   5-HT and PDGF interaction studies in the proliferation and pERK assay.

Enhancement of PDGF-mediated proliferation with a maximal concentration of 5-HT (10 μM) has been reported, where a 2-fold leftward shift of the PDGF CRC and increased maximum response of approximately 30%, was reported in rat HSCs (Ruddell et al., 2006). They also reported that, in the presence of a sub-maximal concentration of PDGF, 5-HT was able to elicit a concentration-dependent increase in proliferation (Ruddell et al., 2006). This was presented as a change in absorbance, not % control BrdU incorporation in the previous study, due to a difference in the methodology used. It is therefore difficult to get a sense of the magnitude of response compared with the rest of the proliferation data presented (Ruddell et al., 2006). These data generated in this study (Figure 5.2.3) did not replicate the 5-HT enhancement of PDGF proliferation observed. There was also no observed effect with a 5-HT_{2A} antagonist, ketanserin, or 5-HT_{2B} antagonist, GSK1606260A, on the PDGF CRC parameters (Figure 5.2.4.). These data therefore suggest, in comparison with Ruddell et al.'s, that 5-HT is not a mitogen in mouse HSCs, and that it does not influence the PDGF proliferation response, despite both compounds exerting clear

signalling events via the ERK pathway (Figure 5.3.1). The differences in results could potentially be due to the methods used. It is possible that the assay format or methodology carried out in these studies was not sufficiently sensitive to detect any enhancement effects of 5-HT on PDGF CRC, or that 5-HT exerts more of a proliferative effect in rat HSCs.

As both 5-HT and PDGF activate receptors that signal via the ERK pathway investigation of PDGF and 5-HT in the pERK assay could offer an insight into whether synergy occurs. PDGF activates a cell surface tyrosine kinase receptor which signals downstream through phosphoinositide 3-kinase (PI3kinase) and ERK/MAPK pathway (Figure 5.3.1) eventually leading to increased proliferation (Figure 1.7.1) (Pinzani, 2002). In HSCs it has been demonstrated that 5-HT activates the ERK pathway (Figure 5.3.1), which leads to signalling through the transcription factor JunD, which is recruited to the TGFβ promoter leading to increased synthesis and eventual release of TGFβ1 (Ebrahimkhani et al., 2011).

The 24 h time course for 5-HT and PDGF to stimulate ERK phosphorylation was investigated to establish whether differences in the profile of response could explain the difference in ability to cause proliferation. 5-HT and PDGF had a similar profile of ERK phosphorylation for about the first 10 min with a maximum pERK response being observed at 10-15 min (Figure 5.2.5). The peak ERK response time with PDGF agrees with the literature data obtained for PDGF in human HSCs (Marra et al., 1995). The 5-HT response decreased to baseline at 8 hours, whereas the PDGF response continued at a low level of activation out to 24 h (Figure 5.2.5), which could explain the difference in proliferation response. Bonacchi et al. (2001) observed a biphasic time course of ERK activation with a second peak being observed at 15 h in human HSCs with PDGF. The 5-HT pERK response kinetics are similar to those observed with the CXCR3 ligand, IP10, which is unable to induce proliferation, with a peak pERK response observed between 15 - 30 min before returning to baseline at 4 h in HSCs. (Bonacchi et al., 2001).
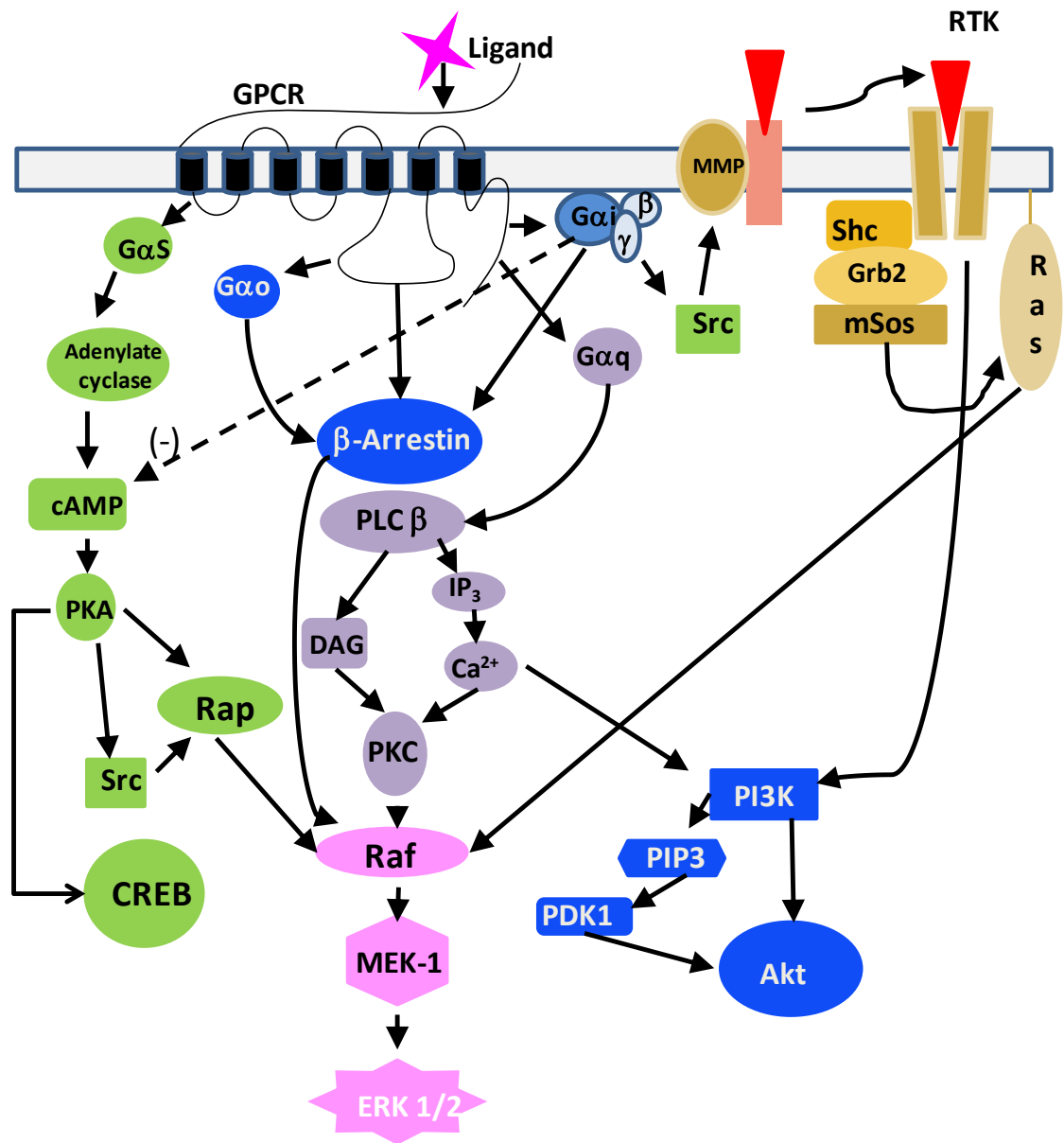
Figure 5.3.1 G protein-coupled receptor (GPCR) and receptor tyrosine kinase (RTK) signalling pathways via ERK1/2. ERK1/2 can be activated by GPCRs, which couple to different G-proteins (Gi,Gs,Gq,Go) which transduce the signal by different pathways. The ERK 1/2 pathway can be activated by activation of a receptor tyrosine kinase receptor .

Whereas in renal glomerular mesangial cells (MCs), a kidney myofibroblast-like cell, IP10 can stimulate proliferation, with the presence of a late phase ERK activation at 15-24 h (Bonacchi et al., 2001). The IP10 biphasic ERK phosphorylation response in MCs, is therefore similar to that observed by PDGF in HSC (Bonacchi et al., 2001) and could be required for proliferation. This therefore may suggest that a biphasic stimulation of ERK activation is related to the stimulation of proliferation which was not observed with 5-HT.

Repeat of the ERK phosphorylation kinetics with PDGF, 5-HT and some other mitogens, such as VEGF or insulin would ascertain if a biphasic ERK phosphorylation kinetics is required for proliferation of the HSCs. There is evidence that growth factors require a prolonged and continuous exposure to commit cells to the cell cycle (Jones and Kazlauskas, 2001) and that other pathways, such as PI3K activity is required for the second wave of PGDF-dependent DNA synthesis (Jones et al., 1999; Pinzani and Marra, 2001a). The use of inhibitors to further dissect the pathway downstream of ERK, such as Elk-1, SAP and transcription factor JunD, may help to further define the proliferative response as well as investigating other pathways which may be involved.

The pERK assay was then used to investigate whether there is any interaction between PDGF and 5-HT, to produce an additive or potential synergistic effect in HSC. Studies were undertaken to examine the effect of sub-maximal concentrations of 5-HT on the PDGF stimulated pERK CRC. The reciprocal studies investigated the effect of a sub-maximal concentration of PDGF, which can elicit a similar level of ERK phosphorylation as a maximum concentration of 5-HT, on the 5-HT CRC. In the presence of a sub-maximal 5-HT concentration, there was a 4-fold leftward shift of the PDGF CRC when compared to the PDGF CRC alone (Figure 5.2.6 A, Table 5.2.5). The actual magnitude of the maximum response achieved by the PDGF CRC, in the presence of 5-HT was not significantly different to that of PDGF alone (Table 5.2.5). This data suggests that there is an enhancement of the PDGF CRC which is suggestive of a synergistic effect. If the effect of 5-HT on the PDGF CRC was additive then the PDGF CRC (+100 nM 5-HT) would have a similar pEC_{50} to that of PDGF alone and the maximum response would be elevated. The predicted additive
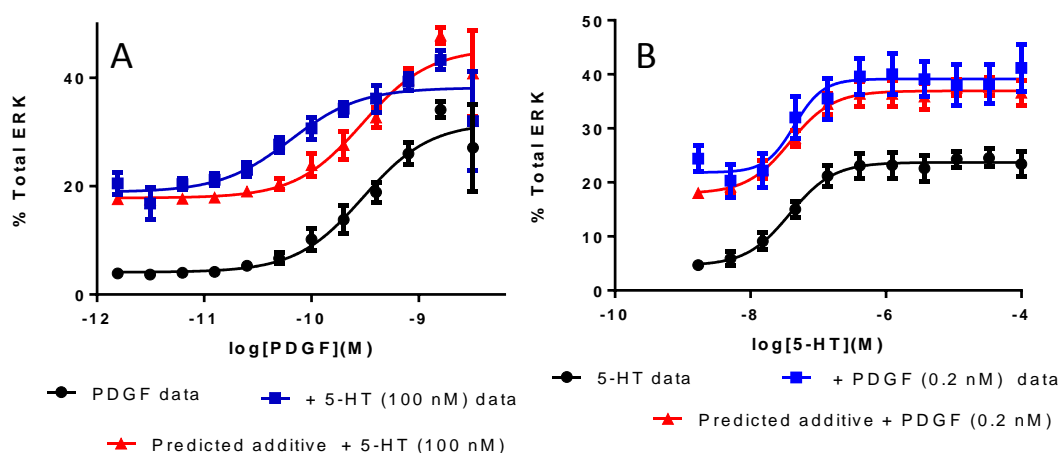
Figure 5.3.2 (A) PDGF CRC (± 5-HT (100 nM)) alongside the predicted PDGF CRC in the presence of 5-HT (100 nM) and (B) 5-HT CRC (± PDGF (0.2 nM)) alongside the predicted 5-HT CRC in the presence of PDGF (0.2 nM) generated in the mouse HSCs pERK assay. PDGF ± 5-HT (100 nM) or 5-HT ± PDGF (0.2 nM) were incubated for 10 min at room temperature before aspiration and addition of ice cold lysis buffer to the cells. The pERK and total ERK levels were measured in the cell lysates using an MSD pERK/Total ERK kit (See Chapter 2: Materials and methods). The data was expressed as the % Total ERK. The predicted curves were plotted by addition of the baseline parameters from the addition of 5-HT(100 nM) or PDGF (0.2 nM) to the control PDGF or 5-HT CRC responses respectively. CRCs were fitted using non-linear regression analysis (four parameter logistic equation with variable slope (Hill, 1909)) (See Chapter 2: Data analysis). Data shown are from a mean ± SEM fit from 3 individual experiments.

	PDGF	PDGF + 100 nM 5-HT	Predicted additive PDGF + 100 nM 5-HT	5-HT	5-HT + 0.2 nM PDGF	Predicted additive 5-HT + 0.2 nM PDGF
Basal % total ERK	4.1	18.9	**17.8**	4.6	21.8	**17.9**
Max % total ERK	31.7	38.2	**45.4**	23.7	39.1	**36.9**
pEC_{50}	9.52	10.2	**9.52**	7.42	7.35	**7.42**
slope	1.39	1.37	**1.39**	1.35	2.06	**1.36**
magnitude of maximum total pERK	27.6	19.3	**27.6**	19.1	17.3	**19**

Table 5.3.1 Fitting parameters obtained from fitting PDGF (± 5-HT (100 nM)) and 5-HT CRC (± PDGF (0.2 nM)) and predicted values based on addition of the 5-HT or PDGF alone CRC or generated in the mouse HSCs pERK assay. Data represents fitting parameters obtained from fitting all the data using non-linear regression analysis (four parameter logistic equation with variable slope (Hill, 1909)) (See Chapter 2: Data analysis) which is graphically represented in Figure 5.3.2. Data shown are from a mean ± SEM fit from 3 individual experiments.

153

effect can be modelled by the addition of the basal effect of 100 nM 5-HT added to the PDGF CRC data (Figure 5.3.2, Table 5.3.1). It can be clearly seen that the predicted PDGF (+ 100 nM 5-HT) CRC is to the right of the actual PDGF (+100nM 5-HT) CRC and elicits a greater maximum response than was actually obtained in the experiment (Table 5.3.1). The actual PDGF (+ 100 nM 5- HT) CRC demonstrates a greater than additive effect until nearing the maximum response. Due to the experiments variability around the maximum response it is difficult to determine if there is a true difference in the values or whether they all reach the same response or there is a limit to the maximum pERK response obtainable. Further experiments could be carried out with higher concentration of PDGF to enable better definition of the top of the PDGF CRC.

Examining the reciprocal experiment, there is no leftward shift of the 5-HT CRC but an increase in the maximum response in the presence of 0.2 nM PDGF. This would therefore suggest that the effect of 0.2 nM PDGF on the 5-HT CRC is additive. To examine the predictive additive effect of 0.2 nM PDGF on the 5-HT CRC the basal response obtained for 0.2 nM PDGF was added to the 5-HT CRC data (Figure 5.2.6 B, Table 5.2.5). The predicted 5-HT CRC was plotted alongside the actual experimental data obtained (Figure 5.3.2). It can be quite clearly seen that the predicted 5-HT CRC (+ 0.2 nM PDGF) and actual data obtained for the 5-HT CRC (+ 0.2nM PDGF) are very similar (Figure 5.3.2) with confirmation from the 5-HT CRC parameters obtained from fitting of the mean data (Table 5.3.1). The actual maximum response obtained by the 5-HT curve in the presence of PDGF was similar to that reached by PDGF CRC alone.

Taken together the data with the different combinations seems to suggest that there be may be a limit to the level of the ERK phosphorylation response achievable in these cells and that PDGF is able to cause a greater degree of ERK activation than 5-HT. We know that 5-HT stimulates two 5-HT receptors, the 5-HT_{2A} and possibly the $5\text{-HT}_{1B,}$ from the ERK phosphorylation studies (See Section 4.2.4.4). These observed effects may be explained by the two 5-HT receptors and PDGF, sharing the same transducer protein. A two-receptor–one-transducer model has previously been proposed in the literature, to explain analogous findings, such as the amplification of

$$A_1 + R_1 \longleftrightarrow A_1R_1$$

$$A_2 + R_2 \longleftrightarrow A_2R_2$$

$$M \longrightarrow E$$
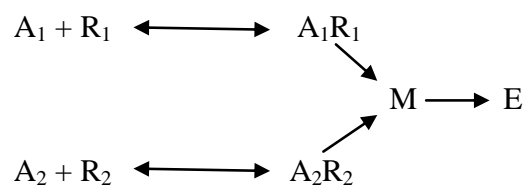
Figure 5.3.3. Schematic of the two receptor–one-transducer model proposed by Leff (1987). Agonists A_1 and A_2 occupy receptors R_1 and R_2 respectively to form complexes. Each agonist-receptor complex is coupled to the formation of an intracellular mediator, M, which leads to a pharmacologic effect E.

5-HT effects in hypertension (Leff, 1987) (Figure 5.3.3). In the scenario we have with the data generated in this system we have two 5-HT receptors stimulating the ERK signal. This model may be applicable to the effects observed with the ERK phosphorylation studies as at the lower concentrations of 5-HT as the 5-HT_{1B} contribution may be negligible.

There are further studies that could be performed to investigate this further to build up a comprehensive data set. These would include generating CRC for both 5-HT and PDGF, in the presence of another higher sub-maximal and a supra-maximal concentration of either PDGF or 5-HT respectively. To understand the contribution of the second 5-HT receptor to the enhancement of the PDGF CRC, experiments could be undertaken after PTX pre-treatment. This should remove the 5-HT_{1B} receptor influence. These data then generated could then be used to explore the applicability of the two-receptor–one-transducer model (Leff, 1987) or whether another model may explain the observed data. The data is consistent with the signals from 5-HT and PDGF converging on the downstream signalling ERK pathway. The effect of PDGF on 5-HT is additive. However the effect of 5-HT on PDGF causes enhancement and possibly synergistic effect in relation to ERK. Further studies could determine the contribution of the different 5-HT receptors to the effect observed.

Although an synergistic effect of 5-HT on PDF has been determined in the ERK phosphorylation this did not translate into an effect on proliferation as had been proposed in the literature (Ruddell et al., 2006). As no effect of 5-HT on proliferation or an enhancement of PDGF proliferation was observed in the proliferation studies it can be concluded that 5-HT does not influence HSC proliferation.

5.3.3 5-HT stimulation of collagen deposition in the Scar-in –a-Jar assay.

The SIAJ assay format was used to investigate the ability of mouse HSCs to produce collagen through 5-HT stimulation of TGFβ1. This methodology introduces macromolecular crowding to occupy a significant volume resulting in the excluded volume effect which enhances the proteolytic cleavage of pro-collagen to collagen (Lareu et al., 2007; Kumar et al., 2015). The methodology used to carry out these

experiments in this thesis, allowed rapid deposition of granular collagen I aggregates within the 72 h timeframe of the assay (Chen et al., 2009).

According to the literature the hypothesis is that 5-HT stimulation of HSCs would drive, through an ERK and JunD phosphorylation, the transcription and release of TGFβ (Ebrahimkhani et al., 2011). The released TGFβ1 in turn activates the TGFβ receptors on the HSCs to stimulate collagen deposition (Ebrahimkhani et al., 2011; Mann and Oakley, 2013). TGFβ1 would be expected to drive collagen deposition, as it has been shown to be a potent stimulator of collagen in fibroblasts (Caraci et al., 2008). Therefore it's important to demonstrate TGFβ1 can drive collagen deposition in HSCs as if this is not the case then 5-HT will be unable to influence the collagen deposition. 5-HT, ketanserin and PDGF produced no effect on the collagen deposition (Figure 5.2.7 B, C and D). The stimulation of collagen I with TGFβ was only observed in one of the two assays carried out, and with only one out of three batches of HSCs (Figure 5.2.8A, Table 5.2.5.).

The activated HSC had been shown to demonstrate a difference in sensitivity to TGFβ1 depending on the activation state of the cell (Dooley et al., 2000). Quiescent and newly isolated HSCs have been found to be more sensitive to TGFβ than HSCs that have been activated through culture on plastic (Dooley et al., 2000; Liu et al., 2003; Dooley and ten Dijke, 2012). The HSCs used in the SIAJ assay were in culture for 3 weeks or more and have been shown to express α-SMA. Interestingly the cells which produced the TGFβ1 driven collagen deposition had been in culture for 5 weeks. It has been reported that HSCs can become senescent whilst in culture (Knittel et al., 1999). It is therefore possible that some of the HSCs could have reverted to a more quiescent phenotype whilst in prolonged culture. This would require further investigation to determine if this had occurred in these cells possibly by investigation of α-SMA expression. Studies investigating HSCs, in the CCl$_4$ model of liver injury, have found that once the CCl$_4$ stimulus was removed, that half of the HSCs acquired a phenotype that was similar but distinct from the quiescent HSCs (Kisseleva et al., 2012). This phenotype of HSCs was shown to exhibit a down regulation of fibrogenic genes and able to respond more rapidly, reactivating into myofibroblasts, in response to fibrogenic stimuli (Kisseleva et al., 2012).

In patients with hepatic fibrosis and in experimental models of fibrogenesis there is an increased expression of TGFβ and extracellular matrix production (Dooley et al., 2000; Inagaki and Okazaki, 2007). TGFβ is a multifunctional cytokine which regulates a large array of cellular responses with further definition of the signalling pathways in Section 1.8.2.4 (Figures 1.8.2 and 1.8.3). Studies with rat HSC have shown that quiescent cells express little TGFβ but once activated they express increased amounts of all three isoforms of TGFβ (Inagaki and Okazaki, 2007). HSCs, both quiescent and activated, express TβRI and TβRII strongly, but in activated HSCs the ligand binding activity is down-regulated (Dooley et al., 2000; Dooley and ten Dijke, 2012). The activated cells become insensitive to TGFβ, such that activated HSC proliferation cannot be inhibited by TGFβ (Dooley et al., 2000; Liu et al., 2003). Deregulated TGFβ signalling, which uncouples the anti-proliferative and profibrotic TGFβ effects during activation of HSCs, is proposed to be due to reduced TβRII expression (Roulot et al., 1999). In the activated HSC the receptor stoichiometry may shift into a more ECM producing phenotype (Roulot et al., 1999). Differences in the relative involvement of SMAD2 and SMAD3 in TGFβ signalling pathway, in quiescent HSC compared to activated HSCs, may therefore be implicated (See section 1.82.4, Figure 1.8.2.) (Dooley et al., 2000; Pinzani and Marra, 2001a; Liu et al., 2003; Inagaki and Okazaki, 2007). TGFβ inhibition of HSC proliferation signals through SMAD2. Activated HSCs, express a constitutively phosphorylated nuclear SMAD2 and therefore TGFβ is only able to induce SMAD3 phosphorylation and translocation to the nucleus (Dooley et al., 2000; Liu et al., 2003; Inagaki and Okazaki, 2007). The lack of response to TGFβ is supported in literature, as it is suggested that upon differentiation into a myofibroblast phenotype the cells lose sensitivity to TGFβ and produce extracellular matrix protein by a TGFβ-independent pathway (Dooley et al., 2001). Furthermore, the activated phenotype may only allow a small window for further activation by TGFβ stimulation. In activated HSCs, collagen expression is similar to that found in quiescent HSCs after incubation with TGFβ for 16 hours (Dooley et al., 2000). The batch of activated HSCs, that demonstrate a TGFβ concentration-dependent increase in collagen deposition, have a lower baseline collagen level, when compared with the other two batches (Figure 5.2.8.). The maximum level of collagen deposition, once

stimulated maximally with TGFβ, was similar to the basal level of collagen of the other two batches of HSCs tested, suggesting the latter two batches were already maximally stimulated. The baseline levels of collagen observed with lung fibroblasts, was reduced when compared to activated HSCs (data not shown) in the SIAJ assay, and that fibroblasts produce a consistent TGFβ concentration-dependent increase in collagen deposition in the assay format. This therefore suggests that the current HSC assay format is not suitable to investigate TGFβ driven collagen deposition in activated HSCs and therefore 5-HT stimulated TGFβ driven collagen deposition.

5.3.4 *In Vivo* CCl_4 liver model

All the experiments in this chapter and Chapter 4 have used a single cell type, the HSC. The liver, is a multi celluar organ and so the interplay between the different populations of cells will have a major role in how the liver responds to the fibrotic stimuli. To investigate this a selective $5\text{-}HT_{2A}$ antagonist, volinanserin, and selective $5\text{-}HT_{2B}$ antagonist, GSK160260A, were chosen, on the basis of their selectivity (> 1000-fold), PK and formulation stability, to explore their effects in a mouse CCl_4 model of lung injury. In the CCl_4 model doses of volinanserin and GSK1606260A were selected to obtain 90% ~ 99% receptor occupancy, ensuring correct targeting of selectivity at the receptors of interest. The blood concentrations achieved throughout the study demonstrated the predicted exposure levels for the two concentrations of volinanserin and GSK1606260A throughout the dosing period (by minipump). Throughout the duration of the study the compounds maintained their solubility and stability whilst being delivered by minipump.

Surprisingly both doses of GSK1606260A demonstrated a significant increase in PSR staining at week 8 and further concentration-related analysis of the data implied a $5\text{-}HT_{2B}$ concentration-related relationship (Figure 5.2.9). This data suggests that 5-HT has an anti-fibrotic activity via the $5\text{-}HT_{2B}$ receptor in the injured liver and blockade leads to increased fibrosis. In the presence of both concentrations of volinanserin there was no significant difference in the PSR staining when compared to week 8. This therefore implies that $5\text{-}HT_{2A}$ antagonism would have no benefit as an anti-fibrotic therapy.

An element that was not assessed in this assay was whether the profibrotic effect of the GSK1606260A was due to toxicity of the compound. Constant very low maintained concentrations of GSK1606260A was achieved throughout the study. Therefore it is unlikely that the effect is driven through an off-target activity, as the compounds is > 300-fold selective for the 5-HT_{2B} receptor and concentrations chosen were in the selective range. The *in vitro* data from the mouse HSCs implied a possible anti-fibrotic role for 5-HT_{2A} and not for 5-HT_{2B}, but these experiments were limited to the HSCs. The liver is a multicelluar organ, so the interplay between the different resident cells (such as hepatocytes, Kupffer cells and sinusoidal endothelial cells), as well as the vasculature, will determine the overall pharmacological effect of the compounds.

The expression of 5-HT_{2A} and $5\text{-HT}_{2B,}$ using immunohistological techniques, were studied in the livers from CCl_4-treated rats (Ruddell et al.,2006). Diffuse 5-HT_{2A} staining throughout, was present in the uninjured livers, which increased following CCl_4 injury. 5-HT_{2B} staining was only found in elongated cells in the fibrotic bands, suggesting that 5-HT_{2B} receptors are associated with activated HSCs (Ruddell et al., 2006). Data from a mouse CCl_4 model, using SB-204741, a reported selective 5-HT_{2B} antagonist, found reduced numbers of activated HSCs, fibrotic matrix, expression of TGFβ1 and fibrogenic genes (TIMP-1 and pro-collagen I) (Ebrahimkhani et al., 2011). The 5-HT_{2B} compound, SB-204741, used in the study has a pK_i of 6.9 for the 5-HT_{2B} receptor and $pK_i < 5$ for the 5-HT_{2A} receptor (Knight et al., 2004). SB-204741 was demonstrated to inhibit 5-HT pERK expression in HSCs at concentrations $\geq 10\mu M$, which would indicate a 5-HT_{2A} interaction. However within this study pharmacokinetics (PK) was not reported and so there was no confirmation of the blood concentrations obtained with SB-204741. The level of exposure and thus, the concentration-response relationship could not be explored to confirm the 5-HT_{2A} pharmacology. An 'in-house' study to determine the PK of SB-204741, following the same dosing protocol as Ebrahimkhani et al. (2011), demonstrated only brief exposure of the parent compound following dosing (all parent compound was cleared by 2 h of dosing). The *in vivo* study reported in this thesis demonstrated that the animals received constant exposure of 90-99% occupancy of the compound throughout the last 5 weeks of CCl_4 dosing. These data

generated in the *in vivo* study therefore contradicts the findings obtained in the *in vivo* CCl$_4$ study with SB-204741 and data obtained using 5-HT$_{2B}$ knockout mice which is suggestive of 5-HT$_{2B}$ involvement (Ebrahimkhani et al., 2011).

In another study, 5-HT$_{2A}$ antagonist, sarpogrelate (30mg/kg) (5-HT$_{2A}$ pK$_i$ = 8.5, 5-HT$_{2B}$ pK$_i$ = 6.7, (Rashid et al., 2003) was dosed in a thioacetamide (TAA) rat model of liver injury and found to reduce lobular inflammation and cause a slight, but not significant, attenuation of periportal fibrosis (Kim et al., 2013). There were no PK studies to confirm exposure of the sarpogrelate, which is reported to have a short half-life (Tanaka et al., 2000) but expression of markers of HSC activation, α-SMA, TGFβ and SMAD2/3 were all significantly reduced following treatment. This data is partially consistent with the volinaserin data, as there was no significant anti-fibrotic effect. Overall there is conflicting data reported in the liver injury models and further comprehensive studies would be needed to explore dose exposure, receptor target engagement and toxicity of compounds. It would also have been beneficial to identify receptor specific biomarkers, although cell specific biomarkers may be an issue but the occupancy data from PK demonstrates effective cover.

The *in vitro* analyses conducted in this chapter demonstrate that 5-HT or specific 5-HT$_{2A}$ or 5-HT$_{2B}$ antagonists, at concentrations selective for their receptor subtype, are unable to exert any effect on HSC proliferation or collagen deposition. This therefore could suggest that 5-HT does not play a major role in these processes. These are the first studies which have focused on measuring actual collagen deposition following incubation with 5-HT and its antagonists rather than expression, as had been carried out previously (Ruddell et al., 2006; Ebrahimkhani et al., 2011; Kim et al., 2013). The *in vivo* mouse CCl$_4$ liver injury study provided evidence that 5-HT$_{2A}$ antagonism is not anti-fibrotic with 5-HT$_{2B}$ antagonism stimulating fibrosis, demonstrating the value of not relying on single cell experimental data. 5-HT has been demonstrated to exert both a pro-fibrotic and pro-regenerative influence during acute injury (Yokoyama et al., 1953; Lesurtel, 2006; Lesurtel et al., 2012; Mann and Oakley, 2013). However, with chronic disease it would be advantageous to modulate the specific 5-HT receptors that trigger activation of fibrogenic signal transduction (Mann and Oakley, 2013). It is clear that a greater understanding of how the different

5-HT receptors together exert both the pro-fibrotic and regenerative effects in the liver is required (Lesurtel and Clavien, 2012; Lesurtel et al., 2012; Mann and Oakley, 2013). The *in vivo* animal models do not truly mimic the human disease but do offer a way to investigate molecules in the intact organ (Constandinou et al., 2005; Starkel and Leclercq, 2011). Whether these molecules will behave in a similar way in the human HSC and the human disease requires further investigation.

CHAPTER 6: CHARACTERISATION OF THE ROLE OF 5-HT IN INTRACELLULAR CALCIUM RELEASE, ERK PHOSPHORYLATION, PROLIFERATION AND COLLAGEN DEPOSITION IN HUMAN HEPATIC STELLATE CELLS.

6.1 Introduction.

The previous three chapters have focussed on characterisation of the 5-HT responses in mouse HSCs, along with a mouse model of liver injury. Ultimately any developed molecule will be dosed in humans and obtaining information on the role of 5-HT in human HSCs is therefore crucial. A key question is whether the data obtained from 5-HT stimulation of mouse HSCs translate into a similar response in human HSCs? Immortalised human HSC lines, such as LX-2, LI90 or HSC180 could be used to explore this question due to their ease of use, unlimited supply and reproducibility of results (Herrmann et al., 2007). However despite the advantages of HSC lines, there are issues around their loss of differentiated morphology, function, growth characteristics and genetics, which have called into question their suitability (Herrmann et al., 2007; Crespo Yanguas et al., 2015). Human liver tissue was therefore ethically sourced to allow isolation and culture of the human HSCs.

The main aim of the experiments in this chapter is to pharmacologically characterise the 5-HT response in human HSCs using the Ca^{2+} release, ERK phosphorylation, proliferation and collagen deposition (Scar in a Jar) assays. Selective 5-HT$_{2A}$, 5-HT$_{2B}$ and 5-HT$_{1B}$ antagonists, at concentrations known to engage the target receptor, were used to pharmacologically characterise the responses, in a similar way that had been carried out for the mouse HSCs.

6.2 Results.

6.2.1 Immunocytochemistry analysis of isolated hepatic stellate cells.

Human hepatic stellate cells, which had been isolated from human livers, maintained in culture on plastic for 7 or 14 days, were stained to detect the expression of α-SMA (Red), a marker for activated HSC, and synaptophysin (Green), a marker for both activated and quiescent HSCs (Cassiman et al., 1992), along with Hoechst nuclear stain (Blue), to identify the nuclei of cells clearly. The majority of the cells that had been in culture for 7 days stained positively for α-SMA and synaptophysin (Figure 6.2.1) confirming the presence of activated HSCs. However, at this time there were a few cells which stained only weakly for α-SMA (Figure 6.2.1 A), as blue nuclei can be seen with a faint α-SMA stain (red) around them. When the 7 day cultured cells

were co-stained with synaptophysin there were a few cells which stained green only (Figure 6.2.1 B) with the majority co-staining for both α-SMA and synaptophysin (orange). This would suggest that not all the cells had fully activated in the 7 day culture. Cells that had been in culture for 14 days stained positive for α-SMA, with clearly defined cytoskeletal fibres of immunocytochemical staining (Figure 6.2.2 A). When the same cells were co-stained with synaptophysin and α-SMA it can be observed that they both stain the same population of cells, as is shown by orange staining (Figure 6.2.2 B). From these images it can be concluded HSCs that had been in culture for 14 days had the characteristics of a population of fully activated HSC. The same pattern of staining was observed for further batches of HSC which had been in culture for up to 21 days (Data not shown).

6.2.2 Pharmacological characterisation of the 5-HT receptor responsible for the $[Ca^{2+}]$ increase in mouse hepatic stellate cells.

Experiments were carried out to investigate whether 5-HT was capable of stimulating an intracellular calcium signal in the human HSCs. 5-HT (0.12 nM to 100 μM) caused a concentration-dependent increase in fluorescent intracellular calcium signal (Fluo4) with a pEC_{50} of 7.35 (Figure 6.2.3). Characterisation of the 5-HT receptor subtype responsible was investigated using $5-HT_{2A}$ antagonists, ketanserin and volinanserin, and $5-HT_{2B}$ antagonists, GSK1606260A and RS-127445, as the expression of both receptors are induced upon HSC activation. $5-HT_{2A}$ and $5-HT_{2B}$ will elicit a downstream increase in intracellular calcium when stimulated, due to their coupling through Gαq. As the $5-HT_{1B}$ receptor, which couples through G_i, is also up-regulated upon HSC activation and it is possible that stimulation of this receptor could also cause an increase in calcium release. Therefore the effects of $5-HT_{1B}$ antagonist, cyanopindolol, were also investigated. The concentration of the antagonists used were chosen based on their selectivity range for the receptor of interest. The affinities for both human $5-HT_{2A}$ and $5-HT_{2B}$ receptors had been confirmed in a simple recombinant assay system (Table 6.2.1, Chapter 9: Appendix, Section 9.2 for recombinant CHO cell assay method).
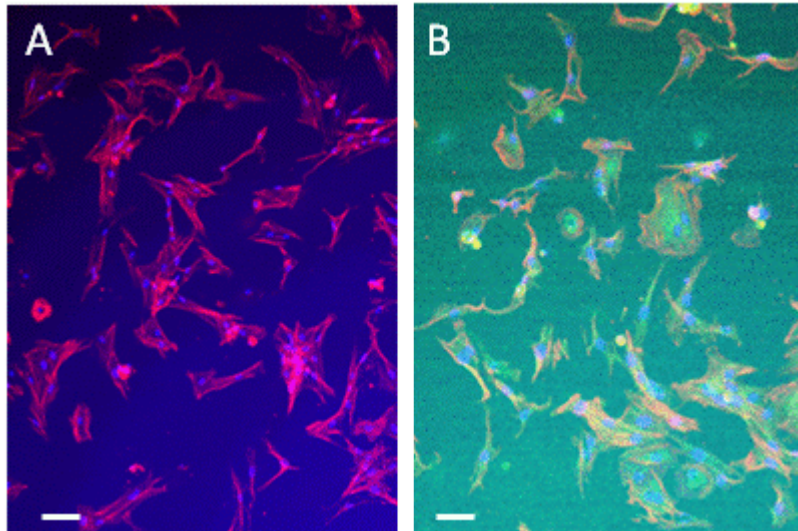
Figure 6.2.1 Expression of α-SMA (A) and co-expression with synaptophysin (B) by immunofluorescent staining of human HSCs which had been in culture on plastic for 7days. Human HSCs were plated out onto 96 well plates for 24 h before being fixed and permeabilised. Cells were incubated with a primary antibody for α-SMA and synaptophysin, followed by incubation with secondary antibodies and cell nuclear stain. The fluorescence was visualised and quantified by the InCell Analyser 2000 (See Chapter 2 :Materials and methods). Data shown are representative images from two different batches of HSCs. Scale bar =250 μm.
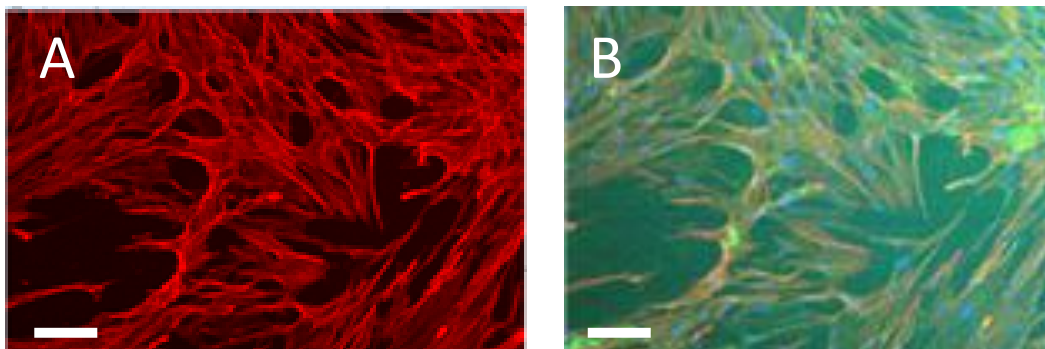
Figure 6.2.2 Expression of α-SMA (A) and co-expression with synaptophysin (B) by immunofluorescent staining of human HSCs which had been in culture on plastic for 14 days. Human HSCs were plated out onto 96 well plates for 24 h before being fixed and permeabilised. Cells were incubated with a primary antibody for α-SMA and synaptophysin, followed by incubation with secondary antibodies and cell nuclear stain. The fluorescence was visualised and quantified by the InCell Analyser 2000 (See Chapter 2 :Materials and methods). Data shown are representative images from two different batches of HSCs. Scale bar =100 μm.
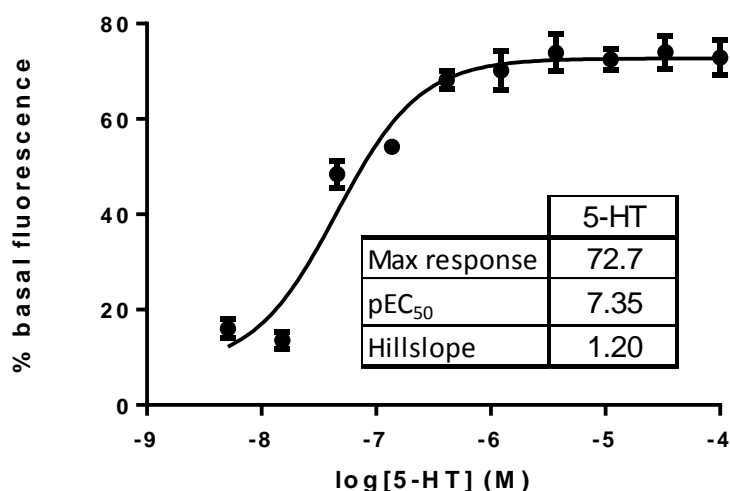
Figure 6.2.3   5-HT concentration-response curve obtained in human HSCs in the FLIPR™ assay with associated curve parameters. Stellate cells were loaded with fluorescent dye (FLUO4) for 1 h before being stimulated with increasing concentrations of 5-HT in the FLIPR. (See Chapter 2: Materials and Methods). Data were captured and analysed to obtain the basal signal and maximum stimulated fluorescence above basal for each concentration, with the response being expressed as a percentage of the basal response. The CRC was fitted using non-linear regression analysis (four-parameter logistic equation with variable slope (Hill, 1909) (See Chapter 2: Data Analysis section). Data are from a single experiment.

	human 5-HT$_{2A}$ fpK$_i$	human 5-HT$_{2B}$ fpK$_i$
Ketanserin	9.6 ± 0.2	<5
Volinanserin	10.7 ± 0.1	$5.9\ (0)$
GSK1606260A	6.0 ± 0.3	$10.2\ (0.1)$
RS-127445	6.3 ± 0.2	$11.3\ (0)$

Table 6.2.1   fpK$_i$ value obtained for ketanserin, volinanserin, GSK1606260A and RS-127445 in recombinant mouse 5-HT$_{2A}$ and 5-HT$_{2B}$ receptor calcium assays. CGE222 cells, expressing hu5-HT$_{2A}$ or 5-HT$_{2B}$, were loaded with fluorescent dye (FLUO4) for 1 h before being stimulated with an EC$_{80}$ concentration of 5-HT in the presence or absence of increasing concentrations of antagonists. (See Chapter 9: Chapter 9: Appendix, Section 9.2). Data presented are the mean $\pm$ SEM n=3 for 5-HT$_{2A}$ and average, n=2 with range for 5-HT$_{2B}$.

No rightward shift of the 5-HT CRC was observed following a 15 min pre-incubation with GSK1606260A (1 μM) and RS-127445 (100 nM) (Figure 6.2.4), as similar 5-HT CRC parameters values were obtained in the absence of the antagonists (Table 6.2.2). A concentration of 1 μM GSK1606260A or 100 nM RS-127445, assuming competitive interaction with the $5-HT_{2B}$ receptor, should have produced a > 1000-fold rightward shift of the 5-HT CRC as predicted from their fpK_i of 10.2 and 10.3 respectively. (Table 6.2.1). Cyanopindolol (1 μM), 15 min pre-incubation, did not cause any rightward shift of the 5-HT CRC (Figure 6.2.5, Table 6.2.3). For cyanopindolol if 5-HT had been eliciting the response through the $5-HT_{1B}$ receptor then a >500-fold shift of the 5-HT CRC would have been observed. These results suggest that the $5-HT_{2B}$ and $5-HT_{1B}$ receptors are not mediating the 5-HT stimulated calcium response in the human HSCs.

To determine if the $5-HT_{2A}$ receptor was the receptor responsible for the 5-HT stimulated calcium response 5-HT CRCs were carried out in the presence of three concentrations of ketanserin and volinanserin (1, 10 and 100 nM). Rightward shift and depression of the maximum 5-HT response was observed with ketanserin (Figure 6.2.6 A, Table 6.2.4 A), with the 10 and 100 nM concentrations almost completely blocking the 5-HT response. Volinanserin, like ketanserin, caused insurmountable antagonism, with a rightward shift and depression of maximum 5-HT CRC, with the 10 and 100 nM concentrations completely blocking the 5-HT CRCs (Figure 6.2.6 B, Table 6.2.4 B). The insurmountable nature of the antagonism obtained with ketanserin and volinanserin means that no antagonist affinity values could be calculated, but does suggest the involvement of the $5-HT_{2A}$ receptor in the 5-HT response. This is due to the concentration range over which the antagonism was observed. Although not all criteria are met for competitive antagonism a pA_2 estimate was determined from the 1 nM shift of ketanserin and of volinanserin of 9.3 and 9.0 respectively. These values are in keeping with an expected $5-HT_{2A}$ antagonist effect. The profile of the antagonism observed may indicate that ketanserin and volinanserin are behaving as non-competitive antagonists but could also be explained by the fact that the antagonist, agonist and receptor are unable to reach a equilibrium in the timeframe of the agonist response (hemi-equilibrium conditions)
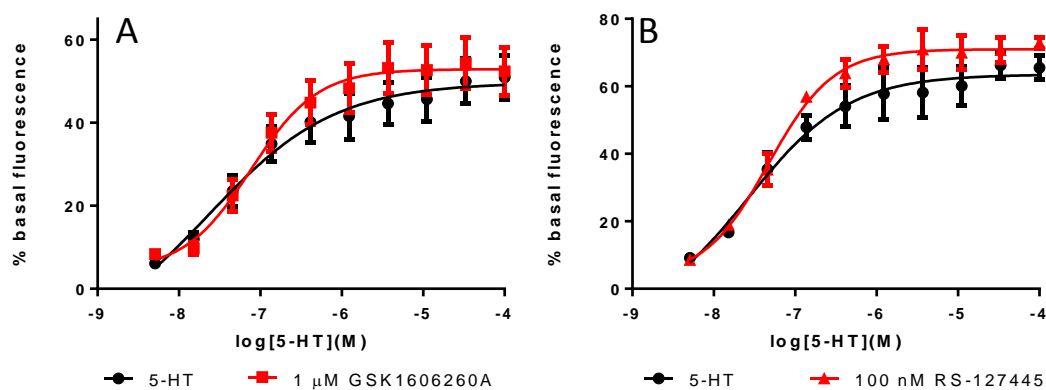
Figure 6.2.4 **Effect of (A) GSK1606260A (1 μM) and (B) RS-127445 (100 nM) on the 5-HT CRC in the human HSC FLIPR™ assay.** Stellate cells were loaded with fluorescent dye (FLUO4) for 1 h before being stimulated with increasing concentrations of 5-HT in the presence and absence of a single concentration of the antagonists in the FLIPR. (See Chapter 2: Materials and Methods). Data were captured and analysed to obtain the basal signal and maximum stimulated fluorescence above basal for each concentration, with the response being expressed as a percentage of the basalfluorescence. CRCs were fitted using non-linear regression analysis (four-parameter logistic equation with variable slope (Hill, 1909)(See Chapter 2: Data Analysis section). Data shown are mean values ± SEM from ≥ 3 experiments carried out in duplicate.

	5-HT	1 μM GSK16060260A		5-HT	100 nM RS-127445
Max Response	55.4 ± 12.3	50.7 ± 8.6		62.1 ± 5.0	69.5 ± 4.3
pEC_{50}	7.36 ± 0.2	7.15 ± 0.1		7.41 ± 0.2	7.35 ± 0.3
Hill slope	0.94 ± 0.2	1.27 ± 0.1		0.97 ± 0.1	1.27 ± 0.1

Table 6.2.2 **5-HT CRC parameters obtained in the presence and absence of GSK1606260A (1 μM) and RS-127445 (100 nM) in the human HSC FLIPR™ assay.** Data represents the mean of the individual parameters obtained from fitting the data from individual experiments represented in Figure 6.2.3 using non-linear regression analysis (four-parameter logistic equation with variable slope (Hill, 1909)(See Chapter 2: Data Analysis section). Data shown are mean values ± SEM from ≥ 3 experiments carried out in duplicate.
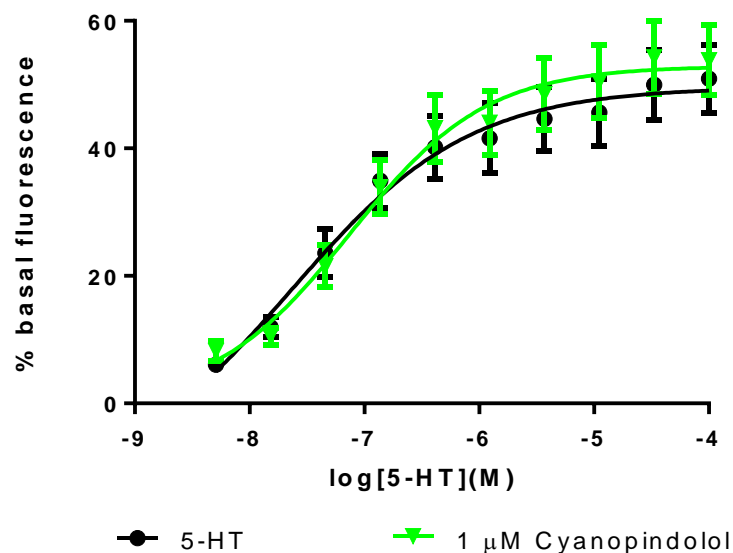
Figure 6.2.5   Effect of cyanopindolol (1 μM) on the 5-HT CRC in the human HSC FLIPR™ assay. Stellate cells were loaded with fluorescent dye (FLUO4) for 1 h before being stimulated with increasing concentrations of 5-HT in the presence and absence of a single concentration of the antagonists in the FLIPR. (See Chapter 2: Materials and Methods). Data were captured and analysed to obtain the basal signal and maximum stimulated fluorescence above basal for each concentration, with the response being expressed as a percentage of the basal response. CRCs were fitted using non-linear regression analysis (four-parameter logistic equation with variable slope (Hill, 1909)(See Chapter 2: Data Analysis section). Data shown are mean values ± SEM from ≥ 3 experiments carried out in duplicate.

	5-HT	1 μM cyanopindolol
Max Response	55.4 ± 12.3	52.7 ± 8.3
pEC_{50}	7.36 ± 0.2	7.06 ± 0.1
Hill Slope	0.94 ± 0.2	0.89 ± 0.1

Table 6.2.3   5-HT CRC parameters obtained in the presence and absence of cyanopindolol (1 μM) in the human HSC FLIPR™ assay. Data represent the mean of the individual parameters obtained from fitting the data from individual experiments represented in Figure 6.2.5. using non-linear regression analysis (four-parameter logistic equation with variable slope (Hill, 1909)(See Chapter 2: Data Analysis section). Data shown are mean values ± SEM from ≥ 3 experiments carried out in duplicate.
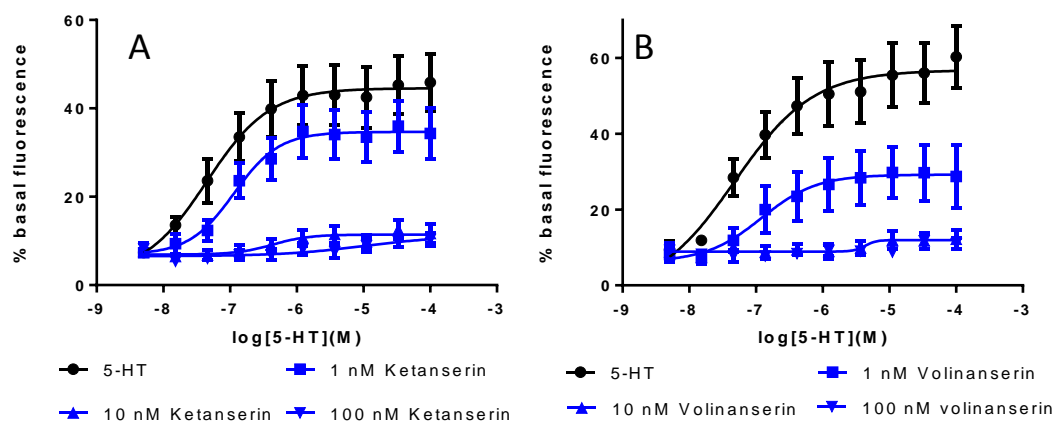
Figure 6.2.6 Effect of (A) ketanserin and (B) volinanserin (1, 10 and 100 nM) on the 5-HT CRC in the human HSC FLIPR™ assay. Stellate cells were loaded with fluorescent dye (FLUO4) for 1 h before being stimulated with increasing concentrations of 5-HT in the presence and absence of the antagonists in the FLIPR. (See Chapter 2: Materials and Methods). Data were captured and analysed to obtain the basal signal and maximum stimulated fluorescence above basal for each concentration, with the response being expressed as a percentage of the basal response. CRCs were fitted using non-linear regression analysis (four-parameter logistic equation with variable slope (Hill, 1909) (See Chapter 2: Data Analysis section). Data shown are mean values ± SEM from 3 experiments carried out in duplicate.

A

	5-HT	1 nM Ketanserin	10 nM Ketanserin	100 nM ketanserin
Max Response	40.3 ± 9.8	28.0 ± 7.8	4.1 ± 1.4	5.74 ± 2.0
pEC_{50}	7.19 ± 0.1	6.71 ± 0.2	<5.35	<5.44
Hill Slope	1.21 ± 0.2	1.20 ± 0.1	1.17 ± 0.1	

B

	5-HT	1 nM Volinanserin	10 nM Volinanserin	100 nM Volinanserin
Max Response	49.7 ± 11.6	22.1 ± 8.8	3.8 ± 1.5	$*4.0 \pm 1.5$
pEC_{50}	7.16 ± 0.1	6.88 ± 0.2	<5.12	
Hill Slope	1.04 ± 0.1	1.30 ± 0.2		

 * maximum response reached

Table 6.2.4   5-HT CRC parameters obtained in the presence and absence of (A) ketanserin and (B) volinanserin (1, 10 and 100 nM) in the mouse HSC FLIPR™ assay. Data represents the mean of the individual parameters obtained from fitting the data from individual experiments represented in Figure 6.2.4 using non-linear regression analysis (four-parameter logistic equation with variable slope (Hill, 1909)) (See Chapter 2: Data Analysis section). Data shown are mean values ± SEM from 3 experiments carried out in duplicate.

(Kenakin et al., 2006). The profile of ketanserin and volinaserin antagonism obtained in the human HSCs is similar to that obtained with the mouse HSCs (See Chapter 4, section 4.2.2).

6.2.3 Characterisation of the 5-HT stimulated ERK phosphorylation in human hepatic stellate cells.

Investigation into the ability of 5-HT to cause ERK phosphorylation in the human HSCs was carried out, using the same methodology as was used for the mouse HSCs (Chapter 2, Section 2.6). 5-HT (1.79 nM -100 μM) was found to cause a very low level of ERK phosphorylation (Figure 6.2.7). A PDGF CRC was generated in the assays too, to confirm that the human HSCs were capable of ERK phosphorylation and that the assay was performing as expected. PDGF caused a concentration-related increase of ERK phosphorylation (Figure 6.2.7), with a pEC_{50} value of 9.36 (Table 6.2.5), which is similar to that observed with mouse HSCs of 9.43 (Table 5.2.4). Due to the level of pERK obtained with 5-HT, no CRC parameters could be reliably generated and further characterisation of the response was not feasible. The basal level of ERK phosphorylation in the human HSCs was found to be ~ 20% (Table 6.2.5) but in the mouse HSC was ~ 4% (Table 5.2.4), which could possibly explain why 5-HT was unable to stimulate ERK phosphorylation in the human HSC.

6.2.4 Hepatic stellate cell proliferation assay.

The bromodeoxyuridine (BrdU) colourimetric ELISA was used to measure proliferation of the human HSCs by measuring the increase in DNA synthesis. Human HSCs were stimulated with increasing concentrations of 5-HT (1.8 nM -100 μM) and PDGF-BB (7.7 pM-7.9 nM). No increase in proliferation was observed with 5-HT (Figure 6.2.8). PDGF caused a concentration-dependent increase in proliferation, with a pEC_{50} value of 9.8 (Figures 6.2.8, Table 6.2.6) confirming that HSCs were capable of proliferating in the assay.

As there had been reports of enhancement of PDGF proliferation with addition of 10 μM 5-HT in rat HSCs (Ruddell et al., 2006), this was investigated using the human HSCs. No leftward shift of the PDGF CRC was observed in the presence of 10 μM
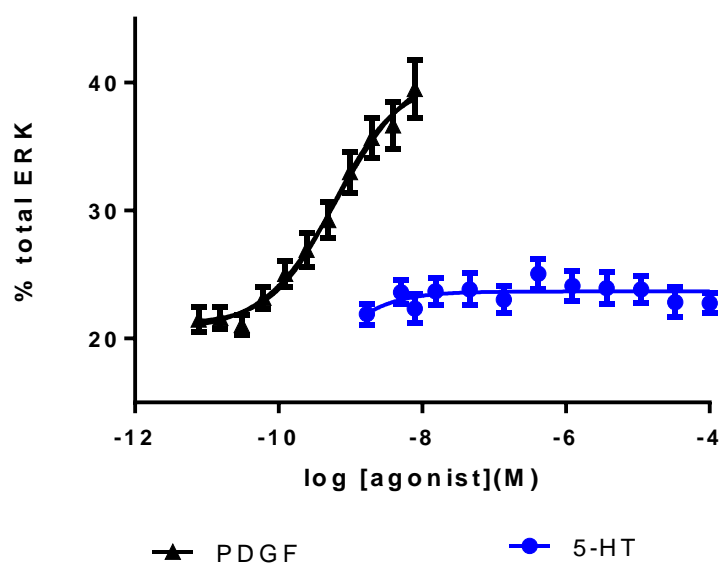
Figure 6.2.7 PDGF and 5-HT CRC in the human HSC pERK assay. HSCs were stimulated for 10 min with 5-HT or PDGF. The pERK and total ERK levels were measured in cell lysates using MSD pERK/Total ERK kit (See Chapter 2: Materials and Methods). pERK response was expressed as a % of total ERK. CRCs were fitted using non-linear regression analysis (four-parameter logistic equation with variable slope (Hill, 1909) (See Chapter 2: Data Analysis section). Data shown are mean values ± SEM from 8 experiments carried out in duplicate.

	PDGF
Minimum response	20.6 ± 1.2
Maximum response	42.5 ± 4.4
pEC$_{50}$	9.36 ± 0.2
Hill Slope	1.44 ± 0.2

Table 6.2.5 PDGF CRC parameters obtained in the human HSC pERK assay. Data represents the mean of the individual parameters obtained from fitting the data from individual experiments represented in Figure 6.2.6 using non-linear regression analysis (four-parameter logistic equation with variable slope (Hill, 1909)(See Chapter 2: Data Analysis section). Data shown are mean values ± SEM from 8 experiments carried out in duplicate.
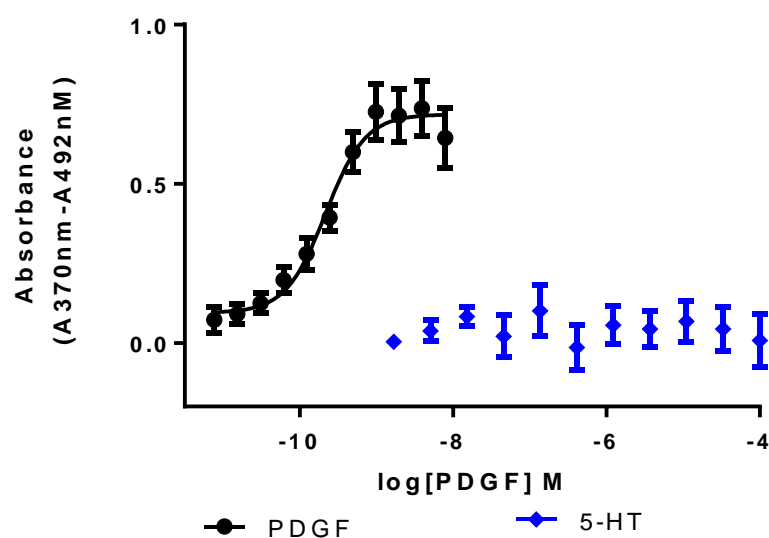
Figure 6.2.8   5-HT and PDGF stimulation of proliferation in human HSCs. Culture-activated human HSCs were cultured in medium containing 0.1% FCS for 24 h before addition of increasing concentrations of 5-HT (A) and PDGF (B) for a further 24 h.The BrdU label was added for a further 4 h incubation at 37°C in 5% CO_2. The proliferation was determined as incorporation of BrdU into the genomic DNA of the proliferating cells using a colourimetric ELISA (See Chapter 2: Material and methods). Response values had the basal values subtracted and was expressed as absorbance. CRCs were fitted using non-linear regression analysis (four parameter logistic equation with variable slope (Hill, 1909)) (See Chapter 2: Data analysis). Data shown are mean values $\pm$ SEM from $\geq$ 6 experiments carried out in duplicate.

	PDGF
Maximum response	0.62 ± 0.1
pEC$_{50}$	9.82 ± 0.1
Hill Slope	1.90 ± 0.2

Table 6.2.6   PDGF CRC parameters obtained in the human HSC proliferation assay. Data represents the mean of the individual parameters obtained from fitting the data from individual experiments represented in Figure 6.2.7 using non-linear regression analysis (four-parameter logistic equation with variable slope (Hill, 1909)(See Chapter 2: Data Analysis section). Data shown are mean values $\pm$ SEM from $\geq$ 6 experiments carried out in duplicate.

5-HT (Figure 6.2.9 A, Table 6.2.7) as would be expected if 5-HT had enhanced the effect of PDGF.

6.2.5 Investigation of the role of 5-HT in driving collagen deposition in human hepatic stellate cells.

Collagen deposition was investigated using human HSCs in a high content imaging method adapted from Chen et al. (2009). 5-HT applied to human HSCs did not elicit a concentration-related increase in collagen deposition (Figure 6.2.10). This therefore demonstrates that 5-HT was unable to stimulate collagen deposition in the human HSCs. TGFβ was found to cause a concentration-dependent increase in collagen deposition in 6 out of the 12 experiments performed from 6 different donors, a representative TGFβ CRC shown (Figure 6.2.11). The ability of TGFβ to elicit a response in the assay was not dependent on batch but was generally observed in the HSCs which had had the shortest length of time in culture for each donor, with one donor not responding at all.

6.3 Discussion.

6.3.1 Immunocytochemistry analysis of isolated hepatic stellate cells.

HSCs have been isolated from the livers of animals and humans since the 1980's, which led to extensive studies being undertaken to understand its role in fibrosis. Culturing the HSCs on plastic causes the cells to differentiate into a myofibroblast phenotype, similar to the population of cells that would be found in fibrotic liver. To confirm that the HSCs used in the experiments were the activated phenotype, immunocytochemical staining of the cells was undertaken. The human HSCs isolated and kept in culture for 7 days or more were shown to express synaptophysin, a marker for quiescent and activated HSCs (Cassiman et al., 1992) and α-SMA, a marker for activated HSC in these studies. This confirmed that the cells that had been isolated were HSCs and that, after at least 7 days in culture on plastic, they had differentiated into the activated phenotype. There were a few cells which stained faintly for α-SMA which could indicate that they were not completely activated. The images of the cells that were in culture for 14 days demonstrated positive staining for
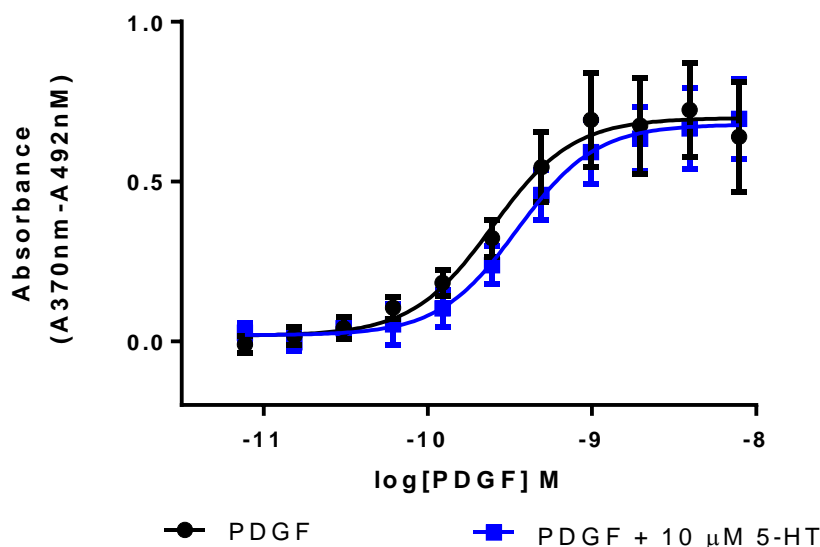
Figure 6.2.9 Effect of 5-HT (10 μM) on PDGF CRCs generated in the human HSCs proliferation assay. Culture-activated human HSCs were cultured in medium containing 0.1% FCS for 24 h before addition of increasing concentrations of PDGF in the presence and absence of 5-HT (10μM) for a further 24 h. The BrdU label was added for a further 4 h incubation at 37°C in 5% CO_2. The proliferation was determined as incorporation of BrdU into the genomic DNA of the proliferating cells using a colourimetric ELISA (See Chapter 2: Material and methods). Response values were normalised to basal and data was expressed as absorbance. CRCs were fitted using non-linear regression analysis (four parameter logistic equation with variable slope (Hill, 1909)) (See Chapter 2: Data analysis). Data shown are mean values ± SEM of 4 individual experiments carried out in duplicate.

	PDGF	PDGF + 5-HT (10 μM)
Maximum response	0.65 ± 0.2	0.55 ± 0.2
pEC$_{50}$	9.79 ± 0.2	9.60 ± 0.1
Hill Slope	1.78 ± 0.2	2.08 ± 0.6

Table 6.2.7 PDGF CRC parameters obtained in the presence and absence of 5-HT (10 μM) in the human HSC proliferation assay. Data represents the mean of the individual parameters obtained from fitting the data from individual experiments represented in Figure 6.2.7. using non-linear regression analysis (four-parameter logistic equation with variable slope (Hill, 1909) (See Chapter 2: Data Analysis section). Data shown are mean values ± SEM of 4 individual experiments carried out in duplicate.
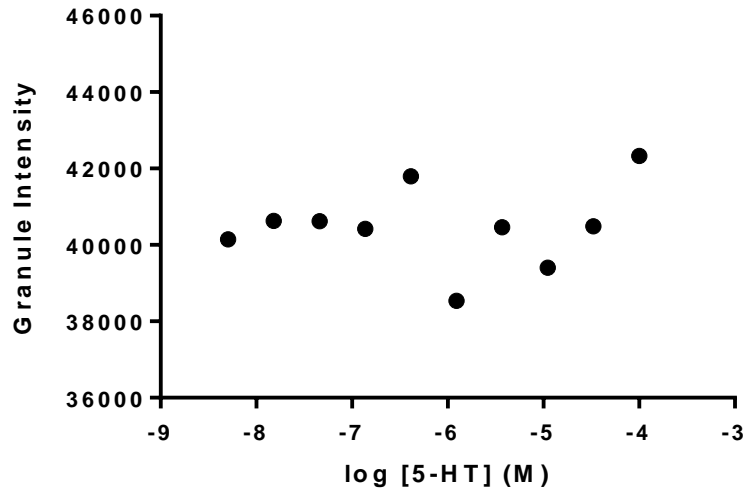
Figure 6.2.10. Effect of 5-HT on stimulation of collagen 1 deposition in human HSCs. Culture-activated human HSCs were cultured in low serum (0.4%) medium at 37°C in 5% CO_2 for 24 h before replacing the medium with Ficoll mix made up in low serum medium containing 0.2mM ascorbic acid. Compounds were added and incubated for 72 h at 37°C in 5% CO_2. Cells were fixed and stained to detect collagen 1 and the nucleus of the cells. The fluorescence was then visualised and data expressed as granule intensity (See Chapter 2: Materials and methods). CRCs were fitted using non-linear regression analysis (four parameter logistic equation with variable slope (Hill, 1909)) (See Chapter 2: Data analysis). Data shown are the individual data from batch 9 p4.
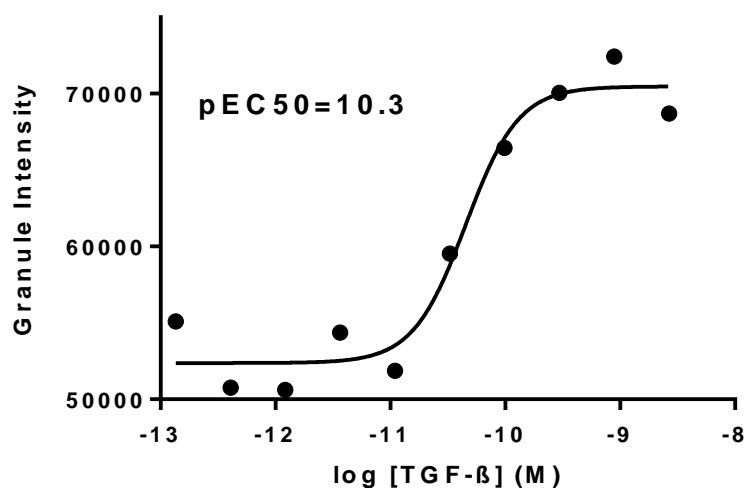
Figure 6.2.11 Effect of TGFβ- on stimulation of collagen 1 deposition in human HSCs.
Culture-activated human HSCs were cultured in low serum (0.4%) medium at 37°C in 5% CO_2 for 24 h before replacing the medium with Ficoll mix made up in low serum medium containing 0.2mM ascorbic acid. TGFβ was added and incubated for 72 h at 37°C in 5% CO_2. Cells were fixed and stained to detect collagen 1 and the nucleus of the cells. The fluorescence was then visualised and data expressed as granule intensity (See Chapter 2: Materials and methods). CRCs were fitted using non-linear regression analysis (four parameter logistic equation with variable slope (Hill, 1909)) (See Chapter 2: Data analysis). Data shown is a representative curve from a single experiment.

α-SMA, with clearly defined cytoskeletal fibres, which were also highlighted by the synaptophysin staining, indicating the cells were fully activated in this culture. This pattern of staining was observed in cultures out to 21 days. These findings confirmed that the cells that were used in these studies were activated HSCs.

6.3.2 Pharmacological characterisation of the 5-HT receptor responsible for the [Ca^{2+}] increase in human hepatic stellate cells.

5-HT was shown to cause a concentration-dependent increase in cytosolic calcium in human HSCs. This confirmed observations in the literature with rat HSCs (Park et al., 2011) and the data obtained in Chapter 4 with mouse HSCs. Due to their increased expression upon activation of HSCs (Ruddell et al., 2006; Ebrahimkhani et al., 2011) and involvement in calcium signalling due to their coupling through $G\alpha q$, 5-HT$_{2A}$ and 5-HT$_{2B}$ receptors are the most likely receptors to be involved. 5-HT$_{2B}$ antagonists GSK1606260A (1 μM) and RS-27455 (100 nM) had no effect on the 5-HT CRCs. This indicated a lack of 5-HT$_{2B}$ involvement in the 5-HT calcium release. 5-HT$_{1B}$ receptor expression has been demonstrated to be up-regulated in the HSCs upon activation (Ruddell et al., 2006) and although this receptor is G_i linked it is possible that it can cause release of calcium in this assay format (Hall et al., 1999; Werry et al., 2002). However cyanopindolol (1μM), a 5-HT$_{1B}$ antagonist, had no effect on the 5-HT CRC which rules out 5-HT$_{1B}$ receptor involvement.

5-HT$_{2A}$ receptor antagonists, ketanserin and volinanserin caused insurmountable antagonism the 5-HT CRC which meant that no affinity could be determined, but the concentration range over which their antagonism of 5-HT CRC was observed indicated a 5-HT$_{2A}$ effect. Ketanserin and volinanserin pA$_2$ estimates are from the 1 nM shifts of the 5-HT CRC, despite criteria for competitive not being met, were determined as 9.3 and 9.0 respectively. These values in keeping with what would be expected for a 5-HT$_{2A}$ antagonist effect. Therefore confirming the 5-HT$_{2A}$ receptor is responsible for the 5-HT stimulated calcium release human HSCs and that this agrees with data generated in the mouse HSC (Chapter 4).

The insurmountable nature of the antagonism may indicate that the antagonists, ketanserin and volinanserin are behaving as non-competitive antagonists but there could be another explanation for their non-competitive behaviour. The non-

competitive nature of the antagonism could be explained by the fact that the antagonist and agonist together are unable to reach equilibrium with the receptor in the time-frame of the agonist response (Hemi-equilibrium) (Figure 4.3.1) (Paton and Rang, 1966; Kenakin et al., 2006). Volinaserin and ketanserin in the human HSCs 5-HT stimulated calcium release assay have exhibited a similar pattern of antagonist behaviour to that observed with the mouse HSCs in the same assay format (See Section 4.2.2). It is therefore likely that ketanserin and volinanserin have a slow off rate and that the 5-HT agonist response is relatively rapid, which means that ketanserin or volinanserin are unable to dissociate from the receptor to allow 5-HT binding to reach the correct equilibrium in these experiments in the human HSCs (Kenakin et al., 2006; Charlton and Vauquelin, 2010). A 'wash off' experiment, similar to that carried out with the mouse HSCs (See Section 4.2.3), could be performed to confirm if the hemi-equilibrium phenomenon is responsible for the non-surmountable antagonism observed in the human HSC. If the level of antagonism observed with ketanserin and volinanserin was reduced (less rightward shift and depression of the 5-HT CRC) once the antagonist was washed out then it can be concluded that ketanserin and volinanserin are not irreversible antagonists.

6.3.3   Characterisation of the 5-HT stimulated ERK phosphorylation in human hepatic stellate cells.

5-HT was found to cause a very low level of ERK phosphorylation of the human HSC using a similar protocol that was used for the mouse HSCs. The human HSC were capable of producing a pERK response in this experimental format as PDGF produced a concentration- dependent increase in ERK phosphorylation. The pEC_{50} of 9.36 for PDGF in the human cells was similar to that obtained for PDGF in the mouse HSC ($pEC_{50} = 9.43$) in the pERK assay (Section 5.2.2). 5-HT did cause a small, concentration-dependent increase in phosphorylation of ERK but this was difficult to quantify due to the low level of response. The basal level of ERK phosphorylation in the human cells was around 20% which was higher when compared to about 4% in the mouse HSC (Section 4.2.4.2). This would seem to suggest that there was a greater level of basal ERK phosphorylation in the human cells.

The HSCs used in these assays were isolated mainly from fibrotic donors over 50 years old. HSCs isolated from mouse livers were from young healthy mice. It has been demonstrated that HSCs isolated from human cirrhotic livers exhibit phenotypic features of myofibroblasts, such as a spindle-like shape, expression of α-SMA and fibronectin with less vitamin A droplets, which is not observed in freshly isolated HSCs isolated from normal livers (Sancho-Bru et al., 2005). HSCs from normal livers which are kept in prolonged culture do then progress into a myofibroblast-like phenotype (Sancho-Bru et al., 2005). It is therefore conceivable that the HSCs isolated for these studies are already partially activated and may possibly explain a higher basal level of pERK stimulation. Further studies could be carried out to determine if this was the case.

The human HSCs obtained from donors suffering from advanced liver fibrosis may not be the best cells to use in our studies. The fibrosis will have developed over decades and is considered less reversible, due to the dense cross-linked collagen, rather than weeks in the case of animal models. Human hepatic stellate cells have been shown to be resistant to apoptosis and this may be due to an over expression of anti-apoptotic protein, Bcl2, *in vitro* (Novo, 2006). The expression of genes implicated in apoptosis regulation in freshly isolated HSCs from diseased livers differ from those cells that have been culture-activated so their apoptotic properties may differ too (Sancho-Bru et al., 2005). The HSCs isolated from fibrotic livers will undergo further activation when cultured on plastic and may develop a different phenotype from HSCs isolated from normal livers cultured on plastic. Culture-activated HSC may not reproduce the activated phenotype of activated HSC from fibrotic liver (Sancho-Bru et al., 2005). This would warrant further investigation to determine if cells isolated from fibrotic liver once cultured on plastic do take on a different phenotype and whether that could explain the higher basal level of pERK observed.

6.3.4   Effect of 5-HT on the proliferation of human activated HSCs.

5-HT was found to have no mitogenic effect or influence the proliferation induced by PDGF in human HSCs, which was similar to that observed in the mouse HSCs (Section 5.2.1). The data also agrees with the finding of Ruddell et al. (2006) who

observed no proliferation with 5-HT in rat HSCs. Other groups have reported that 5-HT can exert a mitogenic effect on cells but these were mesangial cells (Eto et al., 1997) or fibroblasts (Welsh et al., 2004; Chen et al., 2014) so again highlighting differences in particular cell type sensitivity to 5-HT.

6.3.5 Role of 5-HT in driving TGF-β collagen deposition using the Scar in a jar assay.

5-HT was unable to induce collagen deposition in the human HSCs which was also the case in mouse HSCs (Section 5.2.4). In the human HSC, TGFβ was able to cause a concentration-dependent increase in collagen deposition in only 50% of the experiments performed, although this was not dependent on the batch, it was observed with the HSCs that had been in culture for the shortest time. It can be concluded that in this assay we are unable to demonstrate that 5-HT can stimulate the transcription and release of TGFβ to promote collagen deposition in cultured HSCs. The lack of effect on collagen deposition by 5-HT was observed in cells which were able to demonstrate TGFβ concentration-dependent collagen deposition. This may therefore suggests that 5-HT is unable to drive collagen deposition in the human HSCs.

A similar reasoning for the response observed in the mouse HSCs can be used to help understand the response of the human HSC to TGFβ in the collagen deposition assay. TGFβ is the most potent pro-fibrogenic signal for activated HSCs, with an increased expression during activation and a role in regulating extracellular matrix protein genes (Tsukada, 2005). The reason why some cells were able to be stimulated to produce collagen may be due to the state of the cells in the assay, such that they are insensitive to TGFβ and produce extracellular matrix protein by a TGFβ-independent pathway (Dooley et al., 2001; Tsukada, 2005; Tsukada et al., 2006). TGFβ as well as activating classical SMAD signalling can also activate p38 MAPK signalling (Tsukada, 2005). A reduction in α1 (I) collagen gene expression in untreated or TGFβ-stimulated HSCs was observed following inhibition of either of SMAD or p38 MAPK signalling (Tsukada, 2005). It was concluded that both signalling pathways, SMAD and p38 MAPK, independently and additively regulate α1 (I) collagen gene expression through transcriptional activation but the p38 MAPK also increases α1 (I)

collagen mRNA stability (Tsukada, 2005). Furthermore, activated HSCs may only be capable of a small increase in collagen deposition following further activation by TGFβ stimulation. In quiescent rat HSCs, TGFβ-induced collagen expression after 16hrs is similar to that in activated HSCs (Dooley et al., 2000). After full trans-differentiation into a myofibroblast phenotype, collagen mRNA levels are already up-regulated to levels similar to TGFβ treated cells, with no increase with TGFβ treatment and no down-regulation with an anti-TGFβ antibody (Dooley, 2000). Activated HSCs *in vitro* have also demonstrated constitutively activated SMAD2 and SMAD3 that are not associated with endogenous TGFβ signalling (Liu et al., 2003).

The variability in response observed in the human HSC could be due to different activation states of the HSCs. Many studies conducted in cultured rat hepatic stellate cells have shown differences in TGFβ signalling dependent on duration of culture and thus state of activation (Dooley et al., 2000; Liu et al., 2003). In quiescent cells, TGFβ signalling resulted in SMAD2 phosphorylation, whilst signalling after trans-differentiation into an activated phenotype is mediated by SMAD3 (Liu et al., 2003). In addition, SMAD2 activation levels are dependent on time in culture and state of activation (Liu et al., 2003). Inhibitory SMAD7 regulation by TGFβ is also dependent on activation state, with an up-regulation of SMAD7 mRNA with TGFβ treatment in early HSCs but not in cultured cells (Lui et al., 2003).

The results of the studies carried out using human HSCs demonstrate that 5-HT is capable of stimulating intracellular calcium through the 5-HT$_{2A}$ receptor. This is the first time that this 'in-depth', thorough pharmacological characterisation of the 5-HT response has been conducted, in calcium release assays in human HSCs. These data are similar to those observed in the mouse HSC calcium release assays. The 5-HT receptor subtype mediating ERK phosphorylation could not be determined due to the very small 5-HT response and elevated basal level of ERK phosphorylation. In studies investigating proliferation and collagen deposition there was no evidence to demonstrate an effect of 5-HT. These studies are the first to pharmacologically characterise the 5-HT response in the human HSC. The 5-HT studies undertaken in the literature with HSCs have mainly been undertaken with rodent HSCs or human cell lines (Li et al., 2006; Ruddell et al., 2006; Ebrahimkhani et al., 2011; Park et al.,

2011; Kim et al., 2013). Any studies with human HSC have been expression analysis of proteins with no quantitative pharmacology (Ebrahimkhani et al., 2011). None of the literature studies carried out have conducted a rigorous pharmacological analysis of the 5-HT subtype present on HSC from any species (Li et al., 2006; Ruddell et al., 2006; Ebrahimkhani et al., 2011; Park et al., 2011; Kim et al., 2013). The conclusion drawn from the studies carried out in this chapter with the human HSC is that 5-HT may not play a major role in influencing the activated HSC during liver injury.

Chapter 7: General Discussion

7.1   Overview of data generated.

The prevalence of chronic liver disease has been rising worldwide (Lazo and Clark, 2008; Williams et al., 2011). Over the past 30 years there has been much research undertaken in liver fibrosis and it is known that the HSC, a fibrogenic cell type, is responsible for the scarring, as well as playing an immunomodulatory and homeostatic regulatory role in fibrosis (Friedman, 2008a; Jiao et al., 2009; Koyama and Brenner, 2015). During liver injury the quiescent HSC transforms into a proliferating, perpetuating myofibroblast–like cell which produces scarring (Friedman, 2008a; Jiao et al., 2009; Koyama and Brenner, 2015). During the activation of the HSCs expression levels of proteins, such as receptors, have been demonstrated to increase, making targeting the activation of the HSCs an attractive strategy for anti-fibrotic therapy.

One of the targets of interest is 5-HT_2 receptors, which have been demonstrated to promote fibrogenic activity, and whose expression is up-regulated upon activation of the HSCs (Li et al., 2006; Ruddell et al., 2006, 2008; Ebrahimkhani et al., 2011; Park et al., 2011; Kim et al., 2013). Conflicting evidence had been presented in the literature as to the exact 5-HT_2 receptor subtype responsible, 5-HT_{2A} or 5-HT_{2B} (Li et al., 2006; Ebrahimkhani et al., 2011; Park et al., 2011; Kim et al., 2013) (See section 1.6.2 and 4.3). Much of the literature evidence relies upon the use of non-selective concentrations of 5-HT antagonists, with interpretation of the 5-HT receptor subtype responsible being compromised by this approach. The aim of the research presented in this thesis was to undertake an 'in-depth' quantitative pharmacological characterisation of the 5-HT receptor subtype present on mouse and human HSCs. This involved a full evaluation and target validation for a role of 5-HT in driving the fibrogenic process.

7.2   Phenotyping the hepatic stellate cells using immunocytochemistry.

Ensuring that the cells used in the *in vitro* experiments were activated HSCs was crucial for the interpretation of the data generated for this thesis. This is essential as it is the activated HSCs that are responsible for the excessive scarring, which causes loss of function and architectural distortion in liver fibrosis. The immunocytochemistry performed on the primary human and mouse HSCs confirmed

186

that they were activated HSCs. All the cultured mouse and human hepatic stellate cells were demonstrated to express α-SMA, a phenotypic marker for activated HSCs (Friedman, 2008b), with co-expression of synaptophysin, a marker for HSCs (Cassiman et al., 1992). The immunocytochemical analysis confirmed that there were no contaminating cells, such as Kupffer cells, present in the cultures.

7.3 Pharmacological characterisation of the 5-HT receptor responsible for the 5-HT-stimulated calcium response in mouse and human activated hepatic stellate cells.

An *in vitro* assay, investigating the ability of 5-HT to simulate calcium release, was undertaken to enable in-depth pharmacological identification of the 5-HT receptor subtypes in HSCs. Selective 5-HT agonists and antagonists were chosen and were used at selective concentrations, as determined by 'in-house' and literature studies, to clearly identify the 5-HT receptor subtype responsible. Characterisation of the 5-HT-stimulated calcium response in both mouse and human HSCs identified the 5-HT$_{2A}$ receptor as the 5-HT receptor subtype mediating this response. 5-HT$_{2A}$ antagonists ketanserin and volinaserin both behaved as insurmountable antagonists in the concentration range expected for 5-HT$_{2A}$ antagonism. NBOH-2C-CN, a low intrinsic efficacy 5-HT$_{2A}$ agonist, was found to behave as an antagonist in the calcium release assay in mouse HSCs. The concentration range of the antagonism of NBOH-2C-CN was in the correct range for a 5-HT$_{2A}$ receptor-mediated effect. No effect on the 5-HT-stimulated calcium release CRC was observed with the 5-HT$_{2B}$ antagonists GSK1606260A or RS-177445 in the assay. Any contribution of the 5-HT$_{1B}$ receptor was excluded by data demonstrating no effect of a specific 5-HT$_{1B}$ agonist and antagonist or receptor inactivation techniques on the 5-HT-stimulated calcium response in both mouse and human HSCs. The 5-HT-stimulated calcium release data generated in this thesis confirms and expands the pharmacological characterisation reported in the literature (Li et al., 2006; Ruddell et al., 2006; Park et al., 2011). It provides strong evidence that 5-HT$_{2A}$ is the receptor stimulated by 5-HT to cause calcium release in both mouse and human HSCs. The increase in intracellular calcium might influence the contractile nature of activated HSCs and so may be a

contributor to the vascular resistance observed *in vivo* (Park et al., 2011) and in liver fibrosis.

7.4 Pharmacological characterisation of the 5-HT receptor responsible for ERK phosphorylation in mouse and human hepatic stellate cells.

Events downstream of 5-HT stimulation of the HSCs have been shown to involve phosphorylation of ERK (Ebrahimkhani et al., 2011). A similar 'in-depth' pharmacological characterisation in both the mouse and human HSCs was then undertaken to determine the 5-HT receptor subtype involved with literature reports suggesting that the 5-HT_{2B} subtype was responsible (Ebrahimkhani et al., 2011). 5-HT was found to cause a concentration-related increase of ERK phosphorylation in the mouse HSC but in had a limited impact on ERK phosphorylation in human HSCs. This very low level of ERK phosphorylation in the human HSCs prevented any pharmacological characterisation of the response. This lack of pharmacological evaluation therefore does question the role of 5-HT in liver fibrosis.

As observed in the calcium assay, 5-HT_{2B} antagonists, GSK1606260A and RS-127445 caused no rightward shift of the 5-HT CRC for ERK phosphorylation. 5-HT_{2A} antagonists, ketanserin and volinaserin, both behaved as insurmountable antagonists over a 5-HT_{2A} selective concentration range. The nature of the antagonism with ketanserin also suggested the possible presence of a second 5-HT receptor mediating the ERK phosphorylation which is discussed further in Section 7.4.6. NBOH-2C-CN, a selective 5-HT_{2A} agonist (Hansen et al., 2014; Fantegrossi et al., 2015), elicited a concentration-dependent increase in ERK phosphorylation with an intrinsic activity of 0.3. This data therefore confirms that the 5-HT-stimulated ERK phosphorylation was due to activation of the 5-HT_{2A} receptor.

This 'in-depth' pharmacological characterisation of the 5-HT concentration-related increase in ERK phosphorylation carried out with the mouse HSCs identifies the 5-HT_{2A} receptor as mediating the response. This conclusion does not agree with the published data from the analysis of SB-204741, a 5-HT_{2B} selective antagonist, in mouse, rat and human HSCs (Ebrahimkhani et al., 2011). Data presented by Ebrahimkhani et al. (2011) using SB-204741 demonstrated inhibition of 5-HT

stimulated expression of phospho-ERK in mouse, rat, and human HSCs at concentrations of ≥ 10 μM. The 5-HT$_{2B}$ affinity of SB-204741 is about 100 nM (Knight et al., 2004) with a human 5-HT$_{2A}$ receptor binding affinity of > 10 μM. This therefore means that the SB-204741A inhibition, which was only observed at concentrations of ≥ 10 μM, is most likely due to a 5-HT$_{2A}$ receptor related effect. These findings exemplifying how using high non-selective concentrations of specific antagonists can lead to misinterpretation of data. Thus it can be concluded that the ERK phosphorylation data generated in this thesis in the mouse HSCs agrees with the literature.

In the human HSCs it was difficult to define a concentration-dependent ERK phosphorylation effect by 5-HT in the human HSC. Instead a higher basal level of ERK phosphorylation was observed in human HSCs, which was similar to the maximum level of ERK phosphorylation observed in the mouse HSCs (Figure 7.4.1). The cause of the elevated basal ERK phosphorylation was not investigated further but may be due to the source of the cells. The mouse HSCs were isolated from healthy juvenile to mature C57BL/6 mice while the human HSC were isolated from donors who were over 50 years of age, with some coming from fibrotic donors. HSCs isolated from human cirrhotic livers have been demonstrated to exhibit phenotypic features of myofibroblasts, such as a spindle-like shape, expression of α-SMA and fibronectin with less vitamin A droplets, which is not observed in freshly isolated HSCs from normal livers (Sancho-Bru et al., 2005). HSCs from normal livers which are kept in prolonged culture do then progress into a myofibroblast-like phenotype (Sancho-Bru et al., 2005). It is therefore conceivable that the HSCs isolated for these studies are already partially activated and may offer a possible explanation for the higher basal level of ERK phosphorylation. It is therefore conceivable that age and disease stage of the cells affects the signalling pathways or the different results may reflect a species difference.

7.5 Investigation of the insurmountable antagonism obtained with ketanserin and volinaserin in the calcium release and ERK phosphorylation assay.

The 5-HT$_{2A}$ antagonism by ketanserin and volinaserin observed in both the calcium release and ERK phosphorylation assays was insurmountable. In the literature ketanserin is reported to be a competitive antagonist but this can depend on the assay system (Frenken and Kaumann, 1984; Leff and Martin, 1986). Antagonist washout experiments in the calcium release assay suggests that the insurmountable behaviour is due to the antagonist having insufficient time to dissociate from the receptor during the rapid agonist response (hemi-equilibrium) (Paton and Rang, 1966; Kenakin et al., 2006). The response elicited by 5-HT in the ERK phosphorylation assay is slower (10-15 min) compared to the response observed in the calcium release assay (10s). In the ERK phosphorylation assay, ketanserin and volinanserin exhibit a lesser degree of depression of the 5-HT CRCs (Figure 4.2.13) when compared with the 5-HT CRC obtained in the calcium release assay (Figure 4.2.5). The same hemi-equilibrium phenomenon may be applicable but as the 5-HT response is slower we observe a profile expected for a competitive insurmountable antagonism, as partial equilibration occurs (Paton and Rang, 1966). Additional experiments could explore this further, for example using 'washoff' experiments in the ERK phosphorylation assay. Understanding the molecular mechanism of antagonism is important for the drug development process as different types of antagonist can have complex behaviours, which will manifest itself in the therapeutic environment (Kenakin et al., 2006). The behaviour of antagonists in assays with fast agonist responses can be quite different to those determined in assays with slower agonist responses (Leff and Martin, 1986; Kenakin et al., 2006; Charlton and Vauquelin, 2010). Before the advances in molecular biology, where recombinant receptors could be expressed in cell lines, tissue preparations were used in drug discovery such that drugs were discovered in a physiologically relevant system (Leff and Martin, 1986; Kenakin, 2006; Charlton and Vauquelin, 2010). The nature of the antagonism of ketanserin and volinaserin will therefore likely change as more physiologically relevant assay systems are explored.

This is the first time an 'in-depth' pharmacological analysis has been undertaken in this system and confirms that it is the 5-HT$_{2A}$ receptor present on activated mouse HSCs is mediating the 5-HT stimulation of ERK phosphorylation. It also demonstrates the value of performing quantitative 'in-depth' pharmacological characterisation of the *in vitro* response which allows identification of the receptor subtype. Much of the data published in the literature has relied on expression data and use of single high concentrations of nominally specific receptor antagonists. The pharmacological characterisation carried out in both the calcium release and ERK phosphorylation assay reaches the same conclusion: that it is the 5-HT$_{2A}$ receptor expressed on HSCs that is responsible for these 5-HT effects.

7.6   Investigation into the presence of a second 5-HT receptor contributing to the 5-HT response in mouse HSCs.

Closer examination of the 5-HT CRCs obtained in the ERK phosphorylation assay in mouse HSCS revealed a biphasic curve. Further evidence of a biphasic nature came from the 5-HT CRCs, which become progressively more shallow in the presence of increasing concentrations of ketanserin. These findings suggests activation of more than one receptor by 5-HT. Construction of a more defined 5-HT CRC supported this further and suggested that more than one 5-HT receptor subtype could be mediating the ERK phosphorylation response. A model was constructed to explore the influence of activation of two receptors signalling through ERK, which allowed alteration of the affinity and efficacy of the response of the two receptors. The model suggested that two 5-HT receptors are involved in the response with affinities that differ by 100-fold and with different efficacies ($\tau_A = 5$, $\tau_B = 10$). These tau values implying that 5-HT behaves as a partial agonist at both receptors. This model could be further explored by the addition of antagonists to predict their behaviour in the experimental situation.

The most likely candidate for the second 5-HT receptor is 5-HT$_{1B}$, as this receptor had been reported to be induced upon activation of the HCSs. Sumatriptan, a selective 5-HT$_{1B}$/$_{1D}$ receptor agonist behaved as partial agonist in the ERK phosphorylation assay and was not inhibited by GSK1606260A or ketanserin. Cyanopindolol (100 nM), a 5-HT$_{1B}$ antagonist (pK$_B$ = 8.1 - 8.7) (Maroteaux et al.,

1992; Giles et al., 1996), caused a rightward shift of the sumatriptan CRC, with an affinity estimate of 8. This evidence taken together adds support to the hypothesis that sumatriptan is interacting at the 5-HT_{1B} receptor. Two experimental methods were used with the aim to investigate the ketanserin antagonism of 5-HT in a pure 5-HT_{2A} system through removal of the influence of the 5-HT_{1B} receptor by inhibition with cyanopindolol or blocking the G_i-protein activation with PTX. The 5-HT CRC slope in the presence of ketanserin (100 nM) approaches unity in combination with cyanopindolol or PTX pre-treatment, with an estimated pA_2 of ~ 9. The 5-HT_{1B} receptor influence was therefore removed to reveal a pure 5-HT_{2A} response. This data adds further evidence that the 5-HT_{1B} receptor is likely to be the second 5-HT receptor involved in the 5-HT stimulated ERK phosphorylation response.

The effect of PTX pre-treatment on the sumatriptan CRC was investigated as this response should be abolished if it is acting through the 5-HT_{1B} receptor. There was a > 5-fold shift of the sumatriptan CRC but the response was not completely abolished. Due to the low potency (pEC_{50} ~5) of sumatriptan, it is feasible that at the higher concentrations, sumatriptan is causing phosphorylation of ERK via the 5-HT_{2A} receptor, as ketanserin (100 nM) reduced the maximum sumatriptan response. The magnitude of the response is not as much as would be expected for 5-HT_{2A} effect but could depend on how much of the response is elicited by the 5-HT_{2A} receptor. Further experiments investigating sumatriptan with PTX pre-treatment in the presence and absence of ketanserin may be able to further define if 5-HT_{2A} is activated by sumatriptan or via another mechanism.

Indeed, it has been reported that 5-HT_7 and 5-HT_{1F} receptors are present on HSCs and that their expression either reduces or remains stable respectively during activation of HSCs (Ruddell et al 2006). However these receptors were not investigated in this thesis. 5-HT_{1F} like 5-HT_{1B} couples through G_i and so would have also been inhibited by PTX pre-treatment. Sumatriptan is also reported to be an agonist at the 5-HT_{1F} receptor (Adham et al., 1997) but cyanopindolol has not been reported to be a 5-HT_{1F} receptor antagonist. The inhibition of sumatriptan by cyanopindolol would therefore suggest a 5-HT_{1B} receptor mediated effect as opposed to 5-HT_{1F} receptor mediated response. Further investigation is warranted to clearly

define the identity of the second 5-HT receptor, but the evidence so far seems to support this being the 5-HT$_{1B}$ receptor. This is the first time that evidence has been presented for the presence of a second receptor that contributes to the activation of ERK phosphorylation by 5-HT in mouse HSCs.

7.7 Role of 5-HT in driving proliferation in mouse and human hepatic stellate cells.

Next investigations as to the role the 5-HT$_{2A}$ and 5-HT$_{1B}$ receptors, expressed on HSCs, contribute to phenotypic fibrotic endpoints was undertaken. The key phenotypic features of HSCs activation into a myofibroblast–like cell following liver injury are proliferation, contractility, production of collagen, expression of TIMP-1, expression of α-SMA, loss of retinoid storage capability, resistance to apoptosis, and chemotaxis (Murphy et al., 2002; Friedman, 2008). Evidence in the literature had reported that 5-HT was able to exert an effect on proliferation (Ruddell et al., 2006; Ebrahimkhani et al., 2011; Kim et al., 2013).

5-HT did not induce proliferation in mouse and human HSCs whereas PDGF, a potent mitogen, induced proliferation in a concentration-dependent manner in agreement with the findings of Ruddell et al. (2006) in rat HSCs. Myofibroblasts derived from either mesangial cells (Eto et al., 1997) or fibroblasts (Welsh et al., 2004; Chen et al., 2014) have been reported to exhibit a proliferative effect of 5-HT, which may indicate a difference in sensitivity of a particular cell type to 5-HT as a mitogen. Investigation of the 24 h time course of ERK phosphorylation demonstrated a difference profile of response between 5-HT and PDGF in mouse HSCs. 5-HT and PDGF had a similar profile over the first 3 h but then the 5-HT response declined to baseline after 8 h, whereas the PDGF response continued at a low level of activation up to 24 h. This low level of activation possibly sufficient to continually stimulate the proliferation of the cells. In the literature a biphasic time course for ERK phosphorylation was observed in response to PDGF, with a second peak being achieved at 15 h in human HSCs (Bonacchi et al., 2001). The 5-HT pERK response kinetics are similar to those observed with the CXCR3 ligand, IP10, which is unable to induce proliferation. In this case there is a peak pERK response observed between 15 - 30 min before returning to baseline at 4 h in HSCs. (Bonacchi et al., 2001).

These data taken together confirm a different activation profile for both 5-HT and PDGF which may explain why 5-HT does not influence proliferation of HSCs.

5-HT$_2$ antagonists had previously been reported to inhibit proliferation (Ruddell et al., 2006; Lee et al., 2012; Kim et al., 2013). Ketanserin and GSK1606260A failed to inhibit proliferation in the concentration range expected for responses mediated by the 5-HT$_{2A}$ and 5-HT$_{2B}$ receptor respectively. Inhibition of proliferation with ketanserin and GSK1606260A was observed at concentrations > 1 µM, but this is probably a non-specific effect as both inhibitors have nM affinity for their respective 5-HT$_2$ receptor subtypes. These data are similar to those previously reported for ketanserin and a number of different 5-HT$_2$ antagonists in rat HSCs where the IC$_{50}$ values were all greater than 1 µM (Ruddell et al., 2006). This data does not support an effect of 5-HT$_2$ antagonism on proliferation and highlights the problem of using high concentrations of antagonists to confirm specific receptor effects subsequently leading to erroneous interpretation of the result.

7.8 Investigation of a synergistic interaction of 5-HT and PDGF.

An enhancement of proliferation with a maximal concentration of 5-HT, as well as a 5-HT concentration-dependent increase in proliferation in the presence of a sub-maximal concentration of PDGF was reported in rat HSCs (Ruddell et al., 2006). This could not be replicated in the proliferation studies undertaken in this thesis. As both 5-HT and PDGF activate receptors that signal via the ERK pathway, investigation of PDGF and 5-HT in the pERK assay was undertaken to establish whether synergy is observed.

The studies demonstrated that in the presence of a sub-maximal concentration of 5-HT, there was a 4-fold leftward shift of the PDGF CRC with no significant difference in the maximum effect observed with PDGF alone. This data suggests that there is an enhancement of the PDGF CRC, indicative of a synergistic effect. From the data generated it is possible to conclude that 5-HT increases the sensitivity of tyrosine kinase (TRK) activation to PDGF and that PDGF is able to maximally activate all the TRK. The reciprocal experiment demonstrated that a sub-maximally effective concentration of PDGF does not affect the 5-HT CRC potency but causes a

greater maximum response, therefore is suggestive of an additive effect. The data with the different combinations seems to suggest that there may be a limit to the level of the ERK phosphorylation response achievable in the HSCs, with PDGF able to cause a greater degree of ERK phosphorylation or in fact maximally stimulate. Further studies investigating the effect of higher concentrations of 5-HT on the PDGF response and higher PDGF concentrations on the 5-HT response may be able to elucidate if PDGF does maximally stimulate all the TRK.

This is the first time these studies have been undertaken in HSCs using the ERK phosphorylation assay which has clearly demonstrated a synergistic effect of 5-HT on the PDGF response. Translation of this synergistic effect in the proliferation assay was not observed, but the proliferation assay used may not have been as sensitive as the one used in the literature, where an enhancement was observed (Ruddell et al., 2006). It is also possible that PGDF proliferation is achieved at sub-maximal concentrations in terms of TRK activation. Taken together, the lack of effect of 5-HT and any synergistic effect on the PDGF proliferation it is difficult to identify a role for 5-HT in HSC proliferation.

7.9   Investigation of the role of 5-HT in driving collagen deposition in mouse and human hepatic stellate cells.

Activated HSCs are the key cells involved in collagen deposition. In the chronically injured liver HSCs persist, producing excess deposition of collagen, which alters the constituents of the hepatic ECM, such that the liver becomes fibrotic (Benyon and Arthur, 2001). 5-HT was shown to activate the mitogen-activated protein kinase 1 (ERK) and transcription factor JunD to mediate stimulation of TGFβ1 transcription in HSC (Ebrahimkhani et al., 2011). The hypothesis to explain these effect was that 5-HT-stimulates release of TGFβ1, which binds to the TGFβ receptor on the HSCs to stimulate collagen deposition (Ebrahimkhani et al., 2011; Mann and Oakley, 2013).

The effects of 5-HT to induce collagen deposition was investigated in a Scar in a Jar assay. This assay measures rapid deposition of granular collagen I aggregates within a 72 h timeframe through macromolecular crowding. 5-HT had no effect on collagen deposition in both mouse and human HSCs with ketanserin having no effect on

collagen deposition in human HSCs. The ability of TGFβ to stimulate collagen deposition in HSC is key to being able to demonstrate an effect of 5-HT on promoting collagen deposition. In mouse HSCs, TGFβ exhibited a concentration-dependent increase in collagen deposition in only one out of the three batches of cells. The basal collagen levels of the two batches that were insensitive to TGFβ were similar to collagen levels at maximal stimulation by TGFβ in the sensitive batch. There was a greater number of cells in the TGFβ insensitive batches. It is possible that a greater number of HSCs produce more latent and active TGFβ so the cells are less sensitive to TGFβ and a higher basal level of collagen deposition is observed. Therefore if the cells become less sensitive to TGFβ then this would compromise the ability of 5-HT to induce an effect on collagen deposition.

In the human HSCs a TGFβ concentration-dependent increase was observed in 50% of the experiments performed. The HSCs batches that were insensitive to TGFβ tended to be HSCs that had been in culture for longest. This implies that HSCs become resistant to TGFβ with extended time in culture. This is supported by previous work showing that upon differentiation into a myofibroblast phenotype the cells lose sensitivity to TGFβ and produce extracellular matrix protein by a TGFβ-independent pathway (Dooley et al., 2001). Quiescent and newly isolated HSCs have been found to be more sensitive to TGFβ than cells in culture activated on plastic (Dooley et al., 2000; Liu et al., 2003; Dooley and ten Dijke, 2012), so the activated phenotype may only allow a small window for further activation by TGFβ stimulation.

The way each human donor cells responds will depend on the sex, age, genetic makeup and state of liver (Mühlbauer et al., 2004). This suggests that there is strong possibility of variability within other signalling pathways in human HSCs as well as the TGFβ signalling pathway. HSCs isolated from human cirrhotic livers are partially activated, which is not observed in freshly isolated HSCs from healthy livers (Sancho-Bru et al., 2005). This difference may therefore explain the difference in the ability of TGFβ to drive collagen deposition. This could be explored further but would require donor information such as age, sex and liver disease status to be

available for each set of HSCs that are isolated, which has not always been the case in the cells used in these studies.

7.10 *In Vivo* CCl4 liver model.

Studies in this thesis focussed mainly on the HSCs role, as this cell has been shown to play a key role in liver fibrosis and is responsible for the scarring observed in fibrosis (Friedman, 2008a; Jiao et al., 2009). However, the liver, is a multi celluar organ and so the interplay between the different populations of cells will play a major role in how the liver responds to the fibrotic stimuli. The effect of a selective 5-HT$_{2A}$ antagonist, volinanserin, and selective 5-HT$_{2B}$ antagonist, GSK1606260A, were tested in a mouse CCl$_4$ model of lung injury, by administration of selective concentrations by minipump to achieve 90 and 99% receptor occupancy throughout the study. Volinaserin, demonstrated no significant difference in the PSR staining, at week 8, with both doses (0.06 and 0.32 mg/kg/day) implying that 5-HT$_{2A}$ antagonism has no benefit as an anti-fibrotic therapy. GSK1606260A, demonstrated a significant increase in PSR staining at week 8, with both doses (0.15 and 1.53 mg/kg/day) and further analysis of the data implied a 5-HT$_{2B}$ concentration-related relationship. This data suggests that 5-HT has an anti-fibrotic activity via the 5-HT$_{2B}$ receptor in the injured liver and blockade leads to increased fibrosis.

As very low and selective 5-HT$_{2B}$ concentrations of GSK1606260A were maintained in the study it is unlikely that the effect of this inhibitor is driven through an 'off-target' activity. The literature concerning the role of 5-HT in fibrosis demonstrates it to be more likely to be pro-fibrotic (Oates et al., 1966; Graham, 1967; Reimund, 1987; Pavlovic et al., 1995). Data from the withdrawn anti-obesity drug fenfluramine, demonstrated it to cause VHD through activation of 5-HT$_{2B}$ receptors by its metabolite norfenfluramine (Rothman et al., 2000). MDMA, used in Parkinson's disease, was also found to cause VHD through activation of 5-HT$_{2B}$ receptors. In addition data from a mouse CCl$_4$ model, using SB-204741, a selective 5-HT$_{2B}$ antagonist, found reduced numbers of activated HSCs, fibrotic matrix, expression of TGFβ1 and fibrogenic genes (TIMP-1 and pro-collagen I). No SB-204741 PK was reported to confirm the blood concentrations obtained (Ebrahimkhani et al., 2011), but an 'in-house' study, following the same dosing

protocol, demonstrated only brief exposure of the parent compound following dosing (all parent compound was cleared by 2 h of dosing). The *in vivo* study reported in this thesis demonstrated a constant exposure of 90-99% occupancy of GSK1606260A throughout the last 5 weeks of CCl_4 dosing to the animals. The data generated in the *in vivo* study therefore contradicts the *in vivo* CCl_4 study with SB-204741, which suggests a 5-HT$_{2B}$ anti-fibrotic effect (Ebrahimkhani et al., 2011), as well as the literature concerning 5-HT and fibrosis. The data presented in this thesis has been unable to demonstrate a functional 5-HT$_{2B}$ receptor present on HSCs. The interplay between different resident cells, such as hepatocytes, Kupffer cells and sinusoidal endothelial cells along with the vasculature will determine the overall pharmacological effect of the compounds in the liver.

A 5-HT$_{2A}$ antagonist, sarpogrelate, was dosed in a thioacetamide (TAA) rat model of liver injury and found to reduce lobular inflammation and cause a slight, but not significant, attenuation of periportal fibrosis (Kim et al., 2013). Again no PK studies were reported to confirm exposure of the sarpogrelate but expression of markers of HSC activation, α-SMA, TGFβ and Smad2/3 were all significantly reduced following treatment. This data is partially consistent with the volinaserin data, as there was no significant anti-fibrotic effect. Overall there is conflicting data reported in the liver injury models and further comprehensive studies would be needed to explore dose exposure, receptor target engagement and toxicity of compounds.

5-HT is able to exert its effects through 13 distinct GPCRs and one ligand-gated ion channel. Numerous 5-HT receptors are present throughout the liver with expression on vascular endothelium, hepatocytes, Kupffer cells and cholangiocytes (Ruddell et al., 2008; Ebrahimkhani et al., 2011). Expression of 5-HT $_{1A}$, 5-HT $_{1B,}$ 5-HT $_{1D,}$ 5-HT $_{2A,}$ 5-HT $_{2B}$, 5-HT $_{3A,}$ 5-HT $_{3B}$ receptors were shown in liver (Lesurtel, 2006). This would mean that anti-fibrotic medication which targets 5-HT receptors could be hindered by the diverse physiological role of these 5-HT receptors. 5-HT has been shown to exert both a proliferative and anti-proliferative effect on cells (Lesurtel, 2006). Following hepatectomy there was observed a 3- to 4- fold up-regulation of 5-HT$_{2A}$ and 5-HT $_{2B}$ receptors, which suggests a role in liver regeneration (Lesurtel, 2006). Hepatocytes have been reported to express the 5-HT$_{2A}$ receptor, which when

stimulated by 5-HT would promote hepatocyte regeneration (Lesurtel, 2006; Ebrahimkhani et al., 2011). A 5-HT$_{2A}$ antagonist would potentially inhibit regeneration, an undesirable effect in an already injured liver. Conversely 5-HT$_{2A}$ inhibition may be desirable for some of the diverse processes involving 5-HT. Platelets have also been reported to express the 5-HT$_{2A}$ receptor, which when stimulated causes activation and aggregation of the platelets which manifests itself with the release of their stored 5-HT, thus creating a positive feedback loop (Przyklenk et al., 2010; Watts et al., 2012). This would mean that 5-HT$_{2A}$ antagonism might provide the added benefit of preventing 5-HT release from platelets, which is of importance in the development of fibrosis (Ruddell et al., 2006, 2008; Dees et al., 2011; Ebrahimkhani et al., 2011; Mann and Oakley, 2013). 5-HT contributes to the development of portal hypertension by increasing resistance in the intra-hepatic vasculature and in the portal vein itself by signalling through the 5-HT$_{2A}$ receptor (Kaumann and Levy, 2006; Watts et al., 2012). This may therefore identify 5-HT$_{2A}$ targeted therapy to alleviate or protect against the development of portal hypertension. This diversity of effect of 5-HT on the 5-HT$_{2A}$ receptor in the liver may therefore explain why there was no overall anti-fibrotic effect observed with volinanserin in the CCl$_4$ mouse model.

7.11 Summary

The primary aim of these studies was to carry out an 'in-depth' pharmacological characterisation of the 5-HT$_2$ receptor subtype present on activated mouse and human HSCs to fully evaluate and extend the evidence for a role of 5-HT$_2$ antagonists in fibrosis. In the literature this had not been carried out with any quantitative pharmacological rigour with the focus on expression of proteins, which has led to conflicting evidence as to which 5-HT$_2$ receptor was mediating the effect. The data generated in the 5-HT-stimulated calcium release and ERK phosphorylation assay using selective antagonists at selective concentrations have identified conclusively that the 5-HT$_{2A}$ receptor is major receptor responsible for these effects of 5-HT on HSCs. It was not possible to confirm the 5-HT$_{2A}$ receptors involvement in the ERK phosphorylation assay using human HSCs, due to a high basal level of ERK phosphorylation.

Taken together the data generated in this thesis demonstrates that the 5-HT$_{2A}$ is major receptor responsible for mediating the effects of 5-HT on activated HSCs and that a second receptor, 5-HT$_{1B}$ may also play a role. The phenotypic studies have been unable to demonstrate an effect of 5-HT on either proliferation or collagen deposition which suggests that 5-HT does not play a major role in these processes. The synergy studies using the mouse HSCs may indicate that 5-HT plays a role in early fibrosis. The lack of effect of 5-HT on human HSCs to stimulate ERK phosphorylation may indicate that 5-HT does not play a major role in fibrosis in humans. The results from the *in vivo* CCl$_4$ mouse model of liver injury have provided no evidence to imply involvement of 5-HT$_{2A}$ in fibrosis but have found that activation of the 5-HT$_{2B}$ receptor could be profibrotic. This finding is interesting as no functional 5-HT$_{2B}$ receptor was identified on HSCs. The interplay of the 5-HT receptors present on the different cells and vessels in the liver seems to imply that a selective 5-HT receptor anti-fibrotic mechanism is not a viable strategy.

7.12 Future Directions.

There are certainly some future experimental studies which can build on the data generated in this thesis. Radioligand binding studies using selective ligands could be undertaken to identify and confirm the identity of the 5-HT receptors present on HSCs along with the concentrations of receptors present. Confirmation of 5-HT receptor expression on HSCs being undertaken to narrow down the range of binding experiments required. This would aid the identification of the second functional receptor present on HSCs. The radioligand analysis combined with 5-HT receptor expression analysis of the receptors could be undertaken in newly isolated cells and continued as the HSCs activate in culture. In human HSCs the effect of disease status, sex or age on the population of 5-HT receptors could be investigated.

There are some further mechanistic studies which could be undertaken. The insurmountable nature of the antagonism of volinanserin and ketanserin observed in the ERK phosphorylation assay could be investigated further. Similar 'washoff' experiments could be undertaken as were carried out for the calcium release assay. This would be able to confirm whether the hemi-equilibrium phenomenon could account for the insurmountable antagonism observed. Radioligand dissociation

studies could be undertaken to determine if ketanserin and volinanserin do slowly dissociate from the receptor adding further weight to the hemi-equilibrium theory.

The 'phenotypic' fibrotic responses of proliferation and collagen deposition are not the only process that could be studied which the HSCs are involved in. HSCs when activated are also capable of contraction, migration, and releasing TGFβ which are processes that could be further investigated. As activation of the 5-HT$_{2A}$ receptor causes calcium release, which is important for contraction, this maybe something that is a more immediate response and more likely to be influenced by 5-HT. We also have to remember that these cells have been activated through culture on plastic and the stiffness of the plastic can have an influence on how the HSCs respond (Wells, 2008; Olsen et al., 2011; Caliari et al., 2016). Investigation of the response to 5-HT on HSCs cultured on different plastics (exhibiting different degrees of stiffness), or on basement membrane-like matrix Matrigel or stiffening hydrogels may provide further insight into HSC behaviour.

Understanding how 5-HT influences release of TGFβ may help to determine its influence on collagen deposition. Although the data from the *in vivo* studies does cast doubt on 5-HT$_{2A}$ being a viable therapy. There would still be value exploring whether there were any off target effects of the compound in the *in vivo* studies. Understanding the toxicity profile of the compounds used in the *in vivo* studies could greatly enhance the interpretation of the data.

In vivo models of liver fibrosis offer a way to investigate molecules in a multi-cellular environment but it is difficult to replicate the human disease (Constandinou et al., 2005; Starkel and Leclercq, 2011). Human precision-cut liver slices (PCLS) offer a way to investigate the HSCs along with other liver cell types present in a physiological extracellular environment (Olinga and Schuppan, 2013; Trautwein et al., 2015). Human PCLS have been used to investigate HSCs and can be used to test potential anti-fibrotic drugs (Van de Bovenkamp, 2005; Van de Bovenkamp et al., 2006, 2008). PCLS prepared from both normal and diseased liver could be employed to further investigate 5-HT agonists and antagonists on human HSCs. This may therefore provide further insight into the relevance of 5-HT in human liver fibrosis.

CHAPTER 8   REFERENCES

Abergel A, Darcha C, Chevallier M, Ughetto S, Henquell C, Pol S, de Ledinghen V, Canva V, Bronowicki JP, Tran A, Martineau N, Lafeuille H, Dechelotte P, Bommelaer G, Bonny, C, and French Multicentre Study Group (2004) Histological response in patients treated by interferon plus ribvirin for hepatitis C virus reated severe fibrosis. *Eur J Gastroenterol Hepatol* **16**: 1219-1227.

Adams DH and Eksteen B (2006) Aberrant homing of mucosal T cells and extra-intestinal manifestations of inflammatory bowel disease. *Nature Rev Immunol* **6**:246-251.

Adham N, Bard JA, Zqombick JM, Durkin MM, Kucharewicz S, Weinshank RL and Branchek TA (1997). Cloning and characterization of the guinea pig 5-HT1F receptor subtype: a comparison of the pharmacological profile to the human species homolog. *Neuropharmacology* **36**: 569–76.

Akhurst RJ and Hata A (2012) Targeting the TGFβ signalling pathway in disease. *Nat Rev Drug Discov* **11**: 790–811.

Al-Bader A, Mathew TC, Abdul H, Al-Sayer H, Singal PK and Dashti HM (2000) Cholangiocarcinoma and liver fibrosis in relation to changes due to thioactemide. *Mol Cell Biochem* **208**: 1-10.

Alexander SP, Davenport AP, Kelly E, Marrion N, Peters JA, Benson HE, Faccenda E, Pawson AJ, Sharman JL,Southan C and Davies JA (2015) The Concise Guide to PHARMACOLOGY 2015/16: G protein-coupled receptors. *Br J Pharmacol 172*: 5744–5869.

Alkozai EM, Nijsten MW, de Jong KP, de Boer MT, Peeters PM, Slooff MJ, et al. (2010) Immediate postoperative low platelet count is associated with delayed liver function recovery after partial liver resection. *Ann Surg* **251**: 300-6.

Almeida I, Faria R, Vita P and Vasconcelos C. (2011) Systemic sclerosis refractory disease:from the skin to the heart. *Autoimmun Rev* **10**: 693–701.

Arthur MJ (2000). Fibrogenesis II. Metalloproteinases and their Inhibitors in Liver

Fibrosis. *Am J Physiol Gastrointest Lver Physiol* **279**: G245–G249.

Arthur MJP (2002) Reversibility of liver fibrosis and cirrhosis following treatment for hepatitis C. *Gastroenterology* **122**: 1525–1528.

Bachem MG, Melchior R and Gressner AM (1989) The role of thrombocytes in liver fibrogenesis : Effects of platelet lysate and thrombocyte-dervied growth factors on the mitogenic activity and glycosaminoglycan synsthesis of cultured rat liver fat storing cells. *J Clin Chem Biochem* **27**: 555-565.

Bachem MG, Meyer D, Melchior R, Sell KM and Gressner AM (1992). Activation of rat liver perisinusoidal lipocytes by transforming growth factors derived from myofibroblastlike cells. A potential mechanism of self perpetuation in liver fibrogenesis. *J Clin Invest* **89**: 19–27.

Ballardini G, Groff P, Giorgi LB de, Schuppan D and Bianchi FB (1994). Ito cell heterogeneity: Desmin-negative ito cells in normal rat liver. *Hepatology* **19**: 440–446.

Bard JA, Zgombick J, Adham N, Vaysse P, Branchek TA and Weinshank RL. (1993) Cloning of a novel human serotonin receptor (5-HT$_7$) positively linked to adenylate cyclase. *J Biol Chem*, **268**: 23422-23426

Basu S (2003) Carbon tetrachloride-induced lipid peroxidation: eicosanoid formation and their regulation by antioxidant nutrients. Toxicology 189: 113–127

Bataller R and Brenner DA (2005) Liver Fibrosis. *J Clin Invest* 115:209-218.

Bataller R, Gasull X, Ginès P, Hellemans K, Görbig MN, Nicolás JM, Sancho-Bru P, De Las Heras D, Gual A, Geerts A, Arroyo V, Rodés J. (2001). In vitro and in vivo activation of rat hepatic stellate cells results in de novo expression of L-type voltage-operated calcium channels. *Hepatology* **33**: 956-962.

Bataller R, Nicolas J, Gines P, Esteve A, Gorbig NM, Garcia-Ramallo E, Pinzani M, Ros J, Jimenez W, Thomas AP, Arroyo V and Rodes J (1997) Arginine vasopressin

induces contraction and stimulates growth of cultured human hepatic stellate cells. *Gastroenterology* **113**: 615–624.

Bataller R, Nicolas JM, Gine P, Goorbig MN, Garcia-Ramallo E, Lario S, Tobias E, Pinzani M, Thomas AP, Arroyo V and Rodes J (1998) Contraction of human hepatic stellate cells activated in culture: a role for voltage-operated calcium channels. *J Hepatol* **29**: 398–408.

Benyon RC and Arthur MJ (2001) Extracellular matrix degradation and the role of hepatic stellate cells. *Semin Liv Dis* **21**: 373-384.

Benyon RC, Iredale JP, Goddard S, Winwood PJ and Arthur MJ (1996) Expression of tissue inhibitor metalloproteinases1 and 2 is increased in fibrotic human liver. *Gastroenterology* **110**: 821-831.

Berger M, Gray JA and Roth BL (2009) The expanded biology of serotonin. *Annu Rev Med* **60**: 355-366.

Bertaccini G (1960) Tissue 5-hydroxytryptamine and urinary 5-hydroxyindolacetic acid after partial or total removal of the gastro-intestinal tract in the rat. *J Physiol* **153**: 239-249

Black JW, Duncan WA, Durant CJ, Ganellin CR and Parsons EM (1972). Definition and antagonism of histamine H_2-receptors. *Nature* **236**: 385–390.

Black JW, Duncan WA and Shanks RG (1965). Comparison of some properties of pronethalol and propranolol. *Br J Pharmacol* **25**: 577–591.

Bilzer M, Roggel F and Gerbes AL (2006) Role of Kupffer cells in host defence and liver disease. *Liver Int* **26**: 1175-1186.

Blouin A, Bolender RP and Weibel ER (1977) Distribution of organelles and membranes between hepatocytes and non-hepatocytes in the rat liver parenchyma. A Stereological study. *J Cell Biol* **72**: 441-455

Bonacchi A, Romagnani P, Romanelli RG, Efsen E, Annunziato F, Lasagni L, Francalanci M, Serio M, Laffi G, Pinzani M, Gentilini P and Mara F (2001) Signal transduction by the chemokine receptor CXCR3: activation of Ras/ERK, Src and phosphatidylinositol 3-kinase/Akt controls cell migration and proliferation in human vascular pericytes. *J Biol Chem* **276**: 9945-9954.

Bonhaus DW, Flippin LA, Greenhouse RJ, Jaime S, Rocha C, Dawson M, Van Natta K, Chang LK, Pulido-Rios T, Webber A, Leung E, Eglen RM and Martin GR. (1999) RS-127445: a selective, high affinity, orally bioavailable 5-HT$_{2B}$ receptor antagonist. *Br J Pharmacol* **127**: 1075-1082.

Borkham-Kamphorst E, Herrman J, Stroll D, Treptau J, Gressner A M and Weiskirchen R (2004) Dominan- negative soluble PDGF-b receptor inhibits hepatic stellate cell activation and attenuates liver fibrosis. *Lab Invest* **84**: 766-777.

Boyer J (2013) Bile Formation and Secretion. In Comprehensive Physiology, (Hoboken, NJ, USA: John Wiley & Sons, Inc.), pp 1035–1078.

Bradley PB, Engel G, Feniuk W, Fozard JR, Humphrey PP, Middlemiss DN, Saxena, P Mylecharane EJ and Richardson B P (1986) Proposals for the classification and nomenclature of functional receptors for 5-hydroxytryptamine. *Neuropharmacology* **25**: 563–76.

Braet F, and Wisse E (2002) Structural and functional aspects of liver sinusoidal endothelial cell fenestrae: a review. *Comp Hepatol* **1**: 1.

Brauneis U, Gatmaitan Z and Arias IM (1992). Serotonin stimulates a Ca2+ permeant nonspecific cation channel in hepatic endothelial cells. *Biochem Biophys Res Commun* **186**: 1560–6.

Breitkopf K, Haas S, Wiercinska E, Singer MV and Dooley S (2005) Anti-TGF-beta strategies for the treatment of chronic liver disease. *Alcohol Clin Exp Res* **29**:121S-131S.

Brunton G, Cooper I, Hirst D, Orlek BS, Stemp G, Ward, JG and Woodhouse KS (2009) 1-Piperidinyl-6-Piperidinylsulfonylindoles as 5-HT (2B) receptor antagonists. WO 2009/016225 A1

Bryant HU, Nelson DL, Button D, Cole HW, Baez MB, Lucaites VL, Wainscott DB, Whitesitt C, Reel J, Simon R and Koppel GA (1996) A novel class of 5-HT$_{2A}$ receptor antagonists: aryl aminoguanidines. *Life Sci*, **59**: 1259-1268

Buniatian G, Hamprecht B and Gebhardt R (1996). Glial fibrillary acidic protein as a marker of perisinusoidal stellate cells that can distinguish between the normal and myofibroblast-like phenotypes. *Biol Cell* **87**: 65–73.

Caliari SR, Perepelyuk M, Cosgrove BD, Tsai SJ, Lee GY, Mauck RL, Wells RG and Burdick JA (2016) Stiffening hydrogels for investigating the dynamics of hepatic stellate cell mechanotransduction during myofibroblast activation. *Sci Rep* **6**: 21387.

Canbay A, Feldstein AE, Higuchi H, Werneburg N, Grambihler A, Bronk SF and Gores GJ (2003) Kupffer Cell Engulfment of Apoptotic Bodies Stimulates Death Ligand and Cytokine Expression. *Hepatology* **38**: 1188–1198.

Canbay A, Freidman SL and Gores G (2004) Apoptosis: the nexus of liver injury and fibrosis. *Hepatology* **39**: 273-278.

Cao Q, Mak KM and Lieber CS (2006) Leptin enhances alpha1(I) collagen gene expression in LX-2 human hepatic stellate cells through JAK-mediated H2O2-dependent MAPK pathways. *J Cell Biochem* **97**:188–197.

Caraci F, Gili E, Calafiore M, Failla M, Rosa C La, Crimi N, Sortino MA, Nicoletti F, Copani A, Vancheri, C (2008) TGF-B1 targets the GSK-3B/B-catenin pathway via ERK activation in the transition of human lung fibroblasts into myofibroblasts. *Pharmacol Res* **57**: 274–282.

Cassiman D, Denef C, Desmet VJ and Roskams T (2001). Human and rat hepatic stellate cells express neurotrophins and neurotrophin receptors. *Hepatology* **33**: 148–158.

Cassiman D, Van Pelt J, Vos R De, Lommel F Van, Desmet, V, Yap S-H and Roskams T(1992) Synaptophysisn: A novel marker for human and rat hepatic stellate cell. *Am J Pathol* **31**: 273–276.

Charlton SJ and Vauquelin G (2010) Elusive equilibrium: The challenge of interpreting receptor pharmacology using calcium assays. *Br J Pharmacol* **161**: 1250–1265.

Chen C, Han X, Fan F, Liu Y, Wang T, Wang J, Hu P, Ma A and Tian H (2014) Serotonin drives the activation of pulmonary artery adventitial fibroblast and TGF-β1/Smad3-mediated fibrotic responses through 5-HT$_{2A}$ receptors. *Mol Cell Biochem* **397**: 267-276.

Chen CZ, Peng YX, Wang ZB, Fish PV, Kaar JL, Koepsel RR, Russell AJ, Lareu RR and Raghunath M (2009) The Scar-in-a-Jar: studying potential antifibrotic compounds from the epigenetic to extracellular level in a single well. *Br J Pharmacol* **158**: 1196–1209.

Chen JX, Pan H, Rothman TP, Wade PR and Gershon MD (1998) Guniea pig 5-HT transporter: cloning, expression, distribution, and function in intestinal sensory reception. *Am J Physiol* **275**: G433-G448.

Chen W, Gendrault J-L, Steffan A-M, Jeandidier E and Kirn A (1989) Isolation, culture and main characteristics of mouse fat-storing cells: Interaction with viruses. *Hepatology* **9**: 352–362.

Cheng Y and Prusoff WH (1973) Relationship between the inhibition constant (K_I) and the concentration of inhibitor which causes 50 per cent inhibition (I_{50}) of an enzymatic reaction. *Biochem Pharmacol* **22**: 3099-3108.

Clark JM (2006) The epidemiology of nonalcoholic fatty liver diseae in adults. *J Clin Gastroenterol* **40**:S5- S10.

Clavien PA, Petrowsky H, DeOliveira ML and Graf R (2007) Strategies for safer liver surgery and partial liver transplantation. *N Engl J Med* **356** : 1545-1559.

Cohen-Naftaly M and Friedman SL (2011) Current staus of novel antifibrotic therapies in patients with chronic liver disease. *Ther Advn Gastroenterol* **4**:391-417.

Colmenero J, Bataller R, Snacho-Bru P, Domingez M, Menaro M, Forns X, Bruguera M, Arroyo V, Brenner DA and Gines P (2009). Effects of Losartan on hepatic expression of non-phagocytic ADPH oxidase and fibrogenic genes in patients with hepatitis. *Am J Physiol Gastroinvest Liver Physiol* **297**:G726-G734.

Constandinou C, Henderson N and Iredale JP(2005) Modelling liver fibrosis in rodents. In Fibrosis Research. Methods and Protocols. Humana Press. Edited Varga J, Brenner, DA, Phan SH. pp 237–250.

Cools R, Roberts AC, Robbins TW (2008) Serotoninergic regulation of emotional and behavioural control processes. *Trends Cogn Sci* :**12**:31–40.

Costa M, Furness JB, Cuello AC, Verhofstad AAJ, Steinbusch HWJ and Elde RP (1982) Neurons with 5-hydroxytryptamine-like immunoreactivity in the enteric nervous system: Their visualization and reactions to drug treatment. *Neuroscience* **7**: 351–363.

Crespo Yanguas S, Cogliati B, Willebrords J, Maes M, Colle I, Bossche B van den, Souza de Oliveira CPM, Andraus W, Alves VA, Leclercq I and Vinken M (2015) Experimental models of liver fibrosis. *Arch Toxicol* **90**: 1025–1048.

Cummings JL, Cilento EV and Reilly FD. (1993) Hepatic microvascular regulatory mechanisms. XII. Effects of 5-HT2-receptor blockade on serotonin-induced intralobular hypoperfusion. *Int J Microcirc Clin Exp* **13**: 99–112.

Da Prada M, Pletscher A, Tranzer JP and Knuchel H (1967) Subcellular Localization of 5-Hydroxytryptamine and Histamine in Blood Platelets. *Nature* **216**: 1315–1317.

Dees C, Akhmetshina A, Zerr P, Reich N, Palumbo K, Horn A, Jüngel A , Beyer C, Krönke G, Zwerina J, Reite R , Alenina N, Maroteaux L, Gay S , Schett G, Distler O and Distler JHW (2011) Platelet-derived serotonin links vascular disease and tissue fibrosis. *J Exp Med* **208**: 961-972.

Dehmlow C, Erhard J and Groot Hde (1996) Inhibition of Kupffer cell functions as an explanation for the hepatoprotective properties of silibinin. *Hepatology* **23**: 749–54.

De Leeuw AM, Mccarthy SP, Geerts A and Knook DL (1984) Purified Rat Liver Fat-Storing Cells in Culture Divide and Contain Collagen. *Hepatology* **4**: 392–403.

Demoulin J C, Bertholet M, Soumagne D, David JL and Kulbertus HE (1981) 5-HT$_2$-receptor blockade in the treatment of heart failure. A preliminary study. *Lancet* **1**: 1186–1188.

Dooley S, Delvoux B, Lahme B, Mangasser-Stephan K and Gressner AM (2000) Modulation of transforming growth factor beta response and signalling during transdifferentiation of rat hepatic stellate cells to myofibroblasts. *Hepatology* **31**, 1094-1106.

Dooley S and Dijke PT (2012) TGF-β in progression of liver disease. *Cell Tissue Res* **347**: 245–256.

Dooley S, Hamzavi J, Breitkopf K, Wiercinska E, Said HM, Lorenzen J, ten Dijke P and Gressner AM (2003) Smad7 prevents activation of hepatic stellate cells and liver fibrosis in rats. *Gastroenterology* **125**:178–91.

Dooley S, Streckert M, Delvoux B and Gressner AM (2001) Expression of Smads during in vitro transdifferentiation of hepatic stellate cells to myofibroblasts. *Biochem Biophys Res Commun* **283**: 554–62.

Dranoff JA, Ogawa M, Kruglov EA, Gaça MD, Sévigny J, Robson SC and Wells RG (2004) Expression of P2Y nucleotide receptors and ectonucleotidases in quiescent and activated rat hepatic stellate cells. *Am J Physiol Gastrointest Liver Physiol* **287**:G417-G424.

Dreyfus CF and Bornstein MB (1977) Synthesis of serotonin by neurones of the myenteric plexus in situ and in organotypic tissue culture. *Brain Res* **128**: 125-139.

Dufour JF, DeLellis R and Kaplan MM (1997) Reversibility of hepatic fibrosis in autoimmune hepatitis. *Ann Intern Med* **127**: 981-985.

Dumitrascu R, Kulcke C, Konigshoff M, Kouri F, Yang X, Morrell N, Ghofrani HA, Weissmann N, Reiter R, Seeger W, Grimminger F, Eickelberg O, Schermuly RT and Pullamsetti SS (2011) Terguride ameliorates monocrotaline-induced pulmonary hypertension in rats. *Eur Respir J* **37**:1104–1118.

Ebrahimkhani MR, Oakley F, Murphy LB, Mann J, Moles A, Perugorria MJ, Ellis E, Lakey AF, Burt AD, Douglass A, Wright MC, White SA, Jaffre F, Maroteaux L and Mann DA (2011) Stimulating healthy tissue regeneration by targeting the 5-HT$_{2B}$ receptor in chronic liver disease. *Nat Med* **17**: 1668–1673.

Ellis EL and Mann DA (2012) Clinical evidence for the regression of liver fibrosis. *J Hepatol* **56**: 1171–1180.

Elsharkawy AM, Wright MC, Hay RT, Arthur MJP, Hughes T, Bahr MJ, Degitz K and Mann DA (1999). Persistent activation of nuclear factorkappa B in cultured rat hepatic stellate cells involves the induction of potentially novel Rel-like factors and prolonged changes in the expression of IκB family proteins. *Hepatology* **30**:761–769.

Eto Y, Nitta K, Uchida K, Tsutsui T, Natori K, Kawahima A and Yumura W, Nihei H (1997) Anti-mitogenic effects of sarpogrelate in cultured rat mesangial cells. *Life Sci* **60**: PL193–199

Fabre A, Marchal-Somme J, Marchand-Adam S, Quesnel C, Borie R, Dehoux M, Ruffie C, Callebert J, Launay J M, Henin D, Soler P and Crestani B (2008) Modulation of bleomycin-induced lung fibrosis by serotonin receptor antagonists in mice. *Eur Respir J* **32**: 426–436.

Faghihzadeh F, Adibi P, Rafiei R, Hekmatdoost A (2014) Resveratrol, supplementation improves inflammatory biomarkers in patients with nonalcoholic fatty liver disease. *Nutr Res* **34**:837–843.

Fantegrossi WE, Gray BW, Bailey JM, Smith DA, Hansen M and Kristensen JL (2015) Hallucinogen-like effects of 2-([2-(4-cyano-2,5-dimethoxyphenyl)

ethylamino]methyl)phenol (25CN-NBOH), a novel N-benzylphenethylamine with 100-fold selectivity for 5-HT receptors, in mice. *Psychopharmacology* **232**: 1039-1047.

Fickert P, Zollner G, Fuchsbichler A, Stumptner C, Weiglein AH, Lammert F, Marschall HU, Tsybrovskyy O, Zatloukal K, Denk H and Trauner M (2002) Ursodeoxycholic acid aggravates bile infarcts in bile duct-ligated and Mdr2 knockout mice via disruption of cholangioles. *Gastroenterology* **123**:1238–1251

Figueroa KW, Martin GR and Pulido-Rios MT (2009) 5-Hydoxytryptamine Receptor assays. In Current Protocols in Pharmacology, (Hoboken, NJ, USA: John Wiley & Sons, Inc.).

Fitzhugh OG and Nelson AA (1948) Liver tumours in rats fed thiourea or thioacetamide. *Science* **108**: 626-628.

Forbes SJ and Parola M (2011) Liver fibrogenic cells *Best Pract Res Clin. Gastroenterol* **25**: 207–217.

Frenken M and Kaumann AJ (1984) Interaction of ketanserin and its metabolite ketanserinol with $5HT_2$ receptors in pulmonary and coronary arteries of calf. *Naunyn Schmiedebergs Arch Pharmacol* **326**: 334–9.

Friedman SL (1993) The cellular basis of hepatic fibrosis. *N Engl J Med* **328**: 1828–1835.

Friedman SL (2000) Molecular regulation of hepatic fibrosis, an integrated cellular response to tissue injury. *J Biol Chem* **275**: 2247-2250.

Friedman SL (2004) Mechanisms of Disease: Mechanisms of hepatic fibrosis and therapeutic implications. *Nat Clin Pract Gastroenterol Hepatology* **43**: S82-S88.

Friedman SL (2008a) Hepatic fibrosis – Overview. *Toxicology* **254**: 120-129.

Friedmann SL. (2008b) Hepatic stellate cells: Protean, multifunctional, and enigmatic cells of the liver. *Physiol Rev* **88**: 125-172

Friedman SL, Rockey DC, McGuire RF, Maher J, Boyles JK and Yamasaki G., (1992) Isolated hepatic lipocytes and kupffer cells from normal human liver: morphological and functional characteristics in primary culture. *Hepatology* **15**: 234-243.

Friedman SL and Roll FJ (1987) Isolation and culture of hepatic lipocytes, Kupffer cells, sinusoidal endothelial cells by density gradient centrifugation with Stractan. *Anal Biochem* **161**: 207–218,.

Friedman SL, Sheppard D, Duffield JS and Violette S (2013) Therapy for fibrotic disease: Nearing the starting line. *Sci. Trans. Med* **5**:167sr1-17.

Furrer A, Rickenbacher Y, Tian W, Jochum W, Bitterman AG, Kach A, Humar R, Graf W, Moritz PA and Clavian PA (2011) Serotonin reverts age-related capillarization and failiure of regeneration in the liver through a VEGEF-dependent pathway. *Proc Nat Acad Sci* **108**: 2945-2950

Furukawa F, Matsuzaki K, Mori S, Tahashi Y, Yoshida K, Sugano Y, Yamagata H, Matsushita M, Seki T, Inagaki Y, Nishizawa M,Fujisawa J and Inoue K (2003) p38 MAPK mediates fibrogenic signal through Smad3 phosphorylation in rat myofibroblasts. *Hepatology* **38**:879–889.

Furuya CK, Oliveira CP de, Mello ES de, Faintuch J, Raskovski A, Matsuda M Vezozzo DC, Halpern A, Garrido AB, Alves VA and Carrilho FJ (2007) Effects of bariatric surgery on nonalcoholic fatty liver disease: Preliminary findings after 2 years. *J Gastroenterol Hepatol* **22** : 510-514.

Gaddum JH and Picarelli ZP (1957) Two kinds of tryptamine receptor. *Br J Pharmacol Chmeother* **12**: 323-8.

Gatmaitan Z, Varticovski L, Ling L, Mikkelsen R, Steffan AM and Arias IM (1996) Studies on fenestral contraction in rat liver endothelial cells in culture. *Am J Pathol* **148**:2027–2041.

Geerts A (2001) History, heterogeneity, developmental biology and functions of quiescent hepatic stellate cells. *Semin Liv Dis* **3**: 311-335.

Geerts A, Niki T, Hellemans K, De Craemer D, Van Den Berg K, Lazou JM, Geert S, Van De Winkel M and De Blesser P (1998) Purification of rat hepatic stellate cells by side scatter-activated cell sorting. *Hepatology* **27**: 590–598.

Geerts AM, Vanheule E, Praet M, Van Vlierberghe H, De Vos M and Colle I (2008) Comparison of three research models of portal hypertension in mice: macroscopic, histological and portal pressure evaluation. *Int J Exp Pathol* **89**:251–63.

Gentilini A, Marra F, Gentilini P and Pinzani M (2000) Phosphatidylinositol-3 kinase and extracellular signal-regulated kinase mediate the chemotactic and mitogenic effects of insulin-like growth factor-I in human hepatic stellate cells. *J Hepatol* **32**: 227–234.

George J, Roulot D, Koteliansky VE and Bissell DM (1999) In vivo inhibition of rat stellate cell activation by soluble transforming growth factor beta type II receptor: A potential new therapy for hepatic fibrosis. *Proc Nat Acad Sci* **96**: 12719–12724.

Georgiev P, Jochum W, Heinrich S, Jang JH, Nocito A, Dahm F and Clavien PA (2008) Characterization of time-related changes after experimental bile duct ligation. *Br J Surg* **95**:646–656.

Gershon MD and Tamir H (1981) Release of endogenous 5-hydroxytryptamine from resting and stimulated enteric neurons. *Neuroscience* **6**, 2277-2286.

Giles H, Lansdell SJ, Bolofo M-L, Wilson HL and. Martinet GR (1996) Characterisation of a 5-HT$_{1B}$ receptor on CHO cells: functional responses in the absence of radioligand binding. *Br J Pharmacol* **117** 1119-26.

Goto K, Kasuya Y, Matsuki N, Takuwa Y, Kurihara H, Ishikawa T, Kimura S, Yanagisawa M and Masaki T (1989) Endothelin activates the dihydropyridine-sensitive, voltage-dependent Ca2+ channel in vascular smooth muscle. *Proc Natl Acad Sci* **86**: 3915-3918.

Graham JR (1967) Cardiac and pulmonary fibrosis during methysergide therapy for headache. Trans *A Clin Climatol Assoc* **78**: 79–92.

Graves LM, Bornfelt KE, Raines EW, Potts BC, Macdonald SG, Ross R and Krebs EG (1993) Protein kinase A antagonizes platelet-derived growth factor-induced signaling by mitogen-activated protein kinase in human arterial smooth muscle cells. *Proc Natl Acad Sci* **90**: 10300-10304.

Gressner OA, Lahme B, Demirci I, Gressner AM and Weiskirchen R (2007) Differential effects of TGF-β on connective tissue growth factor (CTGF/CCN2) expression in hepatic stellate cells and hepatocytes. *J Hepatol* **47**: 699–710.

Grewal JS, Mukhin YV, Garnovskaya MN, Raymond JR and Greene EL (1999) Serotonin 5-HT2A receptor induces TGF-b1 expression in mesangial cells via ERK: proliferative and fibrotic signals. *Am J Physiol* **276**: F922–F930

Gurtner GC, Werner S, Barrandon Y and Lonaker MT (2008) Wound repair and regeneration. *Nature* **453**: 314-321.

Hadziyannis SJ, Tassopoulos NC, Heathcote EJ, Chang T, Kitis, Rizzetto m, marcellin P, Lim SG, Goodman Z, Wulfshn, Xiong S, Fry J and Brosgart CL (2003) Adefovir dipivoxil for the treatment of hepatitis Be antigen –negative chronic hepatitis B. *New Eng J Med* **348***: 800-7.

Hahn A, Heusinger-Ribeiro J, Lanz T, Zenkel S and Goppelt-Struebe M (2000) Induction of connective tissue growth factor by activation of hepata-helical receptors: modulation by Rho proteins and actin cytoskeleton. *J Biol Chem* **275**: 37429-37435.

Hall DA, Beresford IJ, Browning C and Giles H (1999) Signalling by CXC-chemokine receptors 1 and 2 expressed in CHO cells: a comparison of calcium mobilization, inhibition of adenylyl cyclase and stimulation of GTPγS binding induced by IL-8 and GROα. *Br J Pharmacol* **126**: 810 - 818.

Hamblin MW and Metcalf MA (1991) Primary structure and functional characterization of a human 5-HT1D-type serotonin receptor. *Mol Pharmacol* **40**: 143-148.

Hamlin KE and Fischer FE (1951) The synthesis of 5-Hydoxytrptamine. *J Am Chem Soc* **73**: 5007-5008.

Hammel P, Couvelard A, O'Toole D, Ratouis A, Sauvanet A, Flejou JF, Degott C, Belghiti J, Bernades P, Valla D, Ruszniewski and Levy P (2001) Regression of liver fibrosis after biliary drainage in patients with chronic pancreatitis and stenosis of the common bile duct. *N Eng J Med* **344**: 418-423.

Hannon J and Hoyer D (2008) Molecular biology of 5-HT receptors. *Behav Brain Res* **195**: 198–213.

Hansen M, Phonekeo K, Paine JS, Leth-Petersen S, Begtrup M, Bräuner-Osborne H and Kristensen JL (2014) Synthesis and structure-activity relationships of N-benzyl phenethylamines as 5-HT agonists. *ACS Chem Neurosci* **5:** 243-249

Hasegaea D, Wallace MC and Friedman SL (2015) Stellate cells and Hepatic fibrosis. In Stellate cells in health and Disease : Gandhi C and Pinzani M editors. Elsevier Inc, pp 41–61.

Hayashi1 H and Sakai1 T (2011) Animal models for the study of liver fibrosis: new insights from knockout mouse models. *Am J Physiol Gastrointest Liver Physiol* **300**: G729–G738.

Heldin C and Westermark B (1999) Mechanism of action and *in vivo* role of platelet-derived growth factor. *Phyiol Rev* **79**: 1284- 1316.

Hendrikx M, Van Dorpe J, Flameng W and Daenen W (1996) Aortic and mitral valve disease induced by ergotamine therapy for migraine: a case report and review of the literature. *J Heart Valve Dis* **5**: 235-237.

Herrmann J, Gressner AM and Weiskirchen R. (2007) Immortal hepatic stellate cell lines: Useful tools to study hepatic stellate cell biology and function? *J Cell Mol Med* **11**: 704–722.

Higuchi H and Gores GJ (2003) Mechanisms of liver injury: an overview. *Curr Mol Med* **3**:483-490.

Hill AV (1909) The mode of action of nicotine and curare, determined by the form of the contraction curve and the method of temperature coefficients. *J Physiol* **39**: 361-373.

Hill S J (2006). G-protein-coupled receptors: past, present and future. Br J Pharmacol **147**: S27-S37.

Hoyer D and Martin G (1997) 5-HT receptor classification and nomenclature: towards a harmonization with the human genome. *Neuropharmacology* **36**: 419–28.

Humphrey PPA, Hartig P, Hoyer D (1993) A proposed new nomenclature for 5-HT receptors. *Trends Pharmacol Sci* **14**: 233–6.

Ikeda K, Wakahara T, Wang YQ, Kadoya H, Kawada N, and Kaneda K.(1999) In vitro migratory potential of rat quiescent hepatic stellate cells and it augmentation by cell activation. *Hepatology* **29**: 1760-1767.

Inagki Y and Okazki I (2007) Emerging insights into transforming growth factor beta Smad signal in hepatic fibrogenesis. *Gut* **56**: 284-292.

Iredale JP (2001) Hepatic stellate cells behaviour during resolution of liver injury. *Semin Liv Dis* **21**: 427-436.

Iredale JP, Benyon RC, Pickering J, McCullen M, Northrop, M, Pawley S, Hovell C and Arthur MJ (1998) HSC apoptosis and reducedhepatic expression of metalloproteinase inhibitors. *J Clin Invest* **102:** 538–549.

Iredale JP, Thompson A and Henderson NC (2012). Extracellular matrix degradtion in liver fibrosis: Biochemistry and regulation. *Biochimica et Biophysica Acta.*1832:876-83.

Iwaisako K, Jiang C, Zhang M, Cong M, Moore-Morris TJ, Park TJ, Liu X, Xu J, Wang P, Paik Y-H, Meng F, Asagiri M, Murray LA, Hofmann AF, Iida T, Glass CK, Brenner DA and Kisseleva T (2014) Origin of myofibroblastsin the fibrotic liver in mice. *Proc Natl Acad Sci* **111**: E3297–3305.

Jarnagin WR, Rockey DC, Koteliansky VE, Wang SS and Bissell DM (1994) Expression of variant fibronectins in wound healing : cellular source and biological activity of the EIIIA segment in rat hepatic fibrogenesis. *J Cell Biol* **127**: 2037-2048.

Jiao J, Friedman SL and Aloman C (2009) Hepatic fibrosis. *Current Opin Gastroenterol* **25**: 223-229.

Jones SM and Kazlauskas A. (2001) Growth-factor-dependent mitogenesis requires two distinct phases of signalling. *Nat Cell Bio*. **3**: 165–172.

Jones SM, Klinghoffer R, Prestwich GD, Toker A and Kazlauskas A (1999) PDGF induces an early and a late wave of PI 3-kinase activity, and only the late wave is required for progression through G1. *Curr Biol* **9**: 512–521.

Kasho M, Sakai M, Sasahara T, Anami Y, Matsumura T, Takemura T, Matsuda H, Kobori S and Shichiri M (1998) Serotonin enhances the production of type IV collagen by human mesangial cells. *Kindney Int* **54**: 1083-1092.

Kaumann AJ and Levy FO (2006) 5-hydroxytryptamine receptors in the human cardiovascular system. *Pharmacol Ther* **111**: 674-706.

Kawada N, Uoya M, Seki S, Kuroki T and Kobayashi K (1997) Regulation by cAMP of STAT1 activation in hepatic stellate cells. *Biochem Biophys Res Comm* **233**: 464-469.

Kenakin T. (1997) The pharmacologic analysis of drug receptor interaction. Third edition. Lippincott-Raven, New York.

Kenakin T, Jenkinson S and Watson C (2006) Determining the potency and molecular mechanism of action of insurmountable antagonists. *J Pharm Exp Ther* 319 ;710-723.

Kenakin TP (2006) A Pharmacology Primer. Theory , Applications and Methods. Second Edition. Academic Press.

Kent G, Gay S, Inouye T, Bahu R, Minik OT and Popper H. (1984) Vitamin A containing lipocytes and formation of type III collagen in liver injury. *Proc Natl Acad Sci* **73**: 3719-3722.

Kim DC, Jun DW, Kwon YI, Lee KN,Lee HL, Lee OY, Yoon BC, Choi HS and Kim EK (2013) 5-HT$_{2A}$ receptor antagonists inhibit hepatic stellate cell activation and facilitate apoptosis. *Liver international* **33**: 535-43.

Kim J, Yi NJ, Shin WY, Kim T, Lee KU and Suh KS (2010) Platelet transfusion can be related to liver regeneration after living donor liver transplantation. *World J Surg* **34**: 1052-1058.

Kim SG, Kim YM, Choi JY, Han J-Y, Jang JW, Cho S-H, UM SH, Chon CY, Lee DH, Jang J-J, YU E and Lee YS (2011) Oltipraz therapy in patients with liver fibrosis or cirrhosis: a randomized, double-blind, placebo-controlled phase II trial. *J Pharm Pharmacol*. **63**: 627–635.

Kisseleva T and Brenner DA (2007) Role of hepatic stellate cells in fibrogenesis and reversal of fibrosis. *J Gastroenterol Hepatol* **22**: s73-s78.

Kisseleva T , Cong M, Paik Y, Scholten D, Jiang C, Benner C, Iwasaissko K, Mooer-Morris T, Scott B, Tsukamoto H, Evans, SM, Dillmann W, Glass CK and Brenner DA (2012) Myofibroblasts revert to an inactive phenotype during, regression of liver fibrosis. *Proc Natl Acad Sci* **109**: 9448–9453.

Knight AR, Misra A, Quirk K, Benwell K, Revell D, Kennet G and Bickerdike M (2004) Pharmacological characterisation of the agonist radioligand binding site of 5-HT$_{2A}$, 5-HT$_{2B}$ and 5-HT$_{2C}$ receptors. *Naunyn Schmiedebergs Arch Pharmacol* **370**: 114-123.

Knittel T, Kobold, D, Saile B, Grundmann A, Neubauer K, Piscaglia F and Ramadori G (1999) Rat Liver Myofibroblasts and Hepatic Stellate Cells : Different cell populations of the fibroblast lineage with fibrogenic potential. *Gastroenterology* **117**: 1205–1221.

Knook DL, Seffelaar AM, and De Leeuw AM (1982) Fat-storing cells of the rat liver. Their isolation and purification. *Exp Cell Res* **139**: 468–471.

Konigshoff M, Dumitrascu R, Udalov S, Amarie OV, Reiter R, Grimminger F, Seeger W, Schermuly RT and Eickelberg O (2010) Increased expression of 5-hydroxytryptamine 2A/B receptors in idiopathic pulmonary fibrosis: a rationale for therapeutic intervention. *Thorax* **65**: 949–955.

Koyama Y and Brenner DA (2015) New therapies for hepatic fibrosis. *Clin Res Hepatol Gastroenterol* **39**: S75–S79.

Kristiansen H, Elfving B, Plenge P, Pinborg LH, Gillings NM and Knudsen G (2005) Binding characteristics of the 5-HT$_{2A}$ receptor antagonists altanserin and MDL 100907. *Synapse* **58**: 249–57.

Kubiczkova L, Sedlarikova L, Hajek R and Sevcikova S (2012) TGFβ – an excellent servant but bad master. *J Transl Med* **10**: 183-207

Kumar P, Satyam A, Fan X, Collin E, Rochev Y, Rodriguez BJ, Gorelov A, Dillon S, Joshi L, Raghunath M, Pandit A & Zeugolis DI (2015) Macromolecularly crowded in vitro microenvironments accelerate the production of extracellular matrix-rich supramolecular assemblies. *Scientific reports* **5:** 8729.

Kunisch E, (2004) Macrophage specificity of three anti-CD68 monoclonal antibodies (KP1, EBM11, and PGM1) widely used for immunohistochemistry and flow cytometry. *Ann Rheum Dis* **63**: 774–784.

Lai C, Chien RN, Leung NWY, Chang TT, Guan R, Tai D, Ng K, W P, Dent JC, Barber J, Stephenson SL and Gray FA (1998) One-year trial of Lamivudine for chronic hepatitis C. *New End J Med* **339**: 61-8

Laleman W, Vander Elst I, Zeegers M, Servaes L, Libbrecht L, Roskams T, Fevery J and Nevens F et al., 2006) A stable model of cirrhotic portal hypertension in rat: thioacetamide revisited. *Eur J Clin Invest* **36**: 242-249.

Lang A, Schoonhovan R, Tuvia S, Brenner DA and Rippe RA (2000) Nuclear factor kappaB in proliferation, activation and apoptosis in rat hepatic stellate cells. *J Hepatol* **33**:49–58.

Lareu RR, Arsianti I, Subramhanya HK, Yanxian P and Raghunath M (2007) *In vitro* enhancement of collagen matrix formation and crosslinking for applications in tissue engineering: a preliminary study. *Tissue Eng* **13**: 385–391.

Launay JM, Hervé P, Peoc'h K, Tournois C, Callebert J, Nebigil CG, Etienne N, Drouet L , Humbert M, Simonneau G and Maroteaux L (2002) Function of the serotonin 5-hydroxytryptamine $_{2B}$ receptor in pulmonary hypertension. *Nat Med* **8**: 1129–1135.

Lazo M and Clark JM (2008) The epidemiology of nonalcoholic fatty liver disease: A global pespective. *Semin Liver Dis* **28**:339-350.

Lebrec D, Thabut D, Oberti F, Perarnau JM, Condat B, Barraud H, Saliba F, Carbonell N, Renard P, Ramond M, Moreau R and Poynard T (2010) Pentoxifylline does not decrease short-term mortality but does reduce complications in patients with advanced cirrhosis. *Gastroenterology* **138**: 1755-1762.

Lee JS, Jun DW, Nam HH, Jeon HJ, Kwon HJ, Cho W-K. Kim TY and Sohn JH (2012) 5-HT2A receptor antagonist inhibits hepatic stellate cell activation and facilitates apoptosis via TGF-β and smad 2/3 pathways. *Hepatology* **56**: 811A.

Lee UE and Friedman SL (2011).Mechanisms of hepatic fibrogenesis. *Best Pract Res Clin Gastroenterol* **25**: 195–206.

Leff P (1987) An analysis of amplifying and potentiating interactions between agonists. *J Pharmacol Exp Ther* **243**: 1035–1042.

Leff P and Dougall I G (1993) Further concerns over the Cheng-Prusoff analysis . *Trends in Pharmacol* **14**: 110- 112.

Leff P and Martin GR (1986) Peripheral 5-HT2-like receptors Can they be classified with the available antagonists? *Br J Pharmacol* **88**: 585–593.

Lesage AS, Wouters R, Van Gompel P, Heylen L, Vanhoenacker P, Haegeman G, Luyten WH and Leysen JE. (1998) Agonistic properties of alniditan, sumatriptan and dihydroergotamine on human 5-HT$_{1B}$ and 5-HT$_{1D}$ receptors expressed in various mammalian cell lines. *Br J Pharmacol* **123**: 1655-1665.

Lesurtel M (2006) Platelet-Derived Serotonin Mediates Liver Regeneration. Science 312: 104–107.

Lesurtel M and Clavien PA (2012) Serotonin: A key molecule in acute and chronic liver injury! *Clin Res Hepatol Gastroenterol* **36**: 319–322.

Lesurtel M, Soll C, Graf R and Clavien PA (2008) Role of serotonin in the hepato-gastrointestinal tract: an old molecule for new perspectives. *Cell Mol Life Sci* **65**: 940-952.

Lesurtel M, Soll C, Humar B and Clavien PA (2012) Serotonin: A double-edged sword for the liver? *Surgeon* **10**: 107–113.

Leysen JE, Gommeren W, Heylen L, Luyten WH, Van de Weyer I, Vanhoenacker P, Haegeman G, Schotte A, Van Gompel P, Wouters R and Lesage AS (1996) Alniditan, a new 5-hydroxytryptamine1D agonist and migraine-abortive agent: ligand-binding properties of human 5-hydroxytryptamine1D alpha, human 5-hydroxytryptamine1D beta, and calf 5-hydroxytryptamine1D receptors investigated with [3H]5-hydroxytryptamine and [3H]alniditan. *Mol Pharmacol* **50**: 1567-1580.

Li T, Weng SG, Leng XS, Peng JR, Wei YH, Mou DC, Wang WX (2006) Effects of 5-hydroxytamine and its antagonists on hepatic stellate cells. *Hepatobiliary Pancreat Dis Int* **5**: 96-100.

Liu C, Gaça MDA, Swenson ES, Vllucci VF, Reiss M and Wells RG (2003) Smads 2 and 3 are differentially activated by transforming growth factor-β (TGF-β) in quiescent and activated hepatic stellate cells. *J Biol Chem* **278**: 11721-11728.

Loguercio C, Federico A, Trappoliere M, Tuccillo C, de Sio I, Di Leva A, Niosi M, D'Auriaet MV, Capasso R, Del Vecchio Blanco C and Real Sud group (2007) The

effect of a silybin-vitamin E-phospholipid complex on nonalcoholic fatty liver disease: A pilot study. *Dig Dis Sci* **52**: 2387–2395.

Maher JJ, Friedman SL, Roll FJ and Bissell DM (1988) Immunolocalization of laminin in normal rat liver and biosynthesis of laminin by hepatic lipocytes in primary culture. *Gastroenterology* **94**: 1053–1062.

Mann DA and Oakley F (2013) Serotonin paracrine signaling in tissue fibrosis. Biochim. *Biophys Acta Mol Basis Dis* **1832**: 905–910.

Marek CJ, Tucker SJ, Konstantinou DK., Elrick LJ, Haefner D, Sigalas C, Murray GI, Goodwin B and Wright M C (2005) Pregnenolone-16α-carbonitrile inhibits rodent liver fibrogenesis via PXR (pregnane X receptor)-dependent and PXR-independent mechanisms. *Biochem J* **387**, 601−608.

Marek GJ, Martin-Ruiz R, Abo A and Artigas F (2005b) The Selective 5-HT2A Receptor Antagonist M100907 Enhances Antidepressant-Like Behavioral Effects of the SSRI Fluoxetine. *Neuropsychopharmacology* **30**: 2205–2215.

Maroteaux L, Saudou F, Amlaiky N, Boschert U, Plassat JL, and Hen R (1992) Mouse 5HT1B serotonin receptor: cloning, functional expression, and localization in motor control centers. *Proc Natl Acad Sci* **89**: 3020–3024.

Marra F., Arrighi MC, Fazi M, Caliguiuri A, Pinzani M, Romanelli RG, Efsen E, Laffi G and Gentilini P (1999a) Extracellular Signal-Regulated Kinase Activation Differentially Regulates Platelet-Derived Growth Factor's Actions in Hepatic Stellate Cells, and Is Induced by *In Vivo* Liver Injury in the Rat. *Hepatology* **30**: 951-958.

Marra F, Gentilini A, Pinzani M, Ghosh Choudhury G, Parola M, Herbst H, Laffi G,. Abboud HE and Gentilini P (1997) Phosphatidylinositol 3-kinase is required for platelet-derived growth factor's actions on hepatic stellate cells. *Gastroenterology* **112**: 1297-1306.

Marra F, Pinzani M, De Franco R, Laffi G and Gentilini P (1995) Involvement of phosphatidylinositol 3-kinase in the activation of extracellular signal-regulated kinase by PDGF in hepatic stellate cells. *FEBS Lett* **376**: 141–145.

Marra F, Romanelli RG, Giannini C, Failli P, Pastacaldi S, Arrighi MC, Pinzani M, Laffi G, Montalto P and Gentilini P (1999b) Monocyte chemotactic protein-1 as a chemoattractant for human hepatic stellate cells. *Hepatology* **29**: 140–148.

Martin GR, Leff P, Cambridge D and Barrett VJ (1987) Comparative analysis of two types of 5-hydroxytryptamine receptor mediating vasorelaxation: Differential classification using tryptamines. *Naunyn Schmiedebergs Arch Pharmacol* **336**: 365-373.

Martin GR and MacLennan SJ (1990) Analysis of the 5-HT receptor in rabbit saphenous vein exemplifies the problems of using exclusion criteria for receptor classification. *Naunyn Schmiedebergs Arch Pharmacol* **342**: 111-119.

Martinez-Hernandez A (1984) The hepatic extracellular matrix I. Electron immunochemical studies in normal rat liver. *Lab Invest* **67**: 427-433.

Marzioni M, Glaser S, Francis H, Marucci L, Benedetti A, Alvaro D, Taffetani S, Ueno Y, Roskams T, Phinizy JL, Venter J, Fava G, Lesage GD and Alpini G (2005) Autocrine/paracrine regulation of the growth of the biliary tree by the neuroendocrine hormone serotonin. *Gastroenterology* **128**: 121–137.

Massagué J (1996) TGF-beta signalling: receptors, transducers, and Mad proteins. *Cell* **85** : 47–950.

Massague´ J (1998) TGF-beta signal transduction. *Annu Rev Biochem* **67**: 753-791.

Mastai R, Giroux L, Semret M and Huet PM (1990) Ritanserin decreases portal pressure in conscious and unrestrained cirrhotic rats. *Gastroenterology* **98**:141–145.

Mastai R, Rocheleau B and Huet PM (1989) Serotonin blockade in conscious, unrestrained cirrhotic dogs with portal hypertension. *Hepatology* **9**: 265–268.

Matondo RB, Punt C, Homberg J, Toussaint M J, Kisjes R, Korporaal SJ, Akkerman JW, Cuppen E and de Bruin A (2009) Deletion of the serotonin transporter in rats disturbs serotonin homeostasis without impairing liver regeneration. *Am J Physiol Gastrointest Liver Physiol* **296**: G963–G968.

Matsuzaki K, Murata M, Yoshida K, Sekimoto G, Uemura, Y, Sakaida N, Kaibori M, Kamiyama Y, Nishizawa M, Fujisawa J, Okazaki K and Seki T (2007) Chronic inflammation associated with hepatitis C virus infection perturbs hepatic transforming growth factor β signaling, promoting cirrhosis and hepatocellular carcinoma. *Hepatology* **46**: 48–57.

McGee JO and Patrick RS (1972) The role of perisinusoidal cells in hepatic fibrogenesis. An electron microscopic study of acute tetrachloride liver injury. *Lab Invest* **264**: 429-440.

Medici V, Virata MC, Peerson JM, Stabler SP, French SW, Gregory JF, Albanese A, Bowlus CL, Devaraj S, Panacek EA, Richards JR, Halstead CH (2011) S-adenosyl-l-methionine treatment for alcoholic liver disease: a double-blinded, randomized, placebo-controlled trial. *Alcohol Clin Exp Res* **35**: 1960–1965

Melton AC, Datta A and Yee HFJ (2006) [Ca2+]i-independant contractile force generation by rat hepatic stellate cells in response to Endothelin-1. *Am J Physiol Gastrointest Liver Physiol* **290**: G7-13.

Millan M, Marin P, Bockaert J and Mannoury la Cour C (2008) Signaling at G-protein-coupled serotonin receptors: recent advances and future research directions. *Trends Pharmacol Sci* **29**: 454-464.

Miyoshi H, Rust C, Roberts PJ, Burgart LJ and Gores GJ (1999) Hepatocyte apoptosis after bile duct ligation in the mouse involves Fas. Hepatocyte apoptosis after bile duct ligation in the mouse involves Fas. *Gastroenterology* **117**: 669–677.

Morecroft I, Heeley RP, Prentice HM, Kirk A and MacLean MR (1999) 5-Hydroxytryptamine receptors mediating contraction in human small muscular

pulmonary arteries: importance of the 5-HT$_{1B}$ receptor. *Br J Pharmacol* **128**: 730–734.

Mühlbauer M, Weiss TS, Thasler WE, Gelbmann CM, Schnabl B, Schölmerich J and Hellerbrand C (2004) LPS-mediated NFκB activation varies between activated human hepatic stellate cells from different donors. *Biochem Biophys Res Commun* **325**: 191–197.

Murphy FR, Issa R, Zhou X, Ratnarajah S, Nagase H, Arthur M J P, Benyon C and Iredale J P (2002) Inhibition of Apoptosis of Activated Hepatic Stellate Cells by Tissue Inhibitor of Metalloproteinase-1 Is Mediated via Effects on Matrix Metalloproteinase Inhibition. *J Biol Chem* **277**: 11069-11076.

Nakatani K, Seki S, Kawada N, Kobayashi K and Kaneda K (1996) Expression of neural cell adhesion molecule (N-CAM) in perisinusoidal stellate cells of the human liver. *Cell Tissue Res* **283**: 159–165.

Napier C, Stewart M, Melrose H, Hopkins B, McHarg A and Wallis R (1999) Characterisation of the 5-HT receptor binding profile of eletriptan and kinetics of [3H]eletriptan binding at human 5-HT1B and 5-HT1D receptors. *Eur J Pharmacol* **368**: 259-268.

Neubauer K, Knittel T, Autisch S, Fellmer P and Ramadori G (1996) Glial fibrillary acidic protein - a cell type specific marker for Ito cells in vivo and in vitro. *J Hepatol* **24**: 719–730.

Neuschwander-Tetri BA, Brunt EM, Kent R, Wehmeier KR, Oliver D and Bacon BR (2003) Improved non-alcoholic steotohepatitis after 48 weeks of treatment with the PPAR-gamma ligand rosiglitazone. *Hepatology* **38**: 1008-1017.

Niclauss N, Michel-Reher MB, Alewijnse AE and Michel MC (2006) Comparison of three radioligands for the labelling of human β-adrenoceptors *Naunyn-Schmiedebergs Arch Phamacol* **374**: 99-105.

Nocito A, Georgiev P, Dahm F, Jochum W, Bader M, Graf R and Clavien PA (2007) Platelets and platelet-derived serotonin promote tissue repair after normothermic hepatic ischemia in mice. *Hepatology* **45**: 369–376.

Novo E (2006) Overexpression of Bcl-2 by activated human hepatic stellate cells: resistance to apoptosis as a mechanism of progressive hepatic fibrogenesis in humans. *Gut* **55**: 1174–1182.

Novo E, Busletta C, Valfrè di Bonzo L, Povero D, Paternostro C, Mareschi K, Ferrero I, David E, Bertolani C, Caligiuri A, Cannito S, Tamagno E, Compagnone A, Colombatto S, Marra F, Fagioli F, Pinzani M and Parola M (2011) Intracellular reactive oxygen species are required for directional migration of resident and bone marrow-derived hepatic pro-fibrogenic cells. *J Hepatol* **54**: 964-74.

Novo E, Cannito S, Paternostro C, Bocca C, Miglietta A and Parola M (2014) Cellular and molecular mechanisms in liver fibrogenesis. *Arch Biochem Biophys* **548**: 20–37.

Novo E, Cannito S , Zamara E, Valfrè di Bonzo L, Caligiuri A, Cravanzola C, Compagnone A, Colombatto S, Marra F, Pinzani M and Parola M (2007) Proangiogenic cytokines as hypoxia-dependent factors stimulating migration of human hepatic stellate cells. *Am J Pathol* **170**: 1942-1953.

Oakley F, Meso M, Iredale JP, Green K, Marek CJ, Zhou X, May MJ, Millward Sadler H, Wright M and Mann D (2005) Inhibition of inhibitor kB kinases stimulates hepatic stellate cell apoptosis and accelerated recovery from rat liver fibrosis. *Gastroenterology* **128**: 108-120.

Oakley F, Trim N, Constandinou CM, Ye W, Gray AM, Frantz G, Hillan K, Kendall T, Benyon RC, Mann DA and Iredale JP (2003) Hepatocytes express nerve growth factor during liver injury: evidence for paracrine regulation of hepatic stellate cell apoptosis. *Am J Pathol* **163**: 1849-1858.

Oates JA, Pettinger WA and Doctor RB (1966) Evidence for the release of bradykinin in carcinoid syndrome. *J Clin Invest* **45**: 173–178.

Oben JA (2004) Hepatic fibrogenesis requires sympathetic neurotransmitters. *Gut* **53**: 438–445.

Offord SJ, Wong DF and Nyberg S (1999) The role of positron emission tomography in the drug development of M100907, a putative antipsychotic with a novel mechanism of action. *J Clin Pharmacol* **39**: 17S–24S.

Ogden CL, Carroll MD, Curtin LR, McDowell MA, Tabak CJ and Flegal KM. (2006) Prevalence of overweight and obesity in the United States, 1999-2004. *J Am Med Assoc* **295**: 1549-1555.

Oide H, Tateyama M, Wang XE, Hirose M, Itatsu T, Watanabe S, Ochi Rand Sato N (1999) . Activated stellate (Ito) cells possess voltage-activated calcium current. *Biochim Biophys Acta* **1418**, 158-164.

Oinonen T and Lindros OK (1998) Zonation of hepatic cytochrome P-450 expression and regulation. *Biochem J* **329**: 17–35.

Okanoue T, Burbige EJ and French SW (1983) The role of the Ito cell in perivenular and intralobular fibrosis in alcoholic hepatitis. *Arch Pathol Lab Med* **107**: 459–463.

Olinga P and Schuppan D (2013) Precision-cut liver slices: A tool to model the liver ex vivo. *J Hepatol* **58**: 1252–1253.

Olsen AL, Bloomer SA, Chan EP, Gaça MDA, Georges PC, Sackey B and Uemura M, Janmey PA and Wells RG (2011) Hepatic stellate cells require a stiff environment for myofibroblastic differentiation. *Am J Physiol Gastrointest Liver Physiol* **301**: G110–G118.

Omenetti A, Yang L , Gainetdinov RR, Guy CD, Choi SS , Chen W, Caron MG and Diehl AM (2011) Paracrine modulation of cholangiocyte serotonin synthesis orchestrates biliary remodeling in adults. *Am J Physiol Gastrointest Liver Physiol* **300**: G303–G315.

Pagès G, P. Lenormand G, L'Allemain JC, Chambard JC, Meloche S and. Pouyssegur J (1993) Mitogen-activated protein kinases p42MAPK and p44MAPK are required for fibroblast proliferation. *Proc Natl Acad Sci* **90**: 8319-8323.

Palacios RS, Roderfeld M, Hemmann S, Rath T, Atanasova S, Tschuschner A, Gressner OA, Weiskirchen R, Graf J and Roeb E (2008) Activation of hepatic stellate cells is associated with cytokine expression in thioacetamide-induced hepatic fibrosis in mice. *Lab Invest* **88**: 1192–203.

Papadimas GK, Tzirogiannis KN, Panoutsopoulos GI, Demonakou MD, Skaltsas SD, Hereti RI and papadopoulou-Daifoti Z and Mykoniatis G (2006) Effect of serotonin receptor 2 blockage on liver regeneration after partial hepatectomy in the rat liver. *Liver Int* **26**: 352–61.

Park KS, Sin PJ, Lee DH, Cha SK, Kim MJ, Baik SK, Jeong SW and Kong ID (2011) Switching-on of serotonergic calcium signaling in activated hepatic stellate cells. *World J Gastroenterol* **17**: 164-173

Paton WDM and Rang HP (1966) A kinetic approach to the mechanism of drug action. In Advance in Drug Research, Vol 3, Harper, N.J. & Simmonds, A.B. Eds. Academic Press, New York, pp 57–80.

Pavlovic M, Saiag P, Lotz JP Marinho E, Clerici T and Izrael V (1995) Regression of sclerodermatous skin lesions in a patient with carcinoid syndrome treated by ocreotide *Arch Dermatol* **131**: 1207-1209.

Pellicoro A, Ramachandran P, Iredale JP and Fallowfield JA (2014) Liver fibrosis and repair: immune regulation of wound healing in a solid organ. *Nat Rev Immunol* **14**: 181–194.

Pietrangelo A, Gualdi R, Casalgrandi G, Montosi G and Ventura E (1995) Molecular and cellular aspects of iron-induced hepatic cirrhosis in rodents. *J Clin Invest* **95**: 1824-1831.

Pinzani M, (2002) PGDF and signal transduction in hepatic stellate cells. *Front Biosci* **7**: 1720-1726.

Pinzani M and Gentilini P (1999) Biology of hepatic stellate cells and their possible relevance in the pathogenesis of portal hypertension in cirrhosis. *Semin Liver Dis* **19**: 397-410.

Pinzani M and Marra F (2001) Cytokine receptors and signalling in hepatic stellate cells. *Semin Liver Dis* **21**: 397- 416.

Pinzani M, Marra F, Caligiuri A, De Franco R, Gentilini A, Failli P and Gentilini P (1996) Inhibition of pentoxifylline of extracellular signal-regulated kinase activation by platelet-derived growth factor in hepatic stellate cells. *Brit J Pharmacol* **119**: 1117-1124.

Pinzani M, Vizzutti F and Marra F. (2008) Technology insight: noninvasive assessment of liver fibrosis by biochemical scores and elastography. Nat. Clin. Pract. Gastroenterol. Hepatol. 5, 95-106

Popov Y and Schuppan D (2009) Targeting liver fibrosis: Strategies for development and validation of antifibrotic therapies. *Hepatology* **50**: 1294-1306

Poynard T, Mathurin P, Lai CL, Guyader B, Poupon R, Tainturier MH, Myers RP, Muntenau M, Ratziu V, Manns M, Vogel A, Capron F, Chedid A and Bedossa P (2003) A comparison of fibrosis progression in chronic liver diseases. *J Hepatol* **38**: 257-265.

Poynard T, McHutchison J, Manns M, Trepo C, Lindsay K, Goodman Z, Ling MH and Albrecht J (2002) Impact of pegylated interferon alfa-2b and ribavirin on liver fibrosis in patients with chronic hepatitis C. *Gastroenterology* **122**: 1303–1313.

Przyklenk, K, Frelinger, AL, Linden, MD, Whittaker P, Li Y, Barnard MR, Adams J, Morgan M, Al-Shamma H and Michelson AD (2010) Targeted inhibition of the serotonin 5-HT2A receptor improves coronary patency in an in vivo model of recurrent thrombosis. *J Thromb Haemost* **8**: 331-340.

Puche JE, Saiman Y and Friedman SL (2013) Hepatic Stellate Cells and Liver Fibrosis. In Comprehensive Physiology, (Hoboken, NJ, USA: John Wiley & Sons, Inc.), pp 1473–1492.

Quinn JC, Johnson-Farley NN, Yoon J and Cowen DS(2002) Activation of extracellular-regulated kinase by 5-hydroxytryptamine2A receptors in PC12 cells is protein kinase C independent and requires calmodulin and tyrosine kinases. *J Pharmacol Exp Ther* **303**: 746–752.

Radaeve S, Sun R, Jaruga B, Nguyen VT, Tian Z and Goa B (2006) Natural killer cells ameliorate liver fibrosis by killing activated stellate cells in NKG2D-dependent and tumour necrosis factor-related apoptosis-inducing ligand-dependent manners. *Gastroenterology* 1**30**: 435-452.

Ramachandran P, Pellicoro A, Vernon MA, Boulter L, Aucott RL, Ali A, Hartland SN, Snowden VK, Cappon A, Gordon-Walker TT, Williams MJ, Dunbar DR, Manning JR, van Rooijen N, Fallowfield JA, Forbes S and Iredale JP (2012) Differential Ly-6C expression identifies the recruited macrophage phenotype, which orchestrates the regression of murine liver fibrosis. *Proc Natl Acad Sci* **109**: E3186–95.

Ramond MJ, Poynard T, Reuff B, Mathurin M, Theodore C, Chaput J and Benhamou J (1992) A randomized trial of prednisolone in patients with severe alcoholic hepatitis. *New Eng J Med* **326**: 507-512.

Rang HP (2006) The receptor concept: pharmacology's big idea. *Br J Pharmacol* **147**: S9–16.

Rashid M, Manivet P, Nishio H, Pratuangdejkul J, Rajab M, Ishiguro M, Launay JM, Nagatomo T (2003) Identification of the binding sites and selectivity of sarpogrelate, a novel 5-HT$_2$ antagonist, to human 5-HT$_{2A}$, 5-HT$_{2B}$ and 5-HT$_{2C}$ receptor subtypes by molecular modelling . *Life Sci* **73**: 193-207.

Raymond JR, Mukhin YV, Gelasco A, Turner J, Collinsworth G, Gettys TW, Grewal JS and Garnovskaya MN (2001) Multiplicity of mechanisms of serotonin receptor signal transduction. *Pharmacol Ther* **92**: 179-212.

Reavill C, Kettle A, Holland V, Riley G and Blackburn TP (1999) Attenuation of haloperidol-induced catalepsy by a 5-HT$_{2C}$ receptor antagonist. *Br J Pharmacol* **126**: 572-574.

Reimann T, Hempel U, Krautwald S, Axmann A, Scheibe R, Seidel D and Wenzel KW (1997) Transforming growth factor-β1 inducesactivation of Ras, Raf-1, MEK and MAPK in rat hepatic stellate cells. *FEBS Lett* **403**: 57–60

Reimund E (1987) Methysergide and retroperitoneal fibrosis. *Lancet* **1**: 443

Reynaert H, Thompson MG, Thomas T and Geerts A (2002) Hepatic stellate cells: role in microcirculation and pathophysiology of portal hypertension. *Gut* **50**: 571-581

Richardson PD and Withington PG (1977) A comparison of the effects of bradykinin, 5-hydroxytryptamine and histamine on the hepatic arterial and portal venous vascular beds of the dog: histamine H$_1$- and H$_2$-receptor populations. *Br J Pharmacol* **60**: 123–133.

Rockey DC (2001a) Cellular pathophysiology of portal hypertension and prospects for management with gene therapy. *Clin Liver Dis* **5**: 851-865.

Rockey DC (2001b) Hepatic blood flow regulation by stellate cells in normal and injured liver. *Semin Liv Dis* **21**: 337-350.

Rockey DC (2003) Vascular mediators in the injured liver. *Hepatology* **37**: 4-12.

Rockey DC (2006) Hepatic Fibrosis, Stellate Cells, and Portal Hypertension. *Clin Liver Dis* **10**: 459–479.

Rockey DC (2008) Current and future anti-fibrotic therapies for chronic liver disease. *Clin Liv Dis* **12**: 939-962.

Rockey DC and Weisiger RA (1996) Endothelin induced contractility of stellate cells from normal and cirrhotic rat liver: Implications for regulation of portal pressure and resistance. *Hepatology* **24**: 233–240.

Rodríguez-Garay EA, Agüero RM, Pisani G, Trbojevich RA, Farroni A and Viglianco RA (1996) Rat model of mild stenosis of the common bile duct. *Res Exp Med* **196**:105–116.

Rombouts K, Knittel T, Machesky L, Braet F, Wielant A, Hellemans K, De Bleser P, Gelman I, Ramadori G, and Geerts A (2002) Actin filament formation reorganisation and migration are impaired in hepatic stellate cells under the influence of trichostatin A, a histone deacetylase inhibitor. *J Hepatol* **37**: 788-796.

Ros, R, Raines EW and Bowen-Pope DF (1986) The biology of platelet-derived growth factor. *Cell* **46**: 155–169.

Roth BL (2007) Drugs and valvular heart disease. *N Eng J Med* **356**: 6- 9.

Rothman RB and Baumann M H. (2009). Serotonergic Drugs and Valvular Heart Disease. *Expert Opin Drug Saf* **8**: 317–329.

Rothman RB, Baumann MH, Savage JE, Rauser L, McBride A, Hufeisen SJ, Roth BL (2000) Evidence for possible involvement of 5-HT(2B) receptors in the cardiac valvulopathy associated with fenfluramine and other serotonergic medications. *Circulation* **102**: 2836-2841.

Roulot D, Sevcsik AM, Coste T, Strosberg AD and Maurullo S (1999) Role of transforming growth factor beta type II receptor in hepatic fibrosis: studies of human chronic hepatitis C and experimental fibrosis in rats. *Hepatology* **29** :1730-1738.

Ruddell RG, Mann DA and Ramm GA (2008) The function of serotonin within the liver. *J Hepatol* **48**: 665-675

Ruddell RG, Oakley F, Hussain Z, Yeung I, Bryan-Lluka LJ, Ramm GA, Mann DA (2006) A role for serotonin (5-HT) in hepatic stellate cell function and liver fibrosis. *Am. J Pathol* **169**: 861–876.

Said A and Lucey MR (2008) Liver transplantation: and update 2008. *Curr Opin Gastroenterol* **24**: 339-245.

Sancho-Bru P, Bataller R, Gasull X, Colmenero J, Khurdayan V, Gual, A, Nicolas JM, Arroyo V and Gines P. (2005) Genomic and functional characterization of stellate cells isolated from human cirrhotic livers. *J Hepatol* **43:** 272–282.

Sanyal AJ, Chalasani N, Kowdley KV, McCullough A, Diehl AM, Bass NM, Neuschwander-Tetri BA, Lavine JE, Tonascia J, Unalp A, Van Natta M, Clark J, Brunt EM, Klieiner DE, Hoofnagle JH and Robuck PR (2010) Pioglitazone, vitamin E, or placebo for nonalcoholic steatohepatitis. *N Eng J Med* **362**: 1675-85.

Schmitt-Gräff A, Krüger S, Bochard F, Gabbiani G and Denk H (1991) Modulation of alpha smooth muscle actin and desmin expression in perisinusoidal cells of normal and diseased human livers. *Am J Pathol* **138**: 1233–42.

Selbie LA and Hill SJ (1998) G protein-coupled-receptor cross-talk: the fine-tuning of multiple receptor-signalling pathways. *Trends Pharmacol Sci* **19**: 87-93.

Setola V, Hufeisen SJ, Grande-Allen KJ, Vesely I, Glennon RA, Blough B, Rothman RB and Roth BL (2003) 3,4-Methylenedioxymethamphetamine (MDMA, 'Ecstasy') Induces Fenfluramine-Like Proliferative Actions on Human Cardiac Valvular Interstitial Cells in Vitro. *Mol Pharmacol* **63**: 1223–1229.

Shi Z, Wakil AE, Rockey DC (1997) Strain-specific differences in mouse hepatic wound healing are mediated by divergent T helper cytokine responses. *Proc Natl Acad Sci* **94**: 10663–10668.

Sims DE (1991) Recent advances in pericyte biology--implications for health and disease. *Can J Cardiol* **7**: 431–43.

Slominski A, Pisarchik B, Zbytek DJ, Tobin S, Kauser S and Wortsman J (2003) Functional activity of serotonergic and melatonsergic systems expressed in skin. *J Cell Physiol* **196**: 144-153.

Soon RK and Yee HF (2008) Stellate Cell Contraction: Role, Regulation, and Potential Therapeutic Target. *Clin Liver Dis* **12**: 791–803.

Starkel P and Leclercq IA (2011) Animal models for the study of hepatic fibrosis. *Best Pract Res Clin Gastroenterol* **25**: 319-333.

Stopa M, Anhuf D, Terstegen L, Gatsios P, Gressner AM and Dooley S (2000) Participation of Smad2, Smad3, and Smad4 in transforming growth factor β (TGF-β)-induced activation of Smad7. The TGF-β response element of the promoter requires functional Smad binding element and E-box sequences for transcriptional regulation. *J Biol Chem* **2000**: 275: 29308–29317.

Sunahara RK, Guan HC, O'Dowd BF, Seeman P, Laurier LG, Ng G, George SR, Torchia J, Van Tol HH and Niznik HB. (1991) Cloning of the gene for a human dopamine D5 receptor with higher affinity for dopamine than D1. *Nature* **350**: 614-619.

Tahashi Y, Matsuzaki K, Date M, Yoshida K, Furukawa F, Sugano Y, Matsushita M, Himeno Y, Inagaki Y and Inoue K (2002) Differential regulation of TGF-β signal in hepatic stellate cells between acute and chronic rat liver injury. Hepatology 35:49–61

Tamayo R P (1983) Is cirrhosis of the liver experimentally produced by CCl4 an adequate model of human cirrhosis? *Hepatology* **3:** 112–120.

Tanaka N, Goto R, Ito R, Hayakawa M, Sugidachi A, Ogawa T, Asai F and Fujimoto K (2000) [2-(O-Phenylalkyl)phenoxy]alkylamines III: Synthesis and selective serotonin-2 receptor binding (2). *Chem Pharm Bull (Tokyo)* **48**: 1729–1739.

Teegarden BR, Shamma HA and Xiong Y (2008) 5-HT(2A) inverse-agonists for the treatment of insomnia. *Curr Top Med Chem* **8**: 969–976.

Thimgan MS and Yee HF (1999) Quantitation of rat hepatic stellate cell contraction: stellate cells' contribution to sinusoidal resistance. *Am J Physiol* **277**: G137-143.

Thomas DR, Gittins SA, Collin LL, Middlemiss DN, Riley G, Hagan J, Gloger I, Ellis CE, Forbes IT and Brown AM (1998) Functional characterisation of the human cloned 5-HT7 receptor (long form); antagonist profile of SB-258719. B*r J Pharmacol*, **124**: 1300-1306.

Thrall KD, Vucelick ME, Gies RA, Zangar RC, Weitz KK, Poet TS, Springer DL, Grant DM and Benson JM (2000) Comparative metabolism of carbon tetrachloride in rats, mice, and hamsters using gas uptake and PBPK modeling . *J Toxiciological Environ. Heal* **60**: 531–548.

Tian Y, Graf R, El-Badry AM , Lesurtel M, Furrer K, Moritz W and Clavien PA (2011) Activation of serotonin receptor-2B rescues small-for-size liver graft failure in mice. *Hepatology* **53**: 253–262.

Trautwein C, Friedman SL, Schuppan D and Pinzani M (2015) Hepatic fibrosis: Concept to treatment. *J Hepatol* **62**: S15–S24.

Trebicka J, Hennenberg M, Schulze Pröbsting A, Laleman W, Klein S, Granzow M, Nevens F, Zaagsma J Heller J and Sauerbruch T (2009) Role of beta3-adrenoceptors for intrahepatic resistance and portal hypertension in liver cirrhosis. *Hepatology* **50**: 1924–1935.

Tsuchioka, M, Takebayashi M, Hisaoka K, Maeda N and Nakata Y (2008) Serotonin (5-HT) induces glial cell line derived neurotrophic factor (GDNF) mRNA expression via the transactivation of fibroblast growth factor receptor 2 (FGFR2) in rat C6 glioma cells. *J Neurochem* **106:** 244–257.

Tsukada S (2005) SMAD and p38 MAPK Signaling Pathways Independently Regulate 1(I) Collagen Gene Expression in Unstimulated and Transforming Growth Factor- -stimulated Hepatic Stellate Cells. *J Biol Chem* **280**: 10055–10064.

Tsukada S, Parsons CJ and Rippe RA (2006) Mechanisms of liver fibrosis *Clin. Chim Acta* **364**: 33–60.

Tsukamoto H, Matsuoka M and French SW (1990) Experimental models of hepatic fibrosis: A review. *Semin Liver Dis* **10,** 56–65.

Tsukazaki T, Chiang TA, Davison AF, Attisano L and Wrana JL. (1998). SARA, a FYVE Domain Protein that Recruits Smad2 to the TGF-β Receptor. *Cell*. **95** 779-91.

Tyce GM (1990) Origin and Metabolism of Serotonin. *J Cardiovasc Pharmacol* **16**: S1–S7.

Uemura M, Swenson ES, Gaça MDA, Giordano FJ, Reiss M and Wells RG (2005) Smad2 and Smad3 play different roles in rat hepatic stellate cell function and α-smooth muscle actin organization. *Mol Biol Cell* **16**:4214–4224.

Ueno T, Sata M, Sakata R, Torimura T, Sakamoto M, H Sugawara and Tanikawa K (1997) Hepatic Stellate Cells and Intralobular Innervation in Human Liver Cirrhosis. *Human Pathol* **28**: 953-959.

Van de Bovenkamp M (2005). Precision-Cut Liver Slices as a New Model to Study Toxicity-Induced Hepatic Stellate Cell Activation in a Physiologic Milieu. *Toxicol Sci* **85**: 632–638.

Van de Bovenkamp M, Groothuis GMM, Meijer DKF and Olinga P (2008). Liver slices as a model to study fibrogenesis and test the effects of anti-fibrotic drugs on fibrogenic cells in human liver. *Toxicol Vitr* **22**: 771–778.

Van de Bovenkamp M , Groothuis GMM, Meijer DKF, Slooff MJH and Olinga P (2006). Human liver slices as an in vitro model to study toxicity-induced hepatic stellate cell activation in a multicellular milieu. *Chem Biol Interact* **162**: 62–69.

Verne J (2014) Liver disease: a preventable killer of young adults *Blog: https://publichealthmatters.blog.gov.uk/2014/09/29/liver-disease-a-preventable-killer-of-young-adults.*

Verrecchia F, Mauviel A. (2007) Transforming growth factor-beta and fibrosis. *World J Gastroenterol* **13:** 3056-3062.

Vinas O, Bataller R, Sancho-Bru P, Gines P, Berenguer C, Enrich C, Nicolas JM, Ercilla G, Gallart T, Vives J, Arroyo V and Rodes J (2003) Human hepatic stellate cells shows features of antigen-presenting cells and stimulate lymphocyte proliferation. *Hepatology* **38**: 919-929.

Vorobioff J, Garcia-Tsao G, Groszmann R, Aceves G, Picabea E, Villavicencio R and Hernandez-Ortiz J (1989) Long-term hemodynamic effects of ketanserin, a 5-hydroxytryptamine blocker, in portal hypertensive patients. *Hepatology* **9**: 88–91.

Wade PR, Chen J, Jaffe B, Kassem IS, Blakely RD and Gershon MD (1996) Localization and function of a 5-HT transporter in crypt epithelia of the gastrointestinal tract. *J Neurosci* **16**: 2352-2364.

Wake K (1971)"Sternzellen" in the liver: perisinusoidal cells with special reference to storage of vitamin A *Am J Anat* **132**: 429-462.

Walkin L, Herrick SE, Summers A, Brenchley PE, Hoff CM, Korstanje R and Margetts PJ et al (2013) The role of mouse strain differences in the susceptibility to fibrosis: a systematic review. *Fibrogenesis Tissue Repair* **6**:18.

Wallace K, Burt AD and Wright MC (2008) Liver fibrosis. *Biochem J* **411**: 1-18.

Wallace MC, Hamesch K, Lunova M, Kim Y, Weiskichen R, Strnad P and Friedman SL (2015) Standard operating procedures in experimental liver research: thioacetamide model in mice and rats. *Lab Anim* **49**: 21–29

Waller EA, Kaplan J, Heckman MG (2005) Valvular heart disease in patients taking pergolide. *Mayo Clin Proc* **80**: 10161020.

Watts, SW, Morrison, SF, Davis, RP and Barman, SM. (2012) Serotonin and blood pressure regulation. *Pharmacol Rev* **64**: 359-88.

Weber LWD, Boll M and Stampfl A (2003) Hepatotoxicity and Mechanism of Action of Haloalkanes: Carbon Tetrachloride as a Toxicological Model. *Crit Rev Toxicol* **33**: 105–136.

Wells RG (2008) Cellular Sources of Extracellular Matrix in Hepatic Fibrosis. *Clin Liver Dis* **12**: 759–768.

Welsh DJ, Harnett M, MacLean M ans Peacock AJ (2004) Proliferation and signalling in fibroblasts: role of 5-hydroxytryptamine2A receptor and transporter. *Am J Respir Crit Care Med* **170**: 252–259.

Werry TD, Christie MI, Dainty IA, Wilkinson GF, Willars GB (2002) Ca^{2+} signalling by recombinant human CXCR2 chemokine receptors is potentiated by P2Y neucleotide receptors in HEK cells. *Br J Pharmacol* **135:** 1119-1208.

Williams CD, Stengel J, Asike MI , Torres DM, Shaw J, Contreras M, Landt CL and Harrison SA (2011) Prevalence of nonalchoholic fatty liver disease and nonalcoholic steatohepatitis among a largely middle-aged population utilizing ultrsound and liver biopsy: A prospective study. *Gastroenterology* **140**:124-131.

Wilson S, Chambers JK, Park JE, Ladurner A, Cronk DW, Chapman CG, Kallendar H, Browne MJ, Murphy GJ and Young PW (1996) Agonist potency at the cloned human beta3 adrenoceptor depends on receptor expression level and nature of assay. *J Pharmacol Exp Ther* **279**: 214-222.

Wong L, Yamasaki G, Johnson RJ, Friedman SL (1994) Induction of beta-platelet derived growth factor receptor in rat hepatic lipocytes during cellular activation in vivo and in culture. *J Clin Invest* **94**: 1563–1569.

Wright MC, Issa R, Smart DE, Trim N, Murray GI, Primrose JN, Arthur MJ, Iredale JP and Mann DA (2001) Gliotoxin stimulates the apoptosis of human and rat hepatic stellate cells and enhances resolution of liver fibrosis in rats. *Gastroenterology* **121**: 685–698

Wu J, Dent P, Jelinek T, Wolfman A, Weber MJ and Sturgill TW (1993) Inhibition of the EGF-activated MAP kinase signaling pathway by adenosine 3',5'-monophosphate. *Science* **262**: 1065-1069

Wynn TA (2008) Cellular and molecular mechanisms of fibrosis. *J Pathol* **214**:199-210.

Wynn TA and Ramalingam TR (2012) Mechanisms of fibrosis: therapeutic translation for fibrotic disease. *Nat Med* **18**: 1028–1040.

Xu L, Hui AY, Albanis E, et al (2005) Human hepatic stellate cell lines, LX-1 and LX-2: New tools for analysis of hepatic fibrosis. *Gut* **54**: 142–51.

Yang C, Zeisberg, B, Mosterman M, Sudhakar A, Yerramalla U, Holthaus K, Xu L, Eng F, Afdhal N and Kalluri R (2003) Liver Fibrosis: Insights into migration of hepatic stellate cells in response to extracellular matrix and growth factors. *Gastroenterol* **124**, 147-159.

Yokoi Y, Namihisa T, Kuroda H, Komatsu I, Miyazaki A, Watanabe S and Usui, K (1984) Immunocytochemical Detection of Desmin in Fat-Storing Cells (Ito Cells). *Hepatology* **4**: 709–714.

Yokoyama HO, Wilson ME, Tsuboi KK and Stowell R E (1953) Regeneration of mouse liver after partial hepatectomy *Cancer Res* **13**: 80–85.

Yoneda A, Sakai-Sawada K, Niitsu Y and Tamura Y (2016) Vitamin A and insulin are required for the maintenance of hepatic stellate cell quiescence. *Exp Cell Res* **341**: 8-17.

Yoshida K, Matsuzaki K, Mori S, Tahashi, Y, Yamagata H, Furukawa F, Seki T, Nishizawa M, Fujisawa J and Okazaki K (2005) Transforming growth factor-β and platelet-derived growth factor signal via c-Jun N-terminal kinase-dependent Smad2/3 phosphorylation in rat hepatic stellate cells after acute liver injury. *Am J Pathol* **166**: 1029–1039.

Yoshio R, Taniguchi T, Itoh H and Muramatsu I (2001) Affinity of serotonin receptor antagonists and agonists to recombinant and native alpha1-adrenoceptor subtypes. *Jpn J Pharmacol*, **86**: 189-195.

Yu PL, Fujimura M, Okumiya K, Kinoshita M, Hasegawa H and Fujimiya M (1999) Immunohistochemical localisation of tryptophan hydroxylase in the human and rat gastrointestinla tract. *J Comp Neurol* **411**: 654-665.

Zimmerman T, Muller A, Machnik G, Franke H, Schubert H and Dargel R (1987) Biochemical and morphological studies on production and regression of

experimental liver cirrhosis induced by thioacetamide in Uje:WIST rats. *Z Versuchstierkd* **30**: 165-180.

CHAPTER 9: APPENDIX.

9.1 Additional data.

Where additional data has been generated by co-workers, that was deemed to add value to the author's conclusions by being included, this has been highlighted in the relevant results section and any methodology from those experiments fully described in this appendix section.

9.2 Mouse and human 5-HT$_{2A}$ and 5-HT$_{2B}$ recombinant assay.

9.2.1 FLIPR™ Method.

CGE22cells (CHO/GAM/E1A clone22 cells) were thawed, washed and resuspended in growth media (DMEM/F12 containing 10% FCS (charcoal and dextran treated) and 1% glutaMax). 10% BacMam virus containing either mu5HT$_{2A}$ or mu5HT$_{2B}$ or, h5HT$_{2A}$ or h5HT$_{2B}$ was added to the cells. The cells were plated out at 10,000 cells per well in a black flat-bottom clear bottomed 384 plate and incubated at 37°C in 5% CO$_2$ for 24 h. The media was removed and replaced with loading buffer (FLIPR buffer:-HBSS (137 mM NaCl, 4.24 mM NaHCO$_3$, 5.6 mM glucose, 5.4 mM KCl, 1.3 mM CaCl$_2$, 0.8 mM MgSO$_4$, 0.4 mM K$_2$HPO$_4$ and 20mM N-2-hydroxyethylpiperazine-N'-ethanesulphonic acid (HEPES) pH7.4) 2.5 mM probenicid (to inhibit dye leakage from the cells) with the addition of 250 µM Brilliant Black (to quench the surplus Fluo-4 AM) and 2 µM Fluo-4 AM (Molecular probes, Invitrogen Ltd., Paisley,UK)) and incubated for 1 h at 37ºC. The plate was placed in the FLIPR, where the fluorescence was measured before and after any additions of antagonist, vehicle or agonist. The antagonist was allowed a 15min incubation before addition of an EC$_{80}$ concentration of 5-HT. Basal and maximum responses obtained were determined and the response was expressed as % basal fluorescence.

9.2.2 Data analysis.

Inhibition response curves were fitted using nonlinear regression analysis (four-parameter logistic equation with variable slope) to obtain values for logIC$_{50}$, Hill slope, minimum response and maximum asymptote response using Microsoft Excel add-in XC$_{50}$ module (GlaxoSmithKline in-house module). The fpK$_i$ was obtained by

converting the IC_{50} using the Cheng-Prussoff equation (Cheng and Prusoff, 1973).

$Ki = ([IC_{50}])/(1+([A])/([EC_{50}]))$

Where A is the EC_{80} concentration of the agonist and EC_{50} of the agonist CRC.

The data should have been fitted to the Cheng Prussoff equation which takes into account the shape of the CRC (Leff and Dougall 1993).

$Ki = ([IC_{50}])/((2+([A])/([EC_{50}])^{n})-1)$.

9.2.3   Results

The fpK_i obtained for each compound against each receptor are reported in Table 9.2.1 for the mouse 5-HT_2A and 5-HT_{2B} receptor and Table 9.2.2 for the human 5-HT_2A and 5-HT_{2B} receptor.

	mouse 5-HT$_{2A}$ fpK$_i$	mouse 5-HT$_{2B}$ fpK$_i$
Ketanserin	10.1 ± 0.2	<5
Volinanserin	10.8 ± 0.1	5.4 ± 0.2
GSK1606260A	5.4 ± 0.3	10.2 ± 0.2
RS-127445	6.9 ± 0.1	10.8 ± 0.1

Table 9.2.1 fpK$_i$ value obtained for ketanserin, volinanserin, GSK1606260A and RS-127445 in recombinant mouse 5-HT$_{2A}$ and 5-HT$_{2B}$ receptor calcium assays. CGE222 cells were transfected with mu5-HT$_{2A}$ or 5-HT$_{2B}$ using BacMam virus**.** Cells were loaded with fluorescent dye (FLUO4) for 1 h before being stimulated with and EC$_{80}$ concentration of 5-HT in the presence or absence of increasing concentrations of antagonists. (See Chapter 9: Appendix section 9.2). Data presented are the mean $\pm$ SEM from three replicates.

	human 5-HT$_{2A}$ fpK$_i$	human 5-HT$_{2B}$ fpK$_i$
Ketanserin	9.6 ± 0.2	<5
Volinanserin	10.7 ± 0.1	5.9
GSK1606260A	6.0 ± 0.3	10.2
RS-127445	6.3 ± 0.2	11.3

Table 9.2.2 fpK$_i$ value obtained for ketanserin, volinanserin, GSK1606260A and RS-127445 in recombinant mouse 5-HT$_{2A}$ and 5-HT$_{2B}$ receptor calcium assays. CGE222 cells were transfected with hu5-HT$_{2A}$ or 5-HT$_{2B}$ using BacMam virus**.** Cells were loaded with fluorescent dye (FLUO4) for 1 h before being stimulated with and EC$_{80}$ concentration of 5-HT in the presence or absence of increasing concentrations of antagonists. (See Chapter 9: Appendix section 9.2). Data presented are the mean $\pm$ SEM n=3 for 5-HT$_{2A}$ and average, n=2 for 5-HT$_{2B}$.

9.3 Two-Site receptor binding Model.

A model was developed in order to investigate the interaction of two signals coming from the same receptor contributing to the ERK response (Courtesy of David Hall). The final equation was used to construct CRCs (Equation 9.3.1)

$$E = \frac{\text{Emax}\left(\frac{\tau_A[H]}{K_a} + \frac{\tau_B[H]}{K_b} + \frac{[H]^2(\tau_{A+}\tau_B)}{K_aK_b}\right)}{1 + \frac{[H]}{K_b}(1+\tau_B) + \frac{[H]}{K_a}(1+\tau_A) + \frac{[H]^2(1+\tau_{A+}\tau_B)}{K_aK_b}}$$

Equation 9.3.1.

The parameters of affinity and efficacy for each individual receptor were altered to model the experimental CRCs ie. Emax of the system $=1$, affinity of receptor 1, K_A $=30$nM, affinity of receptor 2 $K_B= 3\mu$M, efficacy for receptor A$\tau_A = 5$ and efficacy for receptor B$\tau_B = 5$

9.3.1 David Halls model: Derivation and assumptions

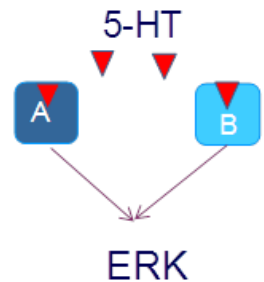Let $[H]$ = conc of 5-HT

K_a = affinity of 5-HT for 5-HTRA

K_b = affinity of 5-HT for 5-HT RB

K_{KA} = affinity of antagonist for Receptor A

K_{KB} = affinity of antagonist 2 for Receptor B

ε_A = efficacy of 5-HT at receptor A

ε_B = efficacy of 5-HT at receptor B

5-HT

A   B

ERK

$$[HB] = \frac{[B]+[H]}{K_b(1+\frac{[K]}{[K_{KB}]})+[H]} \qquad [HA] = \frac{[A]+[H]}{K_a(1+\frac{[K]}{[K_{KA}]})+[H]} \qquad S = \varepsilon_A[HA] + \varepsilon_B[HB]$$

$$E = \frac{EmaxS}{K_E+S} = \frac{Emax(\varepsilon_A[HA]+\varepsilon_B[HB])}{K_E+(\varepsilon_A[HA]+\varepsilon_B[HB])}$$

$$= \frac{Emax\left(\left[\frac{\varepsilon_A[A]+[H]}{K_a(1+\frac{[K]}{[K_{KA}]})+[H]}\right]+\left[\frac{\varepsilon_B[B]+[H]}{K_b(1+\frac{[K]}{[K_{KB}]})+[H]}\right]\right)}{K_E+\left[\frac{\varepsilon_A[A]+[H]}{K_a(1+\frac{[K]}{[K_{KA}]})+[H]}\right]+\left[\frac{\varepsilon_B[B]+[H]}{K_b(1+\frac{[K]}{[K_{KB}]})+[H]}\right]}$$

$$Let \ \frac{\varepsilon_A[A]_T}{K_E} = \tau_A \ \ and \ \frac{\varepsilon_B[B]_T}{K_E} = \tau_B \ then \ [K] = 0$$

Equation used in excel

$$E = \frac{Emax\left(\frac{\tau_A[H]}{K_a}+\frac{\tau_B[H]}{K_b}+\frac{[H]^2(\tau_{A+}\tau_B)}{K_aK_b}\right)}{1+\frac{[H]}{K_b}(1+\tau_B)+\frac{[H]}{K_a}(1+\tau_A)+\frac{[H]^2(1+\tau_{A+}\tau_B)}{K_aK_b}}$$

9.4   *In vivo* CCL4 model of liver injury.

9.4.1   Compound dose selection.

Before embarking on the *in vivo* model work was carried out to identify the compounds to use, formulation and dose to administer. 6 compounds were identified as suitable candidates to investigate, three 5-HT$_{2A}$ and three 5-HT$_{2B}$ antagonists. Based on their selectivity across other receptors, stability of formulation, % protein binding and results of naïve mice pilot PK studies two compounds, volinanserin and GSK1606260A, were chosen. The doses required to achieve about 90 and 99% occupancy were determined using the receptor specific functional pK$_i$ and data generated from the pilot PK study.

9.4.2   Calculation of dose.

Receptor occupancy (RO) was determined from the ligand concentration [L] required and K$_i$ of the ligand.

$$[L] = RO \times ([L] + Ki)$$

Therefore $RO = \dfrac{[L]}{[L] \times Ki}$

Actual blood concentration required

The % protein bound for each ligand is required to determine the blood free fraction (BFF). From this the ligand concentration required divided by the BFF will determine the actual blood concentration which needs to be achieved.

Actual concentration (ng/ml)

[Actual Conc](ng/ml)=(([actual blood conc] X mol wt)/1000))/1e-9

Dose to be given mg/kg/day :

(Actual concentration / ng/ml achieved for a known mg/kg/day)× known mg/kg/day.

Dose concentration mg/ml to be administered in via the mini-pump at a rate of 3.6 µl per day.

((Dose to be given mg/kg/day × weight of mouse (g))/3.6) = dose concentration.

9.4.3   Animal study.

All animal studies were ethically reviewed and carried out in accordance with Animals (Scientific Procedures) Act 1986 and the GSK Policy on the Care, Welfare and Treatment of Animals.

C57Bl/6 mice (n=63) were divided into Groups 1 to 6. Each group was subdivided into two in order to stagger the start date of each sub group by one week. All animals were dosed by the intraperitoneal route twice weekly with CCl_4 (2 µl/g of body weight, 1:3; CCl_4;olive oil) for up to a total of 8 weeks to induce fibrosis.. Group 2 animals were culled at the end of week 3 to determine the baseline level of fibrosis prior to compound administration. All other animals were surgically implanted with minipumps (ALZET 2006, flow rate 3.6 µL/day) that had been loaded with: Group 1: compound vehicle (DMSO : PEG200 : water 10:45:45 (v/v/v); Group 3 and 4: Volinanserin 0.06 and 0.32 mg/kg/day, respectively, Group 5 and 6: GSK1606260A 0.15 and 1.53 mg/kg/day, respectively. The dose levels were selected in order to achieve between 90-99% receptor occupancy as determined by their receptor functional pK_i and exposure from a pilot pharmacokinetic study (Table 9.4.1, Figure 9.4.1).

Blood samples were taken from animals throughout the in life phase and as a terminal procedure to determine drug exposure levels. At the end of the study two liver lobes were removed to determine tissue levels and histological assessment of collagen staining (a combination of collagen 1 and 3) using the percent area of picrosirius red staining (% PSR) . The significance of the % PSR was determined comparing treatment with the 8 week vehicle group to obtain a Dunnetts adjusted p value.

9.4.4   Results.

For the *in vivo* model the blood concentrations obtained were plotted over time for each of the doses with the 90 and 99% occupancy concentrations. The blood concentrations which were determined, following minipump administration of

GSK1606260A   **Receptor occupancy** $\%RO=([L]/[L]+K_i)*100$

mouse fK_i	6.31E-11
5-HT$_{2B}$ fpK_i	10.2
Mol wt	383
5-HT$_{2B}$ fpK_i in (ng/ml)	0.024

Delivery at 2mg/kg/day gave 39ng/ml steady state concentration

25g mouse
given 3.6 ul per day

times Ki	Receptor occupancy	added ligand concentration required	Conc required ng/ml	Mouse protein binding %	Blood free fraction %	Actual conc required to be delivered	Actual conc required ng/ml	Dose mg/kg/day	Dose conc mg/ml
1	50	6.310E-11	0.02	91.9	8.1	7.79E-10	0.30	0.02	0.1
3	75	1.893E-10	0.07	91.9	8.1	2.34E-09	0.90	0.05	0.3
10	90.91	6.310E-10	0.24	91.9	8.1	7.79E-09	2.98	0.15	1.1
30	96.77	1.893E-09	0.72	91.9	8.1	2.34E-08	8.95	0.46	3.2
100	99.01	6.310E-09	2.42	91.9	8.1	7.79E-08	29.83	1.53	10.6
300	99.67	1.893E-08	7.25	91.9	8.1	2.34E-07	89.50	4.59	31.9
1000	99.90	6.310E-08	24.17	91.9	8.1	7.79E-07	298.34	15.30	106.2
3000	99.97	1.893E-07	72.50	91.9	8.1	2.34E-06	895.02	45.90	318.7
10000	99.99	6.310E-07	241.66	91.9	8.1	7.79E-06	2983.42	153.00	1062.5

Volinanserin   **Receptor occupancy**

mouse fK_i	1.58E-11
5-HT$_{2A}$ fpK_i	10.8
Mol wt	373
5-HT$_{2A}$ fpK_i in (ng/ml)	0.006

Delivery at 2mg/kg/day gave 10.2ng/ml steady state concentration

25g mouse
given 3.6 ul per day

times Ki	Receptor occupancy	added ligand concentration required	Conc required ng/ml	Mouse protein binding	Blood free fraction %	Actual conc required to be delivered	Actual conc required ng/ml	Dose mg/kg/day	Dose conc mg/ml
1	50	1.585E-11	0.01	81.9	18.1	8.76E-11	0.03	0.01	0.04
3	75	4.755E-11	0.02	81.9	18.1	2.63E-10	0.10	0.02	0.1
10	90.91	1.585E-10	0.06	81.9	18.1	8.76E-10	0.33	0.06	0.4
30	96.77	4.755E-10	0.18	81.9	18.1	2.63E-09	0.98	0.19	1.3
50.0	98.04	7.924E-10	0.30	81.9	18.1	4.38E-09	1.63	0.32	2.2
100	99.01	1.585E-09	0.59	81.9	18.1	8.76E-09	3.27	0.64	4.4
300	99.67	4.755E-09	1.77	81.9	18.1	2.63E-08	9.80	1.92	13.3
1000	99.90	1.585E-08	5.91	81.9	18.1	8.76E-08	32.66	6.40	44.5
3000	99.97	4.755E-08	17.73	81.9	18.1	2.63E-07	97.98	19.21	133.4
10000	99.99	1.585E-07	59.12	81.9	18.1	8.76E-07	326.61	64.04	444.7

Table 9.4.1. Receptor occupancy calculations for GSK1606260A and volinaserin for the *in vivo* CCl$_4$ study. The lines highlighted in yellow are the receptor occupancy level to be achieved and the does required to be given to achieve that dose taking into account the protein binding and pilot mouse PK study data. This shows all the calculations required that took place to deliver the correct dose. (See Chapter 2: Data analysis section, Appendix 9.4.3 Materials and methods).

Week

0			3	4	5	6	7	8

CCl$_4$ i.p.

CCl$_4$ i.p. + minipump s.c. infusion of compound

Cull Group 2

Blood sampling at weeks 4, 5, 6, 7 & 8

Cull all remaining groups
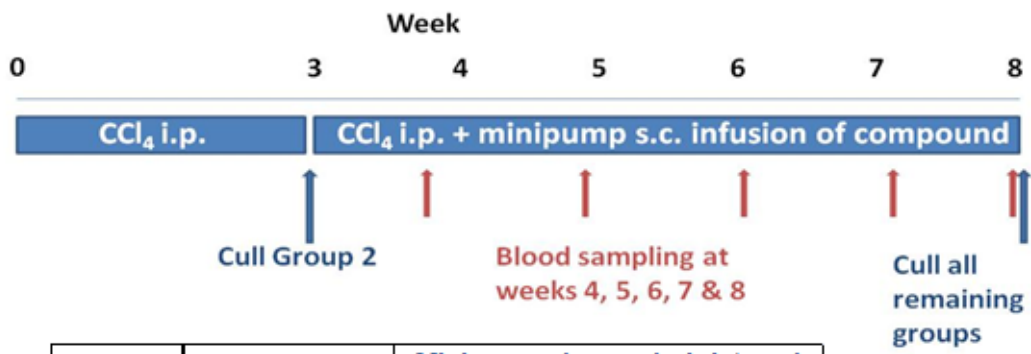
Group	No. of animals	Minipump dose administered weeks 3-8
1	15	Vehicle
2	8	N/A
3	10	0.06 mg/kg/day Volinanserin
4	10	0.32 mg/kg/day Volinanserin
5	10	0.15 mg/kg/day GSK1606260A
6	10	1.53 mg/kg/day GSK1606260A

Figure 9.4.1. Diagram of the *in vivo* protocol for the CCl$_4$ study.

volinanserin (0.06 and 0.32 mg/kg/day) and GSK1606260A (0.15 and 1.53 mg/kg/day) throughout the study, remained stable and at levels predicted to achieve the receptor occupancy required (Figure 9.4.2).
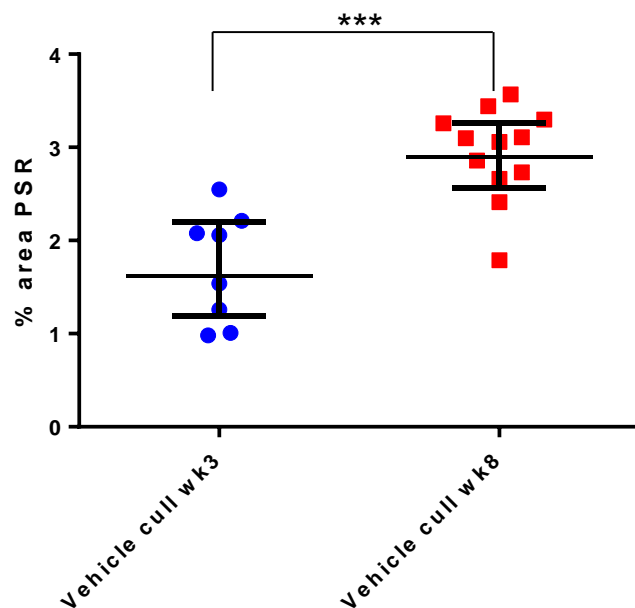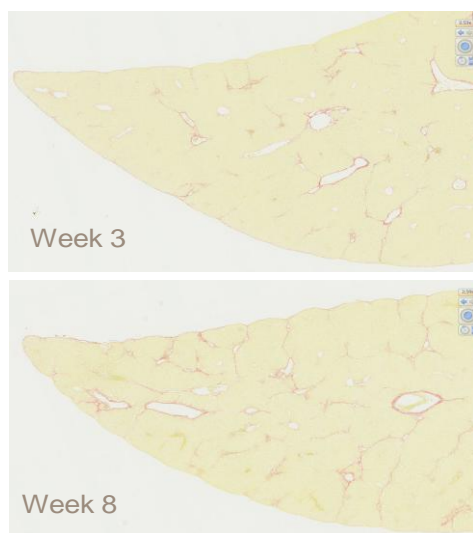
Histological assessment of fibrosis in the model obtained at week 3 and 8 demonstrated a significant increase in % picrosirius red staining observed between week 3 and week 8 vehicle treated animals ($P<0.001$ p value adjusted based on Dunnett's method) (Figure 9.4.3) confirming that this model is capable of demonstrating a disease window with which to compare treatments.

Liver from animals dosed with the 5-HT$_{2B}$ antagonist GSK1606260A had significantly increased % PSR area at both doses compared to the 8 week vehicle (*Dunnetts adjusted   p-value=0.0445 for 0.15mg; **Dunnetts adjusted p-value=0.0036 for 1.53mg) (Figure 9.4.4). Liver from animals dosed with the 5-HT$_{2A}$ antagonist, volinanserin (0.06 and 0.32 mg/kg/day) showed no significant difference in the % PSR area staining compared with liver from vehicle animals at week 8 (Figure 9.4.5).
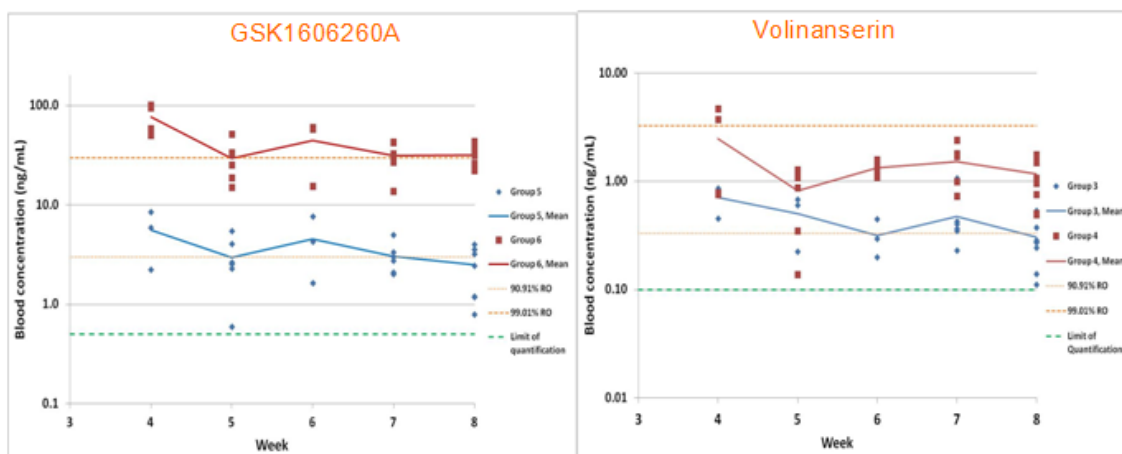
Figure 9.4.2. Blood concentrations achieved following the minipump administration of GSK1606260A and volinaserin to the mouse during the study. Animals were surgically implanted with minipumps (flow rate 3.6 µl/day) that had been loaded with: Group 3 and 4: Volinanserin 0.06 and 0.32 mg/kg/day, respectively, Group 5 and 6 GSK1606260A 0.15 and 1.53 mg/kg/day, respectively. The blood samples were taken throughout the life phase and as a terminal procedure to determine the drug exposure levels (See Appendix 9.4.3. Materials and methods). Data was expressed as blood concentration.
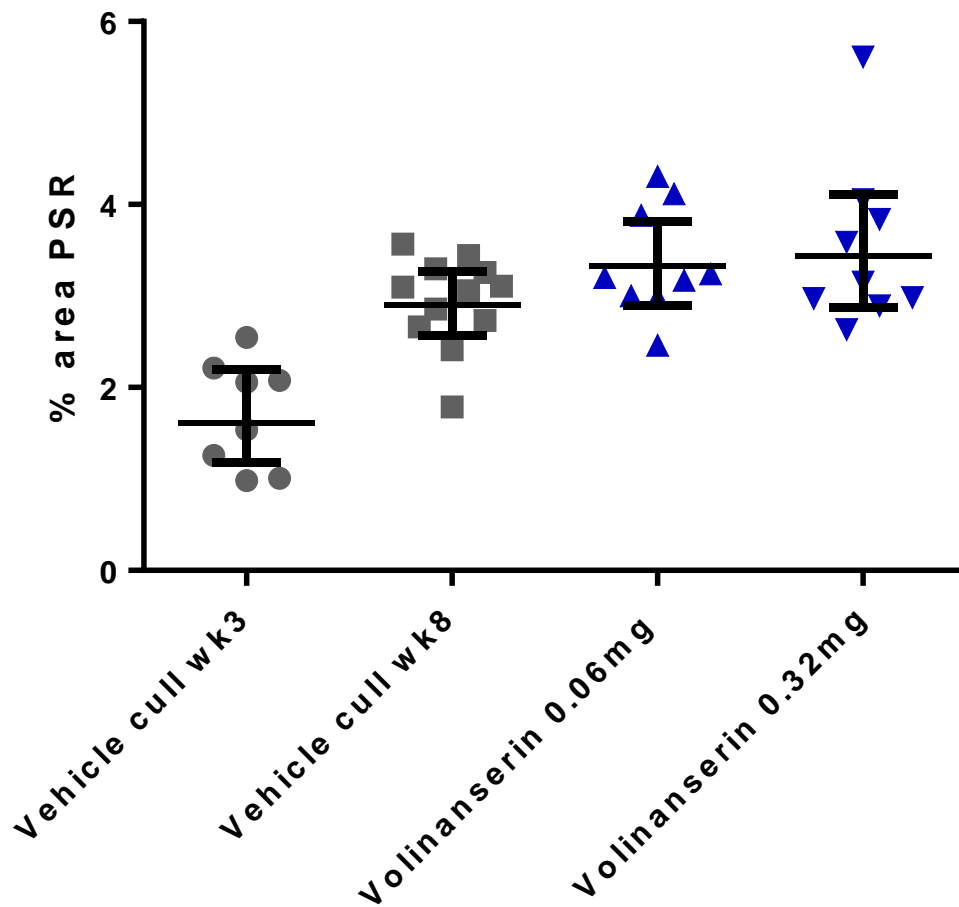
Figure 9.4.3   Histological assessment for percent area of picrosirius red obtained at week 3 and week 8. Animals were injected i.p. with carbon tetrachloride (CCL_4) twice weekly for up to a total of 8 weeks to induce fibrosis. One group of animals was culled at 3 weeks to determine a baseline level. Data shown is a representative slide of the % picrosirius staining obtained at week 3 and week 8. (See Appendix 9.4.3. Material and methods). The graph shows the % picrosirius red staining obtained for all the control animals with the geometric mean with 95 % confidence interval obtained. *** $P<0.001$ (p value adjusted based on Dunnett's method)
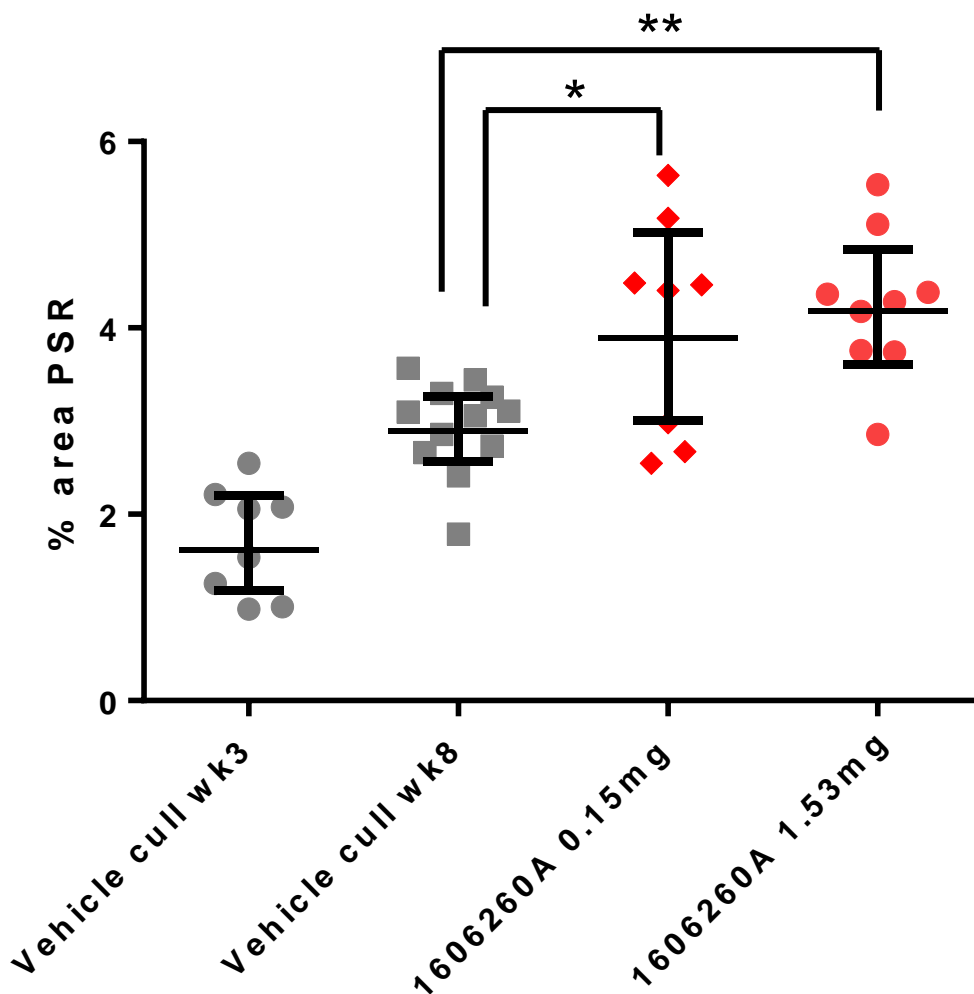
Figure 9.4.4 Histological assessment for percent area of picrosirius red obtained at week 3, week 8, week 8 dosed with GSK1606260A 0.15 mg/kg/day and week 8 dosed with GSK1606260A 1.53 mg/kg/day. Animals were injected i.p. with CCL$_4$ twice weekly for up to a total of 8 weeks to induce fibrosis. On group was culled at 3 weeks to determine baseline and the rest of the groups of animals were surgically implanted with minipumps (flow rate 3.6 μL/day) that had been loaded with vehicle (DMSO : PEG200 : water 10:45:45 (v/v/v), 0.15 mg/kg/day GSK1606260A and 1.53 mg/kg/day GSK1606260A respectively. (See Appendix 9.4.3. Materials and methods). Histological assessment of fibrosis was determined as % picrosirius red staining. Data shown is geometric mean with 95 % confidence interval obtained. ** P<0.01 and * P<0.015 (p value adjusted based on Dunnett's method).

Figure 9.4.5. Histological assessment for percent area of picrosirius red obtained at week 3, week 8, week 8 dosed with volinanserin 0.06 mg/kg/day and week 8 dosed with volinaserin 0.32 mg/kg/day. Animals were injected i.p. with CCL_4 twice weekly for up to a total of 8 weeks to induce fibrosis. On group was culled at 3 weeks to determine baseline and the rest of the groups of animals were surgically implanted with minipumps (flow rate 3.6 μl/day) that had been loaded with vehicle (DMSO : PEG200 : water 10:45:45 (v/v/v), 0.06 mg/kg/day volinanserin and 0.32 mg/kg/day volinanserin respectively. (See Appendix 9.3. Materials and methods). Histological assessment of fibrosis was determined as % picrosirius red staining. Data shown is geometric mean with 95 % confidence interval obtained.